

Alma Mater Studiorum – Università di Bologna

DOTTORATO DI RICERCA IN

Scienze Biomediche

Ciclo XXIX

Settore Concorsuale di afferenza: 06/A4

Settore Scientifico disciplinare: MED/08

**NOVEL, BIO-INSPIRED SUPERPARAMAGNETIC HYBRID
MICROSPHERES FOR BONE TISSUE ENGINEERING**

Presentata da: Tatiana Marisa Fernandes Patrício

Coordinatore Dottorato

Prof. Lucio Cocco

Relatore

Prof. Giovanna Cenacchi

Co-Relatore

Dott. Simone Sprio

Dott.ssa Anna Tampieri

Esame finale anno 2017

Table of contents

Table of contents	II
List of Figures	VI
List of tables	XI
List of equations	XII
Abbreviations.....	XIII
Acknowledgements.....	XIV
Funding	XV
Scope of the work	XVI
Chapter 1: Introduction	17
1.1 Overview: Bone defects and current treatments	17
1.2 Bone tissue	18
1.3 Biomimetic strategies applied on bone tissue engineering.....	21
1.3.1 Scaffolds	21
1.3.2 Nanoparticles /Microbeads	22
1.3.3 Powerful properties of calcium phosphate and ions substitution	23
1.3.4 Nature-inspired approaches	24
1.3.4.1 Biomineralisation Process	24
1.4 Smart strategies for advanced bone regenerative therapies.....	25
1.5 Biocompatible magnetic materials: new approaches for bone tissue regeneration.....	26
1.5.1 Magnetic nanoparticles	27
1.5.2 Magnetic cells	28
1.5.3 Magnetic scaffolds.....	29
1.5.4 Novel biocompatible magnetic nanoparticles: Fe-HA.....	32
1.6 Brief idea on regulatory guidelines and scaffold commercialization	33
Chapter 2. Materials and Methods.....	35
2.1 Application of biomineralisation process to obtain new hybrid biomaterials with superparamagnetic properties.....	35
2.1.1 Raw materials	35
2.1.2 Biomineralisation Process	35
2.1.3 Morphological, chemical, thermal and magnetic characterisation.....	36
2.2 New bioactive bone-like microspheres with intrinsic magnetic properties obtained by bio-inspired mineralisation process	37
2.2.1 Raw materials	37
2.2.2 Reaction of RCP with calcium and iron ions.....	37
2.2.3 Synthesis of hybrid mineralised materials	38

2.2.4	Production of microspheres by emulsification method	38
2.2.5	Physicochemical, morphological and magnetic characterisation	39
2.2.6	Preliminary cytocompatibility test.....	40
2.2.7	Statistical analysis.....	41
2.3	Effect of ions release from hybrid superparamagnetic microspheres on osteogenic differentiation of MC3T3-E1	42
2.3.1	Raw materials	42
2.3.2	Preparation of RCP and RCPfluidMAG-CT solutions	42
2.3.3	Synthesis and functionalisation of mineralised slurries.....	42
2.3.4	Fabrication of microspheres by emulsification process.....	43
2.3.5	Morphological and physicochemical characterisation.....	43
2.3.6	Microspheres degradation study	44
2.3.7	Biological characterisation	44
2.3.7.1	Cell culture	44
2.3.7.2	Cell viability	45
2.3.7.3	Cell damage and cell morphology evaluation	45
2.3.7.4	Western Blot.....	46
2.3.7.5	Quantitative real-time polymerase chain reaction (qPCR).....	47
2.3.8	Statistical analysis.....	47
2.4	Effect of microspheres composition on differentiation of human mesenchymal stem cells.....	48
2.4.1	Materials	48
2.4.2	Microspheres characterisation	48
2.4.3	Cell culture.....	48
2.4.4	Cell viability and proliferation.....	50
2.4.5	Calcium assay	52
2.4.6	Gene expression.....	52
2.4.7	von Kossa staining.....	53
2.4.8	Preparation of histology samples.....	53
2.4.9	Statistical analysis.....	54
2.5	Superparamagnetic microspheres as a sustained carrier for rhBMP-2 delivery	55
2.5.1	Materials	55
2.5.2	Assessment of rhBMP-2 release from microspheres.....	55
2.5.2.1	Microspheres characterisation.....	55
2.5.3	<i>In vitro</i> loading and release of rhBMP-2	56
2.5.4	Loading efficiency of microspheres and interaction with rhBMP-2	57
2.5.5	<i>In vitro</i> rhBMP-2 bioactivity assay.....	58
2.5.6	Optimisation of rhBMP-2 adsorption from microspheres	59

2.5.7	<i>In vitro</i> rhBMP-2 release under pulsed electromagnetic field (PEMF).....	59
2.5.8	Statistical analysis.....	60
2.6	Preliminary investigations on Scaffold fabrication	61
2.6.1	Scaffolds fabrication.....	61
2.6.2	Scaffold characterisation.....	61
Chapter 3.	Results	62
3.1	Application of biomineralisation process to obtain new hybrid biomaterials with superparamagnetic properties.....	62
3.1.1	Collagen I based recombinant peptide.....	62
3.1.2	Development of materials with magnetic and bone-like properties	62
3.2	New bioactive bone-like microspheres with intrinsic magnetic properties obtained by bio-inspired mineralisation process	68
3.2.1	Physicochemical and morphological characterisation of mineralised and non-mineralised materials	68
3.2.2	Characterisation of microspheres.....	73
3.2.3	<i>In vitro</i> cell analysis.....	76
3.3	Effect of ions release from hybrid superparamagnetic microspheres on osteogenic differentiation of MC3T3-E1	78
3.3.1	Physical, chemical and thermal characterisation of RCPFeHA functionalised with Sodium Citrate	78
3.3.2	Phase composition, morphological characterisation, microspheres size distribution and magnetic properties	80
3.3.3	Microspheres degradation studies under physiological and inflammatory mimicking conditions	83
3.3.4	Biological characterisation	87
3.4	Effect of microspheres composition on differentiation of human mesenchymal stem cells.....	93
3.4.1	Cell viability	93
3.4.2	Optimisation of cell seeding	94
3.4.3	<i>In vitro</i> osteogenic differentiation of human mesenchymal stem cells	96
3.5	Superparamagnetic microspheres as a sustained carrier for rhBMP-2 delivery	102
3.5.1	Microspheres properties.....	102
3.5.2	Effect of specific surface area of microspheres on rhBMP-2 release.....	104
3.5.3	Effect of microspheres composition on: Loading efficiency and interaction with rhBMP-2...	105
3.5.4	rhBMP-2 release kinetics.....	108
3.5.5	Evaluation of non-released rhBMP-2	109
3.5.6	rhBMP-2 bioactivity	110
3.5.7	Tailored release of rhBMP-2 by using PEMF	110

3.6 Preliminary investigations on Scaffold fabrication	112
3.6.1 Bone-like scaffolds with superparamagnetic properties	112
Chapter 4. Discussion.....	115
4.1 Application of biomineralisation process to obtain new hybrid biomaterials with superparamagnetic properties.....	115
4.2 New bioactive bone-like microspheres with intrinsic magnetic properties obtained by bio-inspired mineralisation process	116
4.3 Effect of ions release from hybrid superparamagnetic microspheres on osteogenic differentiation of MC3T3-E1	118
4.4 Effect of microspheres composition on differentiation of human mesenchymal stem cells....	120
4.5 Superparamagnetic microspheres as a sustained carrier for rhBMP-2 delivery	122
4.6 Preliminary investigations on Scaffold fabrication	124
Chapter 5. Conclusions and Future perspectives.....	125
References	128
Annex I.....	143
Preliminary investigations on microspheres production with low amount of mineral phase	143
Annex II.....	151
List of Publications	151

List of Figures

Figure 1. A) Hierarchical structure of bone tissue and B) cells activity in bone tissue (Wegst et al. 2014; Long 2011).	19
Figure 2. Steps of bone fracture healing (Lienemann et al. 2012).	20
Figure 3. The use of magnetic nanoparticles in bone tissue regeneration. A) Effect of external magnetic field on cells surface; B) Magnetic cells; C) Interaction of magnetic beads with cells; D, D1) Effect of EMF and magnetic scaffold in tissue regeneration and magnetic stimulation on cell behaviour (D2) (Santos et al. 2015; Gil & Mano 2014).	27
Figure 4. Step from research bench to scaffold commercialization.	34
Figure 5. Schematic design of biomineralisation process.	35
Figure 6. Schematic design of emulsification process.	39
Figure 7. Cells seeding strategy for 3500 cell/cm ² (A) and for 700 and 350 cells/cm ² (B).	50
Figure 8. Pulsed electric magnetic field used on rhBMP-2 release.	60
Figure 9. Composition of RCP (A) and size distribution profile of RCP (B).	62
Figure 10. XRD pattern of the as-produced biomaterials. a) RCP; b) RCP/HA (90/10); c) RCP/FeHA (90/10; 3:2; 25); d) RCP/FeHA (90/10; 3:2; 40); e) RCP/FeHA (90/10; 5:4; 40).	63
Figure 11. (A) FTIR spectrum and (C) XRD pattern of the as-produced biomaterials, #) Calcium phosphate, 40 °C; a) RCP/FeHA (60/40); b) RCP/FeHA (40/60); c) RCP/FeHA (30/70); d) RCP/FeHA (20/80), (* iron oxide pattern with reference code: 00-019-0629; • calcium phosphate hydroxide with reference code: 00-0090432); B) Typical infra-red spectra and XRD pattern (D) of bone tissue (Boskey 2007; Vallet-Regi & Gonzalez-Calbet 2004).	64
Figure 12. (A) FTIR spectrum and (B) XRD pattern of the as-produced biomaterials, #) Calcium phosphate, 40 °C; a) RCP/FeHA (20; 3:2); b) RCP/FeHA (20; 5:4); c) RCP/FeHA (45; 3:2); d) RCP/FeHA (45; 5:4), (• calcium phosphate hydroxide with reference code: 00-0090432).	66
Figure 13. (A) FTIR spectrum and (B) XRD pattern of the as-produced biomaterials, a) RCP/FeHA, 40 °C; b) RCP/FeHA, 50 °C; c) RCP/FeHA, 60 °C; (• calcium phosphate hydroxide with reference code: 00-0090432; * iron oxide diffraction peaks with reference code: 00-019-0629).	67
Figure 14. XRD pattern of RCP (a) and of the as-obtained mineralised materials: b) RCPHA40; c) RCPFeHA40; d) RCPHA60 and e) RCPFeHA60. Iron oxide formation in RCPFeHA60 is indicated by *	68
Figure 15. FTIR spectra of mineralised materials. a) RCP; b) RCPHA40; c) RCPHA60; d) RCPFeHA40 and e) RCPFeHA60. A: full pattern, B: a detail evidencing the position of the absorption bands related to amide, carboxylic groups and phosphate groups.	69
Figure 16. A) FTIR spectra of RCP and mineralised materials. B) a detail on absorption bands relevant for linking the inorganic phase. a) RCP; b) RCP/Ca; c) RCP/Fe3; d) RCP/Fe2.	70

Figure 17. Weight loss of RCP (A) and mineralised materials in absence (B) and presence of iron (C). D): SEM micrograph of 3D network of the mineral nanophase in RCPFeHA60, as obtained after complete decomposition of RCP, at 700 °C, (Scale bar: 200 nm).....	72
Figure 18. TEM micrographs of mineralised materials, RCPHA40 (A), RCPFeHA40 (B) and TEM micrograph with SAED image of RCPFeHA60 (C); Examples of iron oxide nanoparticles, identified with black arrows, formed on hydroxyapatite nanocrystals of RCPFeHA60 (D), (Scale bar: 20 nm); Energy dispersive X-ray (EDX) analysis of RCPFeHA40 and RCPFeHA60 (E).	73
Figure 19. Hybrid microspheres obtained by varying the mechanical stirring velocity, 520 rpm (A), 650 rpm (B), 715 rpm (C) and 975 rpm (D). As-optimised microspheres obtained at 520 rpm and at low cooling temperature, i.e., microspheres jellification (E). Detail surface morphology and shape of pure RCP (F) and hybrid microspheres: RCPFeHA40 (G) and RCPFeHA60 (H), (Scale bar are: 50 µm (A, B, C, D, E) and 10 µm (F, G, H)).	75
Figure 20. FTIR spectra (A) and TGA profile (B) of DHT crosslinked RCP microspheres compared to non-crosslinked microspheres.....	75
Figure 21. RCPFeHA60 microspheres in cell medium in absence (A) and in presence of neodymium magnet (B) and specific magnetisation of RCPFeHA60 obtained by VSM (C).....	76
Figure 22. Analysis of cells proliferation by the MTT assay, after 1, 3 and 7 days of MC3T3-E1 cell culture with RCP, RCPFeHA40 and RCPFeHA60 microspheres at concentration of microspheres of 10 µg/ml (A) and 100 µg/ml (B). (**p≤0.01; ****p≤0.0001; n = 3).	77
Figure 23. Cell viability analysed by the Live/Dead assay after 1, 3 and 7 days of cell culture with 100 µg/ml microspheres. Calcein AM stains for live cells in green, EthD-1 stains for dead cells in red, (scale bar: 200 µm).	77
Figure 24. Effect of sodium citrate concentration on as-fabricated RCPFeHA microspheres. A) Microspheres without sodium citrate in osteogenic differentiation medium (Scale bar: 100 µm); B) Designed set-up of RCPFeHA slurry functionalisation with sodium citrate; RCPFeHA microspheres obtained with different concentrations of sodium citrate: C) 0.55 M; D) 0.28 M; E) 0.06 M; F) 0.006 M; G) 0.0006 M. Well dispersed microspheres functionalised with 0.006M in presence of osteogenic differentiation medium (H), (Scale bar: 200 µm).	79
Figure 25. Chemical and thermal features of functionalised RCPFeHA microspheres, by FTIR (A); XRD (B) and TGA analysis. a) Non-functionalised RCPFeHA microspheres; b) Functionalised RCPFeHA microspheres and cosslinked by DHT (c).	80
Figure 26. XRD pattern of the as-obtained microspheres: RCP (a); RCPfluidMAG-CT (b); RCPHA _{RT} (c); RCPHA (d); RCPFeHA (e). (Iron oxide formation is indicated by *).....	81
Figure 27. SEM micrographs from the as-produced microspheres: A) RCP; B) RCPfluidMAG-CT; C) RCPHA; D) RCPHA _{RT} ; E) RCPFeHA, (Scale bar is 200 µm and in the figure inserts is 20 µm).....	81
Figure 28. Size distribution and respective microspheres size obtained by Gaussian distribution. A) RCP; B) RCPfluidMAG-CT; C) RCPHA _{RT} ; D) RCPFeHA.....	82

Figure 29. SEM micrographs of microspheres, after immersion in physiological mimicking conditions, over the course of 28 days. A) RCP; B) RCPfluidMAG-CT; C) RCPHA _{RT} ; D) RCPFeHA, (Scale bar: 20 μm); (Note: 7D: 7 days; 14D: 14 days; 21D: 21 days; 28D: 28 days).	84
Figure 30. SEM micrographs of microspheres, after immersion in mimicking inflammatory conditions, over the course of 28 days. A) RCP; B) RCPfluidMAG-CT; C) RCPHA _{RT} ; D) RCPFeHA, (Scale bar: 20 μm); (Note: 7D: 7 days; 14D: 14 days; 21D: 21 days; 28D: 28 days).	84
Figure 31. pH changes in DMEM (pH 7.4) and DMEM-IM (pH 5) in presence of microspheres and controls (Mean±SEM).	85
Figure 32. Percentage of calcium adsorbed from DMEM at pH 7.4 (A); Cumulative Fe release of RCPFeHA (B); Cumulative Ca release at pH 5 (C) and Cumulative Fe release from RCPfluidMAG-CT (D); (* p≤0.05; ** p≤0.01; *** p≤0.001).	86
Figure 33. A) FTIR spectrum of RCPHA _{RT} after 28 days in pH 7.4 (a) and in pH 5 (b) and of RCPFeHA after 28 days in pH 7.4 (c) and in pH 5 (d); (B) XRD pattern of RCPHA _{RT} before (a) and after 28 days at pH 7.4 (b) and pH 5 (c) and of RCPFeHA (C), before (d) and after 28 days at pH 7.4 (e) and pH 5 (f).	87
Figure 34. Cell viability in presence of all tested microspheres (*p<0.05; **p<0.01; ***p<0.001).....	88
Figure 35. The effect of microspheres on cells apoptosis/necrosis, at two concentrations: 10 μg/mL and 100 μg/mL and at two experimental time points (Day 1 and Day 3). Apoptotic cells in green, necrotic cells in red, cell nuclei in blue. Negative control (A) and positive control (B), (Scale bar: 50 μm).	89
Figure 36. The effect of microspheres on ROS production, at two concentrations: 10 μg/mL and 100 μg/mL and at two experimental time points (Day 1 and Day 3). (Negative control (A) and positive control (B)), (Scale bar: 50 μm).	90
Figure 37. Morphological analysis of MC3T3-E1 cultured at day 3, in presence of 100 μg/ml of microspheres, evaluated by phalloidin staining (green: actin filaments, blue: cell nuclei) (A) and haematoxylin and eosin staining (B), (Scale bar: 20 μm). C) Bright-field images of RCPFeHA acquired at day 1 and day 7 of cell culture, (Scale bar: 50 μm).	91
Figure 38. Western blot analysis for the expression of osteogenic proteins ALP (A) and BGLAP (B) and autophagy marker C) LC3B-I (graph above) and LC3B-II (graph below). β-Actin was used as an internal control.	91
Figure 39. Relative quantification ($2^{-\Delta\Delta C_t}$) of osteogenic related genes expression after 7 days of MC3T3-E1 culture with all the tested microspheres.	92
Figure 40. Bright-field images (A) and Live (B) & dead (C) cells obtained after 7 days of cell culture in presence of hMSCs, (Scale bar: 200 μm). Live & Dead cells surrounded to RCPHA _{RT} (D) and RCPFeHA (E) microspheres.	93
Figure 41. Cell seeding at density of 3500 cell/cm ² ((A) Percentage of cells adhere to the microspheres after 3 days of cell culture and (B) H&E staining on RCPFeHA); Optical micrographs from cells (700 cells/cm ²) in presence of RCP (C), RCPHA _{RT} (D) and RCPFeHA microspheres (E), (Scale bar: 200 μm).	94

Figure 42. DNA amount obtained from equal cell seeding number (A) and different cell seeding number (B). Cell nuclei were stained with DAPI, in equal cell seeding number (C) and different cell seeding number (D). Live/Dead staining of RCPFeHA after 24 hours of cell culture (E).....	95
Figure 43. (A) hMSCs DNA content in all tested microspheres, over the course of the experiment (n=3), (Cell _s : cell seeding after 2 hours; Exp _F : end of experiment 21 days or 17 days, depending on the Donor); DNA values obtained from independent Donors (B), (Plot values represent Mean ± SD).....	96
Figure 44. (A) Calcium content in osteogenic induction medium, over the course of the experiment with 3D templates (i.e. hMSCs and respective microspheres RCP, RCPHA _{RT} and RCPFeHA) and in all tested Donors, (*p≤0.05; **p<0.01; ***p<0.001, respect to cell monolayer). B) Calcium content in osteogenic induction medium, over the course of the experiment with microspheres (RCP, RCPHA _{RT} and RCPFeHA), (*p≤0.05; **p<0.01; ***p<0.001, respect to osteogenic induction medium (ost. ind. medium)).....	98
Figure 45. A) Osteogenic gene expression levels obtained in presence of RCP, RCPHA _{RT} and RCPFeHA. Gene expression levels of COL I, SPARC (B) and IBSP (C) obtained in presence of RCP, RCPHA _{RT} and RCPFeHA in the different Donors, (*p<0.05; ** p<0.01; ***p<0.001).....	99
Figure 46. A) Optical micrographs of calcium deposits as indicated with white arrow and von Kossa staining of osteogenic differentiated of hMSCs, (B) Donor 1; (C) Donor 2; (D) Donor 3, (Scale bar: A) 200 μm and B, C, D) 100 μm).....	100
Figure 47. Haematoxylin and Eosin staining of representative sections of hMSCs cells cultured in osteogenic induction medium with RCP (A), RCPHA _{RT} (B) and RCPFeHA (C, D) microspheres. E and F) Thionin staining of hMSCs cells cultured in osteogenic induction medium on RCPFeHA, (Scale bar: 100 μm (A, B, C, E) and 50 μm (D, F)).....	101
Figure 48. SEM micrographs from the as-fabricated microspheres; A) RCP; B) RCPfluidMAG-CT; C) RCPHA _{RT} ; D) RCPFeHA and Ca (E); P (F) and Fe (G) distribution, as well as EDS microanalysis on RCPFeHA microspheres (H), (Scale bar: 20 μm).....	102
Figure 49. Variance of contact angle during the time for RCPHA _{RT} and RCPFeHA (A). Representative water drop on RCPFeHA in the beginning (B), after 360 seconds (C) and in the end of the experiment.....	103
Figure 50. C2C12 BRE-Luc cell line in presence of released rhBMP-2 (A) and (B) Luciferase activity after 1 day of released rhBMP-2 from all tested microspheres (SSA: rhBMP-2 adsorption take into account the specific surface area; No SSA: rhBMP-2 adsorption without consider specific surface area), (* p<0.05; *** p<0.001).....	104
Figure 51. Loading efficiency of rhBMP-2 in all tested microspheres, (* p<0.05).....	105
Figure 52. Fluorescence microscope images from microspheres without rhBMP-2 (A), with 900 ng/mL of rhBMP-2 (B) and after washing steps, (Scale bar: 20 μm).....	106
Figure 53. FTIR vibration peaks of RCP and rhBMP-2 (A) and respective deconvolution peaks (B) and (C); RCPHA _{RT} without and with rhBMP-2 (D) and deconvolution of phosphate peaks without rhBMP-2 (E) and in presence of rhBMP-2 (F); RCPFeHA without and with rhBMP-2 (G) and deconvolution of	

phosphate peaks without rhBMP-2 (H) and in presence of rhBMP-2 (I). (Orange trace line: Fit by Sum; Black line: FTIR spectra; blue lines: deconvolution peaks).....	107
Figure 54. Cumulative release of rhBMP-2 in percentage from RCP _{porous} and RCP microspheres, (in all the points of the graph statistically differences of p<0.0001).	108
Figure 55. Cumulative release of rhBMP-2 in percentage (A) and in ng (B), from RCP, RCPHA _{RT} and RCPFeHA microspheres.	109
Figure 56. SEM micrographs of RCPHA _{RT} (A) and RCPFeHA (B) microspheres, after 14 days of rhBMP-2 releasing studies, urea treatment and degradation with 10 mg/mL of collagenase, (Scale bar: 50 μm).	109
Figure 57. Percentage of rhBMP-2 bioactivity from RCP, RCPHA _{RT} and RCPFeHA, (* p<0.05).	110
Figure 58. Cumulative release of rhBMP-2 in percentage of RCPHA _{RT} (A), RCPfluidMAG-CT (B) and RCPFeHA (C) in presence or without PEMF.	111
Figure 59. Scaffolds produced by using the mineralised slurries and freeze-drying process (A) and SEM micrographs from bottom, middle and top of the scaffolds, cut as demonstrated in A*, (B); (a) RCP/HA; b) RCP/FeHA, 40°C; c) RCP/FeHA, 50°C; d) RCP/FeHA, 60°C, (Scale bar: bottom, middle and top: 100 μm and porous detail: 10 μm).	113
Figure 60. A) Thermogravimetric curve of iron containing mineralized scaffolds, obtained by TGA; B) Swelling properties up to 24h of soaking. C) Maximal swelling properties of the mineralised materials.	114
Figure 61. Proposed devices by using magnetic microspheres. A) Bone filler composed with swollen microspheres; B) 3D template composed by magnetic microspheres and cells; C) Bone filler composed by swollen magnetic microspheres as a carrier of rhBMP-2; D) 3D templates composed by swollen magnetic microspheres as rhBMP-2 carrier and cells.	126

List of tables

Table 1. Examples of magnetic scaffolds applied on bone tissue engineering.	30
Table 2. Cells numbers used in the optimisation of cell seeding. (* Values obtained from specific surface area of microspheres; ** based on specific surface area of RCP microspheres).	49
Table 3. Primers sequences used to define the osteogenic expression of the genes.	53
Table 4. Parameters used in both strategies of rhBMP-2 release, (SSA: rhBMP-2 adsorption take into account the specific surface area of the microspheres; No SSA: rhBMP-2 adsorption without consider specific surface area).....	59
Table 5. Parameters used in the biomineralisation process.....	63
Table 6. Splitting factor, quantitative evaluation of different elements, mineral amount and magnetisation of biomineralised materials. (values obtained by: [#] v4 phosphate group analysed by FTIR; [¥] ICP-OES; ** TGA analysis; [§] Susceptometer balance; * (Dorozhkin 2011)).	65
Table 7. Parameters used in the biomineralisation process.....	66
Table 8. Splitting factor (SF) and cell parameters of mineralised materials.....	69
Table 9. FTIR wavenumber obtained for amide I, amide II and carboxylic group in RCP, RCP/Ca, RCP/Fe ₃ , RCP/Fe ₂ and in RCP/Fe ₃ and RCP/Fe ₂ with adjusted pH.	71
Table 10. Chemical features of mineralised materials (results obtained by: * ICP-OES; ** UV-VIS).	71
Table 11. Effect of sodium citrate on surface charge of RCPFeHA slurry.....	78
Table 12. Microspheres composition, ζ-potential and chemical elements of microspheres. (*obtained by ICP-OES)	82
Table 13. Physical properties of microspheres, (obtained by: [§] zetasizer system; [#] contact angle system; *optical micrographs and analysed by Image J software; **BET equipment).	103

List of equations

Equation 1. Percentage of cells adhered on the microspheres.	51
Equation 2. Percentage of swelling capacity of microspheres.	56
Equation 3. Calculation of loading efficiency of microspheres.	57
Equation 4. Calculation of rhBMP-2 bioactivity.	59
Equation 5. Calculation of swelling capacity of the scaffolds.	61

Abbreviations

ANSI	American National Standards Institute
ASTM	American Society for Testing and Materials
BMSC	Bone marrow stromal cells
BSA	Bovine serum albumin
CA	Citric acid
Ca²⁺	Calcium ion
CDC42	Cell Division Cycle 42 gene
Cl⁻	Chloride ion
CO₂	Carbon dioxide
CO₃²⁻	Carbonate ion
DXM	Corticosteroid dexamethasone acetate
F⁻	Fluoride ion
HPO₄²⁻	Hydrogen Phosphate ion
ISO	International Organization for Standardization
Mg²⁺,	Magnesium ion
Na⁺,	Sodium ion
OH⁻	Hydroxide ion
p38/MAPK	Mitogen-activated protein kinases
SiO₄⁴⁻	Orthosilicate anion
SMF	Static magnetic field
Sr²⁺	Strontium ion
γ -Fe₂O₃	Maghemite

Acknowledgements

I would like to express with great satisfaction my sincere thanks to those who made possible the development of the PhD research work.

Thanks to, Doctor Anna Tampieri, Doctor Simone Sprio, Doctor Monica Sandri, Doctor Monica Montesi, Doctor Silvia Panseri, Doctor Michele Iafisco that gave me the possibility of being integrated into Bioceramics and Bio-hybrid Composites Group, CNR-ISTEC, Faenza, Italy.

To my supervisor, Doctor Simone Sprio, for his suggestions, dedication, all the support throughout the development of the research work and exchange of ideas.

To my supervisor, Professor Doctor Giovanna Cenacchi, for her suggestions during the PhD.

To Doctor Monica Sandri, for her support and exchange of ideas.

To Doctor Monica Montesi and Doctor Silvia Panseri for their friendship, patience, dedication, support and availability to teach me about biological issues.

To Doctor Michele Iafisco, for his support, teaching and exchange of ideas.

To Doctor Alessio Adamiano, Doctor Massimiliano Dapporto, Alberto Balardini and Samuel Dozio, for their help during the PhD.

To all my colleagues from Bioceramics and Bio-hybrid Composites Group and from CNR-ISTEC, that directly or indirectly helps me during the PhD.

To Professor Doctor Gerjo Van Osch from Connective Tissue Cells and Repair group, Erasmus Medical Centre (The Netherlands), for having welcomed me at her research centre and for all the support, dedication and exchange of ideas.

To Doctor Eric Farrell from Department of Oral & Maxillofacial Surgery, Erasmus Medical Centre (The Netherlands), for his friendship, support, dedication, patience and exchange of knowledge.

To Janneke Bouma from Department of Oral & Maxillofacial Surgery, Erasmus Medical Centre (The Netherlands), for her friendship, patience and support in the biological tests.

To all the people from Connective Tissue Cells and Repair group, Erasmus Medical Centre (The Netherlands) for having welcomed me at the group.

To Gloria Belén Ramirez-Rodriguez, for her friendship, support, dedication, exchange of ideas and for the great moments that we passed during those three years of PhD.

To all my colleagues and friends from BIOINSPIRE project, in special to Didem Mumcuoglu, Natalia Gostyńska, Shorouk Garcia, Gopal Shankar, for their friendship and support.

To Bas Kluijtmans and Suzan van Dongen, from Fujifilm Manufacturing Europe B.V. (The Netherlands), to welcomed me in the company and to Jonathan Knychala to teach me during the secondment.

Special Thanks to my Best Friends, for their motivation, support and dedication.

Special Thanks to my Parents, my Brother and my Husband for their support, dedication, motivation and to believe in me.

TO EVERYONE, MY SINCERE THANKS.

Funding

The research leading to these results has received funding from the European Union Seventh Framework Programme FP7-PEOPLE-2013-ITN under grant agreement n° 607051.

Scope of the work

The scope of my PhD thesis was to develop novel biomimetic nanomaterials with potential of use in innovative smart and personalized applications in medicine, with particular respect to bone tissue engineering. The relevance of this activity is in the need of bioactive, bioresorbable and smart nanomaterials, able to substantially activate, promote and sustain biologic processes yielding tissue regeneration. Nowadays this need is made extremely crucial by the steady ageing of the population and increase in the occurrence of bone diseases generating high disability and remarkable healthcare costs. Particularly, smart, stimuli-responsive biocompatible materials are highly desired, as they can enable more effective and personalized therapies in nanomedicine. In this respect, the development of magnetically active materials is today raising substantial interest among scientists, as magnetic signalling is considered as minimally invasive mechanism for biomaterial activation that can open to a plethora of new applications in nanomedicine.

Current limitations in this respect are in the achievement of biocompatible materials with factual cell-instructive ability and magnetic properties for which the development of materials exhibiting high physicochemical and ultrastructural mimesis with natural tissues (i.e. biomimetic) are considered as an elective approach.

In this respect the main concept at the basis of my research work was to apply a bio-inspired synthesis process (i.e. biomineralisation) to a recombinant collagen type I-like macromolecule, with the purpose to develop hybrid mineralised composites mimicking natural bone tissue. In particular, I directed the biomineralisation process to obtain the assembling of the organic macromolecule and simultaneous mineralization with nanocrystalline, iron-substituted hydroxyapatite where the precise positioning of iron ions conferred superparamagnetic properties to the final hybrid materials. Then, I settled an emulsification process to engineer the obtained materials into hybrid magnetic microspheres, which were extensively tested by means of their physicochemical, morphological, magnetic and biological properties.

In particular, my thesis describes, after an introductory section illustrating the biomimetic approach to materials development, specific activities dedicated to material synthesis and testing, particularly to assess how physicochemical properties of the new microspheres affected the fate of specific cell lines relevant for bone regeneration such as pre-osteoblasts and human mesenchymal stem cells. Besides, the ability of the new devices to incorporate and release relevant growth factors by mediation of applied magnetic fields was investigated.

As a general conclusion, the unique features exhibited by the new hybrid magnetic microspheres are interesting and promising for application as new smart biomaterials with ability of remote magnetic activation and control, which might be addressed to smart and personalized applications in medicine, particularly in bone tissue regeneration or smart drug delivery systems.

Chapter 1: Introduction

1.1 Overview: Bone defects and current treatments

Bone defects are among the main causes of reduced life quality due to trauma, diseases (e.g. cancer, osteoporosis-related fractures, congenital bone malformations), aging process, intense sport activity, obesity, or ions deficiency (e.g. leads to dysfunction and diseases in bone tissue, such as osteoporosis and osteomalacia). The natural process of bone repair is enough to regenerate in most of the bone fractures, although bone tissue can not handle with large size “critical” lesion (Boskey 2007; Ferreira et al. 2012; Perez et al. 2015; Wang et al. 2014; Fernandez-Yague et al. 2015). Every year in United States, about \$2.5 billion of dollars in replacements of bone defects was expended, while with increasing of life expectance, until 2020, an increase of costs in bone replacements was predicted (Amini et al. 2012).

Autografts, allografts and xenografts were the first used therapeutic approaches in bone tissue replacement and still a major choice for surgeons. Prior to select the ideal graft, i.e. **autografts** (i.e. bone transplantation from one part to another part of the same body), **allografts** (i.e. bone transplantation from donor of the same species) and **xenografts** (i.e. from other species), bone disabilities, bone defect sizes, tissue viability, biomechanical properties, graft handling and costs are studied (Harvey et al. 2010; Oryan et al. 2014; Poinern et al. 2013; Shibuya & Jupiter 2015). Osteoinductivity and osteoconductivity are the main characteristics of allografts and xenografts, while autografts are defined as “gold standard” due to their osteoinductivity, osteoconductivity and osteogenic properties, relevant on bone healing, modelling and remodelling (Oryan et al. 2014). Moreover, various drawbacks, such as risk of rejection, infection, diseases transmission, pain, bone graft loss/resorption, lack of vascularisation, reduced availability and high cost were identified (Harvey et al. 2010; Oryan et al. 2014; Tang et al. 2016); thus new strategies have been designed and investigated. Bone substitutes based on calcium phosphate, bioactive glasses, polymers and composites were approved by Food and Drug Administration (FDA). The problems with bone grafts availability and donor site morbidity were supported, but still new achievements must be implemented, mainly on synthetic materials that closely mimic the structure and function of bone tissue and the production of scaffolds with suitable mechanical properties for regeneration of critical sized bone defects (Di Silvio 2007; Oryan et al. 2014).

Intensive efforts on development of smart materials were performed, with the perspective to present customised and efficient solutions for the recovery of tissue functionality. In respect to bone tissue regeneration, the challenge is to achieve effective therapies that helps on completely function recovery from diseased tissues without second surgery intervention (Tampieri et al. 2012). On the other hand, smart biomaterials can be engineered as systems for delivery of therapeutic substances directly on the target site, thus avoiding systemic administration. Progress in this respect can guarantee standardized performances (e.g. contrary to autologous or heterologous bone), as well as reduced adverse effects and improvement on osteoconductivity, osteoinductivity and osseointegration (Oryan et al. 2014; Tang et al. 2016).

Tissue Engineering (TE) has been investigated as an innovative approach to develop biomimetic templates

for regeneration of bone tissue defects (Di Silvio 2007). In mid-1980s, *Langer* and *Vacanti* defined TE as “an emerging and multidisciplinary scientific area that applies principles of engineering and life sciences towards the development of biological substitutes that repair, restore or enhance tissue and organs functions”, by combining cells, biomaterials and biomolecular signals (e.g. growth factors or bone morphogenic proteins) (Minuth et al. 2006; Bártolo et al. 2011) and osteogenicity, osteoconductivity and osteoinductivity properties of biomaterials are improved (Oryan et al. 2014). On the other hand, suitable mechanical properties and appropriated degradation rate have been achieved on bone scaffold design, as well as easy-to-use in clinical practise (Di Silvio 2007; Panseri et al. 2013; Stevens 2008).

Therefore, new strategy in tissue engineering is the use of magnetic nanoparticles, in particular superparamagnetic iron oxides (SPIONs), where their functionality is controlled by means of external magnetic fields. The introduction of superparamagnetic features in biomaterials is gaining high importance due to the possibility of stimulating cell activity, or to induce hyperthermia effects by applying magnetic field or simply by releasing relevant ions for osteoblasts proliferation and osteogenic activity. This approach can represent a new tool for boosting metabolic activity towards bone regeneration (Gil & Mano 2014; Tampieri et al. 2014; Meng et al. 2010).

1.2 Bone tissue

Bone is a dynamic tissue in constant remodelling to maintain the structural integrity of the skeleton and allowing the maintenance of bone volume, by cascade of phenomena including homeostasis of calcium and phosphorus metabolism, essential to the life (Engel et al. 2009). Therefore, bone is a porous tissue with complex hierarchical structure, from nanoscale to macroscale, mainly composed of calcium phosphate ($\text{Ca}_{10}(\text{PO}_4)_6(\text{OH})_2$; 69-80wt.%), type I collagen (17-20wt.%), non-collagenous proteins (e.g. sialoprotein, osteonectin, osteopontin), growth factors, water and cells (Boskey 2007; Ferreira et al. 2012; Dorozhkin 2011).

Bone is organised in compact (pore size: 1-100 μm and porosity: 5-10 wt%) and spongy bone (pore size: 200-400 μm and porosity: 75-95 wt%) and at the nanoscale level, non-stoichiometric carbonate hydroxyapatite nanocrystals (plate-shaped, 100-50 nm \times 25 nm in size, 1.5–4 nm thick) are heterogeneously nucleated onto non-mineralised organic macromolecules (i.e. type I collagen, \sim 300 nm long, \sim 1.5 nm in diameter) with preferential orientation along the *c* axis and parallel to collagen fibrils and organised in a periodic, staggered array along the fibrils (Wang et al. 2014; Wegst et al. 2014; Saiz et al. 2013; Dorozhkin 2011; Florencio-Silva et al. 2015). The self-assembly of the collagen fibrils and the formation of crystals of the mineral phase are phenomena governed by various control mechanisms activated by the same structure of the protein macromolecule thanks to specific conditions of pH and ion concentrations (Tampieri et al. 2011; Sprio et al. 2012; Perez et al. 2014) (Figure 1A).

The mature skeleton of humans is supported through the equilibrated activity of the bone-forming osteoblasts and the bone-resorbing osteoclasts (Long 2011; Ferreira et al. 2012). In bone tissue various types of cells are presented, i.e. osteoblasts, bone lining cells, osteoclasts and osteocytes, as well as extracellular matrix

(ECM) (Engel et al. 2009). **Osteoblasts** result from mesenchymal progenitor (MPs) via preosteoblasts and control the mineralisation of extracellular collagen protein matrix. The subset of osteoblasts become **osteocytes**, mature bone cells embedded into the bone matrix, which are thought to control and direct the physiological bone turnover based on continuous formation and resorption of bone tissue, in response to damaging or to mechanical stimuli (bone remodelling). In the early stage of new bone formation, osteoblasts attachment, proliferation and differentiation are key phenomena for bone formation, by the production of matrix proteins, such as collagen type I, osteopontin, bone sialoprotein, osteonectin, osteocalcin, fibronectin and bone morphogenetic proteins (BMPs) prior to mineral deposition (Roveri & Iafisco 2010). **Osteoclasts** are multinucleated resorptive cells derived from bone marrow-derived macrophages, which are in turn progenies of haematopoietic stem cells (HSCs). **Osteoclasts** remove bone mineral and bone matrix in a process named as bone resorption, therefore **bone-lining cells** prevents osteoclasts interaction with bone matrix in dysfunctional situation, as well as it seems to be relevant in coupling bone resorption to bone formation (Figure 1B) (Florencio-Silva et al. 2015; Miller et al. 1989; Perez et al. 2015; Long 2011).

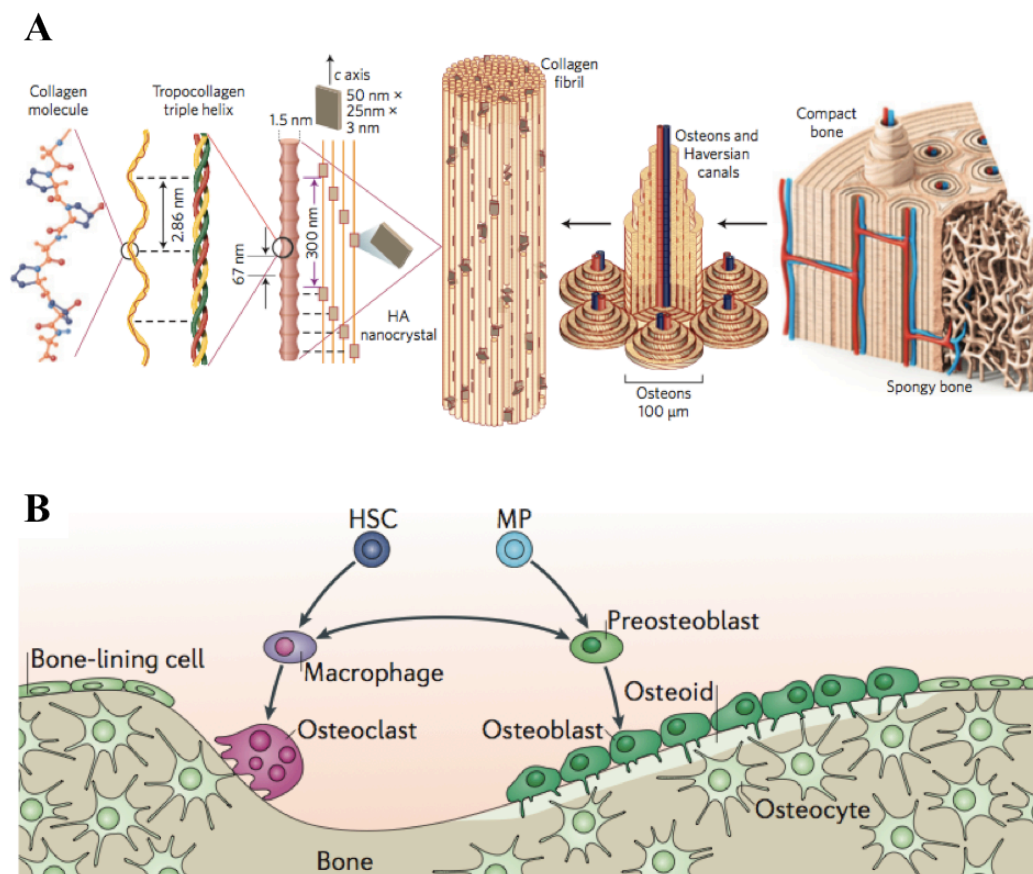


Figure 1. A) Hierarchical structure of bone tissue and B) cells activity in bone tissue (Wegst et al. 2014; Long 2011).

Bone fracture healing occurs via direct intramembranous bone formation, if fractures are well stabilised (e.g. flat bones) or via endochondral bone formation, in the case of large defects, (e.g. long bones) and several molecular regulators are involved in both processes (e.g. indian hedgehog (Ihh), parathyroid hormone related

peptide (PTHrP), bone morphogenetic proteins (BMPs), vascular endothelial growth factor (VEGF) and fibroblastic growth factors (FGFs)) (Amini et al. 2012; Lienemann et al. 2012) (Figure 2). In endochondral bone formation, different stages (i.e. inflammation, soft callus formation, hard callus formation and remodelling) are involved and at the stabilisation of the fracture site mesenchymal progenitor cells differentiated into chondrocytes, to form cartilaginous template that is mineralized and replaced by bone tissue. Therefore, in intramembranous bone formation the differentiation of mesenchymal progenitor cells into osteoblasts and mineralized matrix without chondrogenic differentiation was formed. The as-produced *de novo* bone is remodelled into cortical or trabecular bone at later stages. (Amini et al. 2012; Lienemann et al. 2012; Poinern et al. 2013).

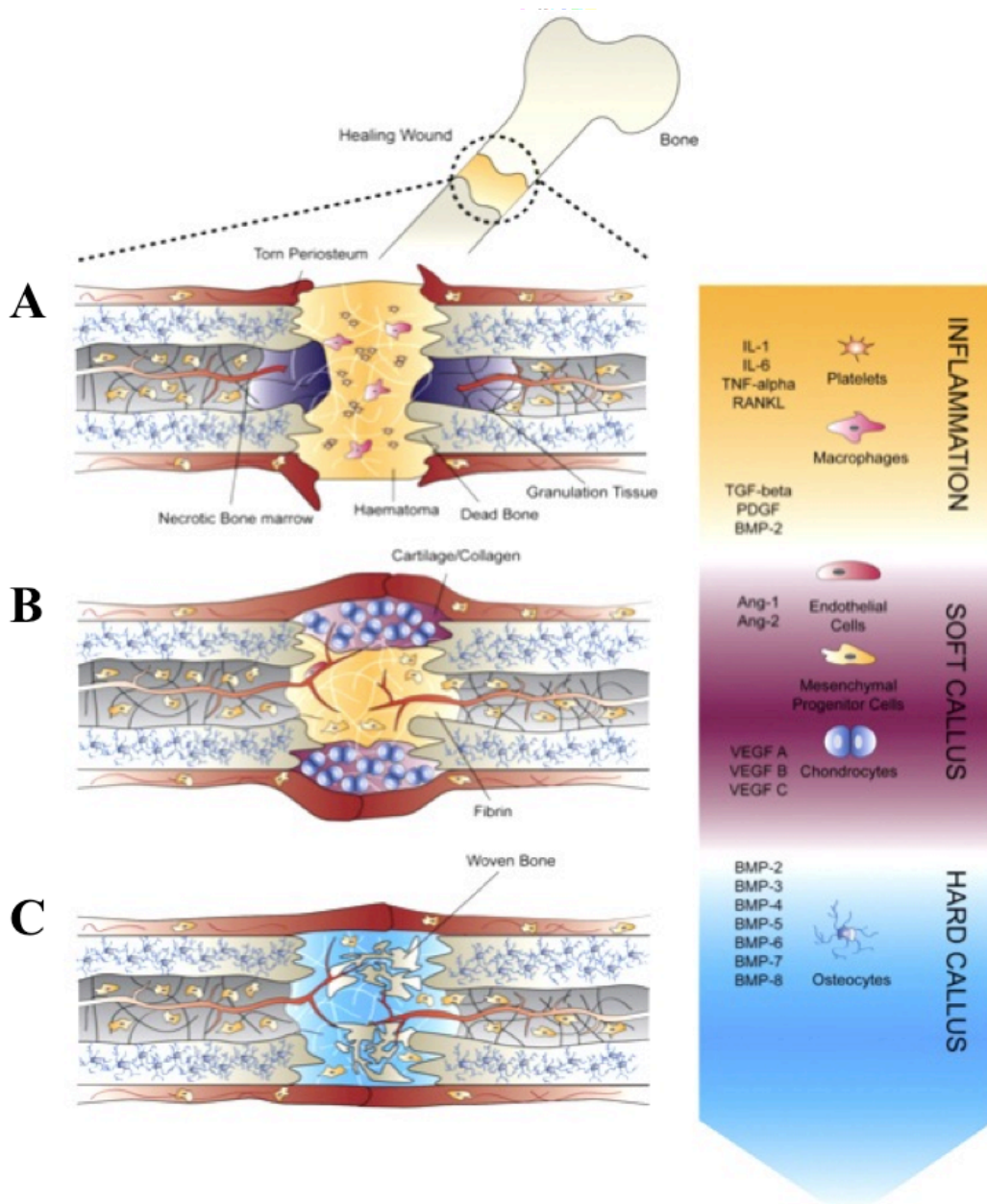


Figure 2. Steps of bone fracture healing (Lienemann et al. 2012).

Bone hydroxyapatite is a non-stoichiometric phase presenting calcium and hydroxyl deficiency with various ion substitutions and vacancies, thus resulting in Ca/P molar ratios different from the stoichiometric hydroxyapatite (1.67) (Boskey 2007; Gomez-Morales et al. 2013). Various ions are presented in physiological environment and the low crystallinity is affected by the presence of those ions into hydroxyapatite lattice (e.g. CO_3^{2-} , Na^+ , Mg^{2+} , SiO_4^{4-} and HPO_4^{2-}) and the typical ion substitutions are: F^- to Cl^- or OH^- position; carbonate for phosphate or OH^- position, while Sr^{2+} , Mg^{2+} and Na^+ for Ca^{2+} position (Yang et al. 2008; Wang & Nancollas 2009; Fernandez-Yague et al. 2015; Tampieri et al. 2011). CO_3^{2-} ions mainly substitute phosphate (B type position) and, in a lesser extent, OH^- ions (A type position). Particularly, B-type substitution is typical of young and immature bone; indeed B-carbonation enhances structural disorder in the mineral phase lattice and consequently increases its chemical reactivity and ability to be remodelled. In young bone, high amount of CO_3^{2-} ions in non-apatitic phase, more disordered domains is also presented, thus representing a reservoir of ions, which enhance the exchange with the extracellular matrix (Sprio et al. 2012; Tampieri et al. 2016). Nevertheless, the presence of ions in physiological conditions represented high importance on cells function, as well as, on bone healing and regeneration (Tampieri et al. 2011; Perez et al. 2015).

1.3 Biomimetic strategies applied on bone tissue engineering

Various devices have been investigated to help in the regeneration of bone tissue, such as scaffolds, microspheres and nanoparticles (Bao et al. 2013). Bone scaffolds are proposed 3D templates to repair critical size bone defects, whereas microspheres and nanoparticles have been applied as drug delivery systems, bone cements, bone fillers, among others (Wang et al. 2011; Wu et al. 2011; Lee & Yun 2014). Nevertheless, biomimetic concept uses bottom-up methodologies to fabricate scaffolds with compositions and pore network similar to the native tissues, by creating a suitable and efficient template able to mimic the characteristics of natural extracellular matrix, including biodegradability and mechanical properties, as well as to provide an appropriate design able to instruct cells to adhere, proliferate, differentiate and neo tissue genesis (Ma 2008; Perez et al. 2015; Pérez et al. 2013).

1.3.1 Scaffolds

In bone tissue engineering, biological, physical and chemical mechanisms of bone tissue were investigated in order to improve the healing or regeneration mechanism (Wu et al. 2014; Cui et al. 2007). The main challenge is to produce a functional scaffold (e.g. by combining biomaterials with cells, growth factors, drugs) able to regulate the healing process and to provide biomechanical support, during the new tissue formation (Fernandez-Yague et al. 2015). Bone scaffolds should exhibit: (i) **biocompatibility** (i.e. non-toxic); (ii) **biodegradability** (i.e. appropriated degradation rate with new tissue formation); (iii) **wide open and interconnected porosity** (with pore size $\geq 50\mu\text{m}$) (i.e. suitable for high surface-to-volume ratio for cells interactions) but maintaining (iv) adequate **mechanical properties**; (v) **osteoconductivity** (i.e. induction of osteoblasts cells, to adhesion, growth and differentiation); (vi) **osteoinductivity**, as well as (vii) easy to

produce, sterilize and handle (Engel et al. 2009). Scaffolds porosity favors the tissue ingrowth by guiding cells to proliferate and differentiate, transport nutrients and integrate with the host bone, as well as controlled degradation rate with osteogenic activity (Ma 2008; Amini et al. 2012; Wu et al. 2014). Equilibrium on physiological, chemical and mechanical properties are key aspects for cell behaviour, thus providing an appropriate framework for bone tissue regeneration (Saiz et al. 2013; Wu et al. 2014; Gil & Mano 2014).

Conventional and additive bio-manufacturing technologies were investigated to produce scaffolds with biocompatible biomaterials (e.g. polymers, ceramics, composites), with suitable porosity, pore interconnectivity and biomechanical properties (Bártolo et al. 2011; Amini et al. 2012). In conventional techniques (e.g. gas foaming, phase separation, freeze-drying) an improvement on scaffold porosity, heterogeneous pore shape and distribution were obtained by the use of porogens (Amini et al. 2012). Additionally, additive bio-fabrication was investigated to guarantee accurate, reproducible and customised scaffolds fabrication. Customised structures with defined size and porosity are created by computer-assisted design (CAD) software or acquired by DICOM data (e.g. from X-ray computed tomography) and printed by computer-assisted manufacturing (CAM). Tailored structures are 3D printed in a wide range of natural or synthetic biomaterials, while another interesting characteristic is to fabricate scaffold assembled with cells and signalling factors, thus creating more efficient scaffold, ready to be implanted (Bártolo et al. 2011).

Poly lactic acid (PLA), poly glycolic acid (PGA), ϵ -polycaprolactone (PCL) are examples of synthetic biopolymers approved by FDA and used by a wide range of technology and proposed in bone tissue engineering (Stevens 2008; Woodruff et al. 2012; Patrício et al. 2014; Engel et al. 2009). Several investigations were carried out on development of biomimetic scaffolds with appropriate properties to enhance cell adhesion, growth, migration and differentiation. For example, PLA was chemically modified with RGD motif (i.e. arginine-glycine-aspartic acid) and cell interaction with biomaterial was improved (Ma 2008). An alternative, is the use of natural derived polymers, such as collagen, glycosaminoglycans (GAGs), gelatin, as well as the use of drugs or growth factors, which enhances the cells activity.

Biomimetic scaffolds based on calcium phosphates were investigated to regenerate bone tissue due to similarity with bone composition and by adding foreign ions into calcium phosphate; degradation rate was controlled; mechanical strength and biological response were enhanced, thus osteogenesis and neovascularization were improved and might be used in bone tissue applications (Wang et al. 2016; Bose & Tarafder 2012; Perez et al. 2015).

Nevertheless, an improvement on physicochemical and biological properties of the scaffolds, in terms of porosity, mechanical properties, biodegradation and bioactivity was achieved by assembling microspheres or nanoparticles into the scaffold (Lee & Yun 2014).

1.3.2 Nanoparticles /Microbeads

Nano and microbeads were investigated as carriers of growth factors, drugs, biomolecules, among others (Solorio et al. 2013; Gu et al. 2013). The small size of nanoparticles yielding to specific biological entity or markers to be coupled at cellular (10 to 100 μ m), subcellular (20 to 250nm), protein (3 to 50 nm) or genetic

(10 to 100nm) scale (Wimpenny et al. 2012). On the other hand, nanoparticles offer the possibility to protect and carry the drug to a specific target. Poly-L-lysine, poly(d,l-lactide-co-glycolide) (PLGA), silica-based mesoporous, calcium phosphates are examples of materials used in nanoparticles production and proposed to be applied in various biomedical fields (Gu et al. 2013; Di Mauro et al. 2016).

Microspheres are defined as particles with spherical shape with diameter from 1-1000 μm and are mainly produced by emulsification process (i.e. single or double), polymerization, photopolymerization, phase separation/coacervation, spray drying and solvent extraction (Oliveira & Mano 2011; Solorio et al. 2013). During the production of microspheres, pore interconnectivity, surface topography, surface chemistry or particle size can be tailored to improve the microspheres functionality (Oliveira & Mano 2011; Solorio et al. 2013). Polymeric based microspheres are the most commonly used material as delivery of several growth factors, drugs and others (Oliveira & Mano 2011). Moreover, hybrid microspheres composed by collagen/hydroxyapatite, gelatin/hydroxyapatite, chitosan/hydroxyapatite, PLGA/hydroxyapatite have greatly showed their potential as growth factor encapsulation of basic fibroblast growth factor (bFGF) and bone morphogenic proteins. Gelatin/chitosan/hydroxyapatite microspheres presented high absorption and controlled delivery of lysozyme and gelatin/hydroxyapatite microspheres was showed as a suitable carrier of human osteoblast-like Saos-2 cells (Lee & Yun 2014).

1.3.3 Powerful properties of calcium phosphate and ions substitution

To mimic bone tissue architecture, composition and to activate the bone regenerative cascade are the main challenges in bone tissue engineering. Hydroxyapatite (HAp) was investigated as a promising biomaterial to substitute damaged bone tissue, due to high biocompatibility, bioactivity, non-toxicity and osteoinductive properties with lack of any immune responses (Boanini et al. 2010; Sprio et al. 2012), as provided by its high similarity with the inorganic part of bone tissue. Wet chemical precipitation, sol-gel synthesis, coprecipitation, hydrothermal synthesis, rapid or continuous precipitation from solution, thermal-decomplexing batch method, are some of the methodologies that have been successfully investigated for the production of synthetic hydroxyapatite (Vallet-Regi & Gonzalez-Calbet 2004; Dorozhkin 2009; Gomez-Morales et al. 2013; Delgado-López et al. 2012). On the other hand, ion substitutions in anionic or cationic positions in the hydroxyapatite lattice strongly improve biomimetic, biological and mechanical properties (Boanini et al. 2010; Sprio et al. 2012). Silicon (Si), strontium (Sr), magnesium (Mg), zinc (Zn) and iron (Fe) are relevant examples (Pon-On et al. 2013; Denry & Kuhn 2016). The use of magnesium doped apatite materials induces osteoblasts and osteoclasts activity, as well as enhanced bone metabolism. Biagini and co-workers showed that substituted HAp with magnesium enhances the solubility of the material at physiological pH, as well as improve adhesion, proliferation and metabolic activation of osteoblasts (Landi et al. 2006). The presence of silicon in calcium phosphates improves cartilage growth, osteoblasts cell activity, thus enhancing bone tissue remodelling and repair (Hing et al. 2006; Tampieri et al. 2012; Tampieri et al. 2016), while the presence of carbonate and strontium improves dissolution behaviour thus facilitating the implant resorption (Boer A., Urk H., Bouwstra J. 2012). Besides, mechanical performance was enhanced by the use of silicates (Vallet-

Regi & Gonzalez-Calbet 2004). Silver and gallium were instead investigated as antibacterial regulator and in the treatment of bone cancer, respectively (Perez et al. 2015).

1.3.4 Nature-inspired approaches

Taking inspiration from nature or by using nature sources are an emerging approach to develop new innovative biomaterials (Stevens 2008; Wegst et al. 2014). Alginate and chitin are two examples of materials that are extracted from nature sources, algae and crustaceans exoskeletons, respectively. Marine coral from *porites species* (Polo-Corrales et al. 2014; Nandi et al. 2015) sea urchins or wood (e.g. rattan, bamboo, palm) are natural sources with interesting properties, e.g. pore size, interconnected pores and high mechanical performance (Wegst et al. 2014). Moreover, by using chemical and physical processes, marine coral and wood can be transformed into suitable bone-like materials. For example, rattan wood showed promising properties to be transformed into biomimetic scaffold for load-bearing bones, due to their similarity with bone morphology (e.g. system of channel-like pores interconnected with smaller channels), presenting 85% of porosity and porous diameter around 240 μm . *In vitro* and *in vivo* tests showed MG63 osteoblasts-like cells viability with bone formation into scaffold channels and no inflammatory response after implantation into adult New Zealand White disease-free rabbits was observed (Sprio et al. 2010; Sprio et al. 2012).

1.3.4.1 Biomineralisation Process

The development of innovative and biomimetic biomaterials has been steadily increased. Particular focus is addressed to **biomineralisation process**, that is defined as a complex cascade of phenomena used by natural organisms to develop hybrid nano-structured materials, that works as endoskeleton (in mammals), exoskeleton (in insects and crustaceans), protective shell (in molluscs), and masticatory systems (i.e., the teeth in vertebrates) (B.- Sprio; et al. 2016; Skinner & Ehrlich 2014)

The formation of bone tissue is an example of biomineralisation process in humans; its translation to laboratory was pursued to develop innovative biomaterials with tailored chemical composition, nano/microstructure and architecture, in order to provide key signalling to cells for activation of the regenerative cascade (Wegst et al. 2014). Various investigations on *in vitro* mineralisation were carried out with non-collagenous proteins and collagen. For example, hydroxyapatite nucleation on polypeptides was improved by hydrophobic alkyl tails covalently bonded to thick hydrophilic peptide head groups with phosphorylated serine, while bone cells adhesion and chemotactic response was improved by adding RGD motifs to the biomaterials (Hartgerink et al. 2001; Stevens & George 2005; Tan et al. 2009). On the other hand, an innovative *in lab* synthesis was optimised to develop bone-like materials made of collagen type I mineralized with hydroxyapatite nanocrystals and was denominated as **Biomineralisation process**. Acidic natural type I collagen in form of nanofibrils was mineralised with hydroxyapatite nanocrystals by mediation of neutralisation process, while the content of additional ions (e.g. Mg^{2+} , Sr^{2+}) can be tailored. Therefore, the crystallization degree of hydroxyapatite nanocrystals can be controlled by the presence of foreign ions into HAp lattice (e.g. Mg^{2+}) (Ramírez-Rodríguez et al. 2016; Tampieri et al. 2016). During the biomineralisation

process, carbonate ions might occupy the phosphate site of hydroxyapatite lattice (B type position) and can be beneficial for cell adhesion and development of new bone tissue (Kon, Delcogliano, et al. 2010; Tampieri et al. 2011; Sprio et al. 2012). The presence of specific functional groups on collagen surface induces the crystal size and the specific orientation of apatite nuclei in respect to the collagen fibrils, thus bone-like properties in HAp/collagen hybrid composites were obtained. Scaffold composed of HAp/collagen composites with good interconnected porosity and adequate pore size was achieved by tailoring the freeze-drying process and biomechanical properties were stabilised by crosslinking methods (B.- Sprio; et al. 2016). Biomineralisation process can be considered as a new approach for the development of biomimetic biomaterials with outstanding properties; in particular, by varying the mineralisation extent, graded scaffolds for osteochondral applications or periodontal regions can be developed. By applying the as-mentioned methodology, a new bio-device with biomimetic properties was developed and investigated for osteochondral regeneration, named as MaioRegen (Finceramica, Italy). MaioRegen is a scaffold composed of 3 different layers and mimics the different zones of osteochondral region (i.e. cartilaginous tissue, tide-mark and subchondral bone structure). The potentiality of MaioRegen was proved by clinical studies, with progressive regeneration of osteo-cartilagineous defects (Finceramica, Italy) (A.- Sprio; et al. 2016). An innovative biomaterial without animal sources and composed by recombinant peptide based on human collagen type I (RCP) and enriched with RGD motif is commercially available as Cellnest® (Fujifilm Manufacturing Europe B.V. (The Netherlands)). Herein, the biomineralisation process was applied to produce RCP mineralized with iron doped hydroxyapatite (Fe-HA) and new devices with potentiality and outstanding properties for bone tissue applications were developed.

1.4 Smart strategies for advanced bone regenerative therapies

Smart biomaterials were designed to be sensitive and to deliver drugs in spatial, temporal and in dosage-controlled fashions. Drug release devices can be controlled by temperature, magnetic field, ultrasound intensity, light, electric pulses or by pH changing, enzyme concentration and / or redox gradients (Mura et al. 2013). The most common stimuli systems in *on demand* drug delivery are pH and temperature, (e.g. drug is released by stimulus from surrounding implantation environment) (Costa 2015).

For example, micro and nanoparticles can be labelled with drugs and introduced in a thermosensitive hydrogel composed of chitosan and β -glycerophosphate (Pérez et al. 2013; Zhu et al. 2015; Anil et al. 2015), while chemically modified gelatin microparticles were used as a pH-sensitive device (Pérez et al. 2013). On the other hand, nanoparticles are well known as a suitable tool in this field, due to their small size, large specific surface area, high drug loading efficiency and faster response to the surrounding environment (Walmsley et al. 2015).

Regards to the lacunae's on reconstruction of critical sized bone defects; the use of biomaterials combined with relevant growth factors can be a promising tool to induce bone healing. Human bone morphogenetic proteins (BMP-2) was approved by FDA and is one of the most studied growth factors in bone tissue engineering, due to its effect in bone healing, by induction of osteogenic differentiation of stem cells, thus

new bone tissue formation. The available BMP-2 carriers use supra-therapeutic doses and non-controlled release over the time often results in severe side effects (Davis et al. 2011; Kim et al. 2016). The scientific interest is therefore focused to innovative systems able to bind, deliver and to guarantee a controlled release of anabolic factors (Davis et al. 2011; Quinlan et al. 2015; Qiao et al. 2015). In particular it was found that mineralised biomaterials allow enhanced BMP-2 adsorption and also exhibit more hydrophilic surface compared with non-mineralised substrate, as well as enhancement of osteogenic response of human mesenchymal stem cells (Davis et al. 2011). A huge variety of biomaterials have been investigated as a suitable device for controlled BMP-2 deliver, although hydroxyapatite is one of the most investigated biomaterials to be applied on bone tissue regeneration, due to chemical bone-like composition, as well as high affinity to growth factors were described (Zhang et al. 2003; Huang et al. 2016; Iafisco et al. 2014; Sprio et al. 2012; Landi et al. 2006).

Nevertheless, new strategies on bone tissue engineering were purposed, as the application of magnetic assisted tissue engineering (Mag-TE) (e.g. cell labelling with magnetic particles) and magnetic biomaterials (Wimpenny et al. 2012; Santos et al. 2015).

1.5 Biocompatible magnetic materials: new approaches for bone tissue regeneration

Several devices are currently available on the market for bone tissue regeneration, but still there is some limitations, with particular respect to induction of cell differentiation and angiogenesis process. Therefore, a new focus in tissue engineering has been highlighted by the use of magnetic particles combined with magnetic fields that might be applied as a carrier of drugs, on cancer therapies and / or stimulation of bone tissue regeneration. Smart magnetic materials were also proposed, as an additional angiogenesis control *in vivo*. The highest advantage of this new concept is to control their activity by mean of an external magnetic field (EMF), and the bone regeneration process can be governed by switching the magnetization input provided by superparamagnetic features of biomaterials, thus boosting tissue regeneration *on demand*, which can be considered a revolutionary approach in medicine (Tampieri et al. 2011; Gil & Mano 2014; Sprio et al. 2012). Iron oxides are an example of those materials, while new bone-like biomaterials with superparamagnetic properties have been developed. Some authors have been investigated scaffolds functionalized with magnetic nanoparticles that increases scaffold stiffness and influence on cell adhesion (Tampieri et al. 2014; Gil & Mano 2014). Cells response to an external magnetic field depends on material surface, as well as a cross-talk between integrin-mediated signals from cells and soluble factors, thus promoting bone tissue regeneration (Xu et al. 2014). In figure 3, various examples of magnetic stimulation on cells behaviour were presented. By applying an external magnetic field the cell membrane is deformed and Rac and CDC42 was activated, as well as the signalling cascade events by p38/MAPK pathway, promoting actin cytoskeleton reorganisation, apoptosis, cytokine production and transcriptional regulation (Figure 3A). On the other hand, magnetic cells (i.e. cells labelled with magnetic nanoparticles (MNPs)) can be moved to a specific target by using external magnetic fields (Figure 3B). By combining external magnetic field with magnetic microspheres various cellular events can be activated, such as migration, survival, cell–

cell interaction and angiogenesis (Figure 3C) (Santos et al. 2015). Moreover, *on demand* release of drugs or growth factors from magnetic carriers can be tailored by applying external magnetic fields (Figure 3D, D1), as well as cells behaviour can be achieved by the exposition of singular magnetic nanoparticle and micromotions at the interface between cells and the scaffold might affect the ion channels in the cell membrane and trigger the mechanotransduction pathway (Figure 3D, D2) (Gil & Mano 2014).

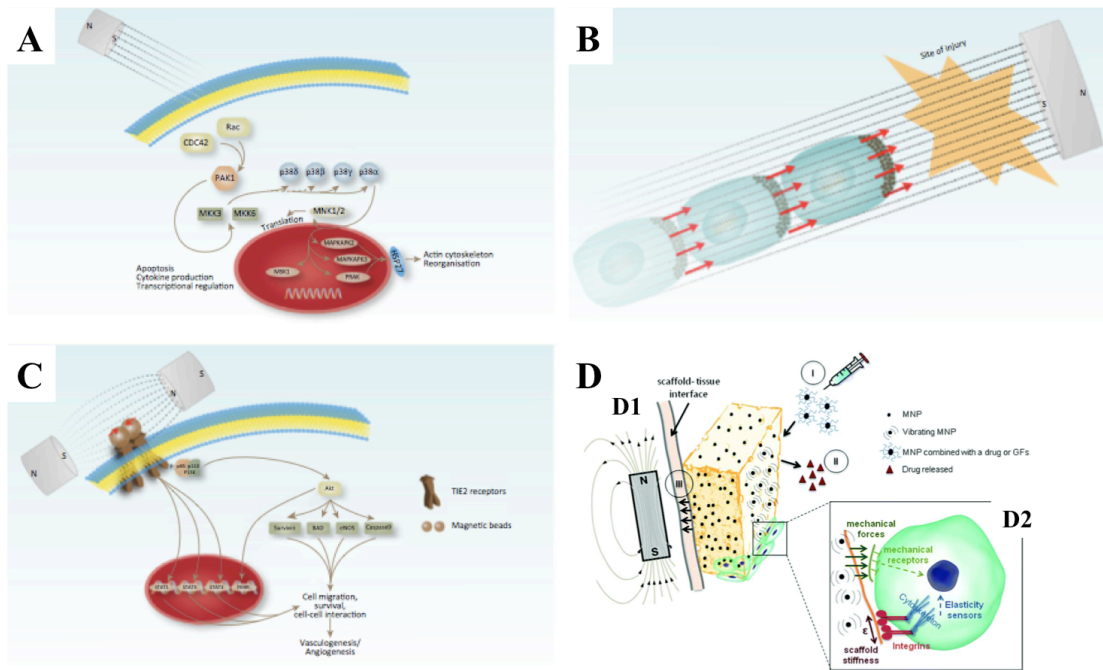


Figure 3. The use of magnetic nanoparticles in bone tissue regeneration. A) Effect of external magnetic field on cells surface; B) Magnetic cells; C) Interaction of magnetic beads with cells; D, D1) Effect of EMF and magnetic scaffold in tissue regeneration and magnetic stimulation on cell behaviour (D2) (Santos et al. 2015; Gil & Mano 2014).

The interest of superparamagnetic materials in medical application was increased and investigated as drug or cell targeting, magnetic resonance imaging (MRI), in the treatment of tumour, by conjugation with antibodies (e.g. tumour growth inhibition), hyperthermia and target therapy (Pankhurst; et al. 2003; Kumar & Mohammad 2011). Research work on magnetic nanoparticles (MNPs), MNPs labelled to cells, MNPs incorporated into the scaffolds, as well as some examples of use MNPs in drug delivery systems, cancer therapy (e.g. hyperthermia) and diagnostic and prognosis by magnetic resonance imaging, as well as the development of innovative magnetic materials (i.e. iron doped hydroxyapatite (Fe-HA)) are followed described (Mura et al. 2013; Singh et al. 2014).

1.5.1 Magnetic nanoparticles

The most common magnetic materials that have been assembled to the cells or to 3D templates are superparamagnetic iron oxide nanoparticles (SPIONS) (size range from 10 nm to 3.5 μm), regards to the

unique magnetic features (Wimpenny et al. 2012). Magnetite and maghemite are the most common SPIONS used in medical applications (Gil & Mano 2014). Excellent magnetic properties, good biocompatibility and low toxicity response, in presence of the cells prompt their use in tissue engineering (Wimpenny et al. 2012; Gil & Mano 2014). Magnetic properties are induced by external magnetic fields, while by removing the magnetic field the crystal-containing regions with disordered unpaired spins and non-magnetic materials are obtained, thus prevents particles aggregation (Gil & Mano 2014; LaConte et al. 2005).

Magnetic nanoparticles loaded with drugs or growth factors are guided to a specific target and dose release is controlled by external magnetic fields, thus improving the therapy efficacy (Chomoucka et al. 2010; Mura et al. 2013; Pankhurst; et al. 2003; Perez et al. 2015). Zhou and co-authors showed magnetic calcium phosphate nanoparticles with suitable properties for cancer therapy. Briefly, nanoparticles through biomineralisation of calcium phosphate on the surface of superparamagnetic iron oxide nanoparticles was synthesised and two types of particles were obtained. Doxorubicin (DOX·HCl) was loaded to the nanoparticles, and by using an external magnetic field an inhibition of tumour growth was observed. On the other hand, DNA was electrostatically compressed to the nanoparticles and by applying external magnetic field high transfection efficiency in A549 (adenocarcinomic human alveolar basal epithelial cells) and HepG2 (human liver carcinoma cell line) cells, was showed (Tang et al. 2014).

In cancer treatment, the potential of hyperthermia on “killing” cancer cells by increasing the temperature, without negative effect on the surrounding healthy cells was successfully investigated (Pankhurst; et al. 2003; Perez et al. 2015). The heating mechanism in superparamagnetic particles is explained by Brown relaxation (i.e. heat effect stimulated by friction arising from total particle oscillations) and Néel relaxation (i.e. heat is mediated by the rotation of the magnetic moment with each field oscillation) (Kumar & Mohammad 2011). An increase of temperature (40 °C – 46 °C) changes the physiology of malignant cells leading to apoptosis, whereas temperatures higher than 46 °C promote necrosis (Silva et al. 2012). This heating phenomenon is improved by the use of an alternating external magnetic field, due to the high Brownian and Neel fluctuation (Singh et al. 2014). Moreover, the use of lower temperature ($T < 41^{\circ}\text{C}$) was investigated in the treatment of rheumatic diseases (Silva et al. 2012). SPIONs coated with growth factors, drugs, RGD peptides, can be a promising tool on bone tissue engineering, but still further investigations must be implemented.

1.5.2 Magnetic cells

The importance of magnetic-mechano actuation in stem cells differentiation, as well as the combination of magnetic functionalisation nanoparticles with osteogenic medium, cyclic magneto-mechanical stimulation and bone morphogenic protein, as a suitable tool for bone biomineralisation has been investigated (Santos et al. 2015; Gil & Mano 2014). It is well known that cells behaviour is affected by physical properties and chemical/ biochemical topography surface of scaffolds, as well as by mechanical stimulation. Regarding to the importance of mechanical stimulation in cells behaviour, MNPs labelled to the cells was investigated and an improvement on cells activity and functional tissue was formed (Gil & Mano 2014; Santos et al. 2015).

The most studied methodologies to produce magnetic cells were described as i) labelling magnetic particles in cells surface integrin or ii) by internalization of MNPs into the cells by using fluid phase endocytosis, receptor-mediated endocytosis or phagocytosis (Gupta & Gupta 2005). By combining magnetic cells with external magnetic fields allowed to conduct the cells to a specific target and to control the delivery of biomolecules, drugs or growth factors; and is non-toxic and do not affect cell differentiation, proliferation, metabolic expression profile, reactive oxygen species formation and apoptosis rate (Wimpenny et al. 2012; Silva et al. 2012; Santos et al. 2015). Magnetite cationic liposomes were electrostatically interacted with human mesenchymal stem cells (hMSCs) and *in vitro* magnetic stimulation was assessed for sheet formation. This tissue was implanted into a cranial defect of F344 nude rats and after 14 days of implantation, significant bone was formed (Shimizu et al. 2007). El Haj group's investigated the interaction of SPIONs with osteoblasts surface (in RGD receptors) and after 3 weeks an upregulation of osteopontin was showed (Wimpenny et al. 2012).

1.5.3 Magnetic scaffolds

Another strategy in bone tissue engineering is the use of magnetic scaffolds, by adding magnetic particles into the scaffold and combined with low-frequency pulsed electromagnetic fields, thus stimulation in bone regeneration was observed (Bock et al. 2010; Tampieri et al. 2014). SPIONs are the most common magnetic particles introduced into the scaffolds and were investigated into ceramic scaffolds (Panseri et al. 2013; Panseri et al. 2012), polymeric scaffolds (Mertens et al. 2014; Lopez-Lopez et al. 2015) or composite scaffolds (e.g. collagen/HAp, chitosan/HAp, among others) (Heidari et al. 2015). Various strategies were used to produce magnetic scaffolds, as by immersing in ferrofluids, incorporation of magnetic nanoparticles or magnetic cells into the scaffolds, among others (Bock et al. 2010). By applying an external magnetic field to superparamagnetic scaffolds the cells activity was enhanced by the compressive or tensile forces produced between nanoparticles and magnetic field (Gil & Mano 2014). In other words, the activation of magnetic field leads to switch on the single magnetic domain from MNPs, promoting an interaction between cells and scaffold, which might influence mechanotransduction pathway (i.e. cells translate physical stimuli into biochemical activity) (Gil & Mano 2014; Santos et al. 2015).

Magnetic scaffolds response to an on/off demand by applying a magnetic field, highlighting their potential compared to the conventional ones. In one hand, the use of magnetic particles into the scaffolds improves cell adhesion, proliferation and differentiation by applying an external magnetic field, due to bone tissue capacity to identify the mechano-electrical conversion leading to improve cellular and metabolic activity, respect to bone differentiation (Singh et al. 2014). On the other hand, magnetic particles into the scaffolds were investigated as a non-invasively assess *in vivo* follow-up and monitor scaffold resorption by magnetic resonance imaging (MRI), leading to therapeutic and diagnostic application (Mertens et al. 2014; Skaat et al. 2012; Perez et al. 2015). Take into account bone tissue composition, a porous scaffold composed by integrated superparamagnetic nanoparticles into HAp and HAp/tricalcium phosphate, were fabricated and were studied in the presence of Ros17/2.8 and MG63 cells, good biocompatibility, cell proliferation and

differentiation was showed. *In vivo* test accelerated BMP-2 expression and new bone-like tissue was formed (Wu et al. 2011). HAp/ collagen composite by direct incorporation of magnetic nanoparticles during HAp nucleation was investigated as a new concept to produce magnetic scaffolds. Cells are activated close to the scaffold and magnetization about 0.5 emu/g was obtained after applying an external magnetic field (Tampieri et al. 2011).

As previously was described, one of TE strategies is to develop 3D complex systems with differentiated and proliferated cells into the scaffolds. Therefore this strategy can leads to a non-homogeneous cell distribution into the scaffold. One possible approach to overcome this drawback is the use of magnetic cells, which by magnetic forces enhance cells distribution into the scaffold structure (Skaat et al. 2012). Homogeneous internationalization and differentiation of magnetic cells into the scaffolds was improved by applying an external magnetic field and it efficiency was monitorised by MRI (Santos et al. 2015; Skaat et al. 2012; Sensenig et al. 2012). Nevertheless, polymeric scaffolds were investigated as a support for magnetic growth factors and suitable 3D framework for cell growth and proliferation was achieved (Skaat et al. 2012).

M. Marcacci and co-authors, showed the potential of *in vivo* magnetic fixation in HAp/collagen magnetic scaffolds and controlled tissue regeneration was showed. As complementary technique, computational stimulation was investigated as a suitable tool to predict scaffolds movements (Panseri et al. 2013; Russo et al. 2012).

In table 1, various examples of proposed magnetic devices to be applied in bone tissue engineering are summarized.

Table 1. Examples of magnetic scaffolds investigated for bone tissue engineering.

Material	Template	Study	Cells/ Animal model	Saturation Magnetization (emu/g)	Remarks	Ref.
CaP coated γ - Fe ₂ O ₃ – BSA CaP coated γ - Fe ₂ O ₃ – CA	Nanoparticles	<i>In vitro</i>	Human osteoblasts	3.47 – 33.58	CaP coated γ - Fe ₂ O ₃ – BSA: high osteoblasts density.	(Pareta et al. 2008)
SPIONs + DXM co-encapsulate in PLGA	Microspheres (1 - 10 μ m)	<i>In vitro</i>	Human synovial fibroblasts	Data not showed	Excellent biocompatibility; Particles internalized through phagocytic process; Do not induce any inflammatory reaction.	(Butoescu et al. 2009)

HAp/collagen (70:30 w/w) immersed in commercial ferrofluids	Porous scaffolds obtained by freeze-dried	<i>In vitro</i>	hBMSC	13-15	Preliminary results: scaffolds are able to support cell adhesion and proliferation <i>in vitro</i> .	(Bock et al. 2010)
γ -Fe ₂ O ₃ MNP, HAp in PLA nanofibers	Nanofibers produced by electrospinning	<i>In vitro</i>	MC3T3-E1	0.0492	High osteoblasts cells proliferation and differentiation, compared to the control ones. Degradation rate of material complement by new bone formation → Applied SMF accelerated tissue repair; Good compatibility.	(Meng et al. 2010) (Meng et al. 2013)
Fe5% -MBG & Fe10%-MGB (MGB – polymer P123 & polyurethane sponges)	Porous scaffolds calcined at 700°C	<i>In vitro</i>	BMSC	5% ≈ 1 10% ≈ 0.2	MNPs - Enhances the mitochondrial activity and gene expression; Maintain sustained drug delivery.	(Wu et al. 2011)
MNP (2, 1 & 0.5%) in discs of HAp	Porous discs immersed in colloid solution of MNP	<i>In vitro</i>	ROS 17/2.8 MC3T3-E1	2% - 0.94 1% - 0.53 0.5% - 0.24	MNP - Stimulated cell adhesion, proliferation, and differentiation by itself; MNP with SMF – enhanced cell proliferation and differentiation.	(Zeng et al. 2012)
HAp/collagen (70/30 wt%) with nucleated 4wt% MNP & HAp/collagen	Porous scaffolds obtained by freeze-dried	<i>In vivo</i>	Male rabbits	Data not showed	Histopathological screening: no inflammatory reaction due to MNPs;	(Panseri et al. 2013)

(70/30 wt%) immersed in ferrofluid						Higher bone healing rate in scaffold nucleated with MNPs.
Bioactive glasses + MNPs + SBF biomineralisation	Scaffolds produced by Salt-leaching techniques (calcined during different timings)	<i>In vitro</i>	HeLa	50': 6.78 70': 3.72 90': 3.19 110': 1.96		Good biocompatibility and cell adherence ability. (Wang et al. 2013)
PCL + MNPs	Nanofibrous produced by electrospun	<i>In vitro</i> <i>In vivo</i>	Osteoblasts Male Sprague- Dawley Rats	1.0 -11.2		<i>In vitro</i> : improve cell adhesion; <i>In vivo</i> : Significant bone formation. (Singh et al. 2014)

1.5.4 Novel biocompatible magnetic nanoparticles: Fe-HA

Some authors defend that magnetite nanoparticles present low stability (Marques et al. 2014; Hoffman-Antenbrink et al. 2009) and tends to aggregate due to strong magnetic dipole-dipole attractions; to avoid that and to improve colloidal dispersion and biocompatibility; the surface charge, surface topography and biocompatibility were modified by surface coating with hydrophilic polymers (e.g. dextran, chitosan, etc. ...) (Chomoucka et al. 2010) or with bovine serum albumin, siloxanes and citric acid (Pareta et al. 2008; Marques et al. 2014).

Nevertheless, a new concept to produce bioactive and bioresorbable biomimetic materials with intrinsic magnetization was investigated. HAp is a biocompatible, bioactive and bioresorbable material and their crystal structure, allows the incorporation of different ions, such as iron sources to create iron-doped apatite (Fe-HA) with superparamagnetic properties (Sprio et al. 2012). Briefly, by adding simultaneously Fe²⁺ and Fe³⁺ ions, during the neutralization process of HAp, Ca²⁺ ions are partially substituted by iron ions into HAp lattice and material with superparamagnetic features is produced. The improvement of magnetic properties can be induced by the formation of minimal amounts of magnetite or maghemite (Tampieri et al. 2011; Tampieri et al. 2012; Panseri et al. 2012; Sprio et al. 2012; Sprio et al. 2010). Fe-HA showed bone-like composition and *in vitro* and *in vivo* tests indicated any cytotoxic effect in presence of rabbit osteoblasts cells after 24h of cell seeding, as well as biocompatible properties were showed with pilot rabbit investigations (Sprio et al. 2010; Panseri et al. 2012). On the other hand, different concentrations of Fe-HA material were tested in presence of Saos-2 human osteoblast-like cells without or under external magnetic field, during 7 days. An improvement on cell activity in presence of static external magnetic field was observed, as well as, good biocompatibility from Fe-HA was obtained after 4 weeks implanted into critical size lesion of rabbit condyle (Panseri et al. 2012), while osteogenic differentiation of human mesenchymal stem cells was

obtained in presence of material composed by Fe-HA and PCL (Gloria et al. 2013).

Fe-HA presented bone-like composition with nanocrystalline hydroxyapatite, cytocompatible, biocompatible, osteoinductive, osteoconductive, bioactivity and prompt their future use in biomedical applications as suitable tool for theranostic, drug delivery, heat mediator for hyperthermia treatment, contrast agent for magnetic resonance imaging or as magnetic nanocarriers, as a possible substitution of commercial iron oxide nanoparticles (Tampieri et al. 2011; Tampieri et al. 2012; Tampieri et al. 2016; Kaygili et al. 2014; Kramer et al. 2013; Panseri et al. 2012; Sprio et al. 2010)

Furthermore, by using a bio-inspired assembling/mineralization process (as previously reported as **biomineralisation process**), which mimics the cascade phenomena occurring *in vivo* during new bone tissue formation, heterogeneous nucleation of Fe-HA onto collagen type I matrix, was successfully achieved (Tampieri et al. 2003; Tampieri et al. 2008; Tampieri et al. 2014). This process activates various physicochemical and morphological mechanisms that constrain the inorganic phase to nucleate in specific *loci* of collagen macromolecule, and limit the crystal growth to few nanometres with very low crystal ordering and specific orientation, similarly as occurring in the newly formed bone (Tampieri et al. 2008; Sprio et al. 2012). As a result of the above mentioned approach, the obtained hybrid construct exhibited high compositional and structural mimicry of bone tissue with excellent biocompatibility, osteogenic ability and intrinsic superparamagnetic properties enabling remote activation by magnetic signalling (Tampieri et al. 2014). This approach opens the new proposed therapies boosting tissue regeneration in the patients with reduced endogenous regenerative potential (Higashi et al. 1993; Kotani et al. 2002; Xu & Gu 2014). The ability of natural polymers such as collagen to expose negatively charged functional groups enabling the link of Ca^{2+} ions and subsequent heterogeneous nucleation of apatite nanophases, opens to the development of hybrid biomimetic materials with tailored mineralization extent by using various macromolecular matrices and could be tailored from cartilage to bone-like level (Tampieri et al. 2008). The bone-like and magnetic properties promote the ability to be used in bone tissue regeneration and be activated by external magnetic field that can be promising on boost regeneration of extended bone or osteochondral regions (A.- Sprio; et al. 2016; Tampieri et al. 2014; Gil & Mano 2014).

1.6 Brief idea on regulatory guidelines and scaffold commercialization

New innovative strategies have been investigated and proposed to develop novel devices for bone tissue regeneration, but still exhaustive bureaucracy processes have been applied in the commercialization of those devices (Pashuck & Stevens 2012; Mehta; 2008). In the book entitled “Biomaterials in the Design and Reliability of Medical Devices, 2002” edited by Michael N. Helmus, the main procedures to commercialize biomaterials and templates, for the different parts of the human body was showed. On the other hand, in the book entitled “Principles of tissue engineering, 3rd ed”, mainly in the chapters three and eighty-five, translate the key points on scaffolds commercialization (Russell & Bertram 2011; Hellman 2011).

Prior to scaffolds implantation a wide range of protocols have been followed and to pass from research bench to clinical testing is important to point: i) the characterisation and evaluation of the raw materials (i.e. cells

and scaffold), ii) the manufacturing process (i.e. cellular processing and testing of biomaterial process, as well as interplay between cells and scaffolds) and then the actions related to iii) translational medicine (i.e. potentiality of the product in small or large animals). An exhaustive screening of *in vitro* and *in vivo* assays to test device-like products is available in ISO10993-1 (approved by FDA). The risk : benefit of new biomaterials must be compared to the materials available in the market, in terms of results reproducibility *in vitro* and *in vivo* that is fundamental in the decisions for human trials.

In figure 4, a general pathway from lab to commercialization of devices was presented. The first step includes the lab research with special focus on research target (e.g. bone tissue, biological and biomechanical mechanisms of bone tissue) and the development of new approaches with cells and scaffolds. Followed by *in vitro* and *in vivo* studies, under regulatory guidelines (e.g. Centre for Devices and Radiological Health (CDRH) and Center for Biologics Evaluation and Research (CBER) from FDA departments that are responsible in the validation of biomaterials and cells, as a support for tissue regeneration). Then, new regulatory guidelines are applied in the clinical studies with humans, followed by business strategies and product commercialization. Actually, it is expected that tissue engineering strategies will bring to the market new devices in 8-10 years. An emerging knowledge from tissue engineering and regenerative medicine will bring new customized solutions to the patients (Russell & Bertram 2011).

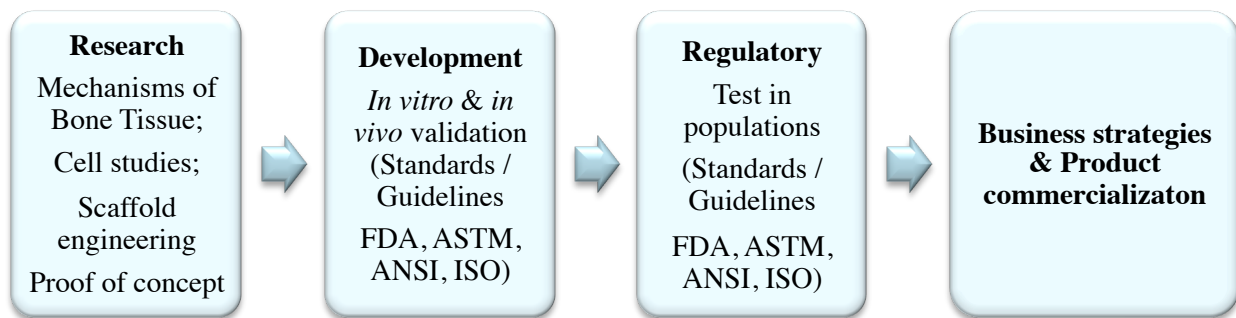


Figure 4. Step from research bench to scaffold commercialization.

Chapter 2. Materials and Methods

2.1 Application of biomineralisation process to obtain new hybrid biomaterials with superparamagnetic properties

2.1.1 Raw materials

RCP, commercially available as Cellnest™, is characterised by molecular weight of 51.7 kDa and isoelectric point of ≈ 10.02 , and was provided by Fujifilm Manufacturing Europe B.V. (The Netherlands). Calcium Hydroxide ($\text{Ca}(\text{OH})_2$, 95%), Phosphoric Acid (H_3PO_4 , 85 wt%), Iron(II) chloride tetrahydrate ($\text{FeCl}_2 \cdot 4\text{H}_2\text{O}$, 99%) and Iron(III) chloride hexahydrate ($\text{FeCl}_3 \cdot 6\text{H}_2\text{O}$) were purchased from Sigma Aldrich (U.S.A.), while nitric acid (HNO_3 , 65%) was purchased from Titolchimica (Italy). Ultrapure water (0.22 mS, 25 °C) was used in all the experiments.

2.1.2 Biomineralisation Process

Biomineralisation process was carried out in presence of Fe^{2+} and Fe^{3+} ions, with the purpose to provide ion substitution in apatite during the neutralization process. Firstly, RCP was dissolved in aqueous environment thermostated at 40 °C during stirring for 40 minutes and then RCP solution was added to an aqueous solution of H_3PO_4 and dropwise into a basic aqueous suspension of $\text{Ca}(\text{OH})_2$ containing $\text{FeCl}_2 \cdot 4\text{H}_2\text{O}$ and $\text{FeCl}_3 \cdot 6\text{H}_2\text{O}$ as sources of Fe^{2+} and Fe^{3+} ions, under constant heating and stirring, for two hours (Figure 5). All the obtained materials were freeze-dried (≈ 0.1 bar) for further physico-chemical characterisation. All the as-used solutions were varied take into account the used $\text{Fe}^{2+}/\text{Fe}^{3+}$ molar ratio, Fe/Ca molar ratio and organic and inorganic ratio, but keeping the Ca/P molar ratio (1.67).

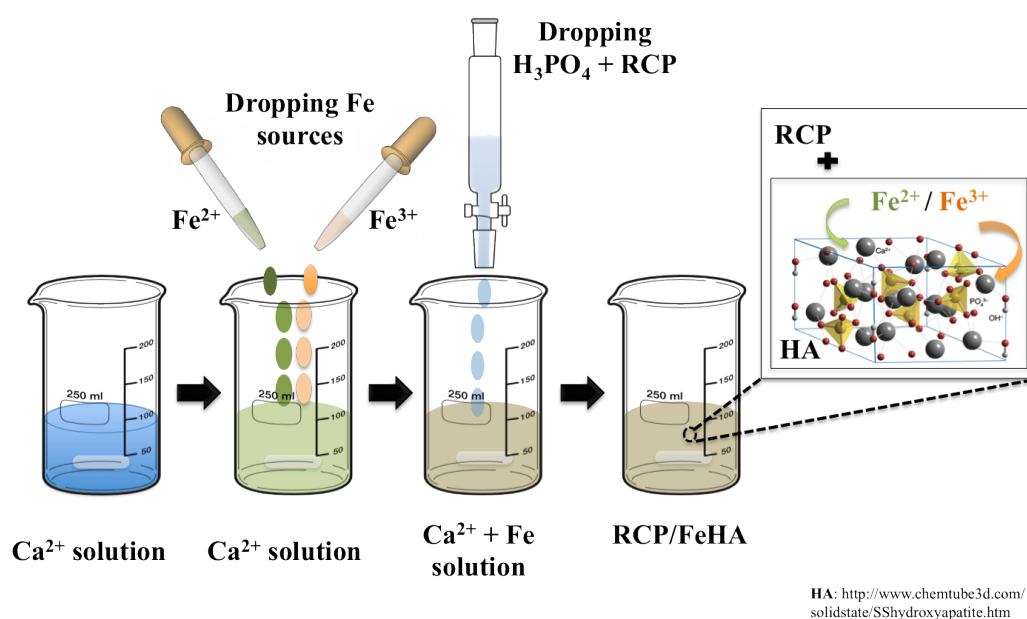


Figure 5. Schematic design of biomineralisation process.

2.1.3 Morphological, chemical, thermal and magnetic characterisation

Size distribution of RCP was evaluated by dynamic light scattering (DLS, Zetasizer Nano Series, Malvern, UK) and was measured by backscatter detection ($\lambda = 630 \text{ nm}$, $\theta = 173^\circ$).

The infrared spectra were collected in the wavelength range from 400 to 4000 cm^{-1} , using KBr pellet technique with 2 cm^{-1} of resolution. The sample ($\sim 2 \text{ mg}$) was mixed with $\sim 150 \text{ mg}$ of anhydrous KBr and the powder pressed at 8000 psi into 7 mm diameter discs. The crystallinity index was measured by evaluating the ratio: $(I_{603} + I_{563}) / I_{588}$, where I is the intensity of the IR band recorded at the wavelength identified by the subscript (Surovell & Stiner 2001) (Weiner & Bar-Yosef 1990).

The phase composition was determined by X-ray powder diffraction (XRD), performed by a D8 Advance Diffractometer (Bruker, Karlsruhe, Germany) using Cu-K α radiation at 40kV and 40mA . XRD spectra were recorded in the 2θ range $10\text{--}80^\circ$, with a step size of 0.02° and a counting time of 0.5s . The Inductively coupled plasma optical emission spectrometry (ICP OES; Liberty200, Varian, Clayton South, Australia) was performed to determine the overall content of calcium (Ca), phosphorus (P) and iron (Fe) into the mineral phase of the different samples. Each type of material were prepared in triplicate by dissolving 20 mg of powder in 2 mL of HNO_3 ($65 \text{ wt}\%$) and the volume of the solution was raised to 100 mL by adding deionized water and further analysed by ICP-OES. Predetermined concentrations of Ca, P, Fe elements were also prepared and used as standard calibration. Thermogravimetric analysis (STA 449C) was carried out to explore the thermal behaviour of the composites and to assess the amount of mineral phase. 10 mg of sample was placed into an alumina crucible and the experiment was conducted in air flux with heating ramp from 30°C to 1100°C and heating rate of $10^\circ\text{C}/\text{min}$. A susceptometer balance YSZ 01C/02C (Sartorius Mechatronics, Italy) was used to evaluate the magnetisation of pelletized materials under a field of 2700 A/m at a distance of 18 mm .

2.2 New bioactive bone-like microspheres with intrinsic magnetic properties obtained by bio-inspired mineralisation process

2.2.1 Raw materials

RCP was kindly provided by Fujifilm Manufacturing Europe B.V. (The Netherlands). Calcium hydroxide ($\text{Ca}(\text{OH})_2$, $\geq 95\%$), phosphoric acid (H_3PO_4 , 85%), iron(II) chloride tetrahydrate ($\text{FeCl}_2 \cdot 4\text{H}_2\text{O}$, $\geq 99\%$), iron(III) chloride hexahydrate ($\text{FeCl}_3 \cdot 6\text{H}_2\text{O}$, 97%), sodium hydroxide (NaOH , $\geq 98\%$), 1,10-phenantroline ($\text{C}_{12}\text{H}_8\text{N}_2$, $\geq 99\%$), sulphuric acid (H_2SO_4 , 99.999%), corn oil, acetone ($\geq 99.9\%$), potassium bromide (KBr , $\geq 99\%$), phosphate buffered saline (PBS), dimethyl sulfoxide ($(\text{CH}_3)_2\text{SO}$, $\geq 99.9\%$), ethanol ($\approx 96\%$ (v/v)), were all obtained by Sigma Aldrich (St Louis, MO, USA), whereas nitric acid (HNO_3 , 65%) was purchased from Titolchimica (Italy). α MEM w/o ascorbic acid, fetal bovine serum (FBS) and penicillin-streptomycin were purchased from Thermo Fisher Scientific (Waltham, MA, USA). 3-(4,5-dimethylthiazol-2-yl)-2,5-diphenyltetrazolium bromide (MTT), calcein acetoxymethyl (calcein AM) and ethidium homodimer-1 (EthD-1) were purchased from Invitrogen (Carlsbad, CA, USA). Ultrapure water (0.22 mS, 25 °C) was used in all the experiments.

2.2.2 Reaction of RCP with calcium and iron ions

The as-used divalent and trivalent ions (i.e. Ca^{2+} , Fe^{2+} and Fe^{3+}) in biomineralisation process were separately bound to RCP in aqueous media. Those reactions were prepared as a reference to be compared with biomineralised materials and to evaluate the involved chemical interactions. The amount of ions dispersed in the solution was defined on the basis of a 1:1 molar ratio with the free carboxylic groups available in the RCP matrix, which are derived from aspartic and glutamic acid (1 mol of RCP corresponds to 57 acids) (Bouwstra J., Sutter M., Kluijtmans S., Hennink W. 2010; Boer A., Urk H., Bouwstra J. 2012).

Firstly, 15.5 mg of $\text{Ca}(\text{OH})_2$ was dispersed in 2 mL of deionized water at room temperature and 200 mg of RCP was dissolved in deionized water, in separated reaction vessel, at thermostated environment (i.e. 40°C). Calcium solution was dropped into RCP solution under vigorous magnetic stirring and continuously mixed at room temperature for 30 minutes to obtain a solution henceforth coded as RCP/Ca.

Similar procedures were carried out to link Fe^{2+} and Fe^{3+} ions to RCP. Two solutions were prepared by dissolving 43 mg of $\text{FeCl}_2 \cdot 4\text{H}_2\text{O}$ and 29 mg of $\text{FeCl}_3 \cdot 6\text{H}_2\text{O}$ in 2 ml of deionized water and dropped in two reaction vessels containing the RCP solution, thus obtaining final materials henceforth coded as RCP/Fe2 and RCP/Fe3, respectively.

On the other hand, new reactions of RCP/Fe2 and RCP/Fe3 were performed and 0.1 M of NaOH was dropped to achieve the conditions of apatite crystallization (as obtained in the biomineralisation process), then the mixture was homogenized for 30 minutes. In all the as-mentioned reactions the final RCP concentration was 5 wt%. The resulting materials were freeze-dried at -40 °C under vacuum (≈ 0.1 bar) overnight, for future investigations.

2.2.3 Synthesis of hybrid mineralised materials

Mineralised materials were synthesised by heterogeneous nucleation of Fe-doped hydroxyapatite on RCP matrix, by following the method showed in the section 2.1.2. However, slightly modification in the amount of reactants was performed. Briefly, an aqueous solution of RCP (0.003 M) was prepared and thermostated at 40°C. An acid solution of H₃PO₄ (1.2 M) was prepared and dropped in the RCP solution, then poured dropwise into a basic aqueous suspension of Ca(OH)₂ (0.8 M) also containing FeCl₂·4H₂O and FeCl₃·6H₂O as sources of Fe²⁺ and Fe³⁺ ions, to establish a Fe²⁺/Fe³⁺ molar ratio of 3:2. The process was carried out at a fixed temperature and under magnetic stirring, to achieve a nominal mineralization extent equal to 40 wt%. The overall ion content was set to achieve Ca/P_{mol} = 1.67 and Fe/Ca_{mol} = 0.2 and the synthesis of materials were carried out at two different synthesis temperatures (i.e. 40 °C and 60 °C) (Figure 5). The as-obtained materials are henceforth coded as RCPFeHA40 and RCPFeHA60, respectively.

Iron-free mineralised materials were synthesised at the same temperature conditions (i.e. 40°C or 60°C) and were used as a control in the chemical-physical characterisation, henceforth coded as RCPHA40 and RCPHA60, respectively.

By the end, the as-obtained hybrid mineralised slurries were used to produce the microspheres by the emulsification process, as described in the section 2.2.4, or to be freeze-dried at -40 °C under vacuum (≈ 0.1 bar) overnight, for further physicochemical investigations.

2.2.4 Production of microspheres by emulsification method

A water-in-oil emulsification process was established, to produce pure RCP and hybrid magnetic microspheres, starting from the previously obtained hybrid mineralised slurries (i.e. RCPFeHA40 and RCPFeHA60).

The emulsification process comprises three different stages, i.e. i) microspheres production in pre-warmed oil; ii) microspheres jellification and iii) oil phase washing. In detail, 20 g of hybrid mineralised slurry was dropped in 45 g of pre-warmed corn oil and kept under mechanical stirring for 20 minutes. The solution was cooled, until microspheres jellification, and dropped into a 300 mL of chilled acetone and kept under mechanical stirring for 5 minutes, then maintained for 1 hour at room temperature, under mechanical stirring. The microspheres were left to sediment and acetone was carefully removed, then 300 mL of clean acetone was added and the microspheres were washed for 10 minutes. This step was repeated twice. The microspheres were filtered, dried overnight in an oven at 40 °C, and sieved to achieve a size distribution in the range 38 to 100 μm (Figure 6). For pure RCP microspheres, predetermined concentrated aqueous solution of RCP (≈ 5 – 36 wt%) was prepared and microspheres were obtained by the aforementioned method. DHT treatment was carried out by placing the dried microspheres in glass vials covered with aluminium foil and heated at 160 °C for 48 hours under vacuum.

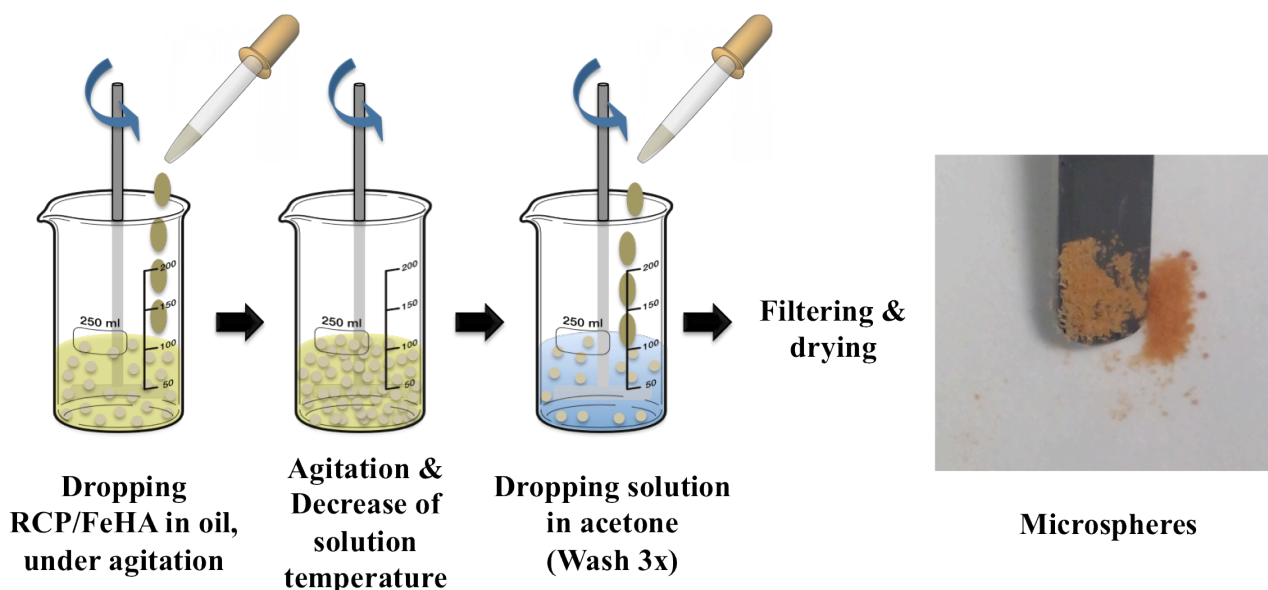


Figure 6. Schematic design of emulsification process.

2.2.5 Physicochemical, morphological and magnetic characterisation

The detailed protocols to perform FTIR, XRD and TGA analysis were showed in the section 2.1.3.

The identification of functional groups of pure RCP and hybrid mineralised materials was made by Fourier Transform Infrared Spectroscopy (FTIR) (Avatar 320 FT-IR, Thermo Nicolet, Canada).

The phase composition of the mineralised materials was obtained by X-ray powder diffraction (XRD, D8 Advance, Bruker, Karlsruhe, Germany). Crystallographic data were then obtained by full profile refinement of the XRD pattern (TOPAS 5, Bruker, Germany).

The overall content of calcium (Ca), phosphorus (P) and iron (Fe) was determined by inductively coupled plasma optical emission spectrometry (ICP-OES; Liberty200, Varian, Clayton South, Australia).

A calorimetric assay with orthophenanthroline was used to determine the amount of Fe^{2+} ions, by means of formation of a stable red-orange Fe (II) orthophenanthroline complex $[(\text{C}_{12}\text{H}_8\text{N}_2)_3\text{Fe}]^{2+}$ in the pH range 4-5 to be detected by UV-Visible spectrophotometry (Lambda 35 UV/VIS Spectrometer; Perkin Elmer Instrument, USA) at 510 nm (Murti et al. 1970; Tampieri et al. 2012). Buffer solution (pH=4), 0.2 % of 1,10-phenanthroline solution and 3M H_2SO_4 was previously prepared. 4 mg of RCPFeHA40 and RCPFeHA60 were separately dissolved in 10 mL of deionized water with 0.1 mL of 3M H_2SO_4 . The final solution to be investigated by UV-vis was: 500 μL of RCPFeHA40 or RCPFeHA60 solution, 500 μL of buffer solution (pH=4), 500 μL of 0.2 % of 1,10-phenanthroline solution and deionized water to the final volume of 5 mL. The concentration of Fe^{2+} was calculated by using a calibration curve obtained by 0.02 mg/ml of $\text{FeCl}_2 \cdot 4\text{H}_2\text{O}$. The Fe^{3+} amount was calculated by the difference between the total iron amount (as obtained by ICP-OES analysis) and the Fe^{2+} amount (as obtained by the calorimetric assay).

Simultaneous thermogravimetric (TGA) analysis (STA 449/C Jupiter, Netzsch, Germany) was carried out to explore the thermal behaviour of RCP and mineralised materials, particularly to assess the amount of the mineral phase in the final obtained materials.

A susceptometer balance YSZ 01C/02C (Sartorius Mechatronics, Italy) was used to evaluate the magnetisation of pelletized materials under a field of 2700 A/m at a distance of 18 mm. The obtained magnetisation was normalised by the mineral phase amount, obtained by TGA analysis. Deeper investigation was carried out by using a vibrating sample magnetometer (VSM) Lakeshore 735, in the range from -15 kOe to 15 kOe. A predetermined amount of sample was loaded into the sample holder and the experiments were carried out at room temperature. The results are presented with uncertainty of about $\pm 2\%$. The potential of magnetic microspheres to be controlled in wet conditions was evaluated by using a neodymium magnet (1.2 T).

The morphology of the microspheres was analysed by using Scanning Electron Microscope (SEM) (FEI Quanta 600, USA) in low vacuum mode with an accelerating voltage of 10 kV and a working distance of 10 mm. The effect of the incorporation of iron ions and the synthesis temperature on the morphology and ultrastructure of the nucleated hydroxyapatite nanocrystals was examined by using transmission electron microscopy (TEM: FEI Tecnai F20 microscope, USA), using an accelerating voltage of 120 kV. Energy dispersive X-ray analysis (EDX) was carried out to detect the presence of iron in the hydroxyapatite nanocrystals. For TEM investigations, the as-obtained mineralised slurries by biomineralisation process were washed three times with deionized water to remove the organic phase and freeze dried at $-40\text{ }^{\circ}\text{C}$ under vacuum (≈ 0.1 bar) overnight. The freeze-dried powder was dispersed in ethanol and placed on carbon/formvar coated-copper grid.

2.2.6 Preliminary cytocompatibility test

Mouse pre-osteoblast cell line, MC3T3-E1 Subclone 14 (ATCC cell bank, USA) was used for the biological study. In detail, MC3T3-E1 cells were cultured in α MEM without ascorbic acid, 10% Fetal Bovine Serum (FBS) and 1% penicillin-streptomycin (100 U/mL-100 $\mu\text{g/mL}$). Cell culture was kept at 37°C in an atmosphere of 5% CO_2 . Cells were detached from culture flasks by trypsinization, centrifuged and re-suspended. Cell number and viability were assessed by trypan-blue dye exclusion test.

For the experiment, cells were plated at a density of 5000 cells/ cm^2 in 96-well and 24-well plate. 24 hours after seeding, different concentrations of each microspheres group (10 $\mu\text{g/mL}$ and 100 $\mu\text{g/mL}$; RCP, RCPFeHA40 and RCPFeHA60) were added to the cell culture. Microspheres, sterilized by 25 kGy γ -ray radiation prior to use and before being added to the cells were vortexed. All the cell-handling procedures were performed in a sterile laminar flow hood and all cell-culture incubation steps were performed at 37°C with 5% CO_2 .

Cell viability was evaluated by quantification of cell metabolic activity using MTT and Live/Dead assay, after 1, 3 and 7 days. MTT reagent was prepared at 5 mg/mL in 1x PBS. Cells seeded in 96-well plate, were incubated with MTT reagent 1:10 for two hours at 37°C . Medium was removed and cells were incubated with 1 mL of dimethyl sulfoxide for 15 min. In this assay, the metabolically active cells react with the tetrazolium salt in the MTT reagent to produce a formazan dye that can be observed at $\lambda_{\text{max}} = 570$ nm, using a Multiskan FC Microplate Photometer (Thermo Fisher Scientific, Waltham, MA, USA). This absorbance is

directly proportional to the number of metabolically active cells. Three samples per group was analysed at each time point.

Live/Dead assay kit (Invitrogen, U.S.A.) was performed according to manufacturer's instructions. Briefly, the cells seeded on 24-well plates were washed with 1x PBS for five min and incubated with Calceinacetoxymethyl (Calcein AM) 2 μ M plus Ethidium homodimer-1 (EthD-1) 4 μ M for 15 min at 37°C in the dark, the samples were rinsed in PBS 1x (Papadopoulos et al. 1994). Images were acquired by an inverted Nikon Ti-E fluorescence microscope (Nikon Corporation, Tokyo, Japan). One sample per group was analysed at each time point.

2.2.7 Statistical analysis

Statistical analysis was performed using two-way ANOVA, followed by Tukey's multiple comparison test, considered statistically significant when $p \leq 0.05$. Calculations were performed using Graph Pad Prisma 6 software. Data is plotted as mean \pm standard error of mean (Mean+SEM) of n. 3 samples per each group.

2.3 Effect of ions release from hybrid superparamagnetic microspheres on osteogenic differentiation of MC3T3-E1

2.3.1 Raw materials

RCP was kindly provided by Fujifilm Manufacturing B.V. (The Netherlands). Calcium hydroxide ($\text{Ca}(\text{OH})_2$, $\geq 95\%$), phosphoric acid (H_3PO_4 , 85%), iron(II) chloride tetrahydrate ($\text{FeCl}_2 \cdot 4\text{H}_2\text{O}$, $\geq 99\%$), iron(III) chloride hexahydrate ($\text{FeCl}_3 \cdot 6\text{H}_2\text{O}$, 97%), sodium hydroxide (NaOH , $\geq 98\%$), corn oil, acetone ($\geq 99.9\%$), potassium bromide (KBr , $\geq 99\%$), phosphate buffered saline (PBS), HEPES sodium salt ($\geq 99.5\%$), acetic acid ($\geq 99.85\%$), sodium acetate ($\geq 99\%$), were all purchased from Sigma Aldrich (St Louis, MO, USA), whereas nitric acid (HNO_3 , 65%) was purchased from Titolchimica (Italy), and fluidMAG-CT from Chemicell (Germany, Berlin). Biological reactants were described in section 2.3.7. Ultrapure water (0.22 mS, 25 °C) was used in all the experiments.

2.3.2 Preparation of RCP and RCPfluidMAG-CT solutions

RCP and RCP combined with fluidMAG-CT (i.e. commercial magnetic nanoparticles, size 50 nm) were prepared. Briefly, 5g of RCP was dissolved in 12 mL of milli-Q water under magnetic agitation and thermostated at about 40°C, and then 2 ml of fluidMAG-CT were dropped in RCP dissolution, for a complete involvement of magnetic nanoparticles in RCP matrix, under magnetic agitation for 30 minutes. The as-obtained material is encoded as RCPfluidMAG-CT. RCP was produced by the as-mentioned method but the volume of magnetic nanoparticles was substituted by milli-Q water.

2.3.3 Synthesis and functionalisation of mineralised slurries

Iron free and iron containing mineralised slurries were obtained by biomineralisation process, as described in the section 2.1.2. Herein, slight modifications in the amount of the reactants were performed, as briefly described: an aqueous solution of RCP (≈ 0.006 M) was prepared and thermostated at 40°C. An acid solution of H_3PO_4 (≈ 3.9 M) was prepared and dropped in the RCP solution, then poured dropwise into a basic aqueous suspension of $\text{Ca}(\text{OH})_2$ (≈ 1.9 M) also containing $\text{FeCl}_2 \cdot 4\text{H}_2\text{O}$ and $\text{FeCl}_3 \cdot 6\text{H}_2\text{O}$ as sources of Fe^{2+} and Fe^{3+} ions, to establish a molar ratio of 3:2. The process was carried out at a fixed temperature and under magnetic stirring, to achieve a nominal mineralization extent (i.e. inorganic : organic fraction) equal to 40 wt%. The overall ion content was set to achieve $\text{Ca/P} = 1.67$ and $\text{Fe/Ca} = 0.2$ and the synthesis of the slurry was carried out at 60°C. The as-obtained material was henceforth coded as RCPFeHA.

Iron-free mineralised slurries were synthesised at 20°C and 60°C to obtain control hybrid mineralised materials with iron-free hydroxyapatite, henceforth coded as RCPHA_{RT} and RCPHA, respectively.

To the as-obtained iron-containing mineralised slurries predetermined concentrations of sodium citrate (i.e. 0.55 M, 0.3 M, 0.06 M, 0.006 M and 0.0006 M) were investigated. Sodium citrate was added to the slurries and maintained under magnetic stirring for about 6h, at room temperature ($\approx 20^\circ\text{C}$). The functionalization time was selected by measuring the surface charge of the slurries at concentration of 0.55 M, by using ζ -potential.

Therefore, functionalised slurries were dropped in pre-warmed corn oil for the production of microspheres, by using water-in-oil emulsification process, as presented in the section 2.2.4.

2.3.4 Fabrication of microspheres by emulsification process

A water-in-oil emulsification process was assessed to produce pure RCP, RCPfluidMAG-CT and hybrid microspheres (i.e. RCPHA_{RT}, RCPHA and RCPFeHA). The used emulsification process was already described in the section 2.2.4. After drying process, microspheres were sieved to achieve a size distribution in the range 50 to 75 μm . Three different batches of each type of microspheres were produced. Dehydrothermal treatment (DHT) was carried out by placing the dried microspheres in glass vials covered with aluminium foil and heated at 160 $^{\circ}\text{C}$ for 48 hours under vacuum.

2.3.5 Morphological and physicochemical characterisation

Functionalised slurries and microspheres surface charge were evaluated by using ζ -potential (Zetasizer Nano analyzer (Malvern, UK)). ζ -potential measurements through electrophoretic mobility were carried out with a using disposable folded capillary cells (DTS1061; Malvern, UK) at 25 $^{\circ}\text{C}$. For functionalised slurries, 100 μL of slurry was diluted in 5 mL of milli-Q water and ζ -potential was evaluated at $t = 0$ and $t = 30'$, 1h30', 3h and 6h. Microspheres surface charge was evaluated in HEPES buffer (i.e. 0.01 M; pH 7.4) at concentration of 1.2 mg/mL of microspheres. The ζ -potential average was calculated from three separate measurements (100 runs each) in each type of microspheres and the results were showed as Mean \pm SEM.

The morphology of the microspheres was analysed by using Scanning Electron Microscope (SEM) (FEI Quanta 600, USA) in low vacuum mode with an accelerating voltage of 10 kV and a working distance of 10 mm. Microspheres size distribution was evaluated by SEM micrographs and analysed by Image J software.

The identification of functional groups of RCPFeHA and functionalised RCPFeHA was evaluated by Fourier Transform Infrared Spectroscopy (FTIR) (Avatar 320 FT-IR, Thermo Nicolet, Canada), by following the protocol described in the section 2.1.3.

The phase composition of the all as-produced microspheres was obtained by X-ray powder diffraction (XRD, D8 Advance, Bruker, Karlsruhe, Germany), as presented in the section 2.1.3.

The overall content of calcium (Ca), phosphorus (P) and iron (Fe) was determined by inductively coupled plasma optical emission spectrometry (ICP-OES; Liberty200, Varian, Clayton South, Australia), by following the method showed in 2.1.3.

Simultaneous thermogravimetric (TGA) analysis (STA 449/C Jupiter, Netzsch, Germany) was carried out to explore the presence of citrate ions on functionalised RCPFeHA microspheres and measured as following the section 2.1.3.

A susceptometer balance YSZ 01C/02C (Sartorius Mechatronics, Italy) was used to evaluate the magnetisation of pelletized materials (i.e. RCPfluidMAG-CT and RCPFeHA) under a field of 2700 A/m at a distance of 18 mm.

2.3.6 Microspheres degradation study

Microspheres degradation tests were carried out under two different conditions that mimic i) the physiological (pH 7.4) and ii) the inflammatory (pH 5.0) environment. For physiological condition, osteogenic differentiation medium was prepared with DMEM (Gibco), 10% Fetal Bovine Serum (FBS), 1% penicillin-streptomycin (100 U/mL-100 µg/mL), 10 mM β-glycerophosphate and 50 µg/mL ascorbic acid. The inflammatory like condition was achieved by buffering the previous medium with sterile sodium acetate-acetic acid buffer solution, reaching pH 5.0. The as-prepared media were named as DMEM and DMEM-IM, respectively.

Each type of microspheres were sterilised in PBS 1X by using autoclave (120°C for 20 minutes). Then PBS 1X was substituted by DMEM or DMEM-IM obtaining a final concentration of 30 mg/mL of microspheres. Three samples of each type of microspheres were investigated. DMEM or DMEM-IM only were used as controls. Microspheres degradation study was carried out in the incubator at 37°C in an atmosphere of 5% CO₂, up to 28 days.

Microspheres morphology was evaluated by SEM, after 7, 14, 21 and 28 days. Moreover, RCPHA_{RT} and RCPFeHA at day 28 were washed four times with milli-Q water, freeze dried and stored for further FTIR and XRD characterisations.

Ions dissolutions evaluation

The elemental concentration of calcium and iron ions released from RCPfluidMAG-CT, RCPHA_{RT} and RCPFeHA in DMEM and DMEM-IM was evaluated by ICP-OES. At predetermined time points (i.e. 12h, 24h, 48h, 7 days, 14 days, 21 days and 28 days), both media (i.e. DMEM and DMEM-IM) were collected from microspheres by centrifugation (13300 rpm, for 12 minutes) and the released ions were investigated, as well as the differences on the pH by using pH meter with electrochemical sensor (XS instruments, Italy). DMEM and DMEM-IM were replaced at the as-mentioned time points. The retrieved media (0.6 mL) were digested with 1 mL of HNO₃ (65 wt%) and the volume of the solution was raised to 3 mL by adding deionized water, and further analysed by ICP-OES. Predetermined concentrations of Ca and Fe elements were also prepared and used as standard calibration. The released ions were normalised to the total concentration of each element (i.e. Ca_{total} and Fe_{total}) in 30 mg of microspheres. Three samples were used per material and the ions concentration was expressed as Mean ± standard error of the mean (SEM).

2.3.7 Biological characterisation

2.3.7.1 Cell culture

Mouse pre-osteoblast cell line, MC3T3-E1 Subclone 14 (ATCC cell bank, Manassas, VA, USA) was used for the biological investigation. In detail, MC3T3-E1 cells were cultured in αMEM without ascorbic acid (Gibco), 10% FBS and 1% penicillin-streptomycin (100 U/mL-100 µg/mL). Cell culture was kept at 37°C in an atmosphere of 5% CO₂, later on the cells were detached from culture flasks by trypsinization, centrifuged

and re-suspended in cell medium. Cell number and cell viability were assessed by trypan-blue dye exclusion test.

For the experiment, cells were plated at a density of 2500 cells/cm² in osteogenic medium in 48-well plates for cell viability with predetermined concentration of each type of microspheres (i.e. 10 µg/mL, 100 µg/mL and 500 µg/mL); in 24-well plates for cell damage evaluation and cell morphology; in 6-well plates for gene expression and western blot analysis, 24 hours after cells seeding, different concentrations of each sterilised microspheres (i.e. 10 µg/mL and 100 µg/mL of RCP, RCPfluidMAG-CT, RCPHA_{RT} and RCPFeHA) were added to the cell culture. All the cell-handling procedures were performed in a sterile laminar flow hood and all cell-culture incubation steps were performed at 37 °C with 5% CO₂.

2.3.7.2 Cell viability

Cell viability as function of cell number based on metabolic activity was evaluated by XTT assay, following the manufacture's protocol (Thermo Fisher Scientific, U.S.A.). Briefly, 6 mg of XTT was dissolved in 6 mL of osteogenic cell medium and then was added 15 µL of 10 mM of PMS solution. After, 75 µL of the as-prepared solution was dropped in each well and incubated at 37 °C in CO₂ incubator for 2 hours and the absorbance was analysed at 450 nm by using a Multiskan FC Microplate Photometer (Thermo Fisher Scientific, USA). All the tested microspheres were prepared in various concentrations and the cell viability was analysed after 1, 3 and 7 days of cell seeding. Cells only and microspheres without cells were used as controls and the experiments were conducted in triplicates and plotted as Mean±SEM.

2.3.7.3 Cell damage and cell morphology evaluation

Apoptotic cells

After 24h and 72h of incubation, cells were evaluated with Annexin V/Dead Cell Apoptosis Kit (Molecular Probes) according to manufacturer's instructions. Briefly, cells were washed with cold PBS 1X, and incubated with 1X annexin-binding buffer, Alexa Fluor 488 annexin V and propidium iodide (PI) working solution for 15 minutes at room temperature following by DAPI staining for cell nuclei. Cells incubated with or without Doxorubicin (0.54 µg/mL; DOX) were used as positive and negative control, respectively. One sample per group was analysed and images were acquired with an inverted Ti-E fluorescence microscope (Nikon).

Reactive Oxygen Species (ROS)

ROS formation at 24h and 72h was analysed by ROS indicator kit (carboxy-2,7-difluorodihydrofluorescein diacetate, carboxy-H2DFFDA, Molecular Probes), according to manufacturer's instructions. Briefly, cells were incubated with ROS detection reagent for 15 minutes at 37°C, then this solution was removed and cell culture medium was added for 10 minutes at 37°C, before washing the cells with PBS 1X following by DAPI staining for cell nuclei. Cells incubated with or without 100 µM of hydrogen peroxide (H₂O₂) were

used as positive and negative control, respectively. One sample per group was analysed and images were acquired with an inverted Ti-E fluorescence microscope.

Actin filament staining

At day 3, cell morphology was evaluated by phalloidin staining. Cells were washed with PBS 1X for 5 min, fixed with 4% (w/v) paraformaldehyde for 15 minutes. Permeabilization was performed with PBS 1X with 0.1% (v/v) Triton X-100 for 5 min. FITC-conjugated phalloidin (Invitrogen, U.S.A.) 38 nM in PBS 1X was added for 20 minutes at room temperature in the dark. For nuclear staining the cells were incubated with 300 nM of DAPI for 5 min. Images were acquired by an Inverted Ti-E fluorescence microscope. One sample per group was analysed.

Haematoxylin and Eosin Staining (H&E)

After 3 days of cell culture, cells were washed with PBS 1X for 5 minutes, fixed with 4% (w/v) formaldehyde for 15 minutes, washed twice with PBS 1X for 5 minutes and stained with H&E. Briefly, the cells were incubated with Mayer's haematoxylin for 7 minutes, then differentiated with tap water for 10 minutes. Cells were then stained with eosin Y (0.25%) for 30 seconds, washed with milli-Q water and mounted. Images were acquired by an Inverted Ti-E fluorescence microscope. One sample per group was analysed.

2.3.7.4 Western Blot

After 7 days of culture the cells, cultured with 100 µg/mL of microspheres, were lysed in a Radioimmunoprecipitation buffer (RIPA buffer) supplemented with a proteinase inhibitor cocktail (Cell Signalling Technology, U.S.A.). Protein concentration in each cell lysate supernatant was determined by a colorimetric assay (Kit DC Protein Assay, Bio-Rad, U.S.A.). The protein sample were diluted in sample buffer (3:1), and loaded and separated in a 4–20% Mini-PROTEAN TGX stain-free protein gels (Bio-Rad, U.S.A.), using a Mini-PROTEAN electrophoresis cell kit (Bio-Rad, U.S.A.). The proteins were then transferred to nitrocellulose membranes by means of a Trans-Blot Turbo™ transfer system (Bio-Rad, U.S.A.), with the blots incubated thereafter for 30 min at room temperature in a blocking solution of 2.5% non-fat dry milk in PBS 1X. The membranes were incubated overnight at 4°C with primary rabbit antibody anti-alkaline phosphatase (ALP, Abcam, UK), anti-osteocalcin (LifeSpan BioSciences, U.S.A.) and anti-β-actin (Cell Signaling Technology, USA) as internal control. Moreover rabbit antibody anti-LC3B-I and LC3B-II (Cell Signalling Technology, USA) was used to detect autophagy as cellular stress marker. Then membranes were incubated with a horseradish goat peroxidase-linked secondary antibody anti-rabbit (Bio-Rad, U.S.A.) for 1h 30 min. An enhanced chemiluminescence kit (ECL, Bio-Rad, U.S.A.) was used to visualize the protein bands with ChemiDoc XRS+ (Bio-Rad, U.S.A.). In order to evaluate the relative protein expression, the ALP, osteocalcin and LC3B-I and LC3B-II band intensities were quantified by densitometry

using ImageLab Software and were then normalized over the signal of the corresponding bands of β -actin (i.e. loading control).

2.3.7.5 Quantitative real-time polymerase chain reaction (qPCR)

The gene expression profile of MC3T3-E1 cells, cultured for 7 days with 100 μ g/mL of microspheres, was assessed by using qPCR. Cells only were cultured in osteogenic differentiation medium and were used as calibrator in order to obtain a relative quantification. Total RNA was harvested by using Tri Reagent, followed by the Direct-zol RNA MiniPrep kit (Zymo Research) according to manufacturer's instructions. RNA integrity was analyzed by native agarose gel electrophoresis and the quantification was performed by using the Qubit® 2.0 Fluorimeter together with the Qubit® RNA BR assay kit, according to the manufacturer's instructions (Invitrogen, U.S.A.). Total RNA (i.e. 500 ng) was reverse transcribed to cDNA using the High-Capacity cDNA Reverse Transcription Kit, according to manufacturer's instructions (Applied Biosystems, U.S.A.). The relative quantification of the expression of the genes, i.e. osteonectin (SPARC, Mn00486332-m1), osteocalcin (BGLAP, Mm00649782_gH), collagen I (COL I, Mm00483888_m1), osteopontin (OPN, Mm004336767) and glyceraldehydes-3-phosphate dehydrogenase (GAPDH, Mm99999915_g1), used as housekeeping gene, were performed by StepOne™ Real-Time PCR System (Applied Biosystems, U.S.A.). Data were collected using the OneStep Software (v.2.2.2) and relative quantification was performed using the comparative threshold (C_T) method ($\Delta\Delta C_T$) where the relative gene expression level equals $2^{-\Delta\Delta C_T}$ (Boanini et al. 2016; Livak & Schmittgen 2001). Experiments were performed in duplicate, using three technical replicates for each experiment and representative results were normalized to RCP. Error bars reflect one standard error of the mean of three technical replicates, as described elsewhere (Liu et al. 2013; Ivey et al. 2008).

2.3.8 Statistical analysis

Statistical analysis was performed by using GraphPad Prism 5 software. The unpaired t-test was used for ions release and two-way ANOVA, followed by Bonferroni post-tests was used for calcium absorption in DMEM. Data is plotted as Mean \pm SEM of n. 3 samples per each group.

Statistical analysis of biological tests was performed by using two-way ANOVA followed by Bonferroni post-tests for XTT analysis and data was plotted as mean \pm SEM of n. 3 samples per each group. All the other biological results were evaluated by one-way ANOVA followed by Tukey's multiple comparison test and data were plotted as mean \pm SEM of n. 2 samples per each group. Results were considered statistically significant when $p < 0.05$.

2.4 Effect of microspheres composition on differentiation of human mesenchymal stem cells

2.4.1 Materials

RCP, RCPHA_{RT} and RCPFeHA microspheres were previously prepared by emulsification process and crosslinked with DHT treatment, as described in section 2.2.4. In the following experiments, microspheres were sterilised by autoclave. Briefly, predetermined amount of microspheres were introduced in Eppendorf and covered with aluminium foil, then were introduced in glass vial and closed with aluminium foil, and sterilised in autoclave at 120°C for 20 minutes. Subsequently, the glass vials were opened into the sterile hood and the microspheres were left to dried for about 30 minutes.

2.4.2 Microspheres characterisation

The specific surface area of microspheres was measured by BET method (Brunauer, Emmett e Teller), using nitrogen adsorption (Sufer, Thermoscientific, U.S.A). Samples were previously degassed at 50°C under vacuum (about 3.0×10^{-3} torr) for 15 hours.

2.4.3 Cell culture

Leftover bone samples from children undergoing facial reconstruction surgery were used to obtain hMSCs under umbrella agreements between patients and Dutch university hospitals for the use of waste materials (MEC2014-106, Erasmus MC Rotterdam). Three independent Donors coded as Donor 1, Donor 2 and Donor 3 were investigated. hMSC's were seeded at density of 5×10^5 cells per T175 flask in 20 mL of standard cell medium (i.e. Minimum Essential Medium alpha (α -MEM, Gibco by Life Technologies, U.S.A.), supplemented with 10% heat-inactivated fetal calf serum (FCS, Lonza), 50 μ g/mL of gentamycin (Invitrogen, U.S.A.), 1.5 μ g/mL fungizone (Invitrogen, U.S.A.), 5 ng/ μ L fibroblast growth factor-2 (Instruchemie B.V., The Netherlands) and 0.1 mM of ascorbic acid (Sigma Aldrich, U.S.A.)) and were cultured at 37°C under humidified incubator and 5% of carbon dioxide (CO₂). Cell medium was renewed every 3-4 days. Cells were detached, upon reaching near confluence (i.e. 80–90%), from culture flasks by trypsinization (0.25% trypsin/EDTA; Life Technologies, U.S.A.), centrifuged and re-suspended in standard cell medium. Cell number and cell viability were assessed by trypan-blue dye exclusion test.

Cell seeding in monolayer

hMSCs (P5) were re-suspended in standard cell medium and were cultured at density of 3000 cells/cm² in 12-well plate. Cells were left to adhere to the well plate for 24 hours, and then 500 μ g of each type of microspheres were added on the top of the cells. The cell culture was kept for 7 days at 37°C under humidified incubator and 5 % of CO₂. Samples were analysed by optical microscope and were treated with Live/Dead assay, for further cell viability evaluation (section 2.4.4).

Cell seeding strategy on microspheres

Preliminary investigations were carried out in presence of hMSC's ($\leq P8$). The amount of cells seeded on the different microspheres was investigated in the range of 3500, 700 and 350 cells/cm² and specific surface area of the microspheres was considered. On the other hand, 350 cells/cm² were seeded in all tested microspheres take into account the specific surface area of RCP microspheres, thus equal cell number in all tested microspheres (Table 2).

Table 2. Cells numbers used in the optimisation of cell seeding. (* Values obtained from specific surface area of microspheres; ** based on specific surface area of RCP microspheres).

Microspheres (Ms)	Specific surface area of microspheres, cm ² /mg	* 3500 cells/cm ²	* 700 cells/cm ²	* 350 cells/cm ²	** 350 cells/cm ²
RCP	1352.8	2 367 400	473 480	236.740	
RCPHA _{RT}	291.1	509 425	101 885	50.942	236.740
RCPFeHA	1941.1	3 396 925	679 385	339.692	

The experiments were carried out with standard cell medium. Previous to cell seeding, for a completely interaction of the cells with all tested microspheres, the bottom of 6-well plate or 12-well plate were filled with 2 % of agarose and left to dried at room temperature. For the cell seeding, 500 µg of each type of microspheres were placed in eppendorf and predetermined amount of cells were seeded on the top of microspheres (Table 2). At density of 3500 cells/cm², the cells were mixed with microspheres by inversion process at each 10 minutes until reaching one hour and then were transferred to the 6-well plate or 12-well plate and kept in culture for three days (Figure 7A).

Moreover, for 700 and 350 cells/cm² the seeding strategy was slightly modified. Briefly, 500 µg of each type of microspheres were introduced in eppendorf and predetermined amount of cells were seeded on the top of microspheres (Table 2), then cells and microspheres were mixed by inversion at each 10 minutes until one hour of seeding. Subsequently, cells and microspheres were left to sediment and standard cell medium was collected and replaced three times, completing another hour (Figure 7B). After 2 hours of seeding, cells and microspheres were placed in the well plates covered with agarose. Cell culture was kept at 37 °C under humidified incubator and 5 % of CO₂. Triplicates of microspheres were prepared and the results were showed as mean of standard deviation (Mean±SD).

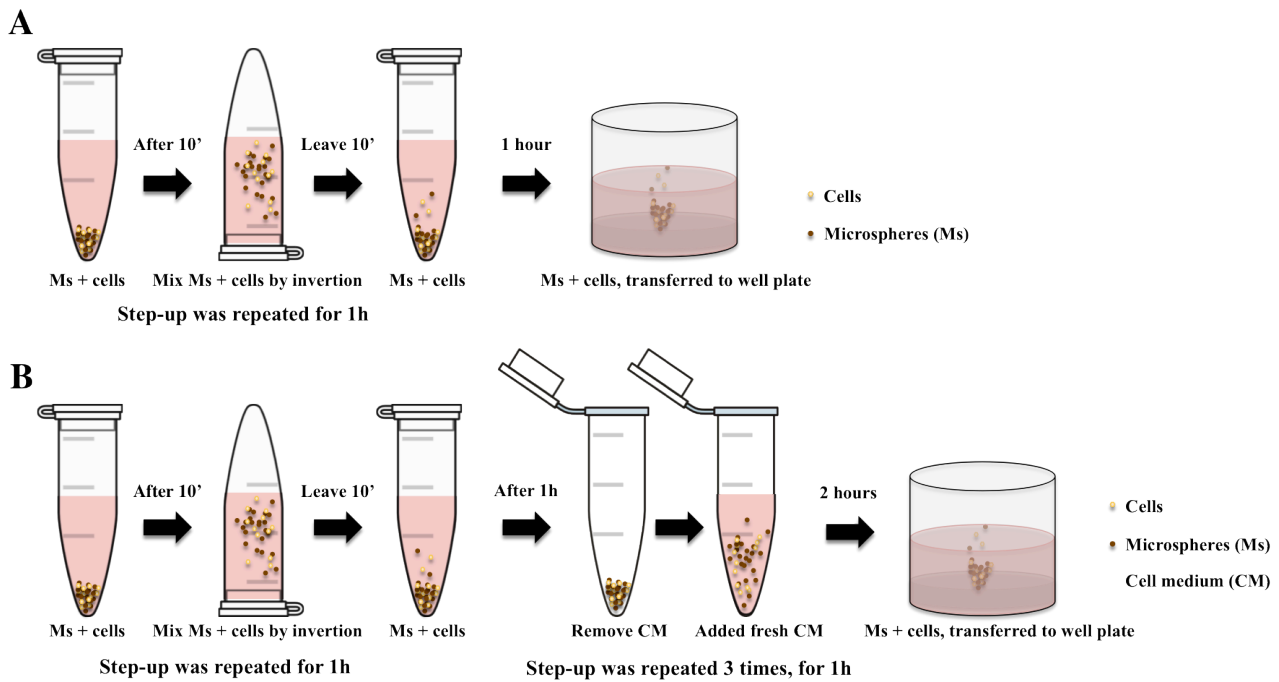


Figure 7. Cells seeding strategy for 3500 cell/cm² (A) and for 700 and 350 cells/cm² (B).

Osteogenesis

hMSCs from the Donor 1, Donor 2 and Donor 3 (P4) were seeded in all tested microspheres at density of 236.740 cells in 500 μ g of microspheres in eppendorfs, by following the previous seeding method (Figure 7B). Cells and microspheres were transferred to 6-well plate or 12-well plates (previous covered with 2% of agarose) in standard cell medium. After 24 hours of incubation, standard cell medium was replaced by osteogenic induction medium (i.e. high-glucose DMEM (Invitrogen, U.S.A.) with 10% of FCS, 50 μ g/mL gentamycin (Invitrogen), 1.5 μ g/mL fungizone (Invitrogen, U.S.A.), 10 mM glycerol 2-phosphate (Sigma Aldrich, U.S.A), 0.1 μ M dexamethasone (Sigma Aldrich, U.S.A) and 0.1 mM ascorbic acid (Sigma Aldrich, U.S.A)). The as-obtained combination of microspheres and cells were encoded as 3D templates, from RCP, RCPHA_{RT} and RCPFeHA. For the controls, cells were seeded in 6-well or 12-well plate at density of 3000 cells/cm². Osteogenic induction medium was replaced twice a week. The samples were harvested at the latest point prior to detachment of the cells monolayer and might varied between 17 days to 21 days, depending on the Donor.

2.4.4 Cell viability and proliferation

DNA assay

At predetermined time points, samples were collected, introduced into eppendorf's and were washed once with PBS. For the digestion of the samples a papain buffer containing 0.2 M of sodium phosphate monobasic ($\geq 99.0\%$, Sigma Aldrich, U.S.A) and 0.01 M of ethylenediaminetetraacetic acid disodium salt dehydrate (Sigma Aldrich, U.S.A) was prepared and freshly was added 0.01 M of cysteine HCL (Sigma Aldrich, U.S.A) and 250 μ g/mL of papain (Sigma Aldrich, U.S.A). Defined volume of papain solution (300 μ L) was dropped in the samples and incubated overnight at 60 °C, then the samples were vortex and incubated for

more one hour at 60°C. DNA assay with ethidium bromide was used to determine the DNA amount in the samples. Samples and calibration curve (0 – 1.25 µg of Deoxyribonucleic acid sodium salt from calf thymus (DNA)) were pipetted in Duplo in 96-well plate (50 µL), then 100 µL of heparin solution (8.3 IU/mL dilution in PBS, Leo Pharmaceutical Products, Denmark) and 50 µL of Ribonuclease type III-A solution (0.05 mg/mL dilution in PBS, Sigma Aldrich, U.S.A) were added to each well, and incubated at 37°C for 30 minutes. After incubation, 50 µL of ethidium bromide (25 µg/mL dilution in PBS, Thermo Fisher Scientific, U.S.A.) were placed in each well and the plate was read on the Wallac Victor (excitation 340 nm and emission 590 nm). The results were expressed Mean±SD in the same Donor and were plotted as Mean±SD from three independent Donors (n=3).

The percentage of cells adhere on the microspheres ($Cell_{MS}$, %) were calculated, as follow:

$$Cell_{MS} = \left(\left(\frac{DNAq}{8.5} \right) / N^{\circ}_{seed} \right) \times 100$$

Equation 1. Percentage of cells adhered on the microspheres.

Where as, $DNAq$ was the DNA quantified by the DNA assay and was expressed in pg ; 8.5 was the DNA amount in each cell, pg (Dormer et al. 2012) and N°_{seed} was the initial cells number seeded in each type of microspheres.

DAPI staining

3D templates were placed in 24-well plate and 1 mL of formalin (4%) was added to fix the cells for one hour at room temperature. 3D templates were washed three times with PBS; were stained 5 minutes with DAPI solution (5 mg/mL) and were washed three times with PBS. The images were acquired by using fluorescent microscope Zeiss Axiovert 200M, with Axiovert software (Germany).

Live & Dead assay

Live/Dead[®] viability/cytotoxicity kit for mammalian cells (Life Technologies, U.S.A.) was performed according to manufacturer's instructions. Briefly, the cell medium was recovered from RCPFeHA 3D template (in 24-well plate) or from cells seeded on 12-well plates and were washed once with saline solution (i.e. 0.9% of NaCl in milli-Q water), then were incubated with Live/Dead solution composed by Calceinacetoxymethyl (Calcein AM) and Ethidium homodimer-1 (EthD-1) (e.g. 1 mL of saline solution with 1 µL of Calcein AM and 1.5 µL of EthD-1), wrap with aluminium foil and incubated for 40 minutes at 37°C in an humidified atmosphere and 5% of CO₂. Live/Dead solution was removed and samples were washed twice with saline solution. Samples were kept in saline solution during the viability analysis with fluorescent microscope Zeiss Axiovert 200M, with Axiovert software (Germany). Three samples per group were analysed and an example of each group was showed.

2.4.5 Calcium assay

The decrease of calcium concentration in the osteogenic induction medium was evaluated over the course of the experiment. At predetermined time points, cell medium was collected from the cell culture and analysed by calcium assay. Briefly, 10 μ L of cell medium or standard curve were pipetted in Duplo in 96-well plate. α -MEM was prepared with known concentration of calcium (i.e. 0 - 3mM) and was used as standard curve. For the detection of the calcium, two distinct solutions were prepared: Solution I) 1 M of ethanolamine buffer (pH 10.6) and Solution II) 0.35 mM O-cresolphthalein complexone, 19.8 mM 8-hydroxyquinoline and 0.6 M hydrochloric acid. Those solutions were mixed in the proportion of 1:1 and 100 μ L was pipetted in each well. The absorbance was measured at 595 nm with Versamax (Molecular Devices). The results were expressed as Mean \pm SD from three independent Donors (n=3) or as Mean \pm SD in each Donor.

2.4.6 Gene expression

RNA isolation and DNA synthesis

Samples were transferred to 1.5 mL eppendorf, washed once with PBS and were snap freezing with liquid nitrogen. RNA was isolated from the 3D templates or cells monolayer by homogenizing samples with a Eppendorf-potter in 350 μ L of Trizol (Thermo Fisher Scientific, U.S.A.). The total RNA was extracted by adding 70 μ L of chloroform (Sigma Aldrich, U.S.A) and three phases after centrifugation were formed. RNA was collected from the top layer and equal volume of 70% v/v of ethanol (Sigma Aldrich, U.S.A) was added. The RNA was purified by using RNeasy Mini Kit with RNeasy MinElute spin columns (Quiagen, The Netherlands), following the manufacturer's instructions and total RNA was quantified by spectrophotometry (NanoDrop 2000, Thermo Scientific, The Netherlands) at wavelength of 260 and 280 nm. 300 ng of RNA was reverse transcribed into complementary DNA (cDNA) by using RevertAid First Strand cDNA Synthesis kit (Thermo Fisher scientific, U.S.A.), according to the manufacturer's protocol.

Quantitative PCR

Osteogenic gene transcriptions were quantified on Bio-Rad CFX thermal cycler (Bio-RAD, U.S.A). Thermocycler conditions comprised an initial holding at 95°C for 10 min, followed by one step at 95°C for 15 s and 60°C for 60 s for 40 cycles. For gene expression tests, three different housekeeping genes were evaluated, such as Ubiquitin C (UBC), Glyceraldehyde-3-phosphate dehydrogenase (GADPH) and Beta-2-microglobulin (B2M), while the investigated osteogenic genes were Gamma-carboxyglutamic acid-containing protein (BGLAP), Collagen type I (COL I), Integrin-binding sialoprotein (IBSP), Alkaline phosphatase (ALPL) and Osteonectin (SPARC).

UBC and B2M mRNA levels were analyzed with qPCRTM Mastermix Plus for SYBR[®] Green I (Eurogentec, Nederland B.V., The Netherlands), while GADPH, BGLAP, COL I, IBSP, ALPL and SPARC, TaqMan Master Mix (Applied Biosystems, U.S.A.) was applied, according to the manufacturer's instructions. The as-corresponding primers were described in Table 3. (Groeneveldt et al. 2014; Leijts et al. 2012; Verseijden et al. 2009). The CT values of the housekeeper genes GADPH, B2M and UBC were averaged by using

geometric averaging of every sample. This average is the best keeper index (BKI) for every single sample. All separate CT values were corrected to the BKI by using the $2^{-\Delta CT}$ formula (Leijts et al. 2012). Values were represented as Mean \pm SD for samples from three independent Donors (n=3) or were plotted as Mean \pm SD in each Donor.

Table 3. Primers sequences used to define the osteogenic expression of the genes.

		Forward	Reverse
Housekeeping genes	GADPH	ATGGGGAAGGTGAAGGTCG	TAAAAGCAGCCCTGGTGACC
	UBC	ATTTGGGTCGCGGTTCTTG	TGCCTTGACATTCTCGATGGT
	B2M	5'-TGCTCGCGCTACTCTCTCTTT-3'	5'-TCTGCTGGAT GACGTGAGTAAAC-3'
Osteogenic genes	ALPL	GACCCTTGACCCCCACAAT	GCTCGTACTGCATGTCCCCT
	BGLAP	GAAGCCCAGCGGTGC	CACTACCTCGCTGCCCTCC
	IBSP	TGCCTTGAGCCTGCTTCC	GCAAAATTAAAGCAGTCTTCATTTG
	COL I	CAGCCGCTTCACCTACAGC	TTTTGTATTCAATCACTGTCTTGCC
	SPARC	ATCTCCCTGTACACTGGCAGTTC	CTGGGTGTGGGAGAGGTACC

2.4.7 von Kossa staining

Cells monolayer were washed once with PBS and fixed with 4% of formaldehyde for one hour, then washed several times with distilled water and milli-Q water and stained with von Kossa staining. Briefly, cells were incubated with 5 % of silver nitrate (AgNO₃, \geq 99.5%, Sigma Aldrich, U.S.A) and incubated in light desk up to 60 minutes. Cells were washed once with milli-Q water and counterstained with thionin solution (0.4% thionin in 0.01 M aqueous sodium acetate, (Sigma Aldrich, U.S.A)) for 5 minutes. By the end, the samples were dehydrate in 70% (10 s), 96% (1 s) and 100% (1 minute) of ethanol (Vector Laboratories, U.S.A.).

2.4.8 Preparation of histology samples

Samples were fixed in 4% formaldehyde (Klinipath) in PBS, embedded in 2% w/v agarose (Eurogentec, Belgium) and subsequently processed in paraffin for light microscopy. The samples were cut into 5 μ m sections by using a microtome (Leica RM 2135).

Haematoxylin and Eosin staining

Pre-treated paraffin sections were deparaffinise in Xylene (2 times, 5 minutes each) and in 100% (2 times, 5 minutes each), 96% (1 time, 5 minutes) and 70% (1 time, 5 minutes) of ethanol, then were washed twice with distilled water for 3 minutes each. Sections were transferred to haematoxylin solution (Sigma Aldrich, U.S.A) for 20 seconds and washed with running tapwater for 10 minutes, then were immersed in eosin Y solution (2% in 50% of ethanol and 0.5 mL of glacial acetic acid, Merck, Germany) during 45 seconds. By the end, the sections were introduced in 70 % of ethanol (10 seconds) and dehydrate one minute in each step,

in 96% and 100% of ethanol and two times in o-xylene (Sigma Aldrich, U.S.A). The stained sections were mounted with Depex mounting medium (Merck, Germany) and analysed on optical microscope.

Thionin Staining

The pre-treated paraffin sections were stained with 0.04% thionin (Gurr, Essex, UK) in 0.01 M aqueous sodium acetate pH 4.5 for up to 15 minutes, and then the sections were counterstained for 5 min with a 0.1 % solution of fast green in water for 5 minutes (Bulstra et al. 1993; Bos et al. 2001). The stained samples were evaluated by using optical microscope.

2.4.9 Statistical analysis

Cell seeding strategies and gene expression were statistically analysed by one-way ANOVA by Tukey's Multiple Comparison Test. The calcium content was evaluated by two-way ANOVA by Bonferroni posttests. The p value < 0.05 was considered statistically significant.

2.5 Superparamagnetic microspheres as a sustained carrier for rhBMP-2 delivery

2.5.1 Materials

Recombinant human bone morphogenetic protein-2 (rhBMP-2) and fluorescent recombinant human bone morphogenetic protein-2 (texas red rhBMP-2) were kindly furnished by Fraunhofer Institute for Interfacial Engineering and Biotechnology (Germany).

Porous microspheres ($\approx 1 \mu\text{m}$) composed by collagen type I like peptide (RCP) were kindly provided by Fujifilm Manufacturing Europe B.V. (The Netherlands) and coded as RCP_{porous}.

Non-mineralised and mineralised microspheres (i.e. pure RCP, RCPfluidMAG-CT, RCPHA_{RT} and RCPFeHA) were obtained by the as-mentioned emulsification process, as described in the section 2.2.4.

2.5.2 Assessment of rhBMP-2 release from microspheres

2.5.2.1 Microspheres characterisation

Predetermined amount of microspheres were placed in warm solution of agarose (2 wt%) and left to solidify, then were introduced in sample holder and embedded with H-OCT compound (Histo-Line Laboratories, Italy). Sliced samples (30 μm thickness) were obtained by using a microtome cryostat (5000 MC, Histo-Line Laboratories, Italy) and the morphology of microspheres' cross-sections were analysed by using Scanning Electron Microscope (SEM) (FEI Quanta 600, USA) in low vacuum mode with an accelerating voltage of 10 kV and a working distance of 10 mm. RCPFeHA was analysed by using Field Emission Scanning Electron microscopy (FE-SEM, Zeiss Sigma) and Ca, P and Fe distribution was evaluated by microanalysis with Energy dispersive spectroscopy (EDS; Oxford X-Act with 10 mm² silicon drifted detector (SDD)). The results were evaluated by INCA microanalysis Suite software.

Microspheres and rhBMP-2 surface charge were evaluated by using ζ -potential (Zetasizer Nano analyzer (Malvern, UK)). ζ -potential measurements through electrophoretic mobility were performed in disposable folded capillary cells (DTS1061; Malvern, UK) at 25 °C. Microspheres surface charge was evaluated in HEPES buffer (i.e. 0.01 M; pH 7.4) at concentration of 1.2 mg/mL of microspheres, while 12 $\mu\text{g/mL}$ of rhBMP-2 was evaluated. The ζ -potential average was calculated from three separate measurements (100 runs each) in each type of microspheres. The results were showed as Mean \pm SEM.

The contact angle measurements of the as-investigated microspheres were carried out by optical contact angle system stabilized with camera (Contact angle, Drop shape analyser with IDS camera, Kruss GmbH, Germany). Briefly, a pellet of each sample was obtained by pressing ≈ 150 mg of microspheres (100 mbar) and deionized water droplets (2 μL) were carefully dropped onto the pelletized microspheres. Contact angle was captured and calculated by applying fitting method (tangent) with approximation by using Kruss advance software. The results were showed as Mean \pm SEM. The effect of surface morphology and microspheres composition on water adsorption was also evaluated for about 12 minutes, and the results were showed as Mean \pm SD.

Predetermined amount of microspheres in PBS were placed in 24-well plate at 37°C for 24 hours to swell. At each time point (i.e. 1h, 3h, 6h, 9h and 24h) the swollen microspheres were observed by inverted Nikon Ti-E

microscope (Nikon Corporation, Tokyo, Japan) and analysed by Image J. The swelling percentage (S_w , %) was calculated according to the following equation,

$$S_w = \left(\frac{D_s}{D_d} - 1 \right) \times 100$$

Equation 2. Percentage of swelling capacity of microspheres.

(where, D_s and D_d are the diameter of the swollen and dried microspheres, respectively). The data was obtained by assuming a spherical shape and measuring the area of microspheres (acquired by Image J) and translate to microspheres diameter. The results were showed as Mean \pm SEM.

Data of total porosity (i.e. the volume percentage of pores) of RCPFeHA microspheres was determined by mercury intrusion porosimetry and was executed into the range between 0 and 200 MPa (Pascal 140/240 series porosimeter, Thermo Finnigan, U.S.A.).

The chemical interaction of microspheres with rhBMP-2 was evaluated by Fourier Transform Infrared Spectroscopy (FTIR) (Avatar 320 FT-IR, Thermo Nicolet, Canada), as presented in section 2.1.3.

The specific surface area (SSA) of RCP, RCPfluidMAG-CT, RCPHA_{RT} and RCPFeHA was measured by BET method (Brunauer, Emmett e Teller) by using nitrogen adsorption (Sufer, Thermoscientific, U.S.A) and were previously degassed at 50°C under vacuum (about 3.0×10^{-3} torr) for 15 hours.

2.5.3 *In vitro* loading and release of rhBMP-2

In vitro rhBMP-2 loading

rhBMP-2 was loaded to the all tested microspheres by adsorption method and the experimental setup was adapted from (Mumcuoglu et al. 2016). Briefly, in 1.5 mL eppendorf LoBind tubes 50 μ L or 75 μ L of predetermined concentration of rhBMP-2 were pipetted on top of 15 mg of dry non-mineralised microspheres (i.e. RCP and RCPfluidMAG-CT) and mineralized microspheres (i.e. RCPHA_{RT} and RCPFeHA), respectively. Soluble rhBMP-2 was used as a control. All the as-prepared samples were overnight incubated at 4 °C to allow the completely adsorption of rhBMP-2 on microspheres during the swelling process.

In vitro release of rhBMP-2

The used release medium was Dulbecco's Modified Eagle's Medium (DMEM), supplemented with 1 % bovine serum albumin (BSA) and 1 % penicillin-streptomycin (100U/mL - 100 μ g/mL). After overnight of rhBMP-2 adsorption, predetermined volume of release medium was added on top of swollen microspheres (i.e. 950 μ L in RCP and RCPfluidMAG-CT and 925 μ L in RCPHA_{RT} and RCPFeHA) to obtain a final concentration of 900 ng/mL or 400 ng/mL of rhBMP-2. Samples were incubated at 37 °C, under three different conditions: agitation (\approx 100rpm), static and pulsed electric magnetic field (PEMF).

At given time points up to 14 days, the release medium was collected after centrifugation at 3000 rpm for 5 min and was replaced by fresh release medium (900 μ L). After 14 days of release assay, 900 μ L of urea solution (6 M) was added to the microspheres and were incubated 4 hours at 37 °C. This supernatant was

collected by centrifugation and dialyzed with cellulose membrane (3500 D, Medicell Membranes Ltd, UK), for 3 days at 4 °C. milli-Q water was replaced twice a day for the completely removal of the salt. Meanwhile, all the microspheres were washed twice with PBS and the supernatant was collect for further analysis. Then, microspheres and soluble rhBMP-2 were digested by using predetermined concentration of collagenase solution in DMEM (i.e. 1 mg/mL, 2 mg/mL, 5 mg/mL and 10 mg/mL) and 900 μL was added to the microspheres and incubated two days at 37°C. All the supernatants were further analysed by sandwich enzyme-linked immunosorbent assay (ELISA) development kit specific for rhBMP-2 (PeproTech, USA), as described below.

Enzyme-linked immunosorbent assay (ELISA)

The detection of rhBMP-2 was investigated by using sandwich ELISA technique, according to the manufacturer's protocol. Briefly, the used 96-well plate was prepared with a known quantity (0.50 μg/mL) of bound antibody to capture the rhBMP-2, then the non-specific binding sites were blocked with solution of bovine serum albumin (1 %) and unknown released rhBMP-2 was added to the plate. A specific detection antibody (1 μg/mL) was added to “sandwiches” the rhBMP-2, then enzyme-linked secondary antibodies were applied to bind detection antibody and unbounded conjugates (antibody-enzyme) were washed off. By the end, substrate was added and was enzymatically converted to a color and color development was monitored with an ELISA plate reader at 405 nm and 620 nm (Gan & Patel 2013). The concentration of unknown released rhBMP-2 was quantified relative to a rhBMP-2 standard calibration curve (ranging from 47 to 3000 pg/mL) run on the same plate, while the percentage of released rhBMP-2 was calculated respect to the positive control (soluble rhBMP-2, at concentration 900 or 400 ng/mL).

Three samples of each group and controls were investigated and the amount or percentage of rhBMP-2 released was expressed as Mean±SEM.

2.5.4 Loading efficiency of microspheres and interaction with rhBMP-2

Quantitative efficiency

In order to evaluate the loading efficiency of all the tested microspheres, predetermined concentration of rhBMP-2 was adsorbed on 15 mg of microspheres and was kept overnight at 4°C.

Further, to the microspheres was added milli-Q water to obtain a final concentration of 900 ng/mL of rhBMP-2 and then washed three times with milli-Q water. At each washing step the milli-Q water was collected by centrifugation (3000 rpm, 5 minutes) and the non-adsorbed rhBMP-2 was evaluated by ELISA development kit. The percentage of loading efficiency (LE, %) of 15 mg of microspheres were calculated, as follow:

$$LE = \left(\frac{Sol_{rhBMP2} - Sum_{nads rhBMP2}}{Sol_{rhBMP2}} \right) \times 100$$

Equation 3. Calculation of loading efficiency of microspheres.

(where, Sol_{rhBMP2} is soluble rhBMP-2 and $Sum_{nads rhBMP2}$ is sum of non-adsorbed rhBMP-2 found in each washing step). The as-showed data were acquired from triplicated samples and presented as Mean+SEM.

rhBMP-2 interaction with microspheres

To evaluate the interaction of rhBMP-2 with all tested microspheres, the previous washed samples were freeze-dried (0.1 mbar) and evaluated by FTIR analysis, following the protocol showed in the section 2.1.3. The relevant vibration modes were analysed by deconvolution and curve fitting technique (Fit by Sum with Lorentzian curve) by using MagicPlot Student 2.5.1 software.

Qualitative efficiency

To further identify the rhBMP-2 adsorption efficiency from RCP, RCPfluidMAG-CT, RCPHA_{RT} and RCPFeHA, predetermined concentration of texas red rhBMP-2 was adsorbed by the microspheres overnight at 4°C. Meanwhile, empty microspheres, used as control and solution of rhBMP-2 was substituted by milli-Q water. Further, predetermined amount of milli-Q water was added to the microspheres to reach a final rhBMP-2 concentration of 900 ng/mL. Non-adsorbed rhBMP-2 was removed by centrifugation and washed three times with milli-Q water. Fluorescent images from empty microspheres, microspheres with 900 ng/mL of rhBMP-2 and washed microspheres were acquired by Inverted Ti-E fluorescence microscope (Nikon) with properly filter (i.e. Excitation of 557 nm and emission of 576 nm).

2.5.5 *In vitro* rhBMP-2 bioactivity assay

rhBMP-2 bioactivity was investigated by using C2C12 BRE-Luc bioassay cell line. To generate the BMP reporter cell line, C2C12 cells were stably transfected with pGL3(BRE)-luciferase reporter construct, as reported in (Herrera & Inman 2009; Brum et al. 2015) and were denominated as C2C12 BRE-Luc cell line. C2C12 BRE-Luc cell line were incubated in complete growth medium (i.e. Dulbecco's modified Eagle's medium without phenol (DMEM) containing 10 % of fetal calf serum (FCS), 1 % penicillin-streptomycin (100 U/mL-100 µg/mL) and 1 mM Sodium Pyruvate, then 200 µg/mL of Geneticin (G418, Thermo Fisher Scientific, USA) was added after 4 hours of plating the cells. Cell culture was kept at 37°C under humidified incubator and in an atmosphere of 5% CO₂. Cells were detached from culture flasks by tripsinization, centrifuged (i.e. 10 minutes at 250 g) and re-suspended. Cell number and viability were assessed by trypan-blue dye exclusion test.

For the rhBMP-2 reporter assay, new investigations on rhBMP-2 release were carried out at final concentration of 900 ng/mL, by following the adsorption assay as mentioned in section 2.5.3. Therefore, the used release medium was growth medium of C2C12 BRE-Luc cell line and the experiments were performed at 37 °C in an atmosphere of 5% CO₂. C2C12 BRE-Luc cell line (≤P19) were seeded into white-walled 96-well culture plates at a density of 10 000 cells per well in 50 µL of complete growth medium. After 30 min, 50 µL of growth medium with released rhBMP-2 from RCP, RCPHA_{RT} and RCPFeHA, growth medium with soluble rhBMP-2 for the controls (900 ng/mL), as well as standard calibration curve with soluble rhBMP-2 (900 ng/mL to 1.6 ng/mL), were added to the well plate in duplicate and incubated for 24 hours at 37°C in an atmosphere of 5% CO₂. Furthermore, lysis reconstitution buffer and lyophilized luciferin (Steady Lite Plus, Perkin Elmer Inc., USA) were combined and 100 µL of the as-prepared solution was added to each

well. The plate was shaken for 15 minutes in the dark and then luminescence signal generated by luciferin was measured 6 seconds by using a Wallac VICTOR Multilabel reader (Perkin Elmer, USA).

On the other hand, the percentage of rhBMP-2 bioactivity (BB, %) was calculated by using the following equation:

$$BB, \% = \left(\frac{Luc_{act}}{Rel_{rhBMP-2}} \right) \times 100$$

Equation 4. Calculation of rhBMP-2 bioactivity.

Where, Luc_{act} was defined as luciferase activity obtained by the assay with C2C12 BRE-Luc cell line and the amount of released rhBMP-2 (ng) calculated by the ELISA sandwich method was denominated as $Rel_{rhBMP-2}$. The results were presented in percentage and as Mean±SEM of triplicates.

2.5.6 Optimisation of rhBMP-2 adsorption from microspheres

rhBMP-2 release studies from RCP, RCPHA_{RT} and RCPFeHA were performed by following two strategies: i) the specific surface area was used to define the amount of microspheres and the concentration of rhBMP-2 and ii) equal amount of microspheres with equivalent concentration of rhBMP-2 adsorbed on the microspheres were investigated (Table 4). The as-mentioned rhBMP-2 concentrations were adsorbed by the microspheres at 4°C and predetermined volume of cell medium was added to obtain a final concentration of 900 ng/mL. After 1 day of releasing studies, the supernatant was collected by centrifugation and evaluated in presence of C2C12 BRE-Luc cell line. For the selection of the best-in-class rhBMP-2 adsorption strategies, the results were presented as luciferase activity (RLU), from Mean±SEM of triplicates.

Table 4. Parameters used in both strategies of rhBMP-2 release, (SSA: rhBMP-2 adsorption take into account the specific surface area of the microspheres; No SSA: rhBMP-2 adsorption without consider specific surface area).

Microspheres	SSA			No SSA		
	Weight of microspheres, mg	Initial concentration of rhBMP-2 to be adsorbed, µg/mL	Volume of rhBMP-2 solution, µL	Weight of microspheres, mg	Initial concentration of rhBMP-2 to be adsorbed, µg/mL	Volume of rhBMP-2 solution, µL
RCP	3.23	83.65	10.76	15	18	50
RCPHA _{RT}	15	12	75	15	12	75
RCPFeHA	2.25	80.2	11.25	15	12	75

2.5.7 In vitro rhBMP-2 release under pulsed electromagnetic field (PEMF)

rhBMP-2 was adsorbed by RCPHA_{RT}, RCPfluidMAG-CT and RCPFeHA and a final concentration of 400 ng/mL was achieved. The releasing studies were performed in static and under pulsed electric magnetic field (PEMF).

PEMF is composed by polymethylmethacrylate tube carrying a home-made eppendorf support and two solenoids (i.e., Helmholtz coils, the planes of which were parallel). The generated magnetic field and the induced electric field were perpendicular and parallel to the samples, respectively. Eppendorf's were horizontally introduced into the home-made support and were 5 cm distant from each solenoid plane (Figure 8). A Biostim SPT pulse generator (Igea, Carpi, Italy) was used to power the solenoids. According to the position of the solenoids and the characteristics of the pulse generator, the electromagnetic stimulus had the following parameters: intensity of the magnetic field equal to 2.0 ± 0.2 mT, amplitude of the induced electric tension equal to 5 ± 1 mV, frequency of 75 ± 2 Hz, and pulse duration of 1.3 ms. The rhBMP-2 adsorption and releasing studies were followed by the previous protocol, as showed in section 2.5.3.

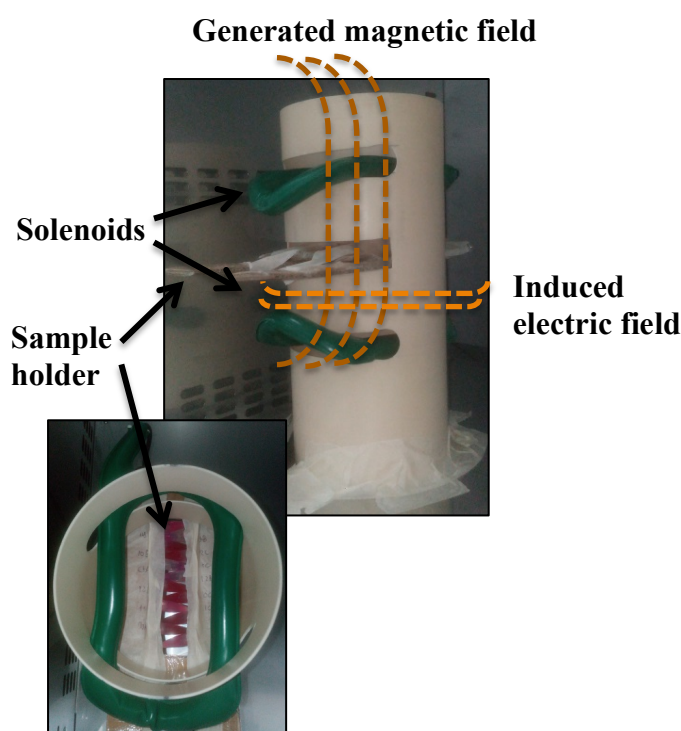


Figure 8. Pulsed electric magnetic field used on rhBMP-2 release.

2.5.8 Statistical analysis

The significant differences of rhBMP-2 adsorption strategies and the effect of porosity on rhBMP-2 release were analysed with two-way ANOVA by Bonferroni's multiple comparison tests. The significant differences on rhBMP-2 release, the effect of microspheres composition on rhBMP-2 release and percentage of rhBMP-2 bioactivity were evaluated by one-way ANOVA with Tukey's multiple comparisons.

Values of $p < 0.05$ were accepted as statistically significant.

2.6 Preliminary investigations on Scaffold fabrication

2.6.1 Scaffolds fabrication

As showed in the section 2.1.2, biomineralisation process was assessed to produce mineralised biomaterials with superparamagnetic properties. For the fabrication of the scaffolds the as-prepared slurries of RCP/FeHA (60/40) at 40, 50 and 60 °C were used to produce the scaffolds. Biomineralised slurries were placed in 48 well plate (i.e. 1 mL per each well), then the material was frozen at -20°C, then the samples were introduced in pre-cooled freeze-drying and the cycle of drying was performed for 48 hours under vacuum (≈ 0.1 bar), and a final porous structure was achieved. Scaffolds were crosslinked under vacuum by DHT at 160 °C for 48 hours.

2.6.2 Scaffold characterisation

Morphological characterisation

The as-produced scaffolds were cut in longitudinal cross-section and were analysed by using Scanning Electron Microscope (SEM) (FEI Quanta 600, USA) in low vacuum mode with an accelerating voltage of 10 kV and a working distance of 10 mm.

Swelling tests

Swelling extent was determined by conventional gravimetric method, in order to observe the water absorption ability of the scaffolds, where the swollen and dried weight of the scaffolds were considered. Crosslinked scaffolds with ≈ 0.04 g in weight were used and swelling tests were performed in PBS (pH 7.4) under incubator with agitation (≈ 100 rpm), at 37°C. After 1h, 3h, 18h and 24h, swollen samples were weighted. RCP/HA (60/40, 40°C) scaffold was used as a control sample. The swelling percentage (S, %) of the scaffolds was calculated as follow:

$$S = \left(\frac{W_s - W_d}{W_d} \right) \times 100$$

Equation 5. Calculation of swelling capacity of the scaffolds.

Where as W_s was the weight of the swollen scaffold and W_d was the weight of the dried scaffold. Three samples of each group were analysed and the results were showed as Mean \pm SEM.

Chapter 3. Results

3.1 Application of biomineralisation process to obtain new hybrid biomaterials with superparamagnetic properties

3.1.1 Collagen I based recombinant peptide

Biomineralisation investigations were carried out in presence of an innovative biomaterial produced by fermentation process and without animal sources and has been commercialized as Cellnest®, by Fujifilm Manufacturing Europe B.V. (The Netherlands). The as-mentioned biomaterial is recombinant peptide based on human collagen type I, α I chain, (RCP) and was designed and addressed to new devices for bone tissue regeneration. RCP is enriched of RGD motif (i.e. arginine – glycine – aspartate) and presented promising properties, such as high cellular adhesiveness, safety, biocompatible, biodegradable and bioabsorbable and can be formulated in scaffolds, microspheres, among others (Van Boxtel 2013; Boer A., Urk H., Bouwstra J. 2012; Mumcuoglu et al. 2016; Ramírez-Rodríguez et al. 2016; Patrício; et al. 2017). The recombinant peptide has an extremely uniform molecular weight distribution of approximately 51 kD, 571 amino acid in length and size distribution about 10 nm (Figure 9A, 9B).

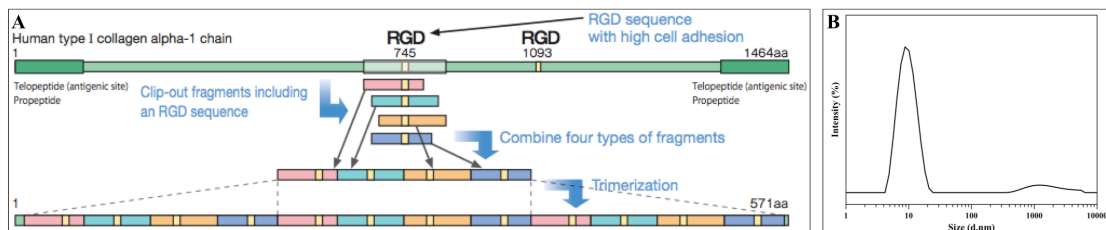


Figure 9. Composition of RCP (A) and size distribution profile of RCP (B).

3.1.2 Development of materials with magnetic and bone-like properties

Biomineralisation process adapted by (Sandri et al. 2010; Tampieri et al. 2003) was used to synthesise biomimetic biomaterials by mediation of neutralisation process and nucleation of hydroxyapatite nanocrystals into collagen fibrils was obtained.

Herein, the biomineralisation of RCP was investigated by following the as-mentioned methodology. RCP is a small molecule, water-soluble and does not form fibres by varying the pH, as in the case of collagen type I. During the biomineralisation process for a completely involvement and interaction with mineral phase, biomineralisation synthesis was kept under stirring for 2 hours and for the formation of low crystalline hydroxyapatite with magnetic properties, several parameters were evaluated, as showed below.

Effect of synthesis temperature and Fe^{2+}/Fe^{3+} molar ratio mineralised with low content of FeHA

The effect of synthesis temperature on phase composition and magnetic properties were evaluated in biomineralised materials synthesised with low amount of inorganic phase (10 wt%) and the synthesis

parameters were presented in Table 5. Iron-containing hybrid biomaterials were synthesised at 25 °C and at 40 °C and iron-free biomineralised material was synthesised at 40 °C.

Table 5. Parameters used in the biomineralisation process.

Sample	Biomineralisation temperature (°C)	Fe/Ca, mol %	Fe ²⁺ /Fe ³⁺ , mol	RCP/FeHA, wt%
RCP/FeHA (90/10; 3:2; 25)	25		3:2	
RCP/FeHA (90/10; 3:2; 40)	40	20	3:2	90/10
RCP/FeHA (90/10; 5:4; 40)	40		5:4	
RCP/HA (90/10)	40	---	---	90/10

Biomineralised materials presented a diffraction peak at about 20 θ°, which reflects the presence of RCP in the biomineralised materials. High hydroxyapatite crystallinity without formation of new phases was showed in RCP/HA, while low synthesis temperature (i.e. 25 °C) promotes the formation of very low crystalline hydroxyapatite, as showed in RCP/FeHA (90/10; 3:2; 25). By increasing the synthesis temperature and changing the Fe²⁺/Fe³⁺ molar ratio the crystallinity was increased. By comparing RCP/FeHA with RCP/HA low crystalline hydroxyapatite was obtained, probably due to the presence of iron ions into apatite lattice (Figure 10).

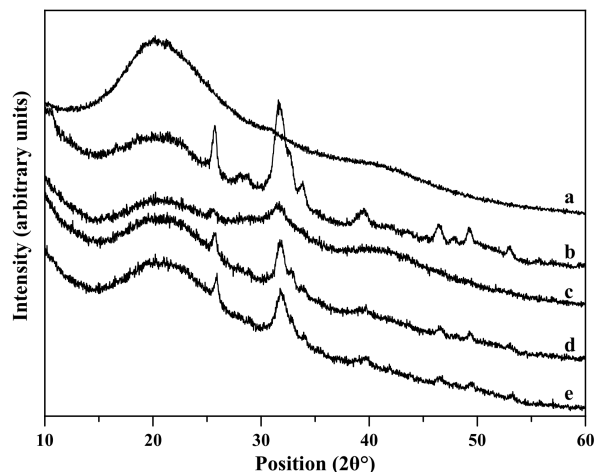


Figure 10. XRD pattern of the as-produced biomaterials. a) RCP; b) RCP/HA (90/10); c) RCP/FeHA (90/10; 3:2; 25); d) RCP/FeHA (90/10; 3:2; 40); e) RCP/FeHA (90/10; 5:4; 40).

Magnetic properties of the as-synthesised biomaterials were evaluated with susceptometer balance and no magnetisation was detected. Moreover, by placing those materials in contact with neodymium magnet, very low magnetisation was presented.

The production of biomineralised biomaterials was showed, although very low magnetisation was demonstrated. The following step was to increase the amount of mineral phase and to evaluate the effect on magnetic properties.

Effect of organic and inorganic ratio

As follow the previous results, $\text{Fe}^{2+}/\text{Fe}^{3+}$ molar ratio (3:2), Fe/Ca molar ratio (20 mol%) and temperature (40 °C) was maintained and the mineral content in the mineralised materials was changed. The effect of mineral content on phase composition was evaluated by FTIR and XRD analysis. FTIR spectrum were showed in Figure 11A and the main vibration modes of RCP (i.e. Amide I, II and III) and formation of hydroxyapatite (i.e. vibration modes of phosphate groups) and the presence of carbonate vibration bands (at 873 cm^{-1}), were presented, thus indicating the formation of carbonate-substituted hydroxyapatite, which is similar to natural bone apatite (Figure 11B). FTIR spectra can also be used to evaluate the calcium phosphate crystallinity index or splitting factor (SF) on biomineralised materials. The results showed that the biomineralised samples presented low splitting factor compared to the calcium phosphate (i.e. splitting factor = 3.29), due to the poorly-crystalline apatite formed during the biomineralisation process (Table 6).

Previous results were also confirmed by XRD analysis (Figure 11C). Low crystalline apatite was formed in all the synthesised materials as assigned by the planes at $(002\text{ (}25^\circ\text{)}; 211(31^\circ); 300(32^\circ)$ (ref. code: 00-0090432). Biomineralised materials with 80 wt% of mineral amount presented small diffraction peak at $35.423\text{ }2\theta^\circ$ that might be related with the formation of secondary phase, such as iron oxide (e.g. magnetite or maghemite) (reference code: 00-019-0629). The phase composition of RCP/FeHA (60/40) was similar with bone tissue (Figure 11D).

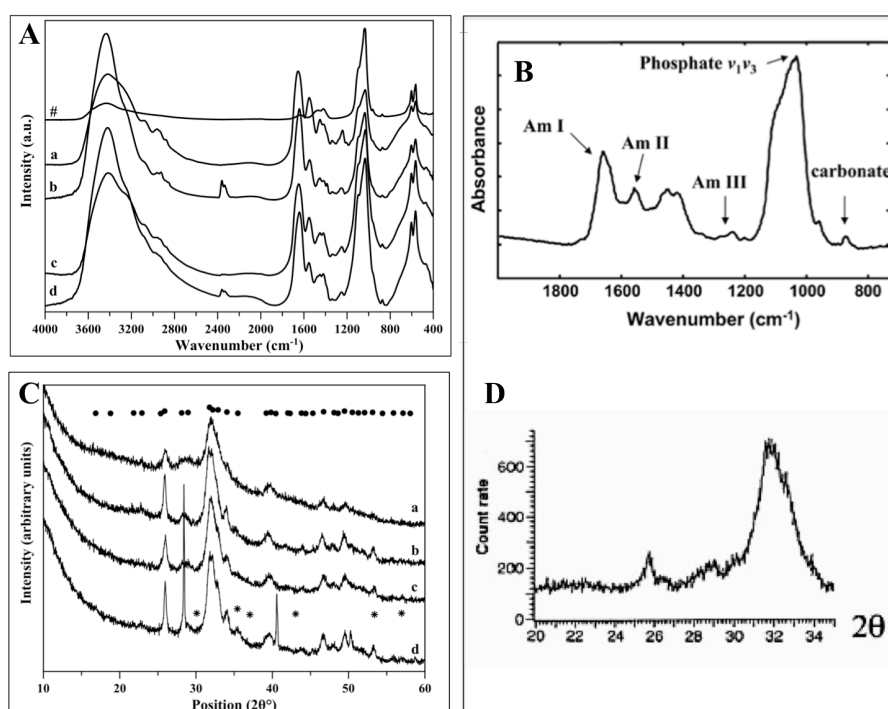


Figure 11. (A) FTIR spectrum and (C) XRD pattern of the as-produced biomaterials, #) Calcium phosphate, 40 °C; a) RCP/FeHA (60/40); b) RCP/FeHA (40/60); c) RCP/FeHA (30/70); d) RCP/FeHA (20/80), (* iron oxide pattern with reference code: 00-019-0629; • calcium phosphate hydroxide with reference code: 00-0090432); B) Typical infra-red spectra and XRD pattern (D) of bone tissue (Boskey 2007; Vallet-Regi & Gonzalez-Calbet 2004).

The as-synthesised biomaterials presented low-crystalline apatite similar to bone tissue composition and the presence of Ca, P, Fe (wt%), Ca/P (mol) and Fe/Ca (mol%) were evaluated by ICP-OES (Table 6). By increasing the mineral ratio in the hybrid biomaterials, slightly increase of Ca, P and Fe was showed, while Fe/Ca ratio was closer to the theoretical one, i.e. 20 mol%.

The mineral amount on the different samples was evaluated by using thermogravimetric analysis, and no significant different were showed with theoretical ones (Table 6).

Magnetic properties of the as-obtained biomaterials were evaluated by susceptometer balance (Table 6), and an improvement on magnetic properties was showed, mainly in RCP/FeHA (20/80). The high magnetisation in RCP/FeHA (20/80) was suggested by the formation of secondary phase, as showed by XRD results.

Table 6. Splitting factor, quantitative evaluation of different elements, mineral amount and magnetisation of biomineralised materials. (values obtained by: [#] v4 phosphate group analysed by FTIR; [¥] ICP-OES; ^{} TGA analysis; [§] Susceptometer balance; * (Dorozhkin 2011)).**

	Bone *	RCP/FeHA (60/40)	RCP/FeHA (40/60)	RCP/FeHA (30/70)	RCP/FeHA (20/80)
[#] Splitting factor	---	2.276	2.393	2.327	2.524
[¥] Ca (wt%)	34.8	12.08±0.41	17.62±0.58	23.37±0.43	18.81±0.77
[¥] P (wt%)	15.2	4.26±0.10	7.28±0.17	7.92±0.18	6.29±0.22
[¥] Fe (wt%)	---	3.14±0.10	5.55±0.15	6.05±0.11	4.8751±0.23
Ca/P (molar)	1.71	2.19±0.18	1.87±0.15	2.28±0.13	2.31±0.25
(Fe+Ca)/P (molar)	---	2.60±0.20	2.29±0.17	2.70±0.15	2.74±0.27
Fe/Ca (mol %)	---	18.65±1.70	22.61±1.94	18.57±0.95	18.60±2.30
Fe/(Ca+Fe) (mol %)	---	0.16±0.01	0.18±0.01	0.16±0.01	0.16±0.02
^{**} RCP/FeHA, wt%	---	54/46	36/64	26/74	16/84
[§] Magnetisation, emu.g ⁻¹	---	0.005±0.00	0.0185±0.02	0.015±0.00	0.18±0.02

Effect of Fe²⁺/Fe³⁺ molar ratio and Fe/Ca molar ratio

RCP/FeHA (60/40) showed similar composition with bone tissue, while RCP/FeHA (20/80) presented high mineral content and magnetisation values. Take into account this result an improvement on magnetic properties were performed on RCP/FeHA (60/40) synthesised at 40 °C and Fe/Ca molar ratio (i.e. 20 and 45) and Fe²⁺/Fe³⁺ molar ratio (3:2 and 5:4) were evaluated (Table 7).

Table 7. Parameters used in the biomineralisation process.

Sample	Biomineralisation temperature (°C)	Fe/Ca, mol %	Fe ²⁺ /Fe ³⁺ , mol	RCP/FeHA, wt%
RCP/FeHA (20; 3:2)	40	20	3:2	60/40
RCP/FeHA (45; 3:2)		45		
RCP/FeHA (20; 5:4)		20	5:4	
RCP/FeHA (45; 5:4)		45		

The effect of Fe²⁺/Fe³⁺ molar ratio and Fe/Ca molar ratio on phase composition and magnetic properties were evaluated. FTIR spectra indicated the presence of RCP in all the as-synthesised biomaterials, as assigned by the main amide groups (i.e. Amide I, Amide II and Amide III). In RCP/FeHA (20; 5:4) and RCP/FeHA (45; 5:4) a strange configuration of phosphate groups (i.e. ν_3 and ν_4) was showed (Figure 12A). By XRD analysis the mineral phase was investigated and narrow diffraction peaks in that materials, suggested the formation of unreacted iron chloride (Figure 12B). A very low crystalline hydroxyapatite was formed in RCP/FeHA (45; 3:2) and non-magnetisation was detected with susceptometer balance. The results suggested that by increasing the Fe/Ca molar ratio or Fe²⁺/Fe³⁺ molar ratio do not improves the magnetic properties.

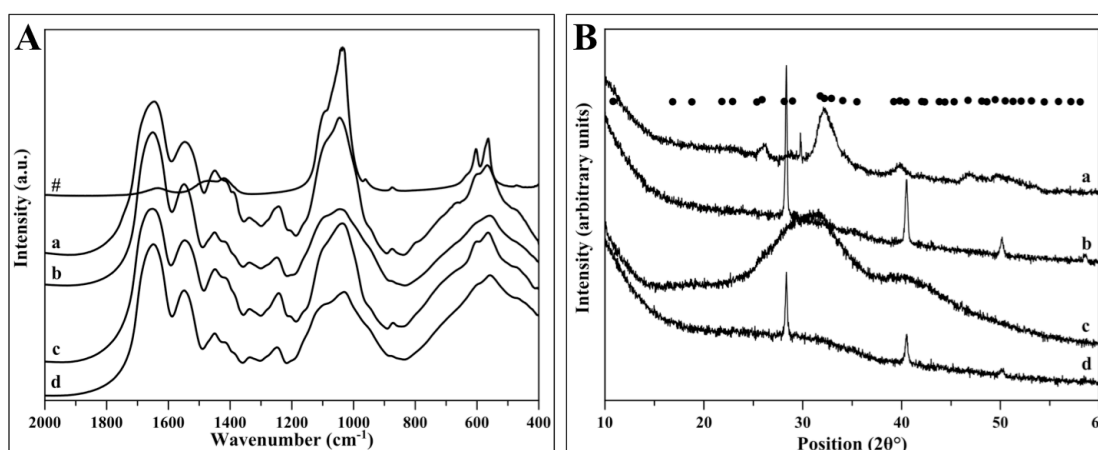


Figure 12. (A) FTIR spectrum and (B) XRD pattern of the as-produced biomaterials, #) Calcium phosphate, 40 °C; a) RCP/FeHA (20; 3:2); b) RCP/FeHA (20; 5:4); c) RCP/FeHA (45; 3:2); d) RCP/FeHA (45; 5:4), (• calcium phosphate hydroxide with reference code: 00-0090432).

Effect of temperature

Regarding to the previous results, magnetic properties were not improved. The hybrid biomaterial that showed relevant properties was RCP/FeHA (3:2, 20) with 40 wt% of mineral phase. The following investigation was based on keeping the optimised parameters and the synthesis temperature was changed. In this study, iron-containing biomaterial was synthesised at 40 °C, 50 °C and 60 °C. Phase composition was evaluated by FTIR and XRD analysis. The presence of organic and inorganic phase was evident by the assignment of the main peaks of RCP and calcium phosphate formation (Figure 13A). Splitting factor

indicates an increase of crystallinity degree from 2.17, 2.45 to 2.46 for materials synthesised at 40, 50 and 60 °C, respectively. By increasing the synthesis temperature the crystallinity of the biomaterialised materials was increased, as showed by the XRD pattern (Figure 13B). A new diffraction peak was presented in the material synthesised at 60 °C (Figure 13B*), suggesting that by increasing the synthesis temperature induces the formation of secondary phase, as iron oxides (e.g. magnetite or maghemite). Magnetite tends to form by increase of temperature during the synthesis process (Tampieri et al. 2012). Magnetic properties were also investigated, 0.005 emu.g⁻¹, 0.007 emu.g⁻¹ and 0.17 emu.g⁻¹ were obtained in the materials synthesised at 40 °C, 50 °C and 60 °C, respectively.

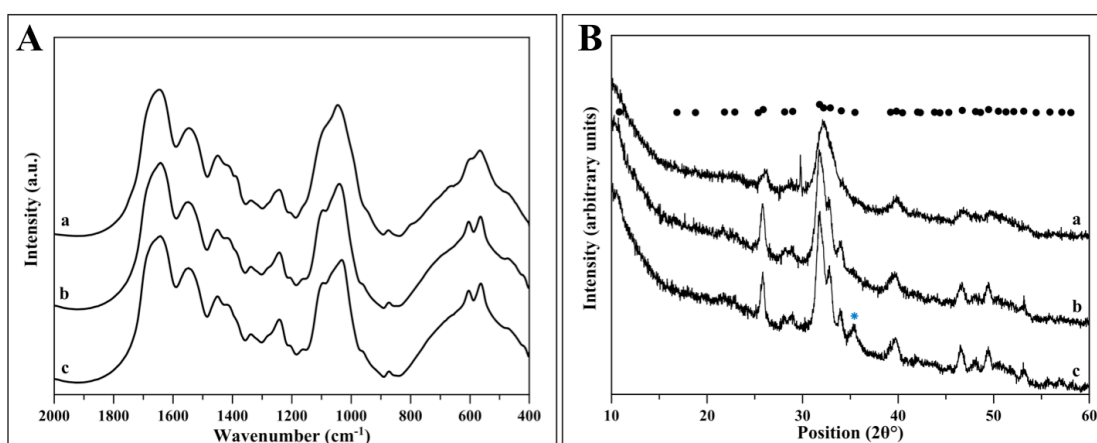


Figure 13. (A) FTIR spectrum and (B) XRD pattern of the as-produced biomaterials, a) RCP/FeHA, 40 °C; b) RCP/FeHA, 50 °C; c) RCP/FeHA, 60 °C; (• calcium phosphate hydroxide with reference code: 00-0090432; * iron oxide diffraction peaks with reference code: 00-019-0629).

Regarding to the as-mentioned results, in the following section was presented the production of two iron containing mineralised materials (40 wt% of mineral extend; Fe/Ca (20 mol%); Fe²⁺/Fe³⁺ (3:2)). On the other hand, the effect of single ions into RCP matrix and the effect of iron in apatite lattice, by using as a control RCP mineralised with hydroxyapatite with the same synthesis conditions were presented.

3.2 New bioactive bone-like microspheres with intrinsic magnetic properties obtained by bio-inspired mineralisation process

3.2.1 Physicochemical and morphological characterisation of mineralised and non-mineralised materials

Compositional and crystallographic analysis

The XRD analysis of pure RCP and the as-obtained hybrid mineralised materials, reported the presence of an amorphous phase that can be ascribed to RCP, as identified by a broad diffraction peak located in the 2θ region 10-30 (Figure 14). In the mineralised compounds a nanocrystalline hydroxyapatite phase was also detected, in agreement with the JCPDS card number: 09-0432 (Figure 14), without any evidence of other calcium phosphate crystalline phases. The full profile analysis of the XRD spectra reported smaller crystallites in RCPFeHA40 and RCPFeHA60 materials, when compared to iron-free materials (i.e. RCPHA40 and RCPHA60), as well as a slight distortion of the lattice, particularly an increase of the a axis and a decrease of c axis (Table 8), thus resulting in a slight lattice volume expansion ($\sim 0.2\%$) in comparison with iron free RCPHA materials. Besides, RCPFeHA60 exhibited an additional diffraction peak at $2\theta \approx 35.4$ (Figure 14 e), indicating the formation of magnetite as secondary phase (in agreement with the JCPDS card number: 01-079-0417). Semi-quantitative phase analysis reported an amount of about 8% of iron oxide formed in RCPFeHA60.

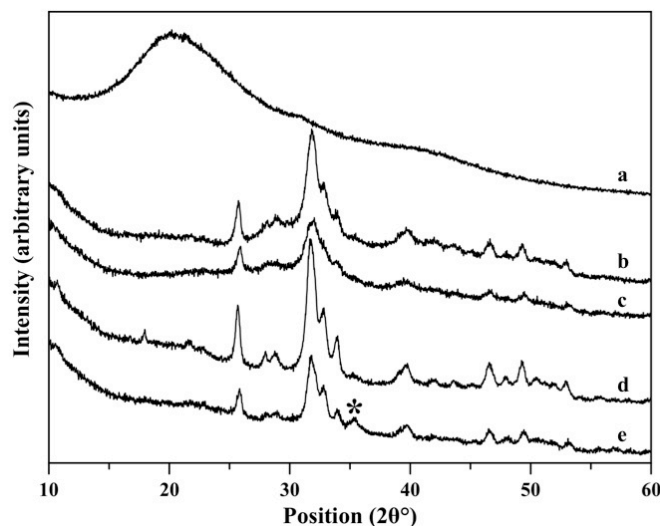


Figure 14. XRD pattern of RCP (a) and of the as-obtained mineralised materials: b) RCPHA40; c) RCPFeHA40; d) RCPHA60 and e) RCPFeHA60. Iron oxide formation in RCPFeHA60 is indicated by *.

Figures 15A-B show FTIR spectra obtained from RCP and mineralised materials. RCP shows large absorption band in the wavelength region $3600-2600\text{ cm}^{-1}$ assigned to the OH^- stretching of water molecules and at $\approx 3074\text{ cm}^{-1}$ could be attributed to the N-H stretching for amide A. Then, three main peaks attributed to the amide groups (i.e. $\approx 1637\text{ cm}^{-1}$ for Amide I, 1550 cm^{-1} for Amide II, 1240 cm^{-1} for

Amide III) were detected, as well as an absorption band at 1390 cm^{-1} , ascribed to the carboxylic group COOH^- (Figure 15B). Besides, in Figures 15A–B the characteristics vibration modes generated by the phosphate group present in the hydroxyapatite phase (i.e. ν_1 and ν_3 stretching at $\approx 960\text{ cm}^{-1}$ and $\approx 1030\text{--}1100\text{ cm}^{-1}$, respectively, and ν_4 bending modes at $\approx 603\text{--}565\text{ cm}^{-1}$) were detected (Gomez-Morales et al. 2013; Yang et al. 2005).

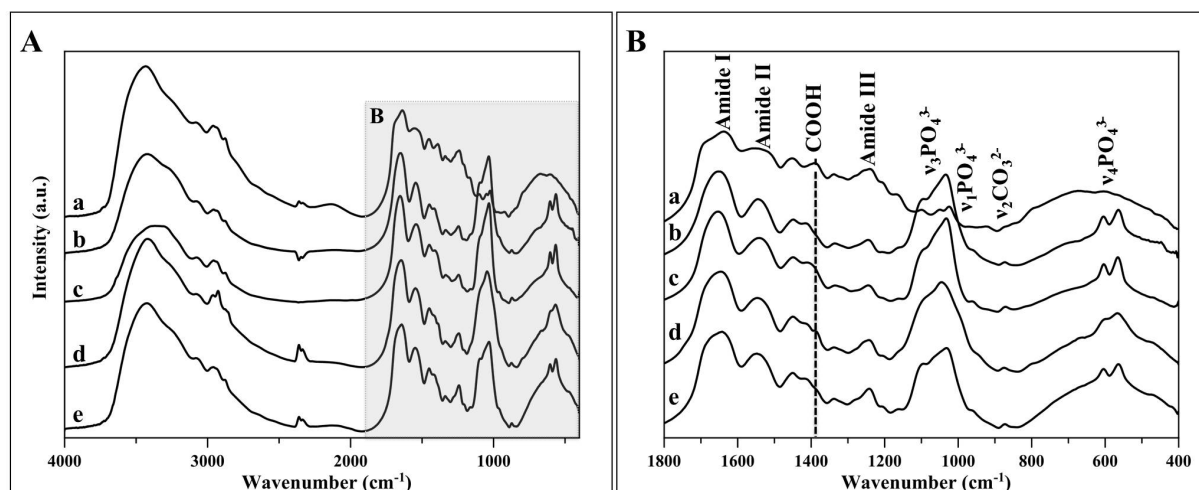


Figure 15. FTIR spectra of mineralised materials. a) RCP; b) RCPHA40; c) RCPHA60; d) RCPFeHA40 and e) RCPFeHA60. A: full pattern, B: a detail evidencing the position of the absorption bands related to amide, carboxylic groups and phosphate groups.

Narrower phosphate bands were associated to iron-free materials (i.e. RCPHA40 and RCPHA60) and, also, to iron-containing materials (i.e. RCPFeHA60) synthesised at higher temperature (Figure 15B and splitting factors in Table 8). The partial replacement of phosphate ions by carbonate (in B position, i.e. the phosphate site) in the HA phase was confirmed by the presence of absorption bands in the FTIR spectra of mineralised materials attributed to the ν_2 stretching modes at $875\text{--}870\text{ cm}^{-1}$ (Addison et al. 2015), which were the only ones visible, as the ν_3 bending modes of carbonate, located at $\sim 1450, 1420\text{--}1400\text{ cm}^{-1}$, were overlapped by the absorption bands generated by the organic matrix (Sprio et al. 2012; Gaihre et al. 2008).

Table 8. Splitting factor (SF) and cell parameters of mineralised materials.

	SF	a (Å)	c (Å)	c/a	Vol (Å ³)	D _{av} (nm)	D ₃₀₀ (nm)	D ₀₀₂ (nm)
RCPHA40	2.63	9.422	6.910	0.733	531.3	13.7	11.3 ± 0.9	22.4 ± 1.1
RCPHA60	2.95	9.424	6.905	0.733	531.1	17.1	15.8 ± 0.6	25.1 ± 0.7
RCPFeHA40	2.17	9.445	6.889	0.729	532.3	11.6	11.6 ± 4.5	23.1 ± 1.2
RCPFeHA60	2.46	9.450	6.890	0.729	532.9	11.3	17.8 ± 1.3	23.1 ± 1.3

FTIR spectra recorded on the hybrid materials showed a slight shift of the adsorption band corresponding to carboxylic group and a higher intensity of the amide II band, if compared to pure RCP. In particular, the carboxylic group band shifted from 1390 cm^{-1} detected in RCP sample to 1402 cm^{-1} (RCPHA40) and 1411 cm^{-1} (RCPHA60). In RCPFeHA40, the vibration modes of carboxylic groups were detected at 1411 cm^{-1} and 1386 cm^{-1} , while in RCPFeHA60 were ascribed at 1413 cm^{-1} , and 1384 cm^{-1} (Mercado et al. 2014).

Further investigation of the interaction between the organic RCP matrix and the inorganic phase was carried out by reacting RCP with well-defined amounts of relevant cations used on biomineralisation process (i.e. Ca^{2+} , Fe^{2+} and Fe^{3+}). Figures 16A – 16B show the FTIR spectra of RCP/Ca, RCP/Fe2 and RCP/Fe3 materials, as obtained by assembling RCP in presence of Ca^{2+} , Fe^{2+} and Fe^{3+} ions, respectively. Both RCP and RCP/Ca solutions were characterised by basic pH (≈ 10 and 12 , respectively); chemical interactions in RCP/Ca were evidenced by an intensity increase and shift of both amide I and II bands (Figure 16A-B and Table 9), possibly induced by the linking with calcium ions. On the other hand, RCP/Fe2 and RCP/Fe3 were characterised by an acidic pH (i.e. $\text{pH} = 6$ and 3 , respectively), consequently in order to reproduce the synthesis conditions of iron-containing mineralised RCP, the pH was adjusted to neutral values by addition of NaOH. In such conditions the band shift in Amide I and II was negligible (Table 9), moreover take also into account the previous results from mineralised materials, we hypothesised that amide and COOH^- groups resulted significantly involved in the biomineralisation process, as sites for heterogeneous nucleation of the apatite nanophase.

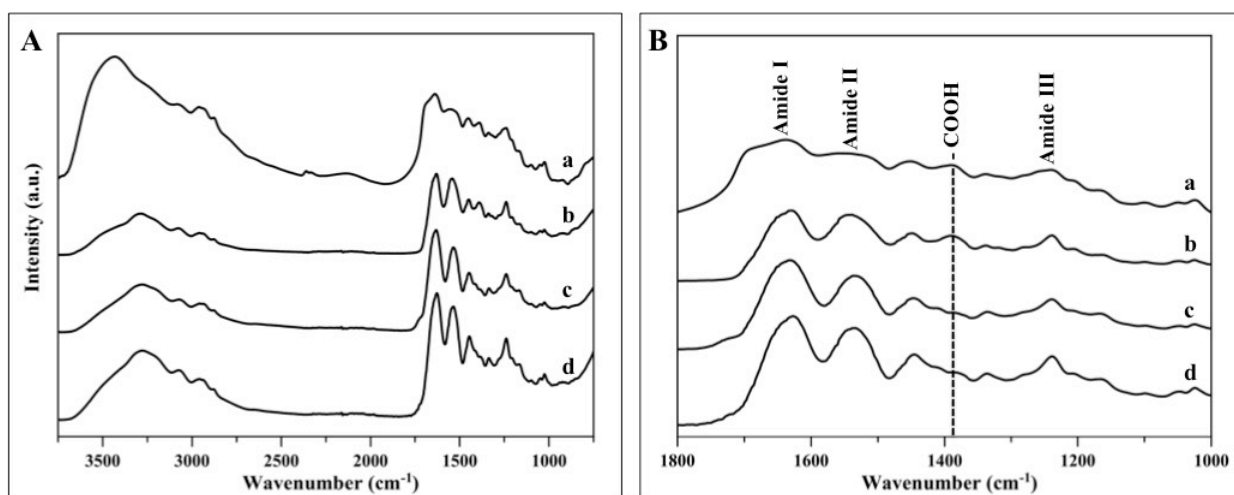


Figure 16. A) FTIR spectra of RCP and mineralised materials. B) a detail on absorption bands relevant for linking the inorganic phase. a) RCP; b) RCP/Ca; c) RCP/Fe3; d) RCP/Fe2.

Table 9. FTIR wavenumber obtained for amide I, amide II and carboxylic group in RCP, RCP/Ca, RCP/Fe3, RCP/Fe2 and in RCP/Fe3 and RCP/Fe2 with adjusted pH.

	Wavenumber, cm ⁻¹					
	RCP	RCP/Ca	RCP/Fe3	RCP/Fe2	RCP/Fe3, Adjusted pH	RCP/Fe2, Adjusted pH
Amide I	1637	1634	1630	1627	1635	1635
Amide II	1537	1542	1532	1534	1537	1537
Carboxylic group	1390	1391	1409	1409	1398	1407

The elemental composition of mineralised materials was investigated by ICP-OES (Table 10). The results showed higher Ca/P molar ratios, if compared to the value typical of stoichiometric hydroxyapatite (i.e. 1.67). The (Fe+Ca)/(P+CO₃²⁻) molar ratio of RCPFeHA60 decreased in comparison with Ca/(P+CO₃²⁻) molar ratio of RCPHA60, thus confirming the partial replacement of Ca²⁺ by iron ions in the structure of the mineral nanophase. The overall amount of Fe detected in RCPFeHA40 and RCPFeHA60 was close to the amount introduced in the reaction vessel. However, a decrease of Fe²⁺/Fe³⁺ molar ratio was detected, ascribed to the reduction of the weight percentage of Fe²⁺. This result suggested a rapid oxidation of Fe²⁺ to Fe³⁺, during the synthesis process.

Table 10. Chemical features of mineralised materials (results obtained by: * ICP-OES; ** UV-VIS).

	* Ca (wt%)	* P (wt%)	* Fe (wt%)	Ca/(P+CO ₃ ²⁻) (mol)	Fe/Ca (mol)	(Fe+Ca)/(P+ CO ₃ ²⁻)(mol)	** Fe ²⁺ (wt%)	Fe ³⁺ (wt%)
RCPHA40	13.6±0.1	4.7±0.0	---	1.91±0.0	---	---	---	---
RCPHA60	13.9±0.1	3.3±0.0	---	2.30±0.0	---	---	---	---
RCPFeHA40	13.1±0.0	4.7±0.0	4.2±0.0	---	0.23±0.0	2.19±0.0	0.10	4.05
RCPFeHA60	13.3±0.0	4.4±0.0	3.9±0.0	---	0.21±0.0	1.91±0.0	0.58	3.28

Figures 17A – 17C show the thermal behaviour of pure RCP and hybrid mineralised materials and 3 different temperature ranges characterised by weight loss were identified. In the lowest temperature range (≈ 25°C – 120°C (a)) the weight loss was ascribed to the evaporation of water. Following, weight loss ascribed to RCP decomposition initiated at about 250°C (b) and completed at about 700°C (Figure 17A). However, careful analysis of the TG profile revealed different onsets of the degradation process in the various investigated materials, i.e. ≈ 250°C (RCP), ≈ 260°C (RCPHA40), ≈ 265°C (RCPHA60), ≈ 285°C (RCPFeHA40) and ≈ 300°C (RCPFeHA60) (Figure 17A – 17C). On the other hand, the presence of the mineral phase induced the complete decomposition and elimination of the RCP matrix already at 550 °C (Figures 17B, 17C). Further, weight loss detected in the range 700–1100 °C can be ascribed to the

evaporation of carbonate ions and hydroxyl incorporated in the apatitic structure during the synthesis process (Mercado et al. 2014).

As a result of complete RCP degradation, the presence of the mineral phase uniformly distributed in the whole mineralised material was evident, as shown by SEM image in Figure 17D.

The synthesis of the mineralised materials was carried out to induce a mineralisation extent of 40 wt%; in this respect the TG analysis reported that the amount of mineral phase in the final materials ranged between approximately 38 – 43 wt% (Figure 17B, 17C).

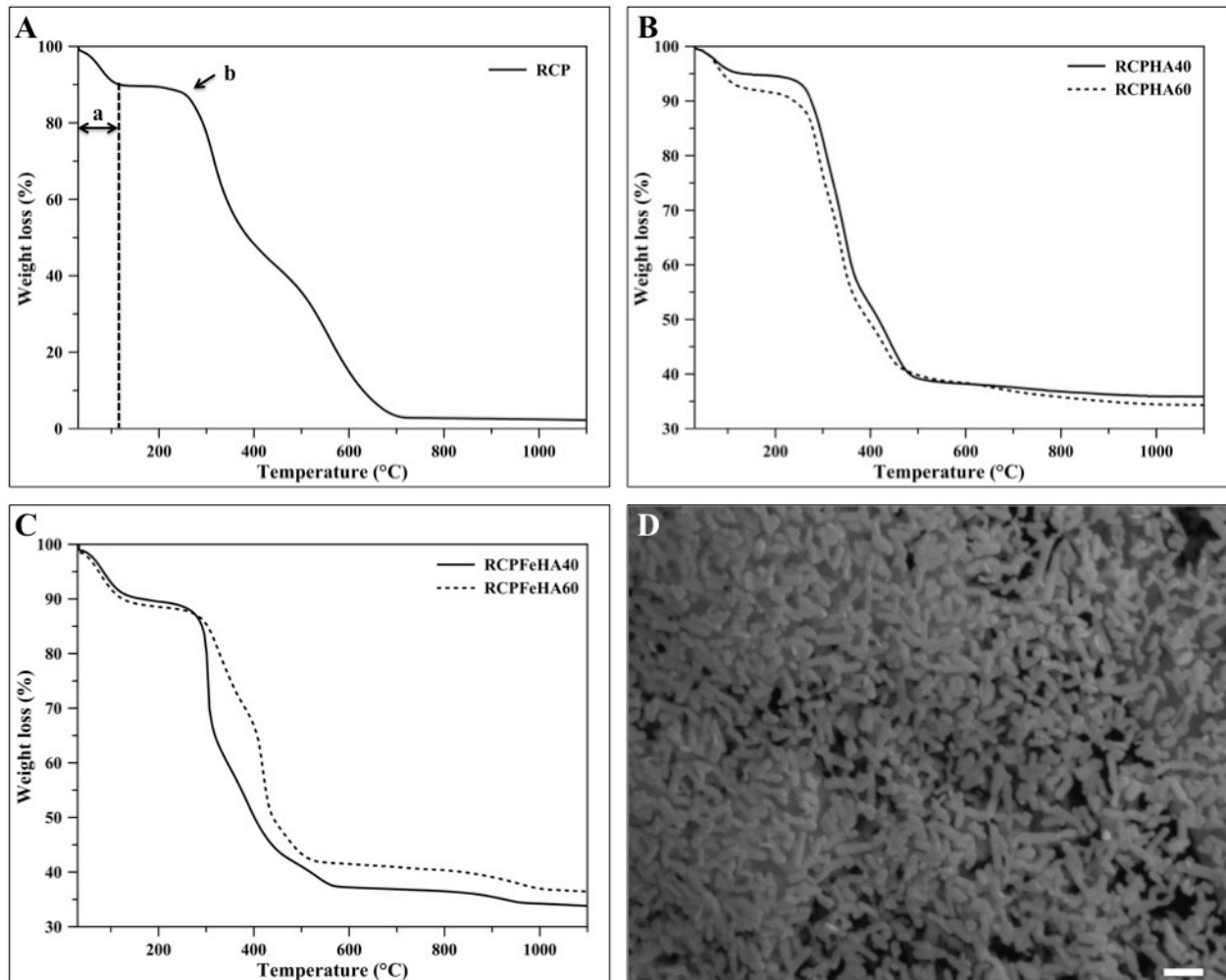


Figure 17. Weight loss of RCP (A) and mineralised materials in absence (B) and presence of iron (C). D): SEM micrograph of 3D network of the mineral nanophase in RCPFeHA60, as obtained after complete decomposition of RCP, at 700 °C, (Scale bar: 200 nm).

Morphological and ultrastructural evaluation by TEM

Figure 18 shows the TEM micrographs and SAED images of hydroxyapatite nanophase obtained upon bio-inspired mineralisation of RCP in different conditions. In all the synthesised materials, TEM analysis showed the formation of nano-crystalline hydroxyapatite with similar morphology. In addition, in RCPFeHA60 dark spots with size about \approx 5-25 nm were detected (Figure 18D, assigned with black

arrows), in close connection with the hydroxyapatite nanocrystals; such spots were identified as iron oxide nanoparticles, nucleated onto the HA nanophase, likely due to the higher temperature adopted where the formation of iron oxide such as magnetite was favoured (Tampieri et al. 2012). The EDX analysis of RCPFeHA40 and RCPFeHA60 is shown in Figure 18E and the presence of iron even in absence of the dark spots in RCPFeHA40, indicated the effective incorporation of iron into the hydroxyapatite structure.

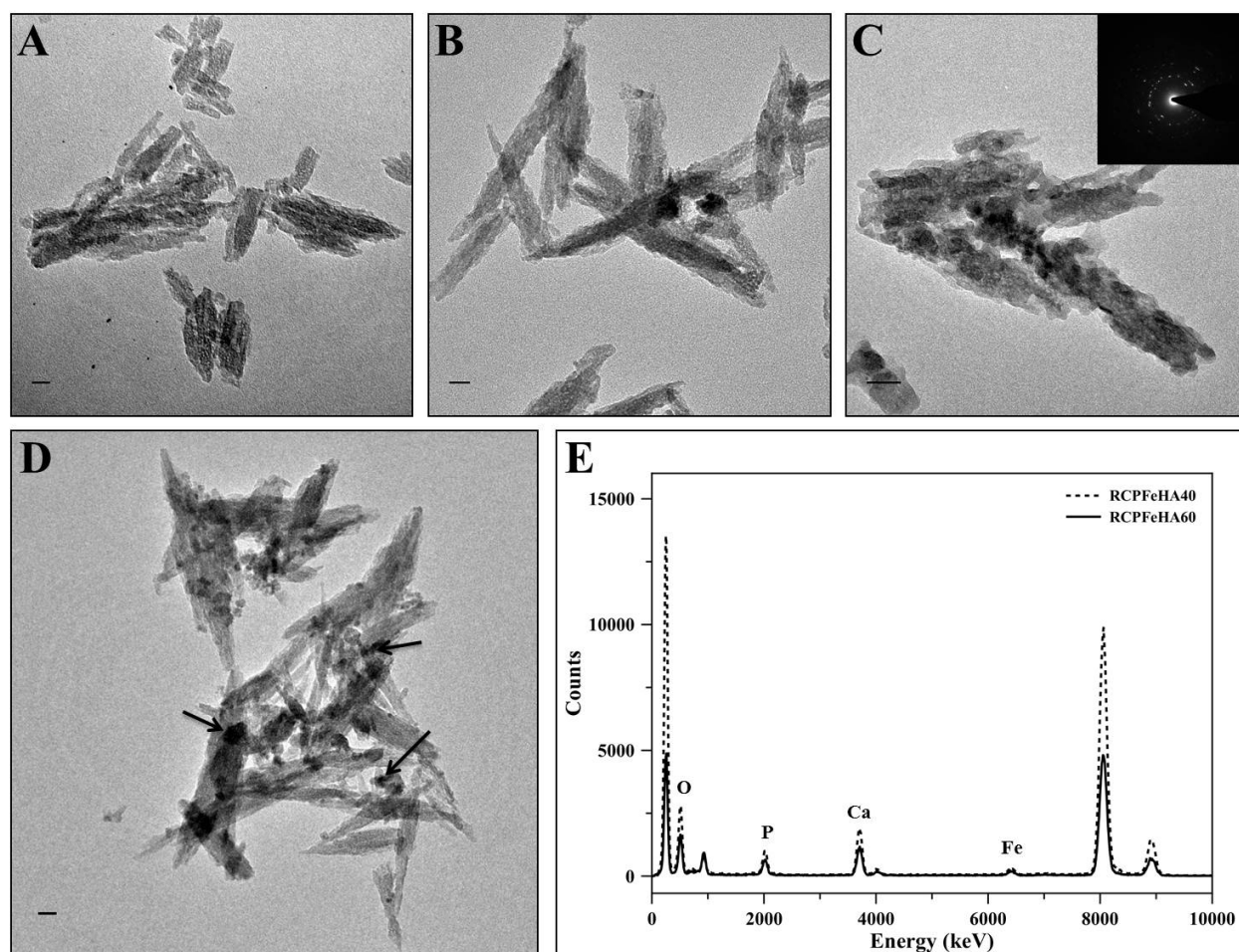


Figure 18. TEM micrographs of mineralised materials, RCPHA40 (A), RCPFeHA40 (B) and TEM micrograph with SAED image of RCPFeHA60 (C); Examples of iron oxide nanoparticles, identified with black arrows, formed on hydroxyapatite nanocrystals of RCPFeHA60 (D), (Scale bar: 20 nm); Energy dispersive X-ray (EDX) analysis of RCPFeHA40 and RCPFeHA60 (E).

3.2.2 Characterisation of microspheres

The as-obtained mineralised slurries were engineered into microspheres by water-in-oil emulsification process and crosslinked by DHT. Several factors affected the production of well-dispersed hybrid microspheres, such as slurry/oil ratio, solution volume, mechanical stirrer velocity, cooling temperature and RCP concentration. Herein, mechanical stirring velocity, cooling temperature and RCP concentration were investigated. Emulsification process was applied to RCPFeHA60 slurry in three distinctive steps (as

mentioned in the methods section). In the first step, dropping of mineralised slurry in pre-warmed oil, associated to various mechanical stirring velocities were studied, from 520 to 975 rpm (Figure 19A to 19D). In all the tested mechanical stirring velocity, well dispersed microspheres were obtained. At higher stirring velocities smaller microspheres were obtained, but coalescence phenomena occurred leading to agglomeration into clusters of heterogeneous shape (Figure 19C, 19D), whereas less agglomerated microspheres were produced at 520 rpm (Figure 19A). Further investigations on emulsification process were carried out by correlating the cooling temperature (2nd step: microspheres jellification) with RCP concentration, in the hybrid mineralised materials ($\approx 5 - 11$ wt%). The results indicated that the formation of well-dispersed microspheres is associated with the gelling kinetics of the slurry/oil phase and the RCP concentration in the slurry. In this respect, the initial RCP concentration played a relevant role, depending on the presence of mineralizing ions. In fact, when preparing pure RCP solutions the concentration of RCP had to be increased from 5 to about 36 wt% in order to obtain well dispersed RCP microspheres; moreover RCP microspheres were successfully obtained when in the second step of emulsification (i.e. microspheres jellification) 5.5 °C was used; whereas in the case of hybrid microspheres the RCP ratio was ≈ 11 wt% and a lower cooling temperature was required, i.e. about 2 °C (Figure 19E).

In order to validate the emulsification process efficiency, the as-obtained microspheres were separated into batches of different size by sieving in the range size of 38 – 50 – 75 – 100 μm and SEM micrographs showed the production of microspheres with well-defined size, i.e. 45.5 ± 0.4 , 68.0 ± 0.7 and 88.3 ± 0.6 μm , respectively. Figures 19F – 19H show SEM images of RCP and iron doped hydroxyapatite microspheres in the range size of 50 – 75 μm . The pure RCP microspheres presented a smooth surface (Figure 19F), whereas the hybrid microspheres exhibited a rougher surface, due to the presence of homogeneously distributed inorganic nanoparticles (Figure 19G, 19H).

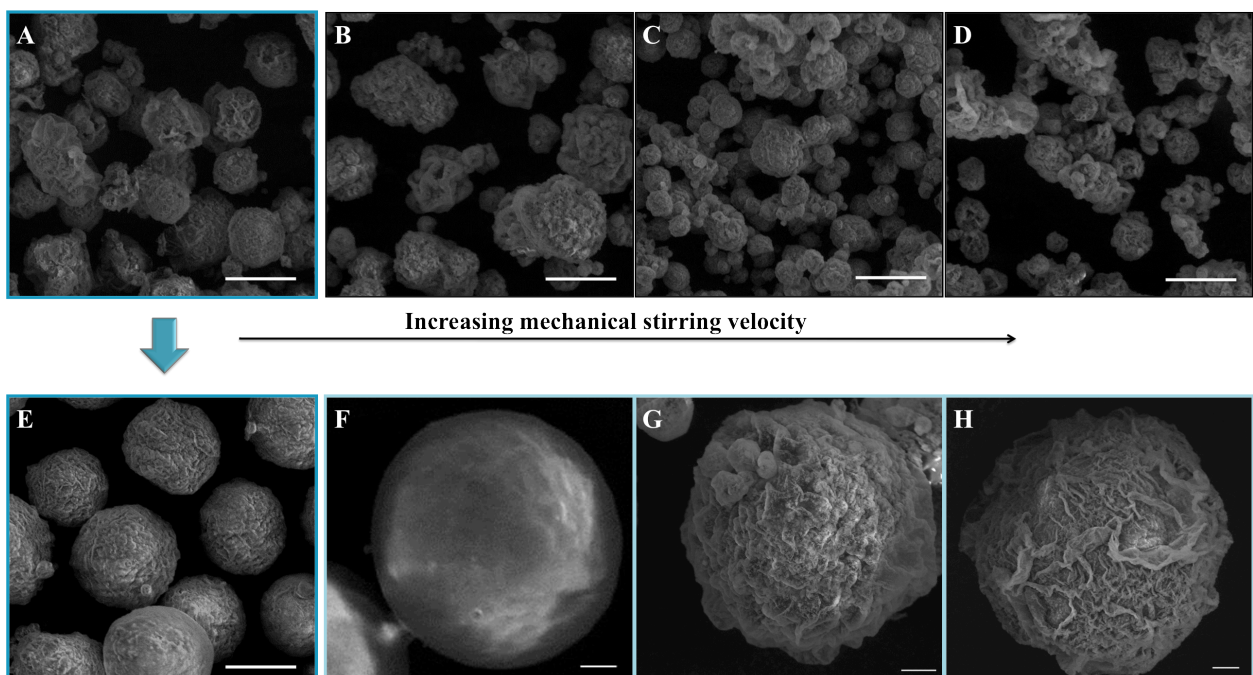


Figure 19. Hybrid microspheres obtained by varying the mechanical stirring velocity, 520 rpm (A), 650 rpm (B), 715 rpm (C) and 975 rpm (D). As-optimised microspheres obtained at 520 rpm and at low cooling temperature, i.e., microspheres jellification (E). Detail surface morphology and shape of pure RCP (F) and hybrid microspheres: RCPFeHA40 (G) and RCPFeHA60 (H), (Scale bar are: 50 μm (A, B, C, D, E) and 10 μm (F, G, H)).

As RCP is a readily water-soluble biomaterial, DHT was used as a crosslinking method to obtain microspheres with enhanced stability in aqueous media. In order to evaluate the effect of DHT on RCP, crosslinked RCP microspheres were characterised by FTIR and TGA (Figure 20A, 20B). In the FTIR spectrum, a slight decrease of amide and carboxylic peaks intensity (in particular amide I and III) was found, whereas an intensity increase for amide II was obtained (Figure 20A*). Those results suggest the formation of intermolecular crosslinking, involving the amide groups and providing a more hydrophobic structure, leading to a high stability when exposed to physiological conditions (Gomes et al. 2013; Drexler & Powell 2011; Haugh et al. 2009). The thermal properties of crosslinked RCP were not significantly altered by the DHT treatment (Figure 20B).

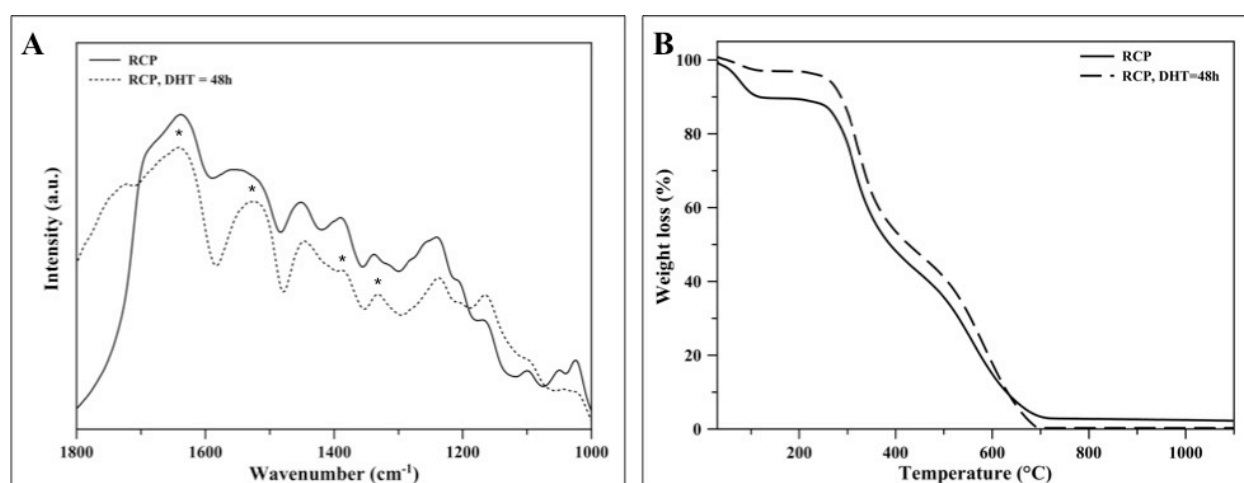


Figure 20. FTIR spectra (A) and TGA profile (B) of DHT crosslinked RCP microspheres compared to non-crosslinked microspheres.

The developed hybrid microspheres RCPFeHA60 are endowed with magnetic properties; in fact, also in cell medium suspension they can be easily attracted from a magnet (neodymium permanent magnet 1.2 T), even at distance of 1 cm. (Figure 21A, 21B). Moreover, the magnetic properties of RCPFeHA40 and RCPFeHA60 were evaluated by using a susceptometer balance and vibrating sample magnetometer (VSM). Different magnetisation values were obtained by susceptometer balance for RCPFeHA40 (0.004 emu/g) and for RCPFeHA60 (0.17 emu/g). Regarding to the high magnetisation obtained in RCPFeHA60, a deeper investigation was performed by VSM, with magnetic field from -15 kOe to 15 kOe. The VSM results indicated that the magnetisation of the RCPFeHA60 microspheres increased with

the magnetic field, until reaching saturation, and a specific magnetisation of 1.65 emu/g was obtained (Figure 21C).

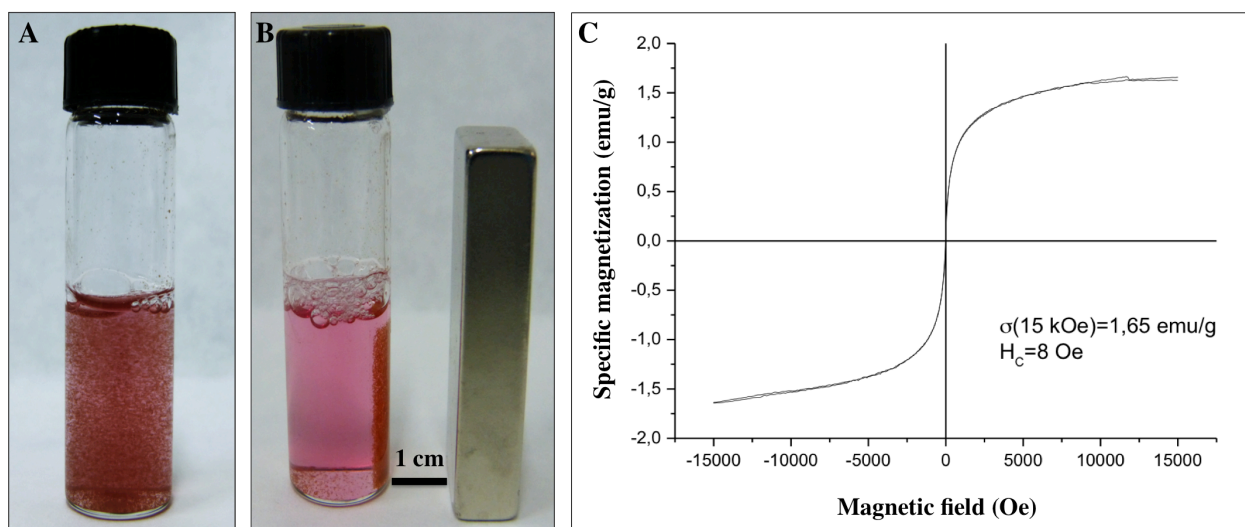


Figure 21. RCPFeHA60 microspheres in cell medium in absence (A) and in presence of neodymium magnet (B) and specific magnetisation of RCPFeHA60 obtained by VSM (C).

3.2.3 *In vitro* cell analysis

Two hybrid microspheres groups (i.e. RCPFeHA40 and RCPFeHA60) with defined magnetic properties and composed by low crystalline hydroxyapatite without and with formation of iron oxide, during the synthesis process, were investigated focusing on cells viability and proliferation. A preliminary *in vitro* cytocompatibility study was performed to evaluate any effect of the magnetic RCP microspheres on pre-osteoblastic cell behaviour using not magnetic RCP microspheres as control. Cell viability was investigated by MTT test and Live/Dead assay (Figure 22 and 23). 24 hours after MC3T3-E1 cell seeding, two concentrations of microspheres (10 $\mu\text{g/mL}$ and 100 $\mu\text{g/mL}$) were added to the culture medium. Quantification of metabolically active cells was performed for each time point. MTT test results demonstrated an increase in cell proliferation from day 1 to day 7 for all the samples highlighting the absence of cytotoxicity (Figure 22). The only statistically significant difference among the groups were identified with the lower microspheres concentration at day 7 (Figure 22).

The cell cultures were also analysed for cell viability with the Live/Dead assay based on the simultaneous determination of live and dead cells with two probes, Calcein and EthD-1, that measure recognized parameters of cell viability: intracellular esterase activity and plasma membrane integrity, respectively. A very high ratio of viable cells were seen with no significant differences among the group at each time point confirming the absence of cytotoxicity induced by the magnetic RCP microspheres at both concentrations (Figure 23).

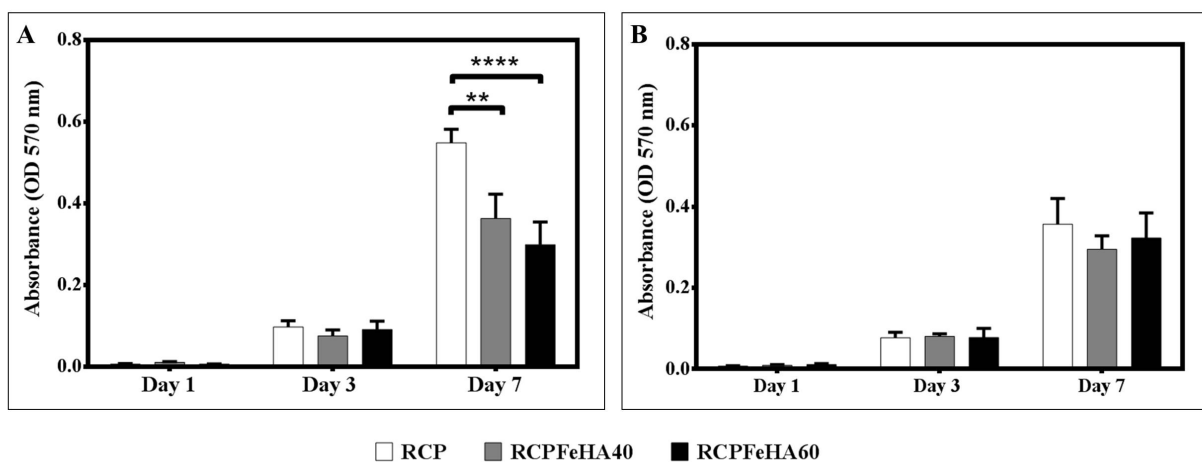


Figure 22. Analysis of cells proliferation by the MTT assay, after 1, 3 and 7 days of MC3T3-E1 cell culture with RCP, RCPFeHA40 and RCPFeHA60 microspheres at concentration of microspheres of 10 µg/ml (A) and 100 µg/ml (B). (**p<0.01; ****p<0.0001; n = 3).

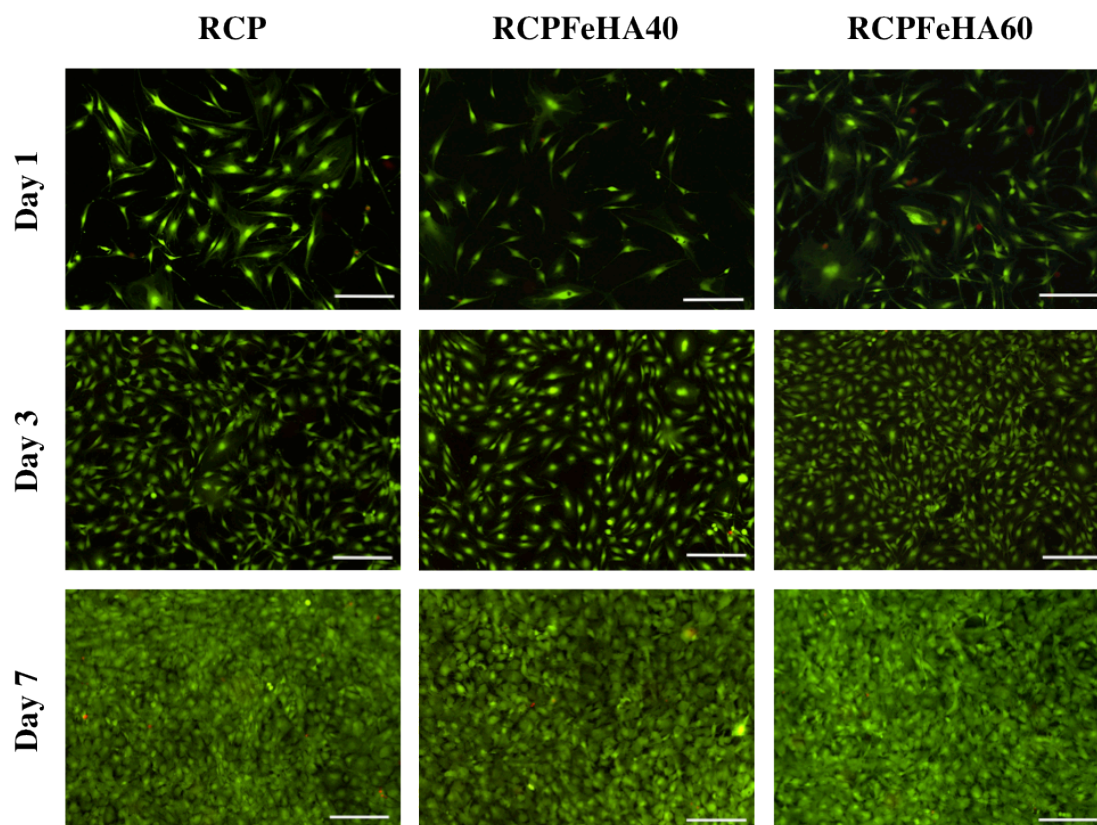


Figure 23. Cell viability analysed by the Live/Dead assay after 1, 3 and 7 days of cell culture with 100 µg/ml microspheres. Calcein AM stains for live cells in green, EthD-1 stains for dead cells in red, (scale bar: 200 µm).

3.3 Effect of ions release from hybrid superparamagnetic microspheres on osteogenic differentiation of MC3T3-E1

3.3.1 Physical, chemical and thermal characterisation of RCPFeHA functionalised with Sodium Citrate

RCPFeHA microspheres in presence of cell medium tend to agglomerate, by forming a lump of microspheres (Figure 24A) and a new strategy was adopted (Figure 24B). RCPFeHA slurry was functionalised with sodium citrate at different concentrations (i.e. 0.55 M, 0.3 M, 0.06 M, 0.006 M and 0.0006 M) and microspheres stability in cell medium was achieved by the surface charge and repulsive interaction between microspheres. Firstly, the effect of sodium citrate (with concentration of 0.55 M) into biomineralised slurry was evaluated by ζ -potential at predetermined time points. By increasing the functionalisation time, a negative charge on biomineralised slurry was improved by the adsorption of citrate ions on the surface of mineral phase, and suitable surface charge for electrostatic repulsion was obtained at 1h 30 min of functionalisation (Table 11).

Table 11. Effect of sodium citrate on surface charge of RCPFeHA slurry.

RCPFeHA slurry	ζ -potential, mV
t = 0, no citrate	12.3±0.36
t = 30'	-13.23±0.21
t = 1h30	-17.2±0.99
t = 3h	-18.8±0.71
t = 6h	-14.4±1.08

Taken into account this result, RCPFeHA slurry was functionalised with sodium citrate at various concentrations during 1h 30 min and microspheres were produced by emulsification process (Figure 24C - 24G). Results indicated that by using high concentration of sodium citrate (i.e. 0.55 M), microspheres with size of 1 mm were produced (i.e. aggregation of small microspheres formed huge particles), while by decreasing the concentration of sodium citrate, smaller aggregates of microspheres were formed. Regarding to the Figure 24F, well dispersed microspheres were produced, thus indicating that successful functionalisation with sodium citrate was obtained with concentration of 0.006 M. Functionalised microspheres were crosslinked by DHT and microspheres were stable in presence of osteogenic differentiation medium for at least 7 days (i.e. no microspheres aggregation) (Figure 24H).

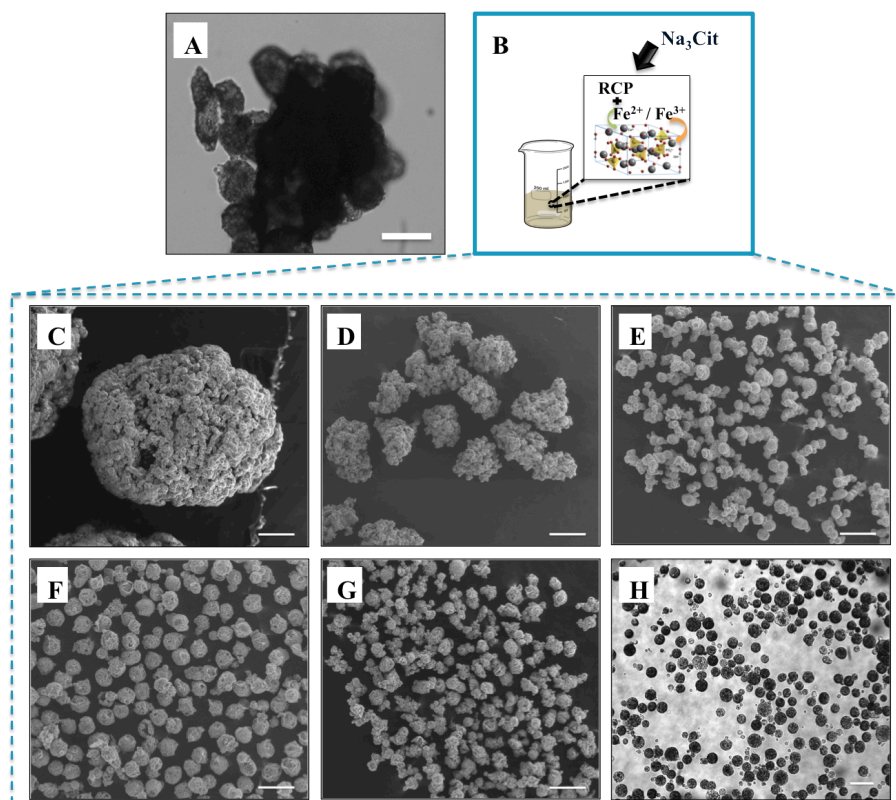


Figure 24. Effect of sodium citrate concentration on as-fabricated RCPFeHA microspheres. A) Microspheres without sodium citrate in osteogenic differentiation medium (Scale bar: 100 μm); B) Designed set-up of RCPFeHA slurry functionalisation with sodium citrate; RCPFeHA microspheres obtained with different concentrations of sodium citrate: C) 0.55 M; D) 0.28 M; E) 0.06 M; F) 0.006 M; G) 0.0006 M. Well dispersed microspheres functionalised with 0.006M in presence of osteogenic differentiation medium (H), (Scale bar: 200 μm).

The effect of sodium citrate (concentration of 0.006 M) on the microspheres was analysed by FTIR, XRD and TGA analysis (Figure 25). FTIR and XRD indicated the formation of poor crystalline and B-type carbonate hydroxyapatite (Figure 25A, 25B). FTIR spectra (Figure 25A) showed the presence of the main vibration peaks of RCP (i.e. amide I, amide II, amide III and carboxylic groups) and calcium phosphate (i.e. phosphate and carbonate assignments) formation in both type of microspheres (i.e. in functionalised and crosslinked functionalised microspheres) (Patrício; et al. 2017). On the other hand, by the introduction of sodium citrate differences were showed in the FTIR spectra. Carboxylic stretching vibrations of citrate were reported at 1755, 1600, 1450 and 1387 cm^{-1} (Mitsionis et al. 2010; Cheraghipour et al. 2012). Moreover, in functionalised microspheres a new peak was detected at 1755 cm^{-1} (Figure 25A*), which was attributed to C=O vibration from -COOH group of sodium citrate, while other vibration modes were overlapped by RCP matrix. XRD patterns showed the formation of low crystalline hydroxyapatite (in agreement with the JCPDS card number: 09-0432) with presence of small amount of iron oxide (e.g. magnetite or maghemite). Thermal investigations provide the decomposition profile of RCPFeHA, functionalised RCPFeHA and crosslinked functionalised RCPFeHA. In RCPFeHA microspheres, the weight loss below to $\approx 140^\circ\text{C}$ was assigned to the

evaporation of the adsorbed water molecules, followed by degradation of RCP matrix until ≈ 600 °C, then evaporation of carbonate and hydroxyl ions from apatitic structure was detected up to 1000 °C. In functionalised RCPFeHA (i.e. RCPFeHA_{Na3Cit}) and crosslinked functionalised RCPFeHA (i.e. RCPFeHA_{Na3Cit} DHT = 48h), slight differences on the thermogram were assigned by the weight loss (≈ 7 wt%) at ≈ 400 °C to 600 °C, indicating the degradation of citrate ions into the microspheres, followed by evaporation of carbonate ions (≈ 600 °C – 1000 °C) (Figure 25C).

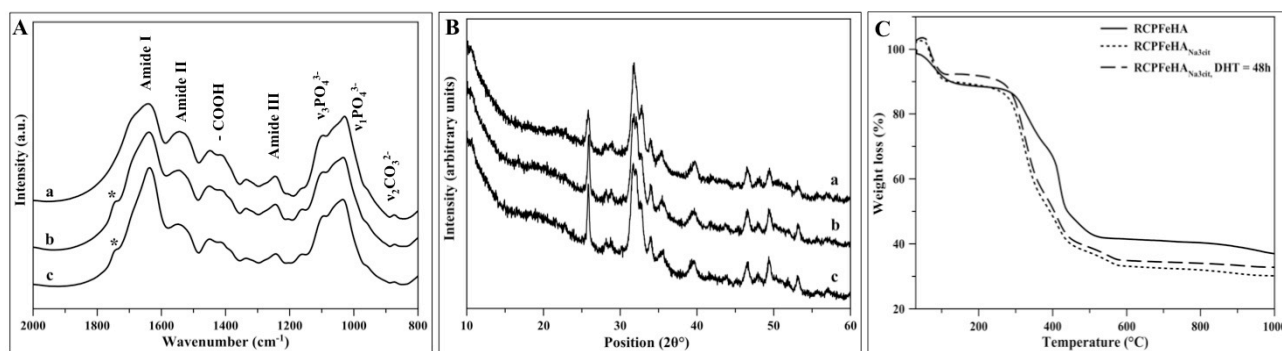


Figure 25. Chemical and thermal features of functionalised RCPFeHA microspheres, by FTIR (A); XRD (B) and TGA analysis. a) Non-functionalised RCPFeHA microspheres; b) Functionalised RCPFeHA microspheres and crosslinked by DHT (c).

3.3.2 Phase composition, morphological characterisation, microspheres size distribution and magnetic properties

XRD pattern of all the as-produced microspheres was presented in figure 26. In RCP and RCPfluidMAG-CT, typical broad diffraction peak ($10 - 30$ Θ°) from the polymeric phase was showed. RCPHA and RCPFeHA were synthesised at 60 °C and in both hybrid biomaterials low crystalline hydroxyapatite was formed, while RCPHA_{RT} was synthesised at 20 °C and very low crystalline hydroxyapatite was obtained. Low intensity and slight shift of diffraction peak at 26 Θ° in RCPFeHA was showed, indicating the partial replacement of Ca ions for Fe ions into hydroxyapatite lattice (Figure 26e).

In RCPfluidMAG-CT, the as-introduced superparamagnetic nanoparticles into RCP matrix was confirmed by the diffraction peak at 35.66 Θ° (in agreement with the JCPDS card number: 01-079-0417), while in RCPFeHA the as-used synthesis temperature induced the formation of secondary phase, as iron oxide (e.g. magnetite or maghemite) and was assigned in the same diffraction signal.

The elements composition of RCPfluidMAG-CT and mineralised microspheres were presented in Table 12. The differences on $(\text{Fe}+\text{Ca})/(\text{P}+\text{CO}_3^{2-})$ mol ratio for RCPFeHA, compared to Ca/P molar ratio of stoichiometric hydroxyapatite (≈ 1.67), can be related to the incorporation of foreign ions into the apatite lattice.

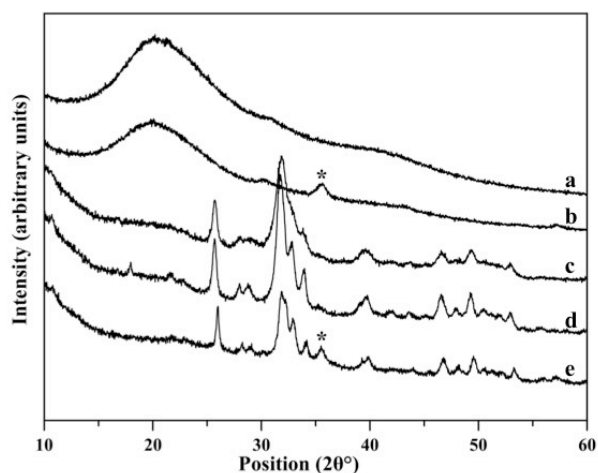


Figure 26. XRD pattern of the as-obtained microspheres: RCP (a); RCPfluidMAG-CT (b); RCPHA_{RT} (c); RCPHA (d); RCPFeHA (e). (Iron oxide formation is indicated by *)

Emulsification process was assessed to produce the microspheres and were separately sieved in the range of 50 – 75 μm and analysed by SEM (Figure 27). All the as-obtained microspheres presented spherical shape, with the exception of RCPHA. The high crystallinity of RCPHA and low viscosity of the biomineralised slurry, might indicate a non-successful microspheres fabrication (Figure 27C). RCP and RCPfluidMAG-CT offered smooth surface, while in RCPHA_{RT} and in RCPFeHA roughness surface by the homogeneous distribution of mineral on the microspheres was obtained. RCP, RCPfluidMAG-CT, RCPHA_{RT} and RCPFeHA microspheres size distribution was evaluated by using the SEM micrographs and analysed by Image J software. Microspheres size distribution and respective Gaussian size distribution were showed in Figure 28 and similar microspheres size was obtained, ranging from $\approx 67 \mu\text{m}$ to $70 \mu\text{m}$.

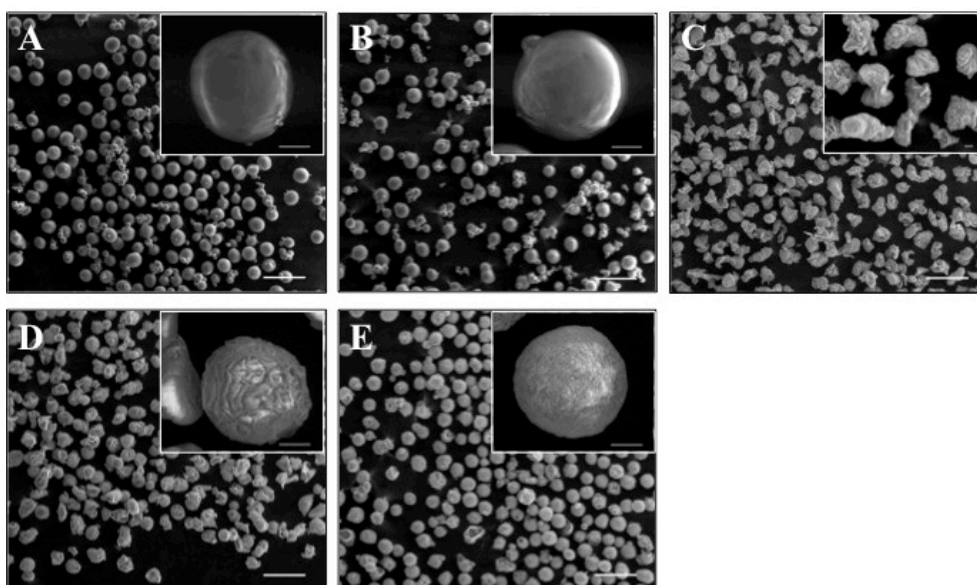


Figure 27. SEM micrographs from the as-produced microspheres: A) RCP; B) RCPfluidMAG-CT; C) RCPHA; D) RCPHA_{RT}; E) RCPFeHA, (Scale bar is 200 μm and in the figure inserts is 20 μm).

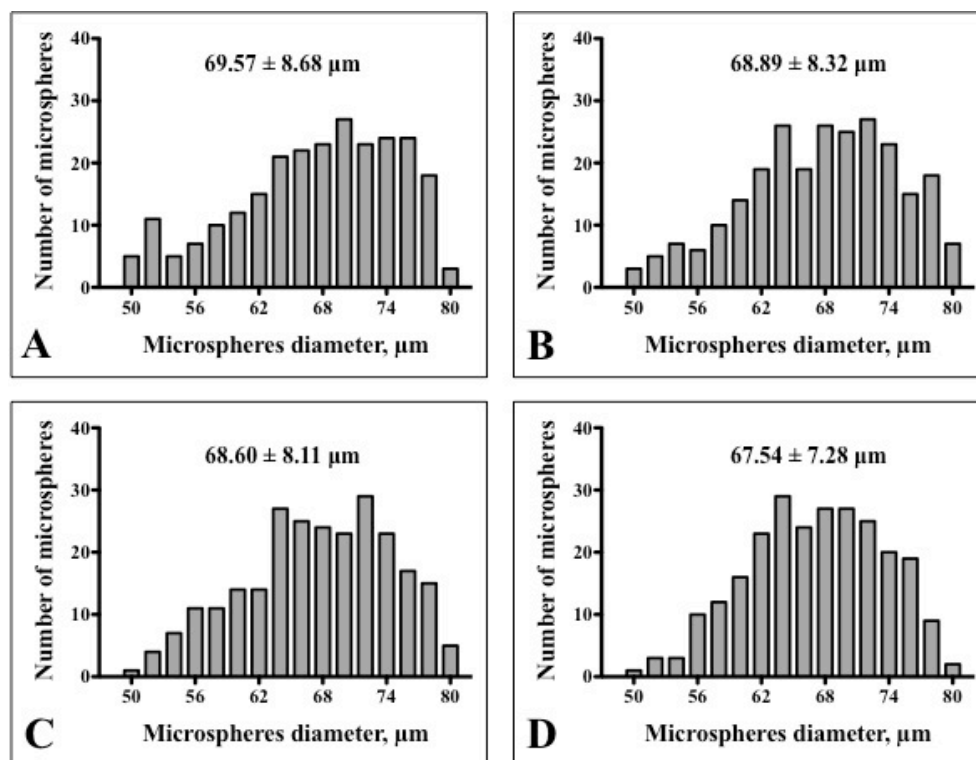


Figure 28. Size distribution and respective microspheres size obtained by Gaussian distribution. A) RCP; B) RCPfluidMAG-CT; C) RCPHA_{RT}; D) RCPFeHA.

Prior to microspheres production RCPFeHA and RCPHA_{RT} slurries were functionalised with sodium citrate at concentration of 0.006 M and microspheres were obtained by emulsification process. The surface charge of microspheres were analysed in HEPES buffer solution (pH 7.4) and low surface charge of all produced microspheres was showed and dispersed microspheres in osteogenic differentiation medium were obtained Table 12. In RCPFeHA, the surface charge in the functionalised microspheres was slightly improved from 2.17 ± 0.63 mV to 5.39 ± 0.12 mV.

Table 12. Microspheres composition, ζ -potential and chemical elements of microspheres. (*obtained by ICP-OES)

Composition of microspheres	Code	ζ -potential, mV	* Ca, mol	* Fe, mol	Ca/(P+CO ₃ ²⁻), mol	(Fe+Ca)/(P+CO ₃ ²⁻), mol
Collagen type I based Recombinant Peptide	RCP	1.53±0.21	---	0.021±0.00	---	---
Collagen type I based Recombinant Peptide prepared with commercial superparamagnetic nanoparticles	RCPfluid MAG-CT	2.195±0.78	---	---	---	---

Collagen type I based Recombinant Peptide mineralised with hydroxyapatite nanophase	RCPHA _{RT}	3.345±0.05	0.51±0.00	---	2.03±0.03	---
Collagen type I based Recombinant Peptide mineralised with iron doped hydroxyapatite	RCPFeHA	5.86±0.11	0.48±0.04	0.09±0.01	---	2.31±0.02

fluidMAG-CT are iron oxide nanoparticles commercially available for Magnetic Resonance Imaging (MRI) diagnostic. RCPfluidMAG-CT microspheres with certain amount of iron oxide nanoparticles were produced and was defined as control to the as-synthesised and produced RCPFeHA microspheres. By susceptometer balance the magnetic properties were evaluated and RCPfluidMAG-CT and RCPFeHA showed similar magnetisation values, i.e. 0.22 emu/g and 0.26 emu/g, respectively.

3.3.3 Microspheres degradation studies under physiological and inflammatory mimicking conditions

RCP, RCPfluidMAG-CT, RCPHA_{RT} and RCPFeHA were immersed in two different DMEM: DMEM (pH 7.4) and DMEM-IM (pH 5), and the degradation studies were evaluated over the course of 28 days. Microspheres morphology was analysed by SEM micrographs at 7, 14, 21 and 28 days and microspheres were not degraded in presence of both conditions (Figure 29 and 30). After 28 days at pH 7.4, small microspheres with wrinkled structure were obtained and RCPFeHA showed a porous surface. Polymeric microspheres showed high stability at pH 5, although the solubility of the mineral phase of RCPHA_{RT} and RCPFeHA was clearly evident by the wrinkled structure.

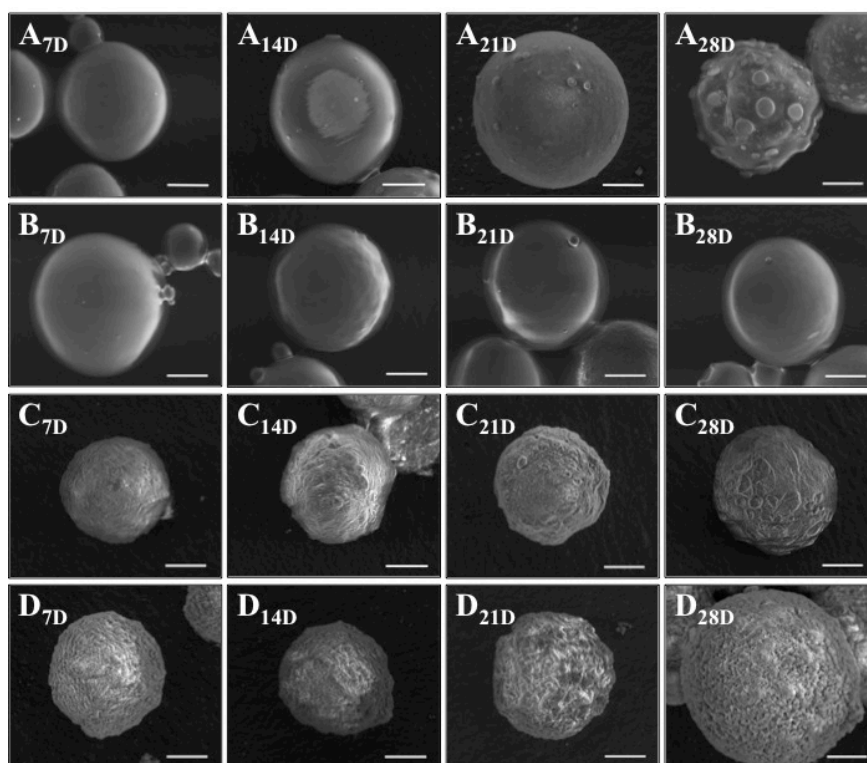


Figure 29. SEM micrographs of microspheres, after immersion in physiological mimicking conditions, over the course of 28 days. A) RCP; B) RCPfluidMAG-CT; C) RCPHA_{RT}; D) RCPFeHA, (Scale bar: 20 μ m); (Note: 7D: 7 days; 14D: 14 days; 21D: 21 days; 28D: 28 days).

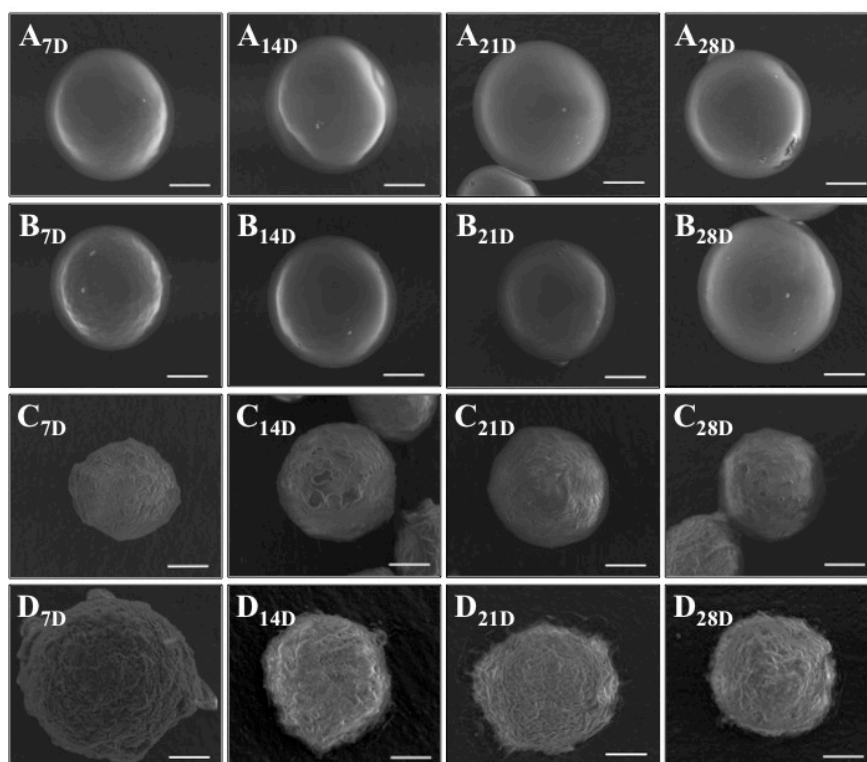


Figure 30. SEM micrographs of microspheres, after immersion in mimicking inflammatory conditions, over the course of 28 days. A) RCP; B) RCPfluidMAG-CT; C) RCPHA_{RT}; D) RCPFeHA, (Scale bar: 20 μ m); (Note: 7D: 7 days; 14D: 14 days; 21D: 21 days; 28D: 28 days).

pH of both controls media (i.e. DMEM and DMEM-IM) and the media used in the degradation studies with all the tested microspheres were evaluated at each predetermined time points (i.e. 12h, 24h, 48h and 7, 14, 21 and 28 days). By comparing the obtained pH (i.e. 7.4 and 5) in the controls or in the media with RCP or RCPfluidMAG-CT, non-significant differences were detected (Figure 31). In physiological mimicking conditions (DMEM, pH 7.4), higher pH (≈ 7.6) on RCPHA_{RT} and an increase of the pH (from ≈ 7.2 to 7.5) on RCPFeHA, were obtained in the first 48h of experiment, then a pH plateau from 7 days to 28 days were presented (≈ 7.4). During 28 days in inflammatory mimicking conditions, a slight increase on the pH of the media in contact with RCPHA_{RT} and RCPFeHA was observed, probably due to the ion exchange or ion release from both microspheres (Figure 31).

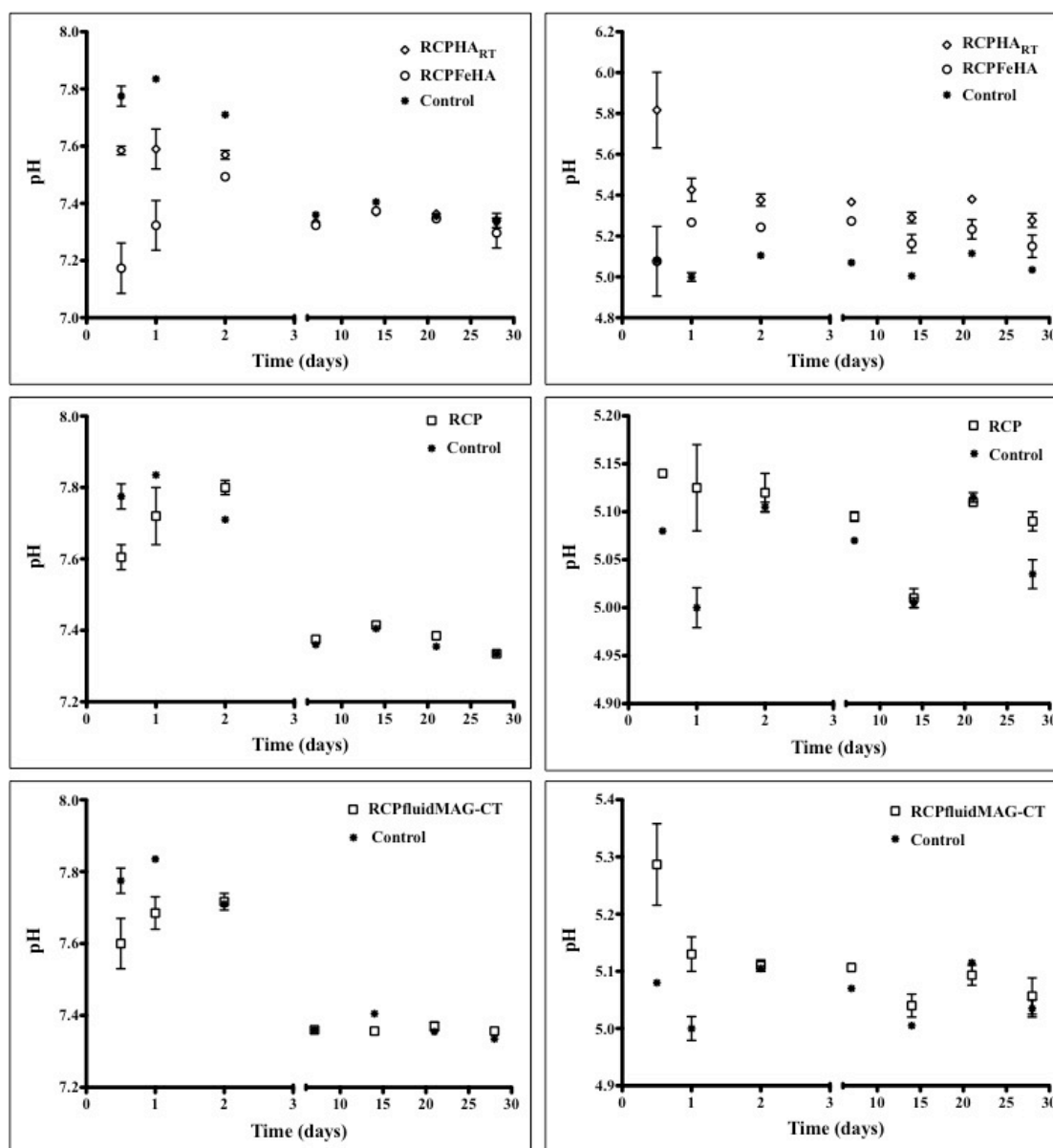


Figure 31. pH changes in DMEM (pH 7.4) and DMEM-IM (pH 5) in presence of microspheres and controls (Mean±SEM).

Calcium and iron ions have been showed an inductive effect on osteogenesis (Tampieri et al. 2014; Tampieri et al. 2016; B.- Sprio; et al. 2016). Regardless, ions release was investigated after incubation of RCPfluidMAG-CT, RCPHA_{RT} and RCPFeHA, at predetermined time points in physiological and inflammatory mimicking conditions. DMEM was a medium enriched of calcium ions (≈ 1.05 mM) and the percentage of adsorbed calcium at each time point was normalised to the total calcium in the replaced medium (Figure 32A), while released ions were normalised to the total amount of ions in 30 mg of microspheres (Table 12). Higher pH values from DMEM in presence of RCPHA_{RT}, was reflected in higher calcium absorption (about 80% of calcium absorption at each time point) until 7 days of experiment, followed by a decrease to $\approx 16\%$ at day 21. From day 21 to 28, slight increase was showed, maybe due to the solubility of the microspheres. In RCPFeHA, over the course of the experiment about ≈ 50 to 90% of calcium was adsorbed, reaching the saturation after 7 days in presence of DMEM. Meanwhile, about 0.13 mM of Fe ion was released from RCPFeHA. Regarding to the Fe release from RCPFeHA in both conditions, significant differences on Fe ion release was presented ($p < 0.05$), indicating the exchange of iron ion to the adsorbed calcium ion in DMEM (Figure 32B). In inflammatory mimicking conditions, a cumulative calcium release was presented without significant differences between RCPHA_{RT} and RCPFeHA (Figure 32C). For RCPfluidMAG-CT in both media, extremely statistically significances on Fe release were showed ($p \leq 0.001$) (Figure 32D).

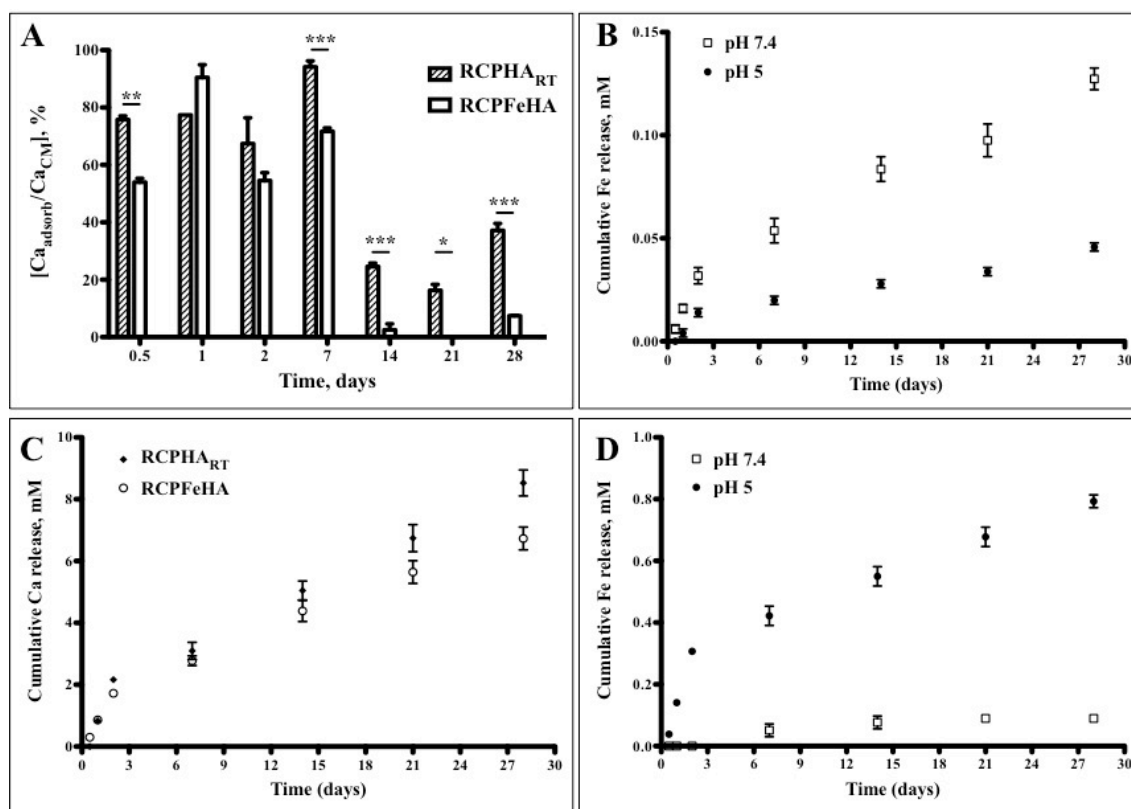


Figure 32. Percentage of calcium adsorbed from DMEM at pH 7.4 (A); Cumulative Fe release of RCPFeHA (B); Cumulative Ca release at pH 5 (C) and Cumulative Fe release from RCPfluidMAG-CT (D); (* $p < 0.05$; ** $p \leq 0.01$; *** $p \leq 0.001$).

The composition of RCPHA_{RT} and RCPFeHA microspheres, after 28 days in mimicking conditions (i.e. physiological and inflammatory) were analysed by FTIR and XRD tests (Figure 33). As showed in FTIR spectrum, organic and inorganic phase were presented in RCPHA_{RT} and RCPFeHA, as observed by the vibration assignments in amide and phosphate groups, respectively (Figure 33A). In RCPHA_{RT} and RCPFeHA, no additional phases formed along 28 days in presence of DMEM or DMEM-IM. In RCPFeHA, lower intensity of diffraction peak at 35.66 Θ° was showed, corroborating the iron release, over the course of 28 days (Figure 33B, 33C).

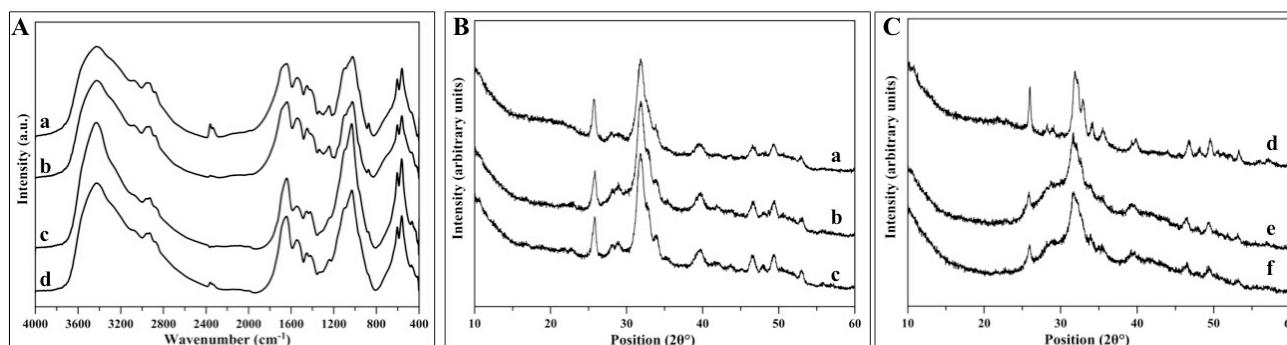


Figure 33. A) FTIR spectrum of RCPHA_{RT} after 28 days in pH 7.4 (a) and in pH 5 (b) and of RCPFeHA after 28 days in pH 7.4 (c) and in pH 5 (d); (B) XRD pattern of RCPHA_{RT} before (a) and after 28 days at pH 7.4 (b) and pH 5 (c) and of RCPFeHA (C), before (d) and after 28 days at pH 7.4 (e) and pH 5 (f).

3.3.4 Biological characterisation

Cell viability

Cell viability was evaluated at predetermined time points and results from XTT test showed an increase on cell viability over the time of the experiment, even at high concentration of microspheres (Figure 34). Statistically significant differences were identified among the groups and in all the tested concentration of microspheres ($p < 0.05$; $p < 0.01$; $p < 0.001$). At concentration of 500 $\mu\text{g/mL}$ higher statistically significant differences were showed among the tested groups, without cytotoxic effect on the cells. After 7 days of cell seeding with the microspheres at 100 $\mu\text{g/mL}$, equivalent cell viability among the groups was showed and this concentration was selected for the further investigations on gene expression and western blot.

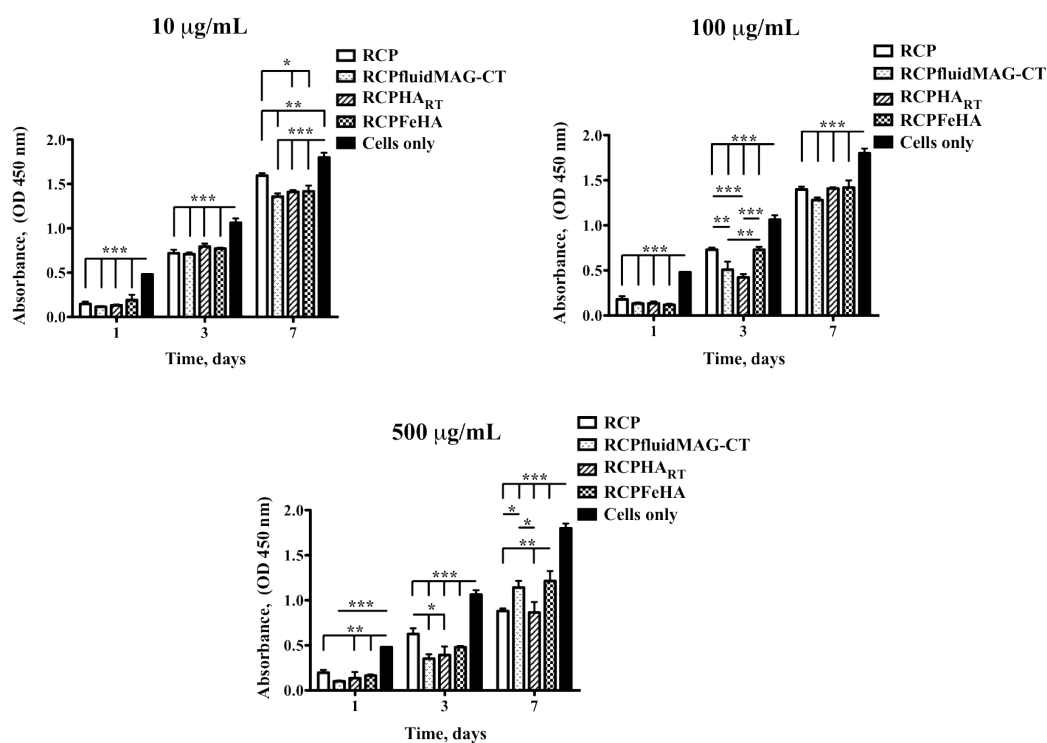


Figure 34. Cell viability in presence of all tested microspheres (*p<0.05; **p<0.01; *p<0.001).**

Cell damage and cell morphology evaluation

In order to evaluate the early stage of apoptosis due to the presence of the microspheres in the culture (Koopman et al. 1994), the cellular protein annexin V, commonly used to detect apoptotic cells, was investigated at day 1 and after 3 days with an assay that also highlight the presence of necrotic cells. As showed in figure 35, all the polymeric and hybrid microspheres tested in both concentrations, do not induce cell apoptosis and necrosis. The cells cultured in standard conditions represented the negative control (Figure 35A), while cells grown in presence of 1 µM doxorubicin were used as positive control (Figure 35B).

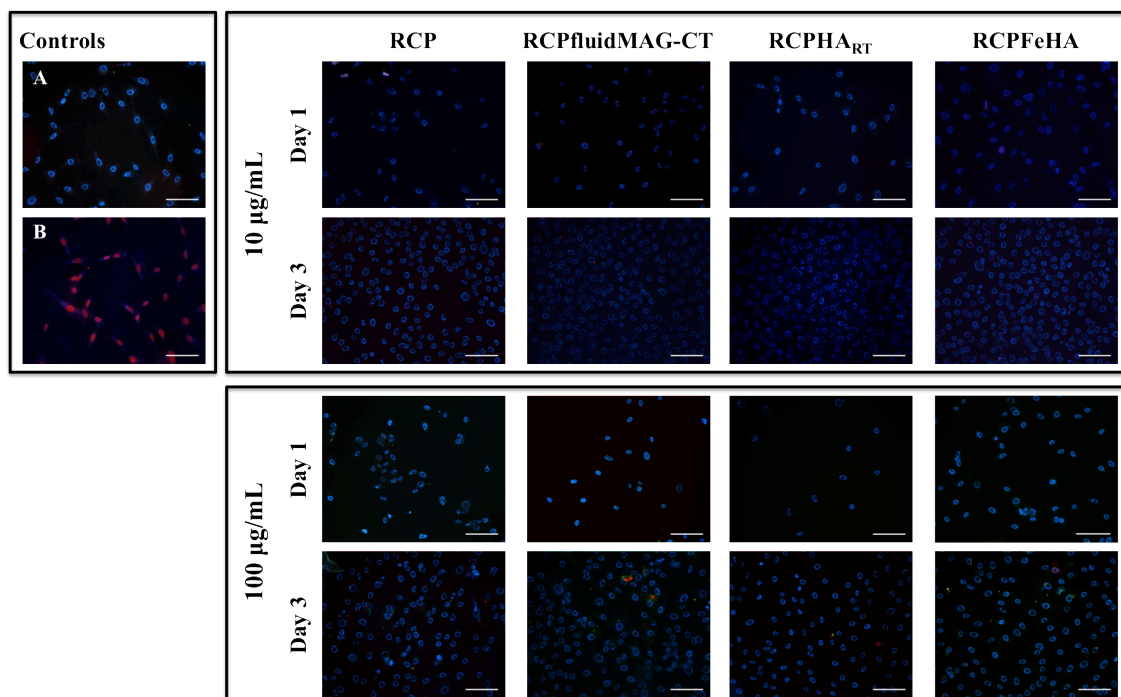


Figure 35. The effect of microspheres on cells apoptosis/necrosis, at two concentrations: 10 µg/mL and 100 µg/mL and at two experimental time points (Day 1 and Day 3). Apoptotic cells in green, necrotic cells in red, cell nuclei in blue. Negative control (A) and positive control (B), (Scale bar: 50 µm).

A further evaluation was performed to verify if the proposed microspheres could induce the production of reactive oxygen species (ROS), as index of cell damage (Stark 2005). The results indicated that for all the microspheres at both concentrations and experimental time points, very low level of ROS were produced (Figure 36), proving that the released ions do not induce oxidative stress on the cells. MC3T3-E1 cells grown in standard condition were used as negative control (Figure 36A), while cells treated with 100 µM of hydrogen peroxide were used as positive control (Figure 36B).

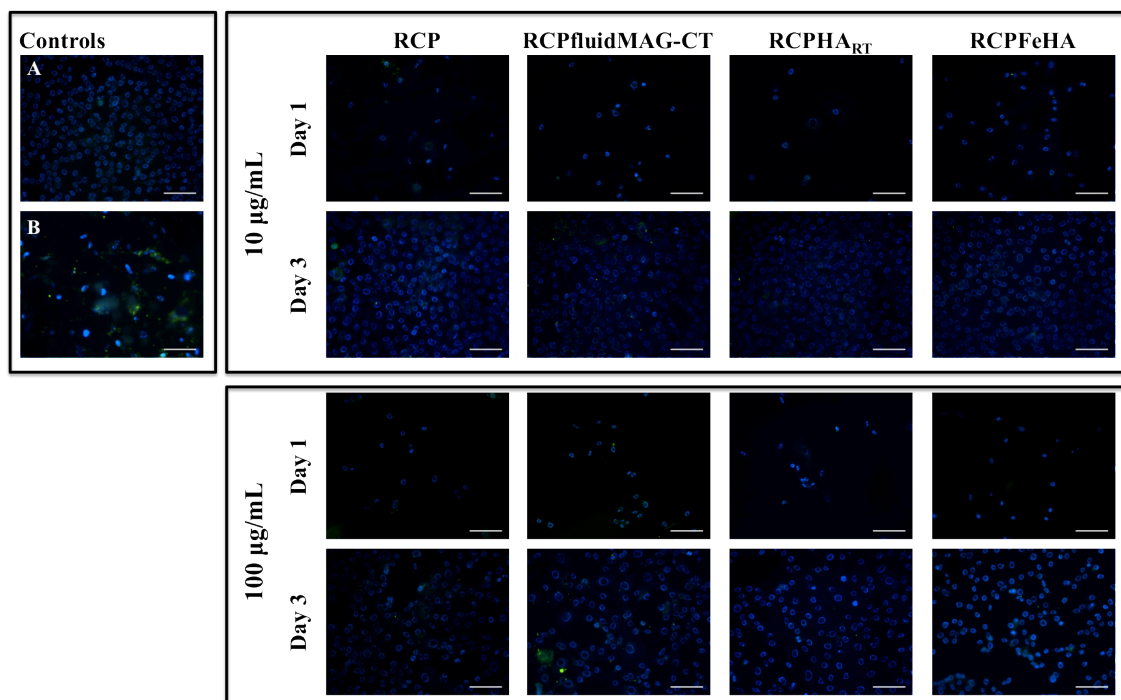


Figure 36. The effect of microspheres on ROS production, at two concentrations: 10 µg/mL and 100 µg/mL and at two experimental time points (Day 1 and Day 3). (Negative control (A) and positive control (B)), (Scale bar: 50 µm).

Cell morphology was analysed by phalloidin staining and H&E staining. The organization of the cytoskeletal structure of actin filaments is an essential element in maintaining and modulating cellular morphology and cell structural integrity (Radulovic & Godovac-Zimmermann 2011). The morphological analysis made by phalloidin staining showed MC3T3-E1 cells well spreaded in the well plate surface without any difference among the group (Figure 37A). These results were confirmed also by H&E staining and in bright field images (Figure 37B-C) the cells were well adhered to the surface of well plate and surrounding the microspheres. Cells showed the typical polygonal shape proving that the microspheres did not induce any macroscopic negative effects to the cell culture.

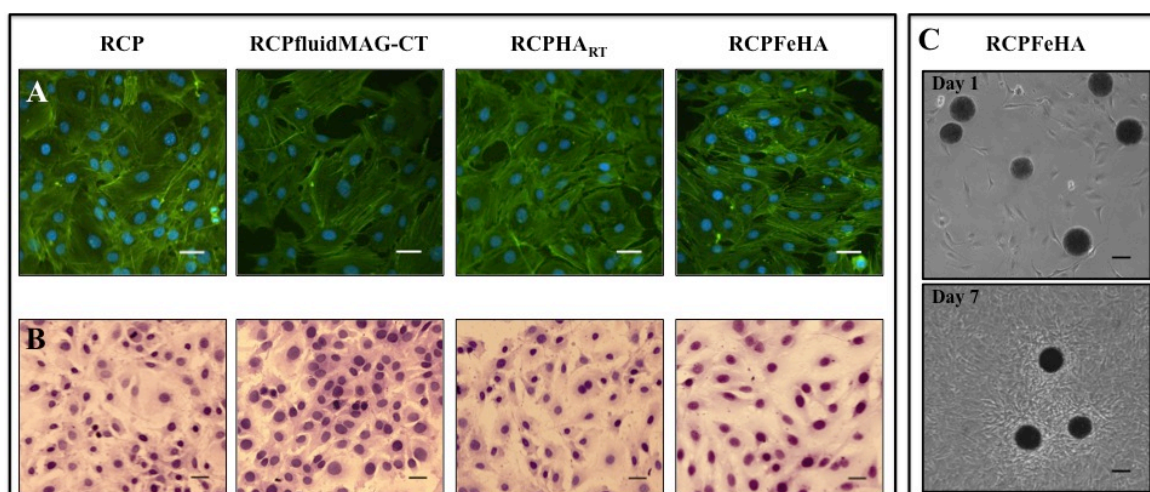


Figure 37. Morphological analysis of MC3T3-E1 cultured at day 3, in presence of 100 µg/ml of microspheres, evaluated by phalloidin staining (green: actin filaments, blue: cell nuclei) (A) and haematoxylin and eosin staining (B), (Scale bar: 20 µm). C) Bright-field images of RCPFeHA acquired at day 1 and day 7 of cell culture, (Scale bar: 50 µm).

Western Blot Analysis

Western blot analysis was performed to evaluate the protein expression of ALP and BGLAP and autophagy regulators (LC3B-I and LC3B-II), after 7 days of cell culture in presence of all tested microspheres (concentration of 100 µg/mL). The results were normalised by the expression of β-Actin (Figure 38). For all the tested microspheres, ALP and BGLAP were expressed without any significant differences among the groups. A slight increase of LC3B-I and LC3B-II, even with any significant differences, was showed in presence of RCPfluidMAG-CT and RCPFeHA microspheres compared to cells only group.

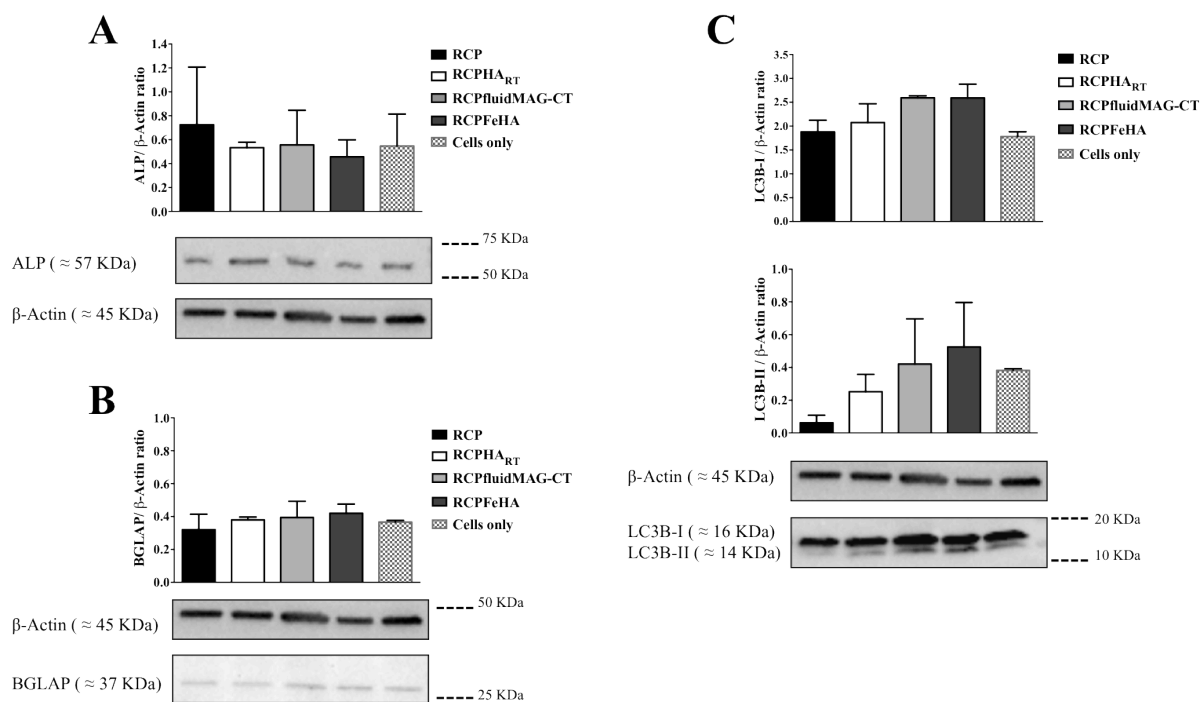


Figure 38. Western blot analysis for the expression of osteogenic proteins ALP (A) and BGLAP (B) and autophagy marker C) LC3B-I (graph above) and LC3B-II (graph below). β-Actin was used as an internal control.

Osteogenic gene expression profile

The effect of microspheres composition at 100 µg/mL on the expression of the osteogenic genes (COL I, SPARC and BGLAP) was evaluated by qRT-PCR (Figure 39). An overall trend in up-regulation of these genes in presence of all hybrid microspheres respect to RCP group was showed. Although no statistical significant differences were detected, BGLAP, a marker of late osteogenic differentiation, seems to be

upregulated in all the tested group. Instead, RCPFeHA exerted, even weakly, higher inductive effect in the expression of COL I and SPARC compared to RCPfluidMAG-CT and RCPHA_{RT}.

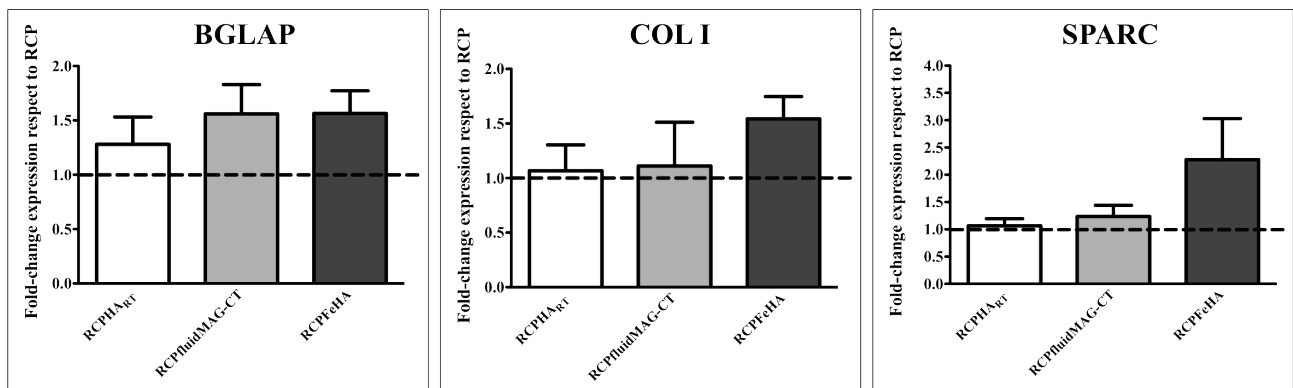


Figure 39. Relative quantification ($2^{-\Delta\Delta C_t}$) of osteogenic related genes expression after 7 days of MC3T3-E1 culture with all the tested microspheres.

3.4 Effect of microspheres composition on differentiation of human mesenchymal stem cells

3.4.1 Cell viability

Optical micrographs indicated great affinity of the cells to the all type of microspheres after 7 days of cell culture (Figure 40A). The effect of microspheres composition on cell viability, cell vitality and cytotoxicity were also evaluated by using the Live/Dead assay after 7 days of cell culture (Figure 40B – 40E). By comparing the images with cell monolayer without microspheres, high density of green cells was observed in all the tested microspheres, demonstrating high cell viability and non-cytotoxic effect on the cells. Microspheres were observed in red and non-dead cells were surrounding the microspheres, as showed at high magnification (Figure 40 D, E). Great cell affinity to the microspheres composed by hydroxyapatite or iron hydroxyapatite nanophase (i.e. RCPHA_{RT} and RCPFeHA) was presented.

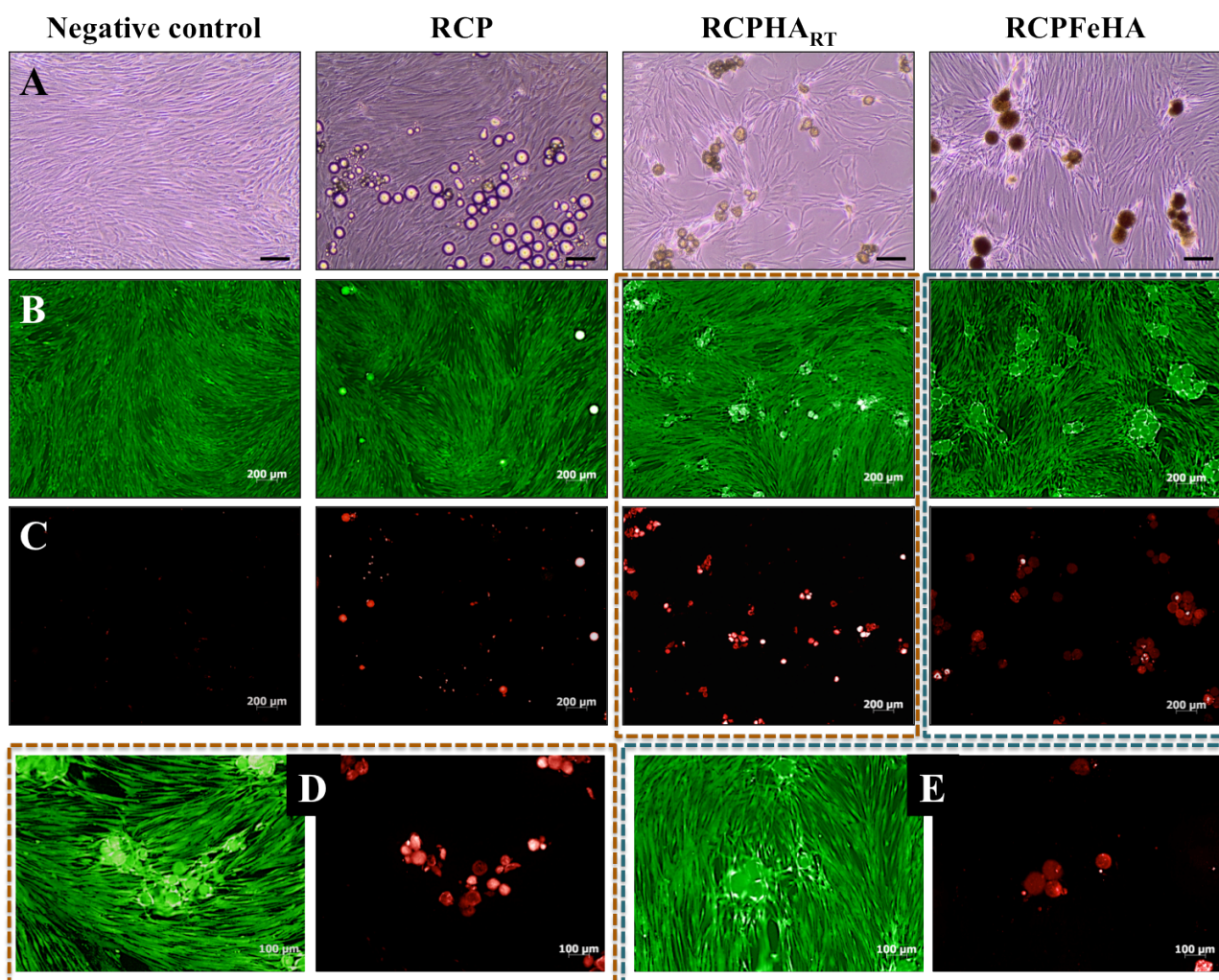


Figure 40. Bright-field images (A) and Live (B) & dead (C) cells obtained after 7 days of cell culture in presence of hMSCs, (Scale bar: 200 μm). Live & Dead cells surrounded to RCPHA_{RT} (D) and RCPFeHA (E) microspheres.

3.4.2 Optimisation of cell seeding

Prior to the investigations in the effect of microspheres composition on osteogenic differentiation of hMSCs, cell-seeding strategy was optimised for 500 μg of microspheres. Preliminary studies on the amount of cell seeding were based on 3500 cells/ cm^2 and specific surface area of each type of microspheres. After three days of cell culture, high percentage of cells was attached to the agarose and a 3D template was formed. The percentage of cells attached to the microspheres was calculated based on DNA extracted from the cells attached to the microspheres and normalised by the nominal amount of DNA in each cell (8.5 pg/cell) (equation 1) (Dormer et al. 2012). Regarding to the high amount of used cells, in one hand low percentage of cells was attached to the different type of microspheres, with statistically significant differences for RCPFeHA ($p < 0.05$) (Figure 41A). On the other hand, this low percentage was reflected in high amount of cells adhering to the microspheres as showed by haematoxylin and eosin staining (H&E) (Figure 41B). Afterwards, the amount of cells seeded on the microspheres was decreased based on 700 cells/ cm^2 and specific surface area of microspheres. Optical micrographs showed the formation of 3D templates for RCP and RCPFeHA, while in RCPHA_{RT} disperse microspheres and cells were presented, after one day of culture (Figure 41 C, D, E).

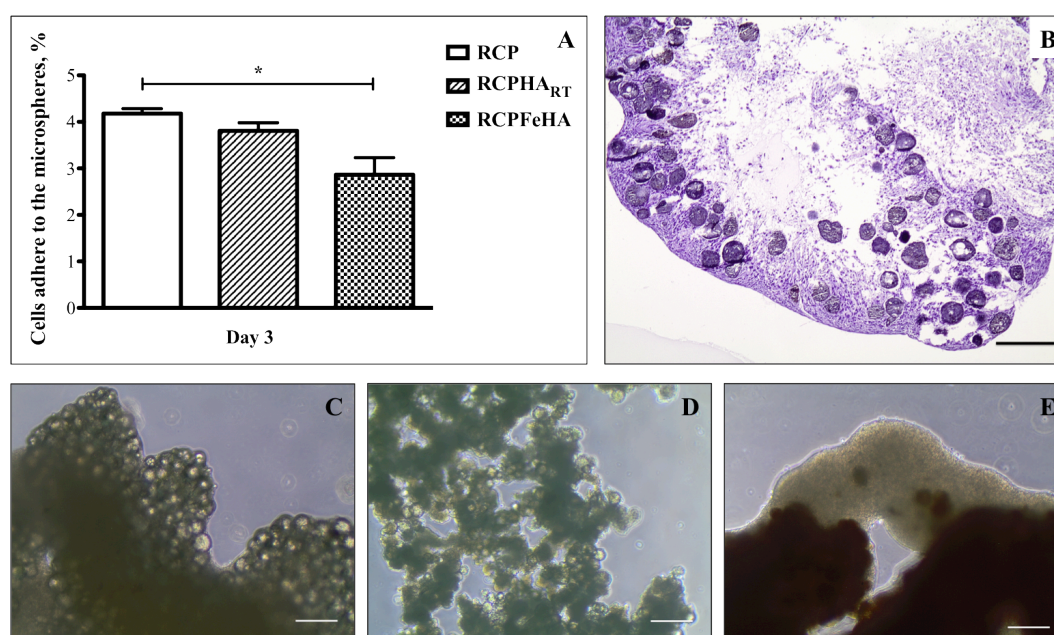


Figure 41. Cell seeding at density of 3500 cell/ cm^2 ((A) Percentage of cells adhere to the microspheres after 3 days of cell culture and (B) H&E staining on RCPFeHA); Optical micrographs from cells (700 cells/ cm^2) in presence of RCP (C), RCPHA_{RT} (D) and RCPFeHA microspheres (E), (Scale bar: 200 μm).

New cell seeding strategy was implemented by reducing the amount of cells (i.e. 350 cells/ cm^2) and based on specific surface area (SSA) of each type of microspheres (i.e. different cell number seeded in the microspheres) or SSA of RCP (i.e. equal cell number seeded in the microspheres). hMSCs (P8) were used in all the tested microspheres and DNA assay, DAPI staining and Live/Dead assay were performed,

after 24h of cell seeding.

Non-adherent cells to the microspheres, during the cell seeding were avoided by using the washing steps. Equivalent DNA quantity with statistical significant differences for RCPFeHA ($p < 0.05$) was presented by seeding the equal cell number. Cell seeding based on specific surface area was translated in differences on DNA amount, with extremely significant statistics differences between all the tested groups ($p < 0.0001$) (Figure 42A, 42B). Take into account the DNA amount in one cell (≈ 8.5 pg/cell) (Dormer et al. 2012; Phuong N. Dang et al. 2016), about half of the number of cells were adhered to all the tested microspheres and in both cell-seeding strategies. By using the equal cell number, 3D templates were obtained after 24h of cell seeding, while by take into account the specific surface area on cells number, dispersed microspheres was showed in RCPHA_{RT}, as showed by DAPI staining (Figure 42C, 42D). Cell nuclei were marked in blue and cells were visualised on the surface of each type of microspheres (Figure 42C, 42D). Meanwhile, 3D template of RCPFeHA was stained with Live/Dead and great cell viability, stained in green, was showed in the surface of the microspheres (Figure 42E). The results suggested that the specific surface area of each type of microspheres do not improve the cell adhesion, thus the use of equal cell number was showed to be the most suitable methodology for the cell seeding.

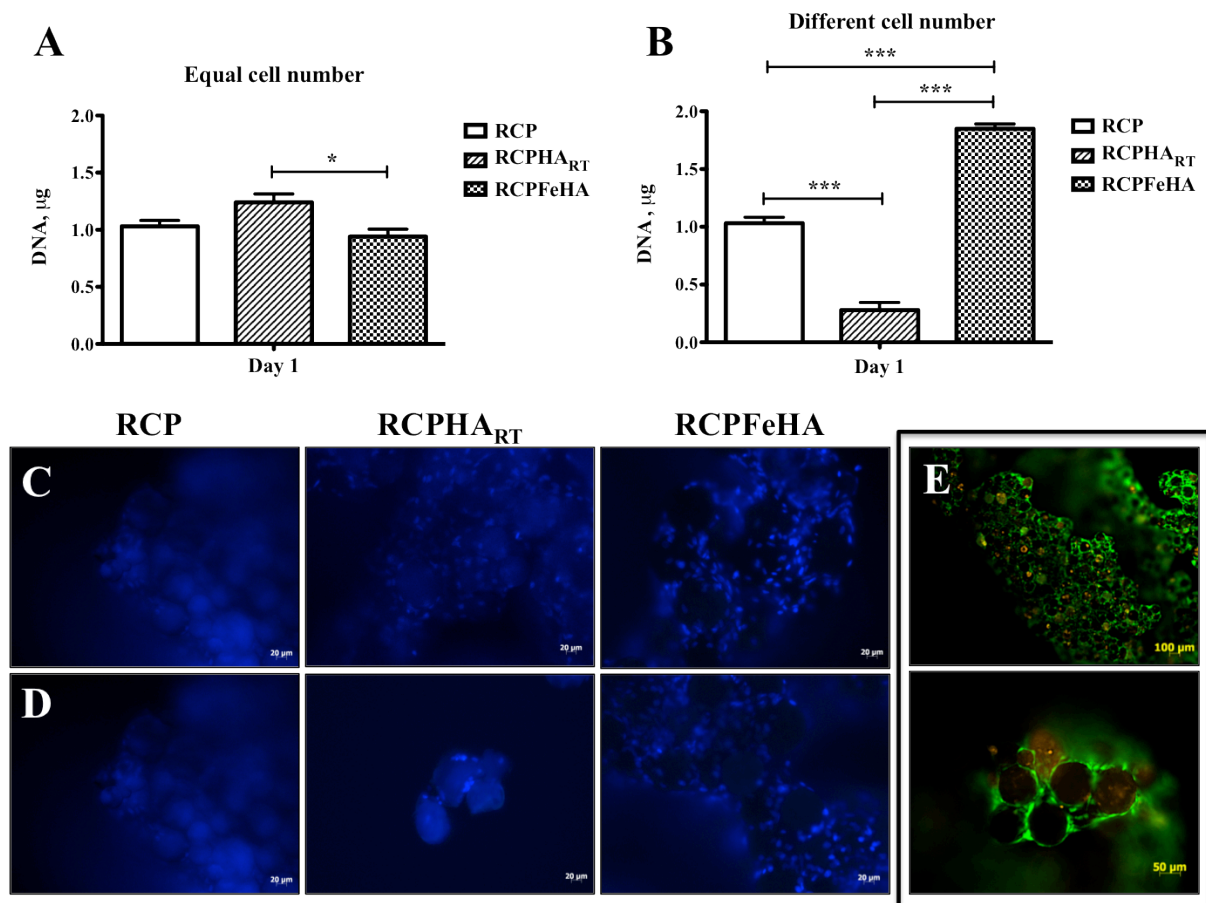


Figure 42. DNA amount obtained from equal cell seeding number (A) and different cell seeding number (B). Cell nuclei were stained with DAPI, in equal cell seeding number (C) and different cell seeding number (D). Live/Dead staining of RCPFeHA after 24 hours of cell culture (E).

3.4.3 *In vitro* osteogenic differentiation of human mesenchymal stem cells

Cell Content

To analyse the amount of cells adhere to the microspheres and the influence of microspheres composition on cell content and consequently on cell proliferation, DNA content was quantified at predetermined time points (i.e. 2h, 1 day, 3 days, 7 days and in the end of the experiment). Similar cell seeding efficiencies in all tested microspheres, without significant differences among the groups, was showed after 2h of cell seeding (Figure 43A). At day 1, slight decrease in the DNA content was showed for RCPFeHA, due to the cell seeding in presence of the Donor 1, although delicate recovery on day 3 and day 7 was presented (Figure 43A, 43B). During the time in culture, no statistically significant differences were noted in the DNA content extracted from the cells in contact with all tested microspheres (n=3). Variability on DNA content was showed among the Donors (Figure 43B).

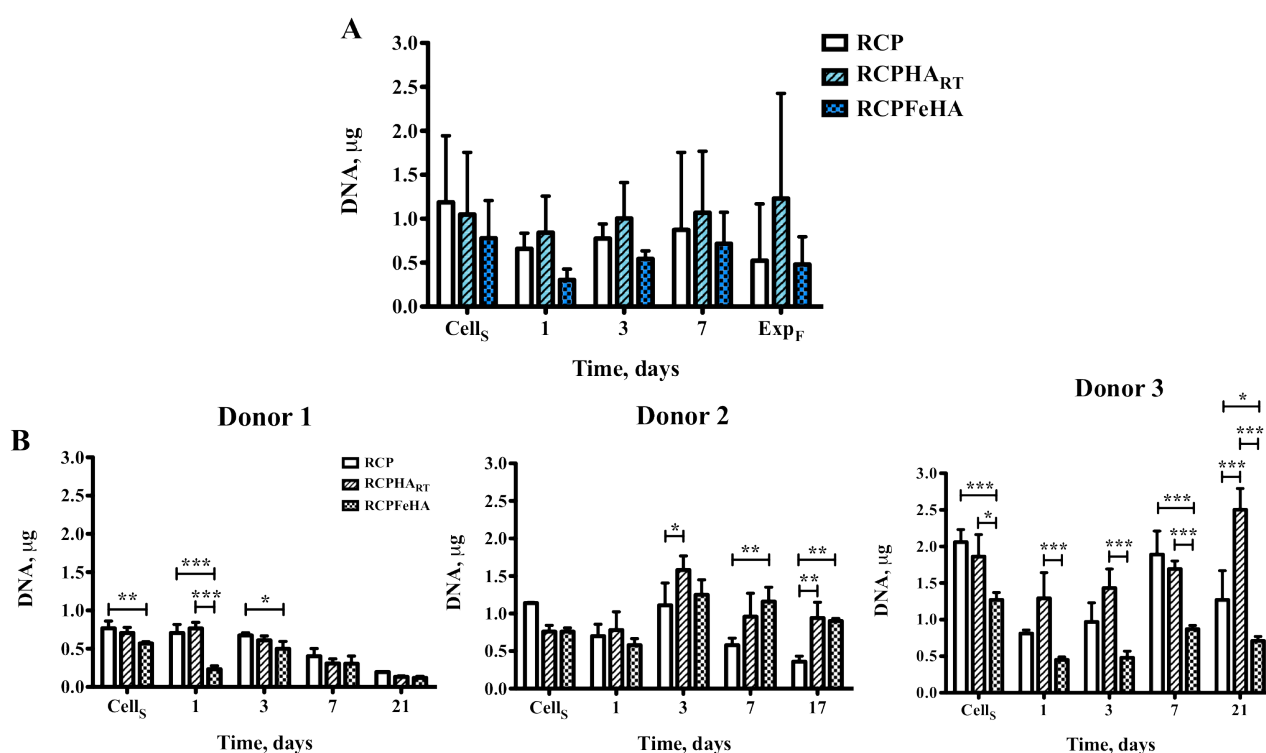
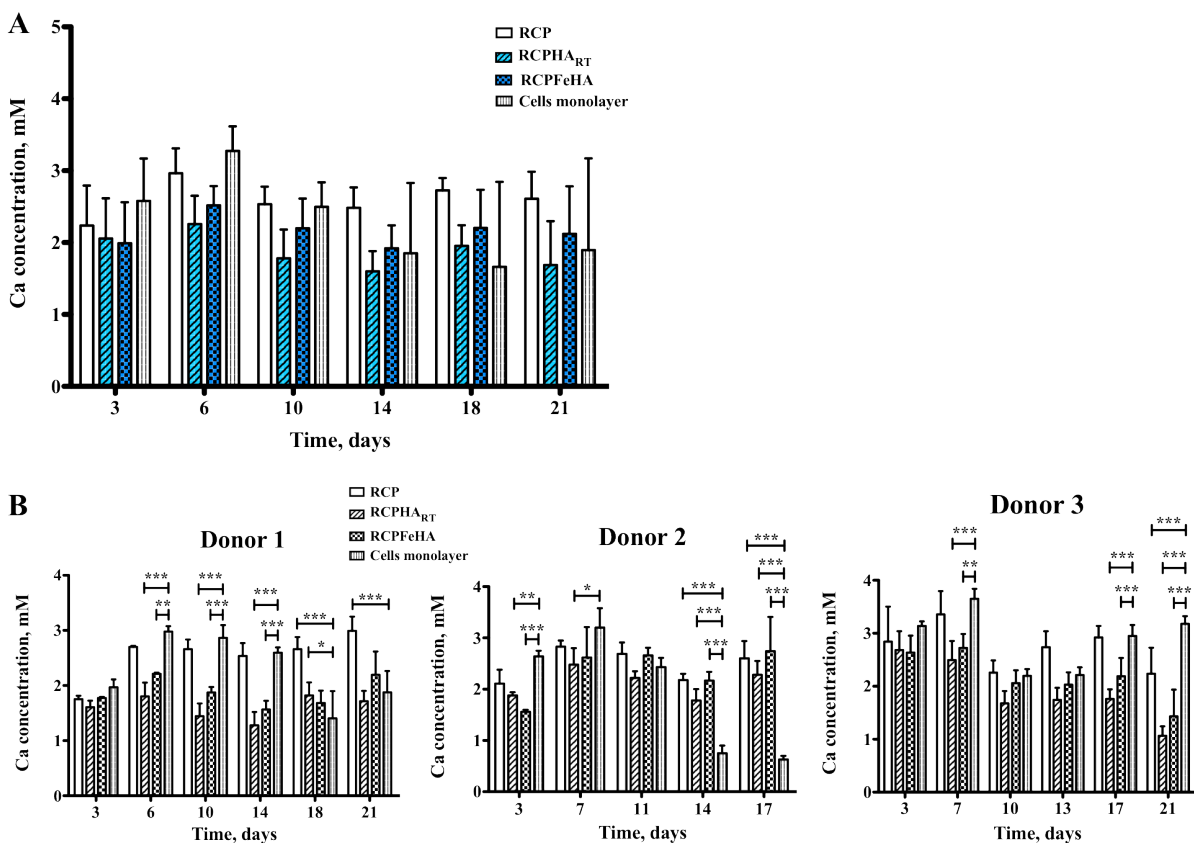


Figure 43. (A) hMSCs DNA content in all tested microspheres, over the course of the experiment (n=3), (Cell_s: cell seeding after 2 hours; Exp_F: end of experiment 21 days or 17 days, depending on the Donor); DNA values obtained from independent Donors (B), (Plot values represent Mean ± SD).

Calcium content

3D templates (i.e. hMSCs with all tested microspheres) were kept in culture for 17 or 21 days in osteogenic induction medium and the calcium content was quantified in presence of all the tested Donors. The values of calcium in the medium were compared with cells monolayer, used as a control. In presence of RCP, no significant reduction of calcium from osteogenic induction medium was presented, while in RCPHA_{RT} and RCPFeHA compared to RCP low calcium values in the medium were detected (Figure 44A). In order to evaluate the effective trend of the results on calcium absorption from the cells or microspheres, individual

Donors were analysed (Figure 44B). In the Donor 1, from day 3 to day 14, no significant differences on calcium content were showed between microspheres, while at day 18 a decrease of calcium content was reflected from RCPHA_{RT}, RCPFeHA and cell monolayer with statistically significant differences for RCPHA_{RT} ($p < 0.05$). In the Donor 2, at day 14 low calcium content in the medium was showed in presence of cell monolayer with very statistically significant differences with all tested microspheres ($p < 0.001$). Controversial results were showed in the Donor 3, the decrease on calcium content was showed in RCPHA_{RT} and RCPFeHA with very statistically significant differences at day 17 ($p < 0.001$) (Figure 44B). The calcium content in osteogenic induction medium in presence of microspheres without cells was also evaluated. In RCP, no significant differences on calcium uptake were presented, while in mineralised microspheres (i.e. RCPHA_{RT} and RCPFeHA) very statistically significant differences on calcium content were obtained ($p < 0.01$; $p < 0.001$), due to ion exchange between microspheres and osteogenic induction medium (Figure 44C). By comparing mineralised microspheres in presence of cells and without cells, high calcium content in cell medium in presence of cells was showed, suggesting the calcium uptake from the cells.



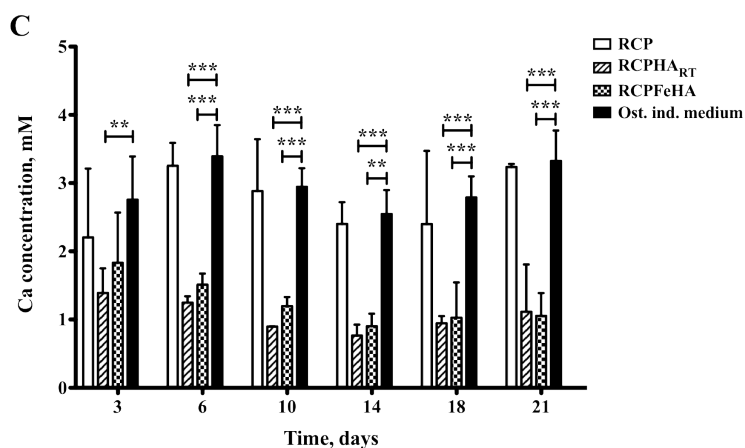


Figure 44. (A) Calcium content in osteogenic induction medium, over the course of the experiment with 3D templates (i.e. hMSCs and respective microspheres RCP, RCPHA_{RT} and RCPFeHA) and in all tested Donors, (* $p \leq 0.05$; ** $p < 0.01$; * $p < 0.001$, respect to cell monolayer). B) Calcium content in osteogenic induction medium, over the course of the experiment with microspheres (RCP, RCPHA_{RT} and RCPFeHA), (* $p \leq 0.05$; ** $p < 0.01$; *** $p < 0.001$, respect to osteogenic induction medium (ost. ind. medium)).**

Gene Expression

The calcium in osteogenic induction medium was quantified in all tested microspheres and cells monolayer. As showed previously, mineralised microspheres slightly uptake the calcium from the cell medium, thus for the gene expression the samples were harvested after calcium drop in cell monolayer. Osteogenic differentiation of hMSCs were evaluated by the expression of important genes, such as early markers of osteogenic differentiation (i.e. ALPL, COL I and IBSP) and late marker of osteogenic differentiation (i.e. BGLAP), as well as Osteonectin (SPARC), by real-time PCR.

The as-obtained results showed a very low expression of the osteogenic genes, mainly BGLAP and ALPL in all tested microspheres, without statistically significant differences. Moreover, good levels of osteogenic differentiation were presented in COL I and SPARC (Figure 45A). Figure 45B demonstrated the expression of COL I and SPARC obtained separately in the different Donors among the tested microspheres and high variability between Donors was showed. High induction of osteogenesis was acquired with Donor 1 and 2, while lower expression was showed with the Donor 3. Regarding to the Donor 1, high expression of COL I, and IBSP with statistically significant differences and slight expression of SPARC in presence of RCPFeHA compare to RCP and RCPHA_{RT} was showed ($p < 0.05$, $p < 0.01$) (Figure 45B, 45C).

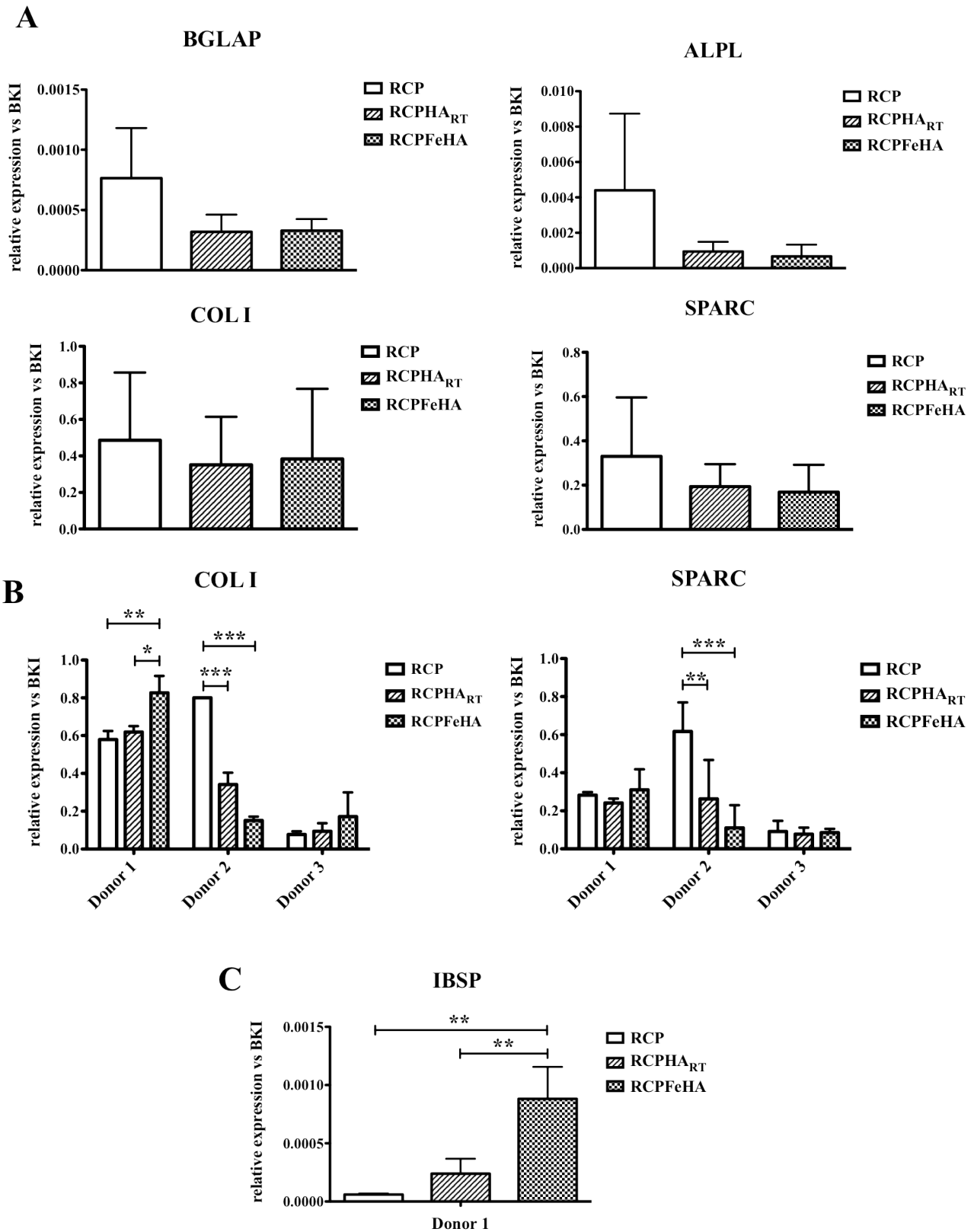


Figure 45. A) Osteogenic gene expression levels obtained in presence of RCP, RCPHA_{RT} and RCPFeHA. Gene expression levels of COL I, SPARC (B) and IBSP (C) obtained in presence of RCP, RCPHA_{RT} and RCPFeHA in the different Donors, (*p<0.05; ** p<0.01; ***p<0.001).

von Kossa staining

The evidence of osteogenic differentiation of all hMSCs donors exposed to osteogenic factors was evaluated in the end of the experiment. Optical micrograph showed the presence of calcium deposits, as indicated by the white arrows (Figure 46A). On the other hand, by von Kossa staining the advanced osteogenesis was investigated and in the Donors 1 and 2 was confirmed by the formation of calcium deposits (i.e. stained in black), while low mineralisation extend was developed by the Donor 3 (Figure 46B, 46C, 46D).

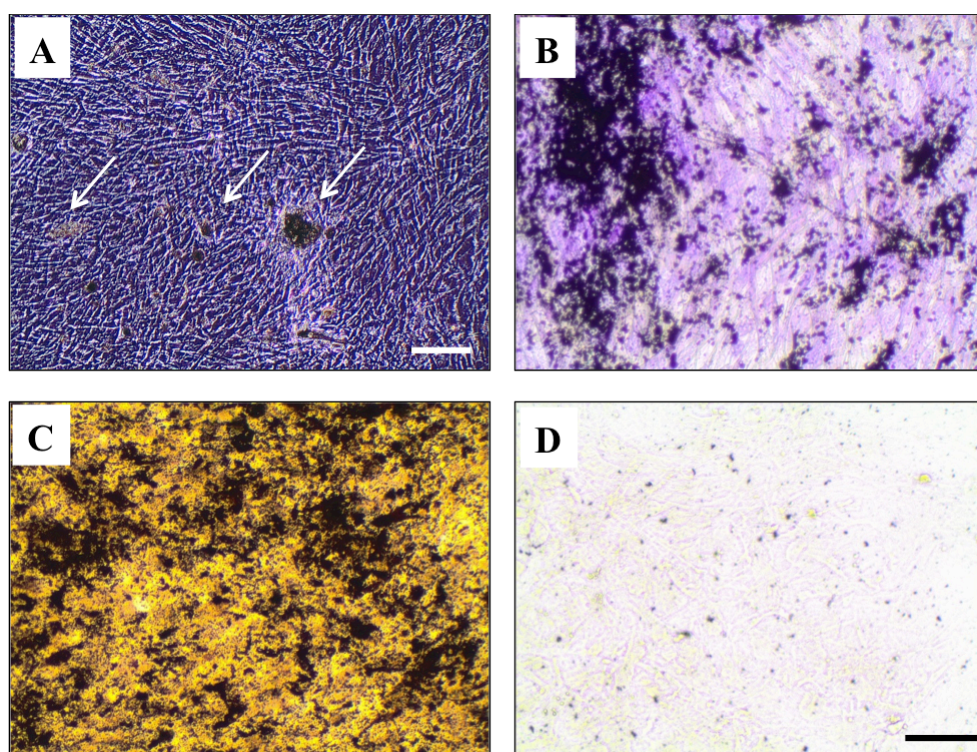


Figure 46. A) Optical micrographs of calcium deposits as indicated with white arrow and von Kossa staining of osteogenic differentiated of hMSCs, (B) Donor 1; (C) Donor 2; (D) Donor 3, (Scale bar: A) 200 μm and B, C, D) 100 μm).

Haematoxylin & Eosin Staining and Thionin staining

After 21 days of cell culture, RCP, RCPHA_{RT} and RCPFeHA were stained with haematoxylin & eosin. The sections obtained from RCP, showed disperse microspheres and cells, while in presence of mineralised microspheres (i.e. RCPHA_{RT} and RCPFeHA) high compact structure was obtained. In both mineralised microspheres, cells nuclei were stained in purple and the produced extracellular matrix or collagen fibers from cells were stained in pink (Figure 47A, 47B, 47C). In Figure 47D, the interaction of cells with microspheres was showed with clear evidence of cells nuclei and extracellular matrix.

RCPFeHA was stained with thionin after 21 days of cell culture. Cells nuclei and cytoplasm were visualized in blue and violet-purple, respectively and great density of cells was surrounding the microspheres. Meanwhile, at high magnification the as-observed purple color from the cells might suggest the formation of glycosaminoglycan in presence of RCPFeHA microspheres (Figure 47E, 47F).

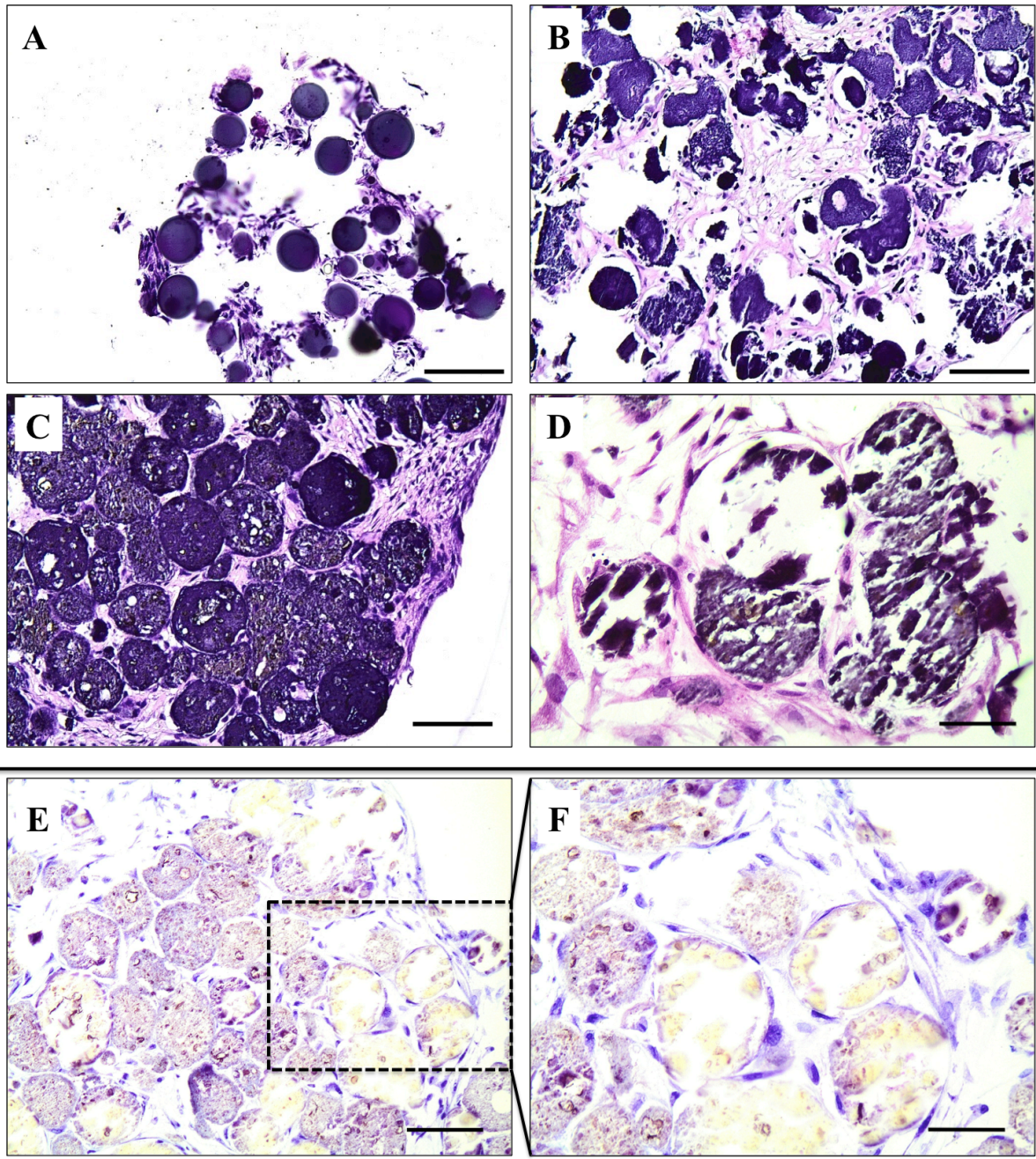


Figure 47. Haematoxylin and Eosin staining of representative sections of hMSCs cells cultured in osteogenic induction medium with RCP (A), RCPH_{ART} (B) and RCPFeHA (C, D) microspheres. E and F) Thionin staining of hMSCs cells cultured in osteogenic induction medium on RCPFeHA, (Scale bar: 100 μ m (A, B, C, E) and 50 μ m (D, F)).

3.5 Superparamagnetic microspheres as a sustained carrier for rhBMP-2 delivery

3.5.1 Microspheres properties

Surface topography, electrostatic interactions, hydrophobic interactions, hydrogen bond and surface chemistry of microspheres were described as the main factors involved in adsorption of protein (i.e. rhBMP-2) (Huang et al. 2016; King & Krebsbach 2012). Regarding to that, surface morphology, surface charge, wettability, swelling and specific surface area of all as-produced microspheres were analysed.

Microspheres were cut and cross-sections were evaluated by SEM. By the cross-section analysis, all the as-produced microspheres presented a dense structure. Smooth internal morphology in RCP was presented, while in RCPfluidMAG-CT slight roughness surface was obtained by the incorporation of magnetic nanoparticles in RCP matrix (Figure 48A, 48B). Mineralised microspheres showed an internal roughness surface, due to the homogeneous distribution of mineral (Figure 48C, 48D). The distribution of Ca, P and Fe was mapped and analysed in RCPFeHA, by EDS microanalysis. The micrographs presented a homogeneous distribution of all the tested elements, indicating a well interaction of organic and inorganic matrix, as well as a production of homogeneous microspheres (Figure 48E, 48F, 48G).

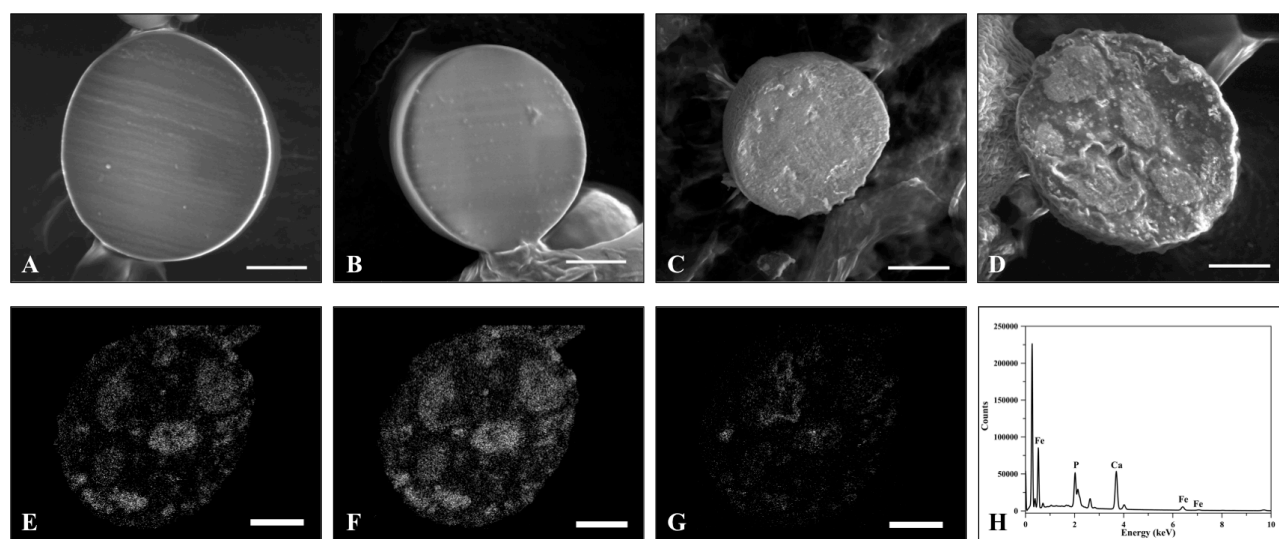


Figure 48. SEM micrographs from the as-fabricated microspheres; A) RCP; B) RCPfluidMAG-CT; C) RCPHA_{RT}; D) RCPFeHA and Ca (E); P (F) and Fe (G) distribution, as well as EDS microanalysis on RCPFeHA microspheres (H), (Scale bar: 20 μ m).

The surface charge of all tested microspheres was evaluated and higher surface charge in RCPHA_{RT} and RCPFeHA was presented. The wettability of the microspheres was evaluated and the contact angle of RCP and RCPfluidMAG-CT were lower than RCPHA_{RT} and RCPFeHA (Table 13). Moreover, the water adsorption was evaluated in presence of RCPHA_{RT} and RCPFeHA, for about 12 minutes. In both microspheres the water was slowly adsorbed, reaching a final contact angle of 42.27 ± 1.76 and 49.06 ± 0.11 , respectively, suggesting that mineralized microspheres were hydrophobic (Figure 49).

The effect of microspheres morphology and composition on swelling properties was analysed (equation 2) and the dense structure of RCP and RCPfluidMAG-CT microspheres allowed lower uptake of PBS, while RCPFeHA showed higher swelling properties, due to the presence of micro-porous with total porosity of 69.15%, as measured by mercury porosimetry (Table 13). The specific surface area of the microspheres was also evaluated and higher specific surface area was showed in RCPFeHA microspheres, while RCPHA_{RT} presented lower specific surface area. RCP and RCPfluidMAG-CT presented similar specific surface areas (Table 13).

Table 13. Physical properties of microspheres, (obtained by: §zetasizer system; #contact angle system; *optical micrographs and analysed by Image J software; **BET equipment).

Microspheres	§Zeta Potential, mV	#Wettability, °	*Swelling, %	** Specific surface area, m ² /g
RCP	1.53 ± 0.12	89.87 ± 4.13	16.45 ± 1.62	135.28
RCPfluidMAG-CT	2.19 ± 0.55	75.67 ± 0.92	18.47 ± 1.82	121.60
RCPHA _{RT}	-4.21 ± 0.86	111.4 ± 0.26	21.22 ± 1.76	29.11
RCPFeHA	5.86 ± 0.07	111.9 ± 0.37	43.25 ± 2.27	194.11

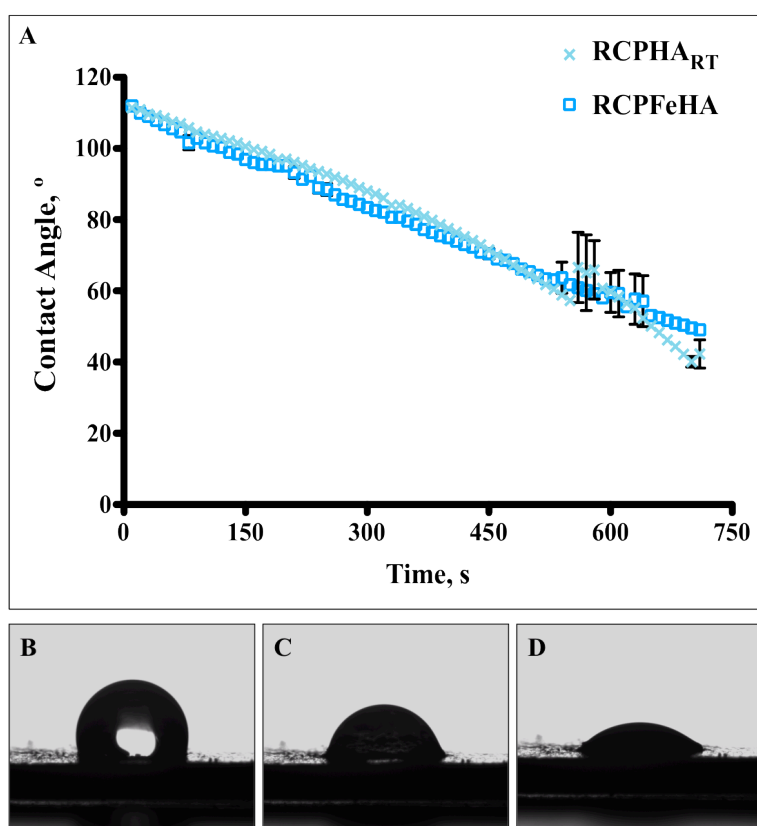


Figure 49. Variance of contact angle during the time for RCPHA_{RT} and RCPFeHA (A). Representative water drop on RCPFeHA in the beginning (B), after 360 seconds (C) and in the end of the experiment.

3.5.2 Effect of specific surface area of microspheres on rhBMP-2 release

Preliminary investigations on rhBMP-2 release were evaluated in presence of C2C12 BRE-Luc cell line. As reported previously, RCPHA_{RT} showed lower specific surface area comparing to RCP and RCPFeHA microspheres, with 4.7 and 6.7 of fold change of difference, respectively. Two rhBMP-2 adsorption strategies were adopted by take into account or no the specific surface area of the tested microspheres.

After one day of rhBMP-2 release, the supernatant was collected by centrifugation and analysed in presence of C2C12 BRE-Luc cell line. This cell line is genetically modified with BMP responsive element-luciferase construct that in presence of BMP, the luciferase gene is expressed (Herrera & Inman 2009). Therefore, the use of this test can indicate the bioactivity of released rhBMP-2, which is important on cellular response (Figure 50A, 50B).

In both tested strategies the rhBMP-2 released from all the microspheres was bioactive, as indicated by the luminescence signal generated by the luciferin. Moreover, independently of the strategy a trend on luciferin signalling was observed. Take into account the specific surface area of each type of microspheres, very statistical significant differences among the tested microspheres were presented ($p < 0.001$) (Figure 50B). Additionally, high luciferase activity from rhBMP-2 released by RCP microspheres was showed, while low luciferin signal for RCPFeHA microspheres with very statistically significant differences ($p < 0.001$) in both strategies was presented (Figure 50B). Furthermore, the following investigations were carried out on equal amount of microspheres loaded with equivalent concentration of rhBMP-2.

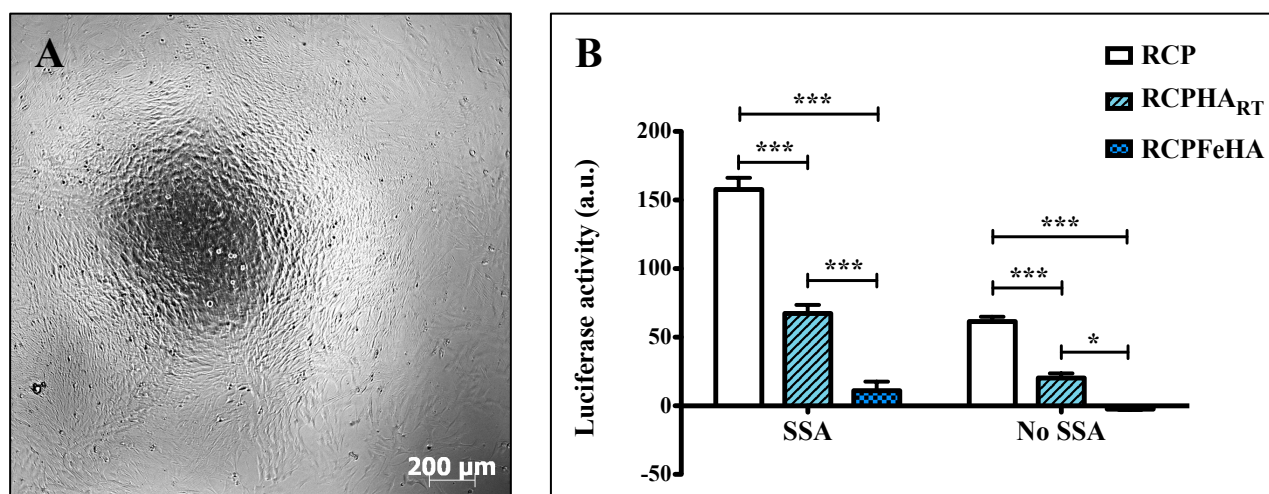


Figure 50. C2C12 BRE-Luc cell line in presence of released rhBMP-2 (A) and (B) Luciferase activity after 1 day of released rhBMP-2 from all tested microspheres (SSA: rhBMP-2 adsorption take into account the specific surface area; No SSA: rhBMP-2 adsorption without consider specific surface area), (* $p < 0.05$; *** $p < 0.001$).

3.5.3 Effect of microspheres composition on: Loading efficiency and interaction with rhBMP-2

rhBMP-2 loading efficiency

All the tested microspheres were washed three times with milli-Q water and evaluated by ELISA development kit. High amount of non-adsorbed rhBMP-2 was obtained from the first and second washing steps. The percentage of loaded rhBMP-2 in all the microspheres was presented in figure 51 (equation 3). Low percentage of rhBMP-2 was loaded from RCP and RCPfluidMAG-CT, while statistical significant differences and higher percentage of rhBMP-2 was loaded from RCPFeHA microspheres ($99.4 \pm 0.03 \%$; $p < 0.05$).

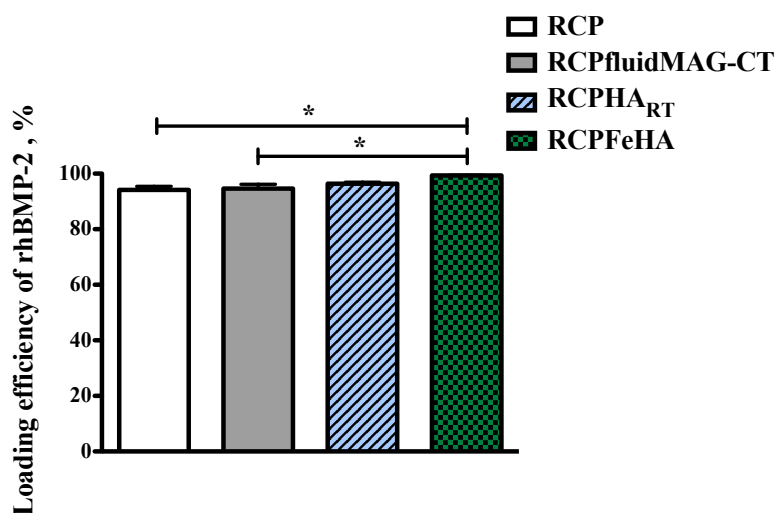


Figure 51. Loading efficiency of rhBMP-2 in all tested microspheres, (* $p < 0.05$).

Loading efficiency by using fluorescent rhBMP-2

Empty microspheres and loaded microspheres with red texas rhBMP-2 were analysed by fluorescence microscopy at equal exposure time (Figure 52). Low fluorescent background was presented from empty RCP, RCPHA_{RT} and RCPFeHA microspheres, while high fluorescence was showed for RCPfluidMAG-CT microspheres, probably due to the presence of magnetic nanoparticles into RCP matrix (Figure 52A). The presence of rhBMP-2 was detected by the high red fluorescence among the tested microspheres, at concentration of 900 ng/mL (Figure 52B). After washing steps, the fluorescent in the samples was maintained, particularly detected in the surface of the microspheres, indicating the high affinity and loading efficiency (Figure 52C). Moreover, with the presented technique was difficult to evaluate the localisation of the rhBMP-2 (i.e. inner or outer of the microspheres).

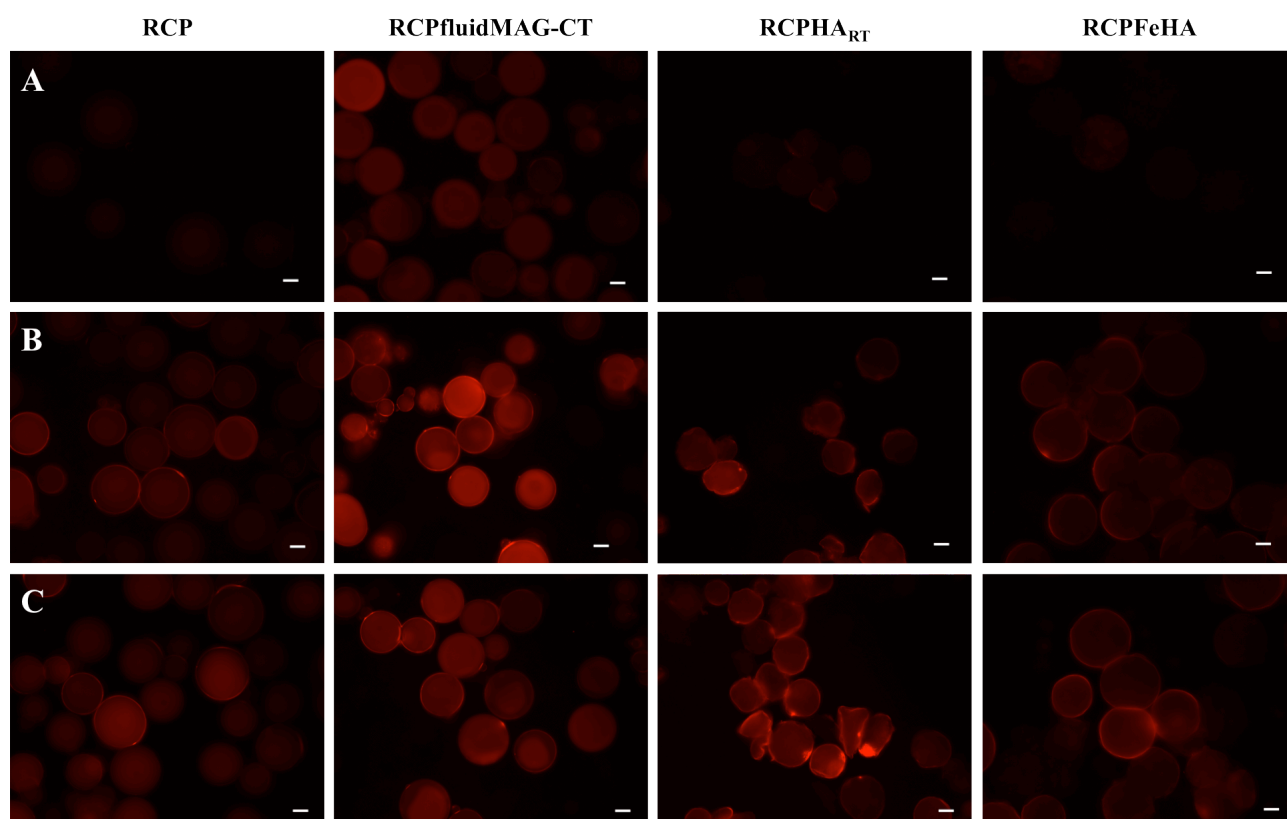


Figure 52. Fluorescence microscope images from microspheres without rhBMP-2 (A), with 900 ng/mL of rhBMP-2 (B) and after washing steps, (Scale bar: 20 μm).

Chemical evaluation of interaction of rhBMP-2 with microspheres

The interaction of rhBMP-2 with microspheres was evaluated by FTIR analysis. rhBMP-2 presented the typical vibration modes of proteins, with mainly assignments at 1600, 1560, 1200 cm^{-1} , for Amide I, Amide II and Amide III, respectively and assignments in the range of 980 – 1130 cm^{-1} (Figure 53), that can be assigned to -COC and -CO stretching (Figure 53 A*) (Jeevithan et al. 2014). In RCP and RCPfluidMAG-CT with adsorbed rhBMP-2, no significant differences were obtained on the vibration modes of the FTIR spectra, while deeply investigation was performed with mineralised microspheres (i.e. RCPHA_{RT} and RCPFeHA). Three types of adsorption functional groups from rhBMP-2 (i.e. -OH; -NH₂; -COO⁻) are showed to interact with hydroxyapatite nanophase (Dong et al. 2007), thus positive charge rhBMP-2 binds to the phosphate groups of hydroxyapatite layer (Gomez-Morales et al. 2013; Huang et al. 2016). Most of the investigations on rhBMP-2 are on Amide I and Amide II (Gilde et al. 2012; Schwartz et al. 2006), moreover the hybrid composition of microspheres limited the evaluation of interactions with rhBMP-2 in that region. Therefore, slightly differences on the stretching phosphate vibration mode (ν_3) were presented (i.e. 1106 and 1036 cm^{-1}) (Figure 53F, 53I). In RCP spectra, six assignments were presented, while seven assignments were obtained for rhBMP-2 by the deconvolution of the FTIR peaks (Figure 53B, 53C). A narrower phosphate peak was showed in RCPHA_{RT} and RCPFeHA without rhBMP-2. By the deconvolution of the peaks in range of 830 to 1190 cm^{-1} indicates the possible interaction of rhBMP-2 with RCPHA_{RT} and RCPFeHA (Figure 53F, 53I). In fact, the presence of rhBMP-2 in RCPHA_{RT} was identified by the formation of broad phosphate

group, mainly by the shift of 1026.1 to 1014.4 cm^{-1} and the formation of larger peak at 1065.6 cm^{-1} (Figure 53E, 53F). In RCPFeHA, the modification in the phosphate region was presented by the shift of the peak from 1018.5 to 1024.9 cm^{-1} and the broad peak at 111.7 cm^{-1} (Figure 53H, 53I).

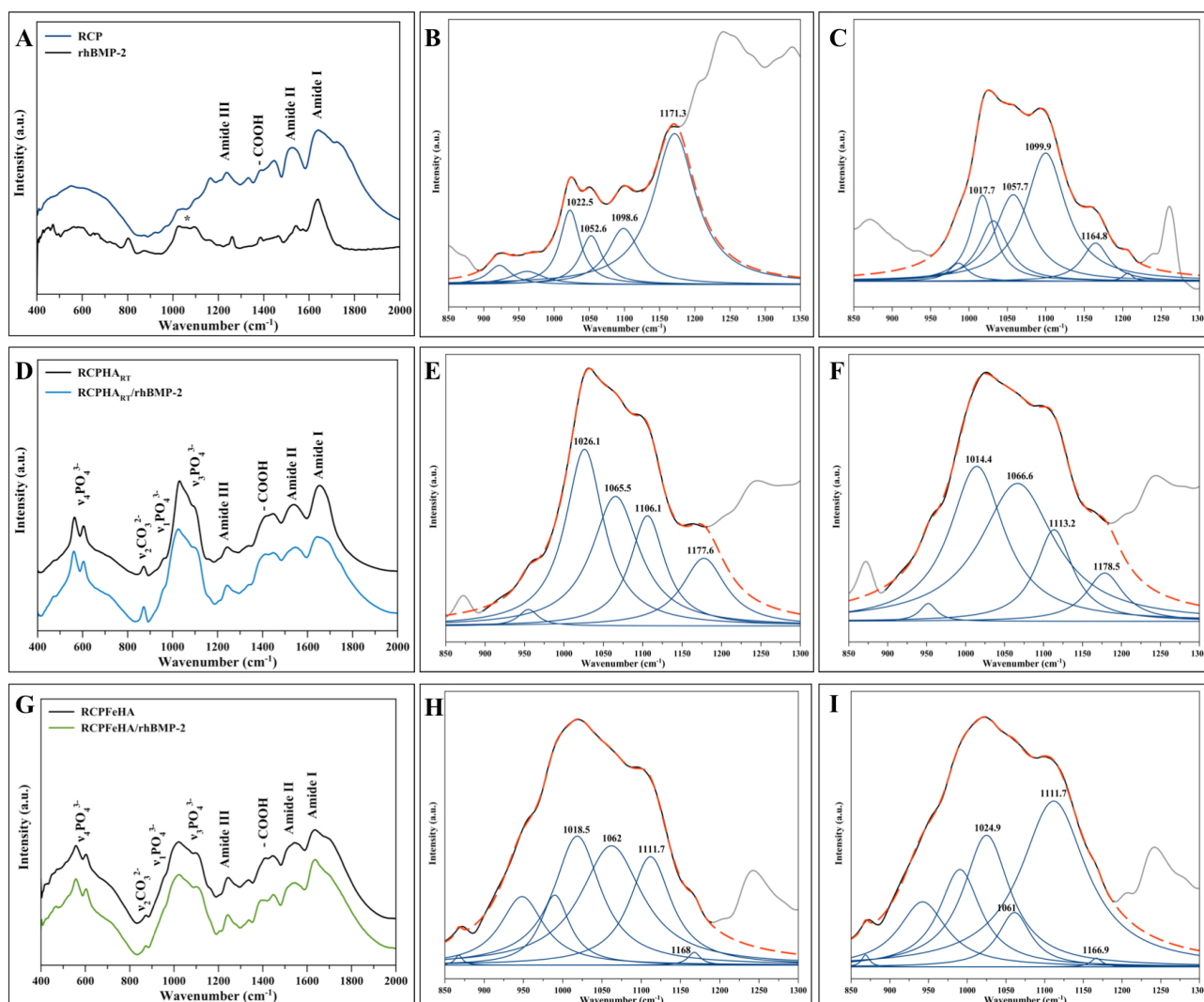


Figure 53. FTIR vibration peaks of RCP and rhBMP-2 (A) and respective deconvolution peaks (B) and (C); RCPHA_{RT} without and with rhBMP-2 (D) and deconvolution of phosphate peaks without rhBMP-2 (E) and in presence of rhBMP-2 (F); RCPFeHA without and with rhBMP-2 (G) and deconvolution of phosphate peaks without rhBMP-2 (H) and in presence of rhBMP-2 (I). (Orange trace line: Fit by Sum; Black line: FTIR spectra; blue lines: deconvolution peaks).

3.5.4 rhBMP-2 release kinetics

The rhBMP-2 release kinetics was evaluated under dynamic conditions (agitation, 100 rpm) and the effect of porosity and microspheres composition on rhBMP-2 release was investigated.

Effect of porosity on rhBMP-2 release

For this study, porous microspheres (RCP_{porous}, 1 μm) with rhBMP-2 loading efficiency (i.e. $71.65 \pm 3.87\%$) were used as a comparative model to the as-produced dense RCP microspheres. *In vitro* release tests showed that RCP_{porous} and RCP microspheres were able to release the rhBMP-2 over the time of the experiment (Figure 54), while an initial burst release was presented. After 24h, the rhBMP-2 cumulative release was about 65 % and 93 % for RCP_{porous} and RCP microspheres, respectively. Moreover, after 3 days, rhBMP-2 was completely released from dense RCP microspheres, while in RCP_{porous} microspheres a slower and more controlled release over the time of the experiment (i.e. 83 % in 14 days) was detected with extremely statistical differences on rhBMP-2 release ($p < 0.0001$).

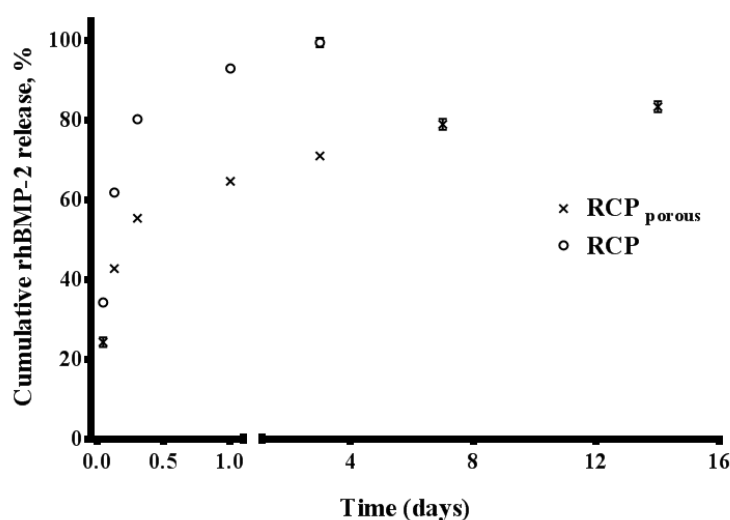


Figure 54. Cumulative release of rhBMP-2 in percentage from RCP_{porous} and RCP microspheres, (in all the points of the graph statistically differences of $p < 0.0001$).

Effect of microspheres composition on rhBMP-2 release

RCP dense microspheres and two types of mineralised microspheres (i.e. RCPHA_{RT} and RCPFeHA) were investigated as rhBMP-2 carriers. As mentioned previously, a burst release for RCP microspheres was presented, while sustained release of rhBMP-2 from mineralised microspheres was experienced. After 1h of rhBMP-2 release, extremely significant differences on rhBMP-2 release was showed (i.e. between RCP and RCPHA_{RT}; between RCP and RCPFeHA; **** $p < 0.0001$), while very significant differences between RCPHA_{RT} and RCPFeHA was presented (** $p < 0.01$). About 57 % and 24 % of rhBMP-2 were respectively released from RCPHA_{RT} and RCPFeHA microspheres, during 14 days of experimental investigations. Over the course of the experiment, extremely statistically significant differences were presented between all the

tested microspheres ($p < 0.0001$) (Figure 55A). Therefore, for RCP microspheres 900 ng of rhBMP-2 were released at day 3, while 400 ng and 200 ng were delivered by RCPHA_{RT} and RCPFeHA, respectively after 14 days of investigations (Figure 55B).

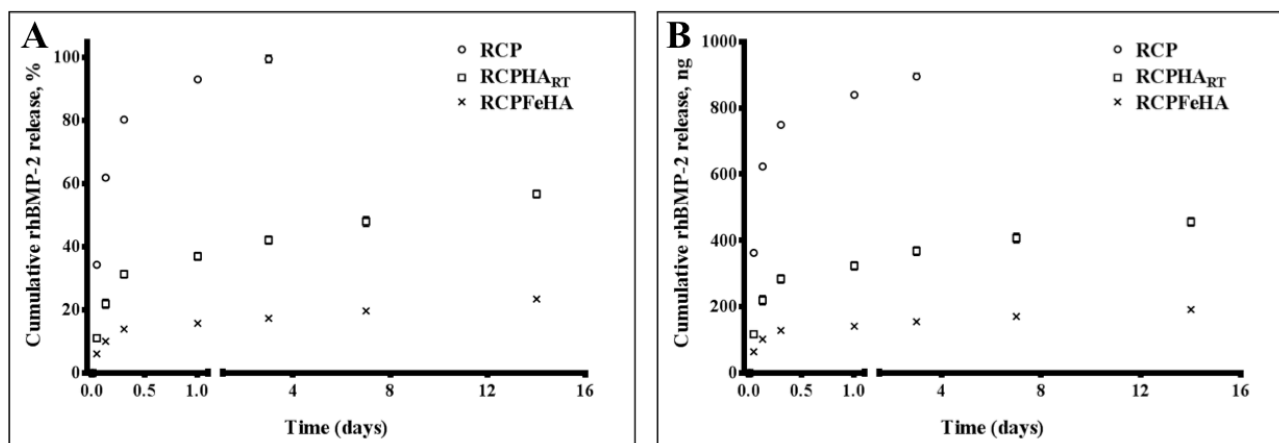


Figure 55. Cumulative release of rhBMP-2 in percentage (A) and in ng (B), from RCP, RCPHA_{RT} and RCPFeHA microspheres.

3.5.5 Evaluation of non-released rhBMP-2

After 14 days of rhBMP-2 release studies, microspheres were treated with urea and collagenase, in order to evaluate the residual attached rhBMP-2 to the microspheres. Predetermined concentrations of collagenase were investigated (i.e. 1 mg/mL; 2 mg/mL; 5 mg/mL and 10 mg/mL) and 10 mg/mL was selected as suitable concentration to degrade the microspheres and mineral nanophas was maintained (Figure 56). For RCP_{porous} microspheres, almost all the rhBMP-2 was recovered, while in mineralised microspheres about 30 % and 15 % of rhBMP-2, was obtained respectively from RCPHA_{RT} and RCPFeHA. From those results, was hypothesised that the rhBMP-2 linked to RCP was obtained after degradation of RCP with collagenase, while residual rhBMP-2 was linked to the mineral phase in the microspheres. Besides, the results suggested that rhBMP-2 presented higher chemical interaction with iron containing mineralised microspheres, as showed previously with FTIR analysis.

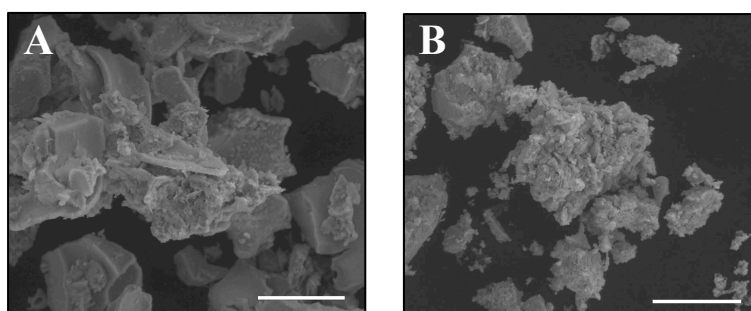


Figure 56. SEM micrographs of RCPHA_{RT} (A) and RCPFeHA (B) microspheres, after 14 days of rhBMP-2 releasing studies, urea treatment and degradation with 10 mg/mL of collagenase, (Scale bar: 50 μ m).

3.5.6 rhBMP-2 bioactivity

After one hour of releasing studies, the released medium was collected by centrifugation and predetermined volume was added to the C2C12 BRE-Luc cell line, as well as quantified by ELISA sandwich method and the results were showed as percentage of rhBMP-2 bioactivity (equation 4). High rhBMP-2 bioactivity was showed from all the tested microspheres, while statistically significant differences on rhBMP-2 bioactivity was showed for RCPFeHA compared to RCP microspheres ($p < 0.05$) (Figure 57).

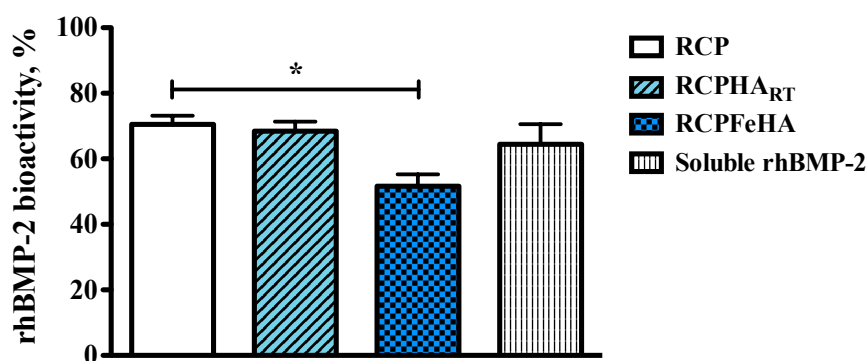


Figure 57. Percentage of rhBMP-2 bioactivity from RCP, RCPHA_{RT} and RCPFeHA, (* $p < 0.05$).

3.5.7 Tailored release of rhBMP-2 by using PEMF

The effect of external magnetic fields on rhBMP-2 release was evaluated in presence of RCPHA_{RT}, RCPfluidMAG-CT and RCPFeHA under pulsed electric magnetic field (PEMF). rhBMP-2 was adsorbed by the tested microspheres and a final concentration of 400 ng/mL was achieved and the releasing studies were performed without (static, NO PEMF) and under PEMF. In agreement with the previous results, all the tested microspheres were able to release rhBMP-2 over the time of the experiment. As was expected for RCPHA_{RT} any significant differences in releasing profile at both condition was presented (Figure 58A). Meanwhile, the effect of magnetic properties on delivery of rhBMP-2 was analysed in RCPfluidMAG-CT and RCPFeHA. Any significant differences were showed in the rhBMP-2 releasing profiles from RCPfluidMAG-CT at both conditions (i.e. No PEMF or PEMF), suggesting that rhBMP-2 was not linked with magnetic nanoparticles but only on the surface of the microspheres (i.e. RCP matrix), thus no improving on releasing profile with PEMF was showed (Figure 58B). Therefore, in RCPFeHA slight increase on rhBMP-2 release in presence of PEMF was showed without statistically significant differences (Figure 58C). The explanation of this result might be correlated by the use of low magnetic field and low magnetisation from RCPFeHA (1.65 emu/g).

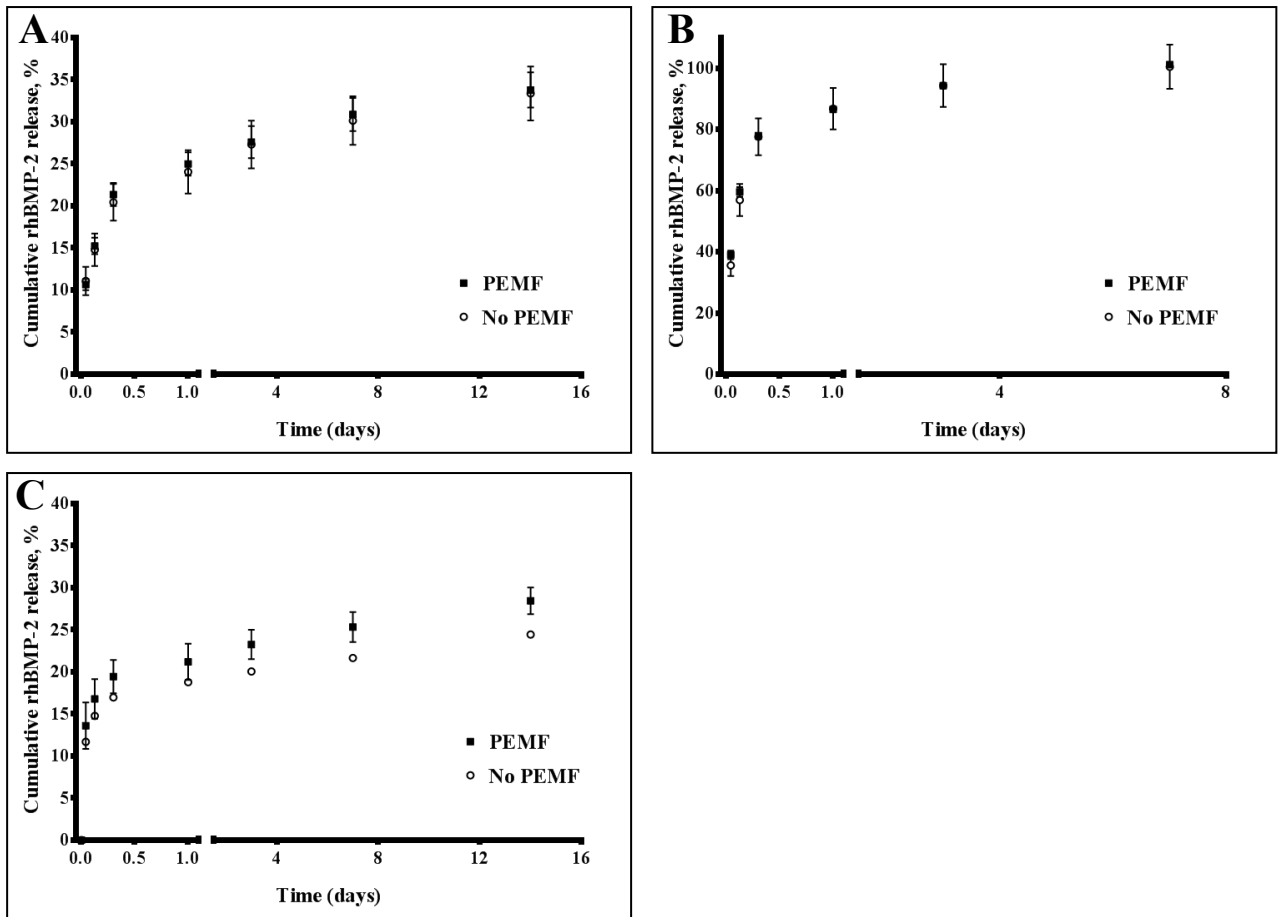


Figure 58. Cumulative release of rhBMP-2 in percentage of RCPHART (A), RCPfluidMAG-CT (B) and RCPFeHA (C) in presence or without PEMF.

3.6 Preliminary investigations on Scaffold fabrication

3.6.1 Bone-like scaffolds with superparamagnetic properties

Phase composition of the scaffolds was showed in the section 3.1.2. By keeping the mineral amount of 40 wt%, and by increasing the temperature of biomineralisation process material crystallinity and magnetic properties were improved. Herein, biomineralised slurries synthesised at 40 °C, 50 °C and 60 °C were used to produce iron-free and iron containing mineralised scaffolds, by freeze-drying process. The effect of synthesis temperature on scaffold structure and morphology was analysed by SEM.

Scaffolds and SEM micrographs from longitudinal cross-section of the scaffolds were showed in Figure 59A, 59B. From macroscopic point of view, the scaffold composed by the slurry synthesised at 60 °C showed weak 3D structure, compared to the other scaffolds synthesised at different temperature. By SEM micrographs, scaffolds presented internal and external porous structure, although in the bottom part small porous were obtained. RCP/FeHA, 60 °C exhibited heterogeneous and undefined porous structure. By analysing the porous detail of the scaffolds, in RCP/HA scaffolds synthesised at 40 °C, heterogeneous distribution of the mineral was presented. In RCP/FeHA scaffolds mineralised at 40 °C, homogeneous mineral distribution inside of the porous was showed, compared to the ones synthesized at 50 °C and 60 °C. The heterogeneous structure of the scaffolds and non well-defined shape of the porous does not allowed to evaluate the porous size. The results suggested that morphological structure of the scaffolds were probably affected by the induced crystallinity promoted by the synthesis temperature and resulted in fragile scaffolds above a critical extent of mineralization.

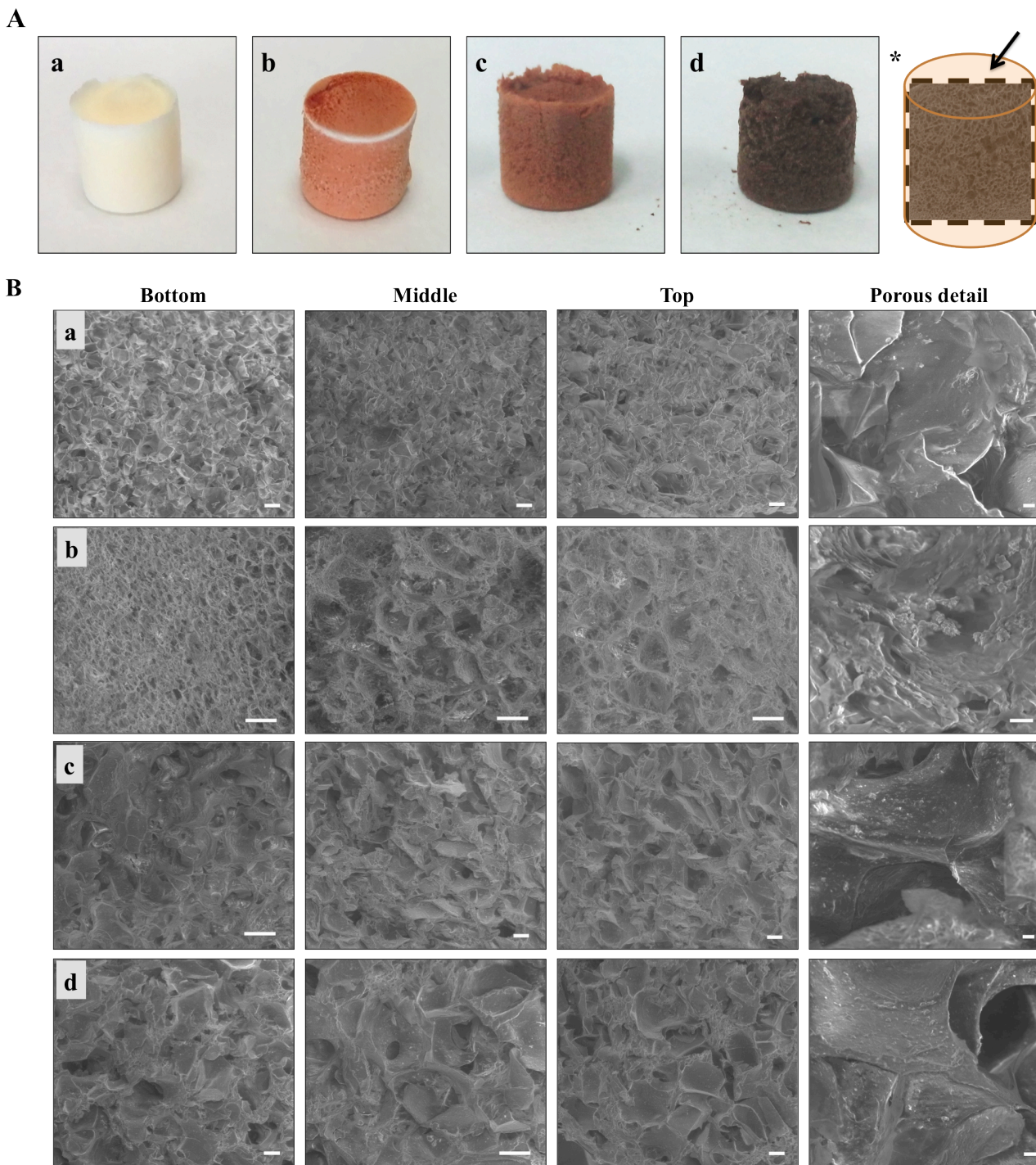


Figure 59. Scaffolds produced by using the mineralised slurries and freeze-drying process (A) and SEM micrographs from bottom, middle and top of the scaffolds, cut as demonstrated in A*, (B); (a) RCP/HA; b) RCP/FeHA, 40°C; c) RCP/FeHA, 50°C; d) RCP/FeHA, 60°C, (Scale bar: bottom, middle and top: 100 μm and porous detail: 10 μm).

The mineral content in the scaffolds was quantified by using the thermogravimetric curve obtained by TGA and higher mineral content was showed by using high synthesis temperature ($\approx 49.3\%$), while similar mineral amount with theoretical one was showed in RCP/FeHA, 40°C ($\approx 46\%$) (Figure 60A).

The effect of scaffold morphology and mineral content on adsorption of PBS was assessed by swelling tests (equation 5). After 1h of swelling tests, scaffolds absorbed higher amount of medium and then an osmotic equilibrium in the samples, until 24h was obtained (Figure 60B). RCP/FeHA (i.e. 40 and 50 °C) scaffolds presented higher swelling behaviour compared to RCP/HA. High mineral content in RCP/FeHA, 60°C was reflected in low swelling properties (Figure 60C).

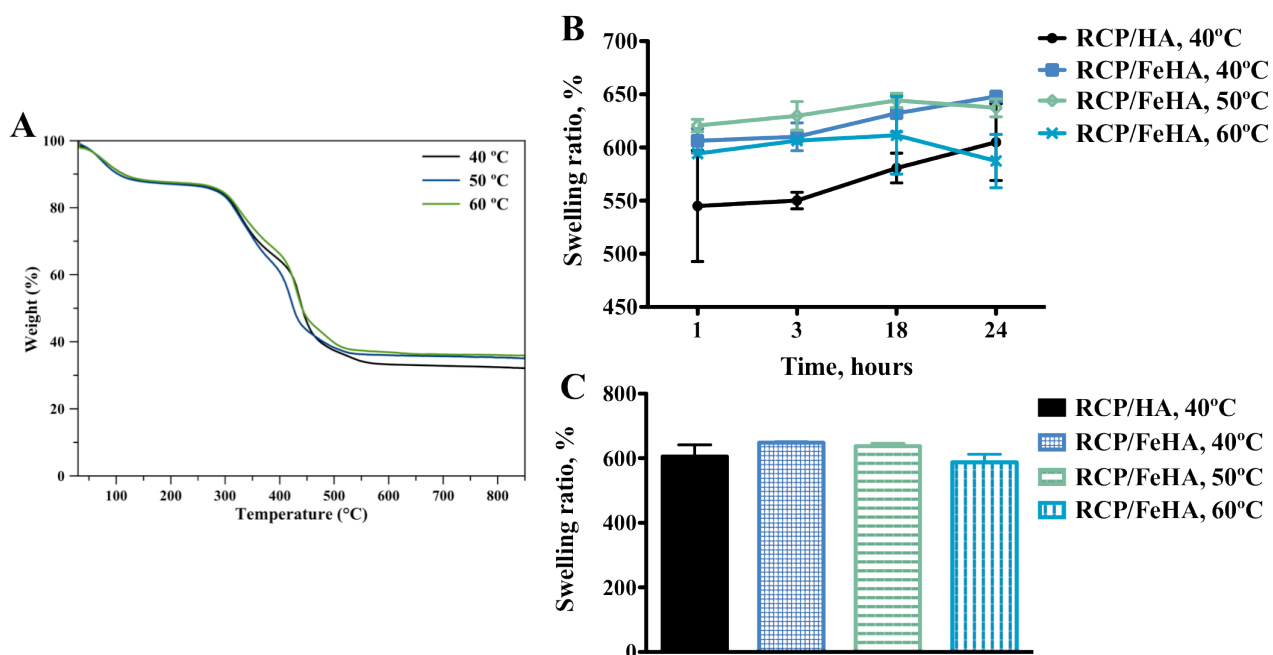


Figure 60. A) Thermogravimetric curve of iron containing mineralized scaffolds, obtained by TGA; B) Swelling properties up to 24h of soaking. C) Maximal swelling properties of the mineralised materials.

Chapter 4. Discussion

4.1 Application of biomineralisation process to obtain new hybrid biomaterials with superparamagnetic properties

Preliminary investigations were carried out to produce new hybrid biomaterials with superparamagnetic and bone-like properties. As described in Tampieri et al. 2012, various parameters were investigated in the synthesis of FeHA to produce bone-like apatite with magnetic properties and by increasing the synthesis temperature an enhancement on magnetic properties were obtained.

Fe/Ca molar ratio, $\text{Fe}^{2+}/\text{Fe}^{3+}$ molar ratio, organic / inorganic ratio and synthesis temperature were investigated. By varying $\text{Fe}^{2+}/\text{Fe}^{3+}$ molar ratio and Fe/Ca molar ratio magnetic or bone-like properties were not improved. On the other hand, in the case of those mineralised materials, the increase of mineral phase up to 80 wt% does not significantly improve the magnetic properties. Moreover, the as-obtained results indicated that by using RCP/FeHA with 40 wt% of mineral phase, $\text{Fe}^{2+}/\text{Fe}^{3+}$ molar ratio (3:2), Fe/Ca (20 mol%) and by applying various synthesis temperature, bone-like and superparamagnetic properties were achieved.

4.2 New bioactive bone-like microspheres with intrinsic magnetic properties obtained by bio-inspired mineralisation process

The application of bio-inspired processes for the synthesis of smart, highly bioactive materials is a relatively recent approach that in the last decade has been successfully followed, particularly in the pH-driven assembling and mineralisation of natural polymeric matrices such as collagen, with bone-like apatitic nano-phases. Such approach generated hybrid bone and osteochondral scaffolds with high biomimesis and regenerative ability (Tampieri et al. 2014; Tampieri et al. 2008; Sprio et al. 2012; Kon, Filardo, et al. 2010; Kon, Delcogliano, et al. 2010), and a number of novel biomaterials with smart properties for applications in medicine (Ramírez-Rodríguez et al. 2016; Campodoni et al. 2016).

The main features of biomineralisation processes is the ability to transfer information from the macromolecular template to the nucleating inorganic phase; such information consists in an ensemble of physico-chemical, morphological and ultrastructural control mechanisms that control the crystallization pathway of the inorganic phase and limit its growth (Sprio et al. 2012; Bouwstra J., Sutter M., Kluijtmans S., Hennink W. 2010; Boer A., Urk H., Bouwstra J. 2012).

In the present work, the biomineralisation process was translated to a hydrosoluble bioengineered collagen derived polypeptide matrix (RCP) obtained by an animal-free yeast fermentation process. The collagen I derived recombinant peptide is by design enriched with cell-binding RGD motifs, thus being able to support cell adhesion, proliferation and differentiation, in the form of hydrogel, scaffolds or microspheres (Bouwstra J., Sutter M., Kluijtmans S., Hennink W. 2010; Boer A., Urk H., Bouwstra J. 2012; Van Boxtel 2013). The biomineralisation process was applied to achieve the heterogeneous nucleation of Fe²⁺/Fe³⁺-doped hydroxyapatite onto the RCP matrix. The synthesis process was optimised on the basis of previous studies on the nucleation and crystallization of intrinsically superparamagnetic apatite phases, for which precise substitution extent with divalent and trivalent iron ions into the apatite structure was required (Tampieri et al. 2012; Tampieri et al. 2014). In this respect XRD, TEM and spectroscopic analyses confirmed the doping of the apatite lattice with both ion species during the biomineralisation process. Two different synthesis temperatures were used (i.e. 40 °C and 60 °C) to investigate the effect on the inorganic phase formation, crystal growth and magnetic properties, by using RCP mineralised with stoichiometric apatite in the same conditions (i.e. RCPHA), as a control material. As an effect of iron substitution, RCPFeHA exhibited lower crystallinity than RCPHA, and a lattice distortion consistent with selective doping of the Ca crystal sites with both Fe²⁺ and Fe³⁺ ions, and also carbonation in B site, was observed by FTIR analysis. The results confirmed that the synthesis temperature and the presence of foreign ions into hydroxyapatite lattice strongly influenced the crystallinity of the mineral phase; besides, a further control level, imparted by the macromolecular template (RCP) was evident when comparing with Fe-doped HA obtained in the present work with one obtained by wet synthesis at the same conditions without any templating matrix (Tampieri et al. 2012).

In order to study the early stages of RCP biomineralisation process, deeper investigation was carried out by studying the chemical interaction of divalent (i.e. Ca²⁺ and Fe²⁺) and trivalent (i.e. Fe³⁺) ions with RCP amide

and carboxylic groups and both are the main functional active groups for the coordination of different ions, like was reported in the biomineralisation of collagen or gelatin (Sprio et al. 2012; Mercado et al. 2014; Wang et al. 2015; Choi et al. 2013).

Besides, a clear trend was identified, where the band shift was stronger in the iron-containing materials, and also in the ones prepared at higher temperatures. This finding confirms the role of exposed iron ions in mediating the biomineralisation process, particularly in inducing a stronger bond with the organic matrix by a specific and preferential link to the carboxylic group, together with calcium ions. On the other hand, the detected shifts of amide groups might suggest the formation of new chelate bonds between Ca or Fe ions and C=O bonds from RCP, that however seemed active only at acidic pH conditions. In fact, when the experiment was carried out at neutral pH the vibration modes of amide I and II were similar to those of pure RCP. This behaviour reflects the gelatin-like character of RCP macromolecule, particularly in respect to the interaction with iron (Gaihre et al. 2008; Yonezawa et al. 2008; Wang et al. 2015; Choi et al. 2013).

The low crystallinity detected in the nucleated inorganic phase, particularly in RCPFeHA synthesised at 40 °C, likely reflected a poor ordering in the coordination of Fe ions in the apatite structure thus inducing very low magnetization values; on the other hand an increase of synthesis temperature promoted the crystallization of iron oxide, as detected by XRD and TEM and the establishment of higher magnetisation, by means of superparamagnetic-like behaviour and single magnetic domain, as obtained by the trend of the magnetisation curve and the low coercive force (H_c).

An emulsification process was optimised to produce RCP and hybrid microspheres and a dehydrothermal treatment (DHT) was used as method to crosslink and improves the microspheres stability in physiological conditions. Mechanical stirring velocity, cooling temperatures and RCP concentration, were the most relevant parameters to be controlled and well-dispersed hybrid microspheres with defined size and composition were obtained. DHT physical treatment is one of the methods used to crosslink gelatin or collagen scaffolds (Vandelli et al. 2004; Haugh et al. 2009; Prasertsung I. & Damrongsakkul S. 2010) and in crosslinked RCP microspheres, intermolecular bonds were formed and confirmed by both FTIR and thermal analysis.

Preliminary biological study with murine pre-osteoblast cells investigated the effect of microspheres composition, polymeric or hybrid iron-containing, on cell behaviour. Cell viability showed no significant difference between materials at the highest microspheres concentration. The small amount of iron oxide formed in RCPFeHA60 did not compromise the cells viability, after 7 days of culture *in vitro*.

4.3 Effect of ions release from hybrid superparamagnetic microspheres on osteogenic differentiation of MC3T3-E1

Calcium phosphate biomaterials presented interesting chemical and physical cues to be doped with relevant ions to mimic bone tissue composition (Boda et al. 2016). Recently, an innovative magnetic hydroxyapatite was synthesised by adding two iron sources (i.e. Fe^{2+} and Fe^{3+}) into the HAp lattice and interesting chemical and physical properties and inductive effect on cell behaviour were showed (Panseri et al. 2012; Tampieri et al. 2014; Panseri et al. 2016). By using a biomineralisation process, RCP matrix was mineralised with $\text{Fe}^{2+}/\text{Fe}^{3+}$ doped hydroxyapatite and iron-containing microspheres with superparamagnetic cues were achieved (RCPFeHA). The effect of ions release and microspheres composition on osteogenic differentiation of MC3T3-E1 was evaluated, as well as the release of ions was proposed as therapeutic purposes for bone tissue regeneration.

Both mineralised microspheres (i.e. RCPHA_{RT} and RCPFeHA) presented bone-like composition and microspheres aggregation in cell medium was improved by the functionalisation with citrate ions, that complex the calcium or the iron ions (present in the mineral phase of the slurries) and non-agglomerated microspheres in cell medium were obtained. Moreover, a partial replacement of calcium ions for iron ions in RCPFeHA was showed, without significant modifications on materials composition.

Further, the beneficial effect of calcium and iron release from RCPHA_{RT}, RCPfluidMAG-CT and RCPFeHA microspheres was investigated as a potential use to enhance bone regeneration. Calcium and iron ions are relevant on bone metabolism and essential on cell growth and functionality. Calcium ion plays a key role in the polarization of macrophages from M1 (inflammatory) to M2 (regeneration), supporting the homeostasis and bone regeneration, while iron deficiency increases the risk of osteoporosis (Wang et al. 2016; Boda et al. 2016; Perez et al. 2015; Toxqui & Vaquero 2015).

Microspheres were immersed in two different mimicking conditions (i.e. physiological or inflammatory), over the course of 28 days, and microspheres morphology, ions release, differences in the pH and phase composition were evaluated. In physiological mimicking conditions, the concentration of calcium in DMEM with RCPHA_{RT} and RCPFeHA was decreased, suggesting an uptake of Ca ion from the DMEM, mainly up to 7 days of immersion, and a precipitation of calcium/phosphate onto microspheres surface, as proved by the XRD analysis performed after 28 days immersed in DMEM. On the other hand, an increase of iron release on mimicking physiological conditions was showed, probably due to the iron ion exchange with calcium ion from DMEM. Some investigations have been corroborate the importance of adding extracellular Ca ion and osteogenic differentiation of human bone marrow stromal cells (hBMSCs) was enhanced (Zhang et al. 2014), although an increase of the number of death MC3T3-E1 cells was showed (Tsang et al. 2011). The dissolution of the as-produced superparamagnetic microspheres can make available Ca and Fe ions and can be defined as promising device for new effective applications in bone tissue engineering. In the blood the pH can be affected by the presence of tumour, inflammation and fractures, thus cellular responses are affected and reduced (Nakamura et al. 2016; Arnett 2010). Regarding to that, microspheres properties were evaluated under mimic inflammatory conditions. RCP and RCPfluidMAG-CT showed good morphologic

surface after 28 days of experiment, while from RCPfluidMAG-CT, RCPHA_{RT} and RCPFeHA ions were released. Calcium solubility was similar from both mineralised microspheres and low iron was released from RCPFeHA. In acidic environment, the resorption activity of osteoclasts is increased and the deposition of alkaline mineral in bone is reduced by osteoblasts, promoting the mineral homeostasis (Nakamura et al. 2016; Arnett 2010). The released ions from RCPFeHA could help or stimulate the surrounding inactivated osteoclasts to differentiate and to be activated, as well as improving osteoclasts formation *in vivo* (Nakamura et al. 2016).

The effect of non-mineralised and mineralised microspheres on cell viability, cell morphology and their ability on promoting osteogenic differentiation of MC3T3-E1 were evaluated. All the tested microspheres were cytocompatible, without apoptotic activation or reactive oxygen species production, until 3 days of cell culture. Therefore, the staining of actin filaments showed cell adhesion and spreading, that are relevant on interaction with biomaterials for further activities like cell migration, proliferation, differentiation and extracellular matrix production (Lin et al. 2013).

Real-time PCR analysis of osteogenic markers (i.e. BGLAP, COL I, and SPARC) was performed for evaluation of osteogenic differentiation promoted by microspheres composition. BGLAP is secreted by osteoblasts, as well as is the main noncollagenous compound of bone matrix deposition and mineralisation (Lin et al. 2013). Interestingly, an up-regulation of the genes was showed from all the tested microspheres. COL I is defined as an early osteogenic marker and is important on bone matrix formation (Lin et al. 2013). COL I expression was up-regulated in all the tested microspheres and slightly higher in RCPFeHA. SPARC gene encodes an important protein for collagen in bone tissue to become calcified (Rosset & Bradshaw 2016). SPARC expression was higher up-regulated in RCPFeHA. The as-mentioned expression levels of the genes suggested that all the microspheres have the ability to stimulate osteogenic differentiation of murine pre-osteoblasts cells, probably due to the calcium deposition in the microspheres surface (Zhang et al. 2014). The magnetic mineral phase of RCPFeHA provided an ion exchange and slightly improves the expression of osteogenic genes. The low concentration of iron released from calcium phosphate cements have enhanced osteogenesis and angiogenesis in mouse BMSCs and in human umbilical vein endothelial cells, respectively (Boda et al. 2016).

4.4 Effect of microspheres composition on differentiation of human mesenchymal stem cells

The main goal was to engineer a new 3D template composed by microspheres and human mesenchymal stem cells that provides an ideal biomimetic microenvironment for bone tissue applications. The cytotoxicity of RCP, RCPHA_{RT} and RCPFeHA microspheres were assessed after 7 days of cell culture and the effect of those microspheres combined with human mesenchymal stem cells triggering the regulation of osteogenesis *in vitro* was evaluated.

hMSCs were grown, spread and high cell viability in presence of all tested microspheres was showed. Moreover, high density of live cells was surrounding the hybrid microspheres indicating the great affinity to the microspheres and non-cytotoxicity effect in the presence of hMSCs.

The cell-seeding efficacy was similar in all the tested 3D templates, as showed by the DNA content after two hours of seeding, while DNA content among the Donors and in all the tested microspheres was maintained over the course of the experiment. In recent studies with hMSCs aggregates, the DNA amount decreased after 2 weeks of cell culture in osteogenic medium and the slightly variances on DNA level were suggested as occurrence of calcification of cartilage matrix (Phuong N. Dang et al. 2016; Phuong N Dang et al. 2016). After 21 days of cell culture, the formation of extracellular matrix and possibly formation of glycosaminoglycan in presence of RCPFeHA was showed by haematoxylin & eosin and thionin staining.

Several ions and proteins are presented in biological environments and by immersion of calcium phosphate biomaterials, a sustained dissolution-precipitation cascade was presented. In concordance with the results showed in previous topic of this thesis, an ion exchange in the cell medium was showed in presence of RCPHA_{RT} and RCPFeHA. The non-equilibrium of ions in cell culture medium due to ion exchange might affect the cells activity, while in *in vivo* the ion equilibrium is regulated by homeostasis (Barrere et al. 2006). The effect of microspheres composition on osteogenic differentiation was evaluated by the expression of relevant genes on bone formation. Osteoblasts synthesize and secrete collagen type I (COL I), alkaline phosphatase (ALPL), osteocalcin (BGLAP), osteopontin, osteonectin (SPARC) and bone sialoprotein (IBSP). In the beginning of cell proliferation and extracellular matrix synthesis and in post-proliferative of extracellular matrix, COL I and ALPL are expressed. On the other hand, osteopontin, osteocalcin and bone sialoprotein are expressed during the extracellular matrix mineralisation (Barrere et al. 2006; Calabrese et al. 2016; Boda et al. 2015; Westhrin et al. 2015). Low expression of BGLAP and ALPL osteogenic genes were presented. The mineral composition of mineralised microspheres (i.e. RCPHA_{RT} and RCPFeHA) may inhibit the production of ALPL from the hMSCs (Barrere et al. 2006), without inhibition of mineralisation, as showed by the high expression of SPARC and IBSP in Donor 1. Hydroxyapatite scaffolds in presence of hMSCs do not significantly improve the expression of osteogenic genes *in vitro* (i.e. BGLAP and SPARC), although a completely cellular maturation and *in vivo* bone formation was observed (Viti et al. 2016). On the other hand, iron based biomaterials in presence of cells were showed as potential device to improve the osteogenic differentiation of genes. For example, superparamagnetic nanoparticles (SPIONS) were labelled with hMSCs and an up-regulation of osteogenic related genes were showed (Wang et al. 2017). An improvement on bone-related gene expression by human bone marrow mesenchymal stem cells in presence

of iron containing mesoporous bioactive glass scaffolds was obtained (Wu et al. 2011). Or going further, the use of mineralised collagen with biomimetic iron doped hydroxyapatite showed an improvement on osteogenesis by applying an external magnetic field (Tampieri et al. 2014).

The as-investigated 3D template with RCPFeHA, non-cytotoxic effect on hMSCs and improvement in expression of relevant genes for bone tissue formation was showed and prompt the use of this template in bone tissue applications.

4.5 Superparamagnetic microspheres as a sustained carrier for rhBMP-2 delivery

rhBMP-2 is one of the most investigated growth factors in bone tissue regeneration, due to induce the osteogenic differentiation of stem cells and improve the formation of high quality of new bone tissue (Kim et al. 2016; Autefage et al. 2009). Herein, hybrid superparamagnetic microspheres were proposed as carrier for sustained release of rhBMP-2 over the time and the effect of porosity, microspheres composition and physical-chemical properties of microspheres were evaluated on rhBMP-2 release.

The main challenge is to understand and tailor the adsorption and bioactivity of rhBMP-2 in engineered bone devices. Protein-material interactions are influenced by charge, chemistry, topography and hydrophobicity, as well as nature of proteins, and surrounding environment (e.g. pH and ions). By adsorption process, the first interactions between proteins and materials surfaces are hydrophobic interaction, electrostatic interaction, hydrogen bond, surface topography and surface chemistry (Huang et al. 2016). The surface morphology, surface charge, wettability and swelling properties were different by comparing non mineralised (i.e. RCP and RCPfluidMAG-CT) with mineralised microspheres (i.e. RCPHA_{RT} and RCPFeHA). Regarding to the rhBMP-2 adsorption strategies by take into account the specific surface area of microspheres, statistical significant differences on luciferase activity from collected supernatant among the microspheres were obtained, while a trend of luciferase activity was similar in both strategies. This result suggested that the specific surface area did not improve the control release of rhBMP-2, although the surface chemistry was showed as an important factor. Moreover, limitations are still presented on evaluation of the effect of the binding mode of rhBMP-2 to bone morphogenetic protein receptors, as well as the mechanism involved to guarantee the rhBMP-2 activity (Huang et al. 2016). The binding sites of proteins adsorbed in hydroxyapatite can be divided in C-sites or N-sites, as well as protein interacted with hydroxyapatite during the protein adsorption until matching the specific crystal surface. Therefore, the adsorption phenomena is mainly conducted by electrostatic interactions (i.e. negatively charged carboxylate groups and calcium cations on hydroxyapatite surface) and intermolecular H-bonds between N-containing groups and phosphate groups of hydroxyapatite (Zhou et al. 2007; Dong et al. 2007). The as-investigated rhBMP-2 had pH = 6.5 and positive surface charge (i.e. 35.1±5.4 mV), thus high affinity to the mineral phase of the microspheres was showed.

The release profile of rhBMP-2 from all tested microspheres and their bioactivity were evaluated *in vitro*. A controlled release profile of rhBMP-2 from RCPHA_{RT} and RCPFeHA was showed, over 14 days, whereas a burst release was showed for RCP microspheres, suggesting the strong interaction with mineral phase of the microspheres. Moreover, the released rhBMP-2 was showed to be bioactive for all the tested microspheres.

High fluorescence of texas red rhBMP-2 was obtained in presence of mineralised microspheres, while by deconvolution of phosphate vibration mode, various peaks were detected and broad peaks or slight shift were showed in presence of rhBMP-2. Altogether, adsorption of rhBMP-2 in mineralised microspheres was suggested by chemical, electrostatic and hydrophobic interactions.

RCPFeHA was previously showed to improve the osteogenic differentiation of MC3T3-E1 and human mesenchymal stem cells, thus combining the sustained release of rhBMP-2 might improve the regenerative

ability of the device, as well as its clinical application. On the other hand, the biomimetic, osteogenic properties and the sustained release of rhBMP-2 and tailored release with PEMF provide interesting advantages compared to the available commercial devices (Quinlan et al. 2015).

4.6 Preliminary investigations on Scaffold fabrication

Several approaches have been reported in the functionalization of scaffolds with magnetic properties, for bone tissue engineering and iron oxide nanoparticles has been extensively used (Bock et al. 2010; Xu et al. 2014; Singh et al. 2014; Mertens et al. 2014; Skaat et al. 2012; Wu et al. 2011).

Taking into account the promising properties of magnetic biomineralised scaffolds, in this work the biomineralisation of iron-doped apatite nanophase on synthetic collagen peptide matrix was studied. The main aim was to produce porous scaffolds with magnetic and adequate biomechanical properties for bone tissue applications. By applying a biomineralisation synthesis to RCP matrix, chemical interaction of carboxylic groups from RCP with iron and calcium ions from mineral phase were presented. The optimisation of the synthesis parameters, temperature and inorganic phase (until a certain amount, 40 wt%) were showed as fundamental parameters to obtain superparamagnetic properties.

Biomineralisation of RCP matrix with hydroxyapatite or magnesium doped hydroxyapatite and applied to scaffolds fabrication by freeze-drying process was described as successful methodology (Ramírez-Rodríguez et al. 2016). However, by applying and modifying this methodology for the fabrication of superparamagnetic materials, the as-produced scaffolds composed by RCP mineralised with iron-doped hydroxyapatite showed non-adequate 3D porous structure and weak biomechanical properties. Non-adequate cell migration, cell proliferation, cell viability, as well as transport of oxygen and nutrients, were hypothesised as additional drawbacks of those scaffolds. The results suggested that was reached the degree of mineralization on RCP matrix and the biomaterial was not suitable for the production of the scaffolds.

Furthermore, the production of RCP mineralised with hydroxyapatite and superparamagnetic properties might be attempted by applying one of the following strategies: i) Mineralisation of RCP with hydroxyapatite nanophase at room temperature, scaffold production by freeze-drying followed by crosslinking and then scaffolds can be soaked in ferrofluid (i.e. solution composed by iron oxide nanoparticles); or ii) during the biomineralisation of RCP matrix the as-used iron sources might be substituted by predetermined concentration of iron oxide nanoparticles.

The first strategy was investigated with mineralised collagen scaffolds and iron oxide nanoparticles were kept inside of the scaffold up to 8 days, without significant modifications on 3D structure of the scaffold and preliminary *in vitro* tests with human bone marrow stem cells, indicated cell adhesion and cell proliferation (Bock et al. 2010).

Chapter 5. Conclusions and Future perspectives

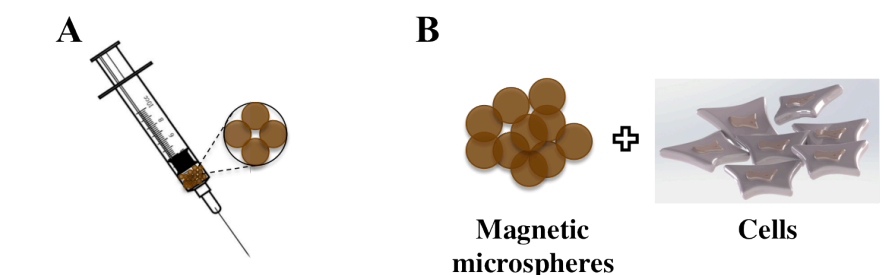
The growing numbers of bone defects, diseases and fractures create a high impact on public health and new solutions must be implemented. Bioactive magnetic based materials are promising solutions that have been investigated to treat bone tissue, through release of ions, composition and surface topography.

This thesis describes a bio-inspired mineralisation process and water-in-oil emulsification method that were successfully optimized and used to produce new hybrid microspheres with bone-like composition, composed by collagen type I based recombinant peptide mineralised with Fe²⁺/Fe³⁺-doped apatite nanophase. Biom mineralisation process confirmed to be a promising synthesis approach that can be flexibly directed to a variety of biomimetic materials with properties tailored on the basis of the nature and chemistry of the organic matrix and designed ion doping in the mineral nanophase. The high active surface exhibited by the apatite nanophase provides specific sites to link several drugs or growth factors. On this basis, such new magnetic microspheres with bone-like composition, cytocompatibility and by immersing microspheres in physiological mimicking conditions, an ion exchange was observed and can be an inductive factor on osteogenic differentiation and bone regeneration, as was showed by the improvement on osteogenic genes expression. Those promising features prompt the use of magnetic microspheres in medicine, particularly in bone tissue engineering, to regulate the osteogenic differentiation *in vitro* and supposedly bone metabolism *in vivo*. Biomimetic composition of microspheres promotes high cell viability, adhesion and proliferation, thus the use of 3D templates composed by cells and microspheres can be proposed for bone tissue engineering. On the other hand, the interesting chemical – physical features of superparamagnetic microspheres enable a sustained release of rhBMP-2 and can be suggested to overcome the actual rhBMP-2 carriers, by offering bone-like composition, slow degradation rates and sustained release over the time. The superparamagnetic properties of the new microspheres can enable smart mechanisms for the *on demand* release of therapeutic factors *in situ* by low alternated magnetic signals.

Regarding to clinical perspective, magnetic microspheres are suggested to be use as **bioactive bone filler**, or as **bioactive bone filler as a carrier of rhBMP-2**, or as **3D template composed by microspheres and cells**. Take into account the swelling properties of magnetic microspheres the injectability might be tailored by the amount of adsorbed water. On the other hand, the use of water does not change the phase composition of microspheres, as well as cytocompatibility and the induction of osteogenic differentiation (Figure 61A). The use of 3D template composed by microspheres and human mesenchymal stem cells showed interesting results on improvement of gene expression and prompt their use as support for bone tissue regeneration (Figure 61B). Furthermore, superparamagnetic microspheres were investigated as suitable carrier of rhBMP-2. In this case, might be suggested as bone filler and the adsorbed water might contain predetermined concentration of rhBMP-2 (Figure 61C). A new 3D template composed by magnetic microspheres with adsorbed rhBMP-2 and human mesenchymal stem cells was also proposed (Figure 61D). In the last two purposes, the osteogenic differentiation of the cells might be improved by i) using a bone-like biomaterial and by ii) the use of important growth factor on bone tissue regeneration (i.e. rhBMP-2). Nevertheless, after

implantation of one of the as-mentioned devices the regeneration of bone tissue can be enhanced by applying an external magnetic field. As showed in the introduction of this thesis, the use of magnetic fields improves the cell activity and also can induces the release of rhBMP-2 and iron ions, both important on boost bone tissue regeneration.

No rhBMP-2



rhBMP-2

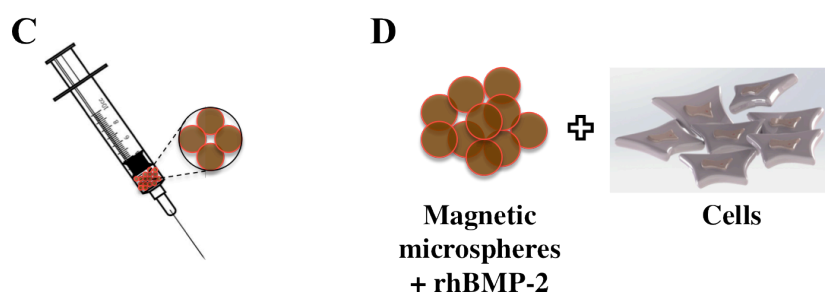


Figure 61. Proposed devices by using magnetic microspheres. A) Bone filler composed with swollen microspheres; B) 3D template composed by magnetic microspheres and cells; C) Bone filler composed by swollen magnetic microspheres as a carrier of rhBMP-2; D) 3D templates composed by swollen magnetic microspheres as rhBMP-2 carrier and cells.

The main scope of the thesis was achieved and superparamagnetic microspheres showed promising properties to be used in bone tissue regeneration, although to achieve the as-mentioned applications it will be necessary to go further and to evaluate some of the following aspects. First, concerning on the production of 3D templates (i.e. hMSCs with cells) and to conclude the effect of microspheres composition in the development of mineralisation will be interesting to evaluate the calcium deposition in the microspheres surface, by SEM and by ICP-OES analysis; sliced samples can be stained with several indicators and maybe to perform *in vivo* tests. Second, will be relevant to perform *in vitro* tests and to evaluate the effect of superparamagnetic microspheres with external magnetic field on cells viability and osteogenic differentiation. Moreover, if from those tests an interesting effect on cells behaviour is achieved; *in vivo* tests are proposed without and with magnetic stimulation. Third, effect of superparamagnetic microspheres as a

carrier of rhBMP-2 in presence of human mesenchymal stem cells can be analysed, then *in vivo* tests might be planned and the effect of this device in the development of new bone tissue might be evaluated by applying or not an external magnetic field. Fourth, the as-mentioned superparamagnetic microspheres can be used in clinical practice as bone filler and tests on rheological properties, injectability and microspheres size and the effect in the formation of new bone tissue *in vivo* might be clarified. Furthermore, if all these aspects showed promising properties for bone tissue engineering will be relevant to scale-up the production of superparamagnetic microspheres, thus to facilitate the future clinical trials and future microspheres commercialization.

References

- Addison, W.N. et al., 2015. Extracellular matrix mineralization in murine MC3T3-E1 osteoblast cultures: An ultrastructural, compositional and comparative analysis with mouse bone. *Bone*, 71, pp.244–256. Available at: <http://dx.doi.org/10.1016/j.bone.2014.11.003>.
- Amini, A.R., Laurencin, C.T. & Nukavarapu, S.P., 2012. Bone tissue engineering: recent advances and challenges. *Critical reviews in biomedical engineering*, 40(5), pp.363–408. Available at: <http://www.ncbi.nlm.nih.gov/pubmed/23339648><http://www.pubmedcentral.nih.gov/articlerender.fcgi?artid=PMC3766369>.
- Anil, S. et al., 2015. Drug Delivery Systems in Bone Regeneration and Implant Dentistry. *Current Concepts in Dental Implantology*, pp.239–65. Available at: <http://www.intechopen.com/books/current-concepts-in-dental-implantology>.
- Arnett, T.R., 2010. Acidosis, hypoxia and bone. *Archives of Biochemistry and Biophysics*, 503(1), pp.103–109. Available at: <http://dx.doi.org/10.1016/j.abb.2010.07.021>.
- Autefage, H. et al., 2009. Adsorption and release of BMP-2 on nanocrystalline apatite-coated and uncoated hydroxyapatite/ β -tricalcium phosphate porous ceramics. *Journal of Biomedical Materials Research - Part B Applied Biomaterials*, 91(2), pp.706–715.
- Bao, C.L.M. et al., 2013. Advances in Bone Tissue Engineering. In Rijeka: InTech, p. Ch. 0. Available at: <http://dx.doi.org/10.5772/55916>.
- Barrere, F., van Blitterswijk, C.A. & de Groot, K., 2006. Bone regeneration: molecular and cellular interactions with calcium phosphate ceramics. *Int J Nanomedicine*, 1(3), pp.317–332. Available at: <http://www.ncbi.nlm.nih.gov/pubmed/17717972><http://www.ncbi.nlm.nih.gov/pmc/articles/PMC2426803/pdf/nano-0103-317.pdf>.
- Bártolo, P.J. et al., 2011. Biofabrication strategies for tissue engineering. In *Advances on Modeling in Tissue Engineering*. Springer, pp. 137–176. Available at: https://link.springer.com/chapter/10.1007%2F978-94-007-1254-6_8.
- Boanini, E. et al., 2016. Alendronate Functionalized Mesoporous Bioactive Glass Nanospheres. *Materials*, 9(3). Available at: <http://www.mdpi.com/1996-1944/9/3/135>.
- Boanini, E., Gazzano, M. & Bigi, A., 2010. Ionic substitutions in calcium phosphates synthesized at low temperature. *Acta Biomaterialia*, 6(6), pp.1882–1894. Available at: <http://dx.doi.org/10.1016/j.actbio.2009.12.041>.
- Bock, N. et al., 2010. A novel route in bone tissue engineering: Magnetic biomimetic scaffolds. *Acta Biomaterialia*, 6(3), pp.786–796. Available at: <http://dx.doi.org/10.1016/j.actbio.2009.09.017>.
- Boda, S.K. et al., 2016. Competing Roles of Substrate Composition, Microstructure, and Sustained Strontium Release in Directing Osteogenic Differentiation of hMSCs. *ACS Applied Materials & Interfaces*, p.acsami.6b08694. Available at: <http://pubs.acs.org/doi/abs/10.1021/acsami.6b08694>.
- Boda, S.K., Thirvikraman, G. & Basu, B., 2015. Magnetic field assisted stem cell differentiation – role of

-
- substrate magnetization in osteogenesis. *J. Mater. Chem. B*, 3(16), pp.3150–3168. Available at: <http://www.scopus.com/inward/record.url?eid=2-s2.0-84927951033&partnerID=tZOtx3y1>.
- Boer A., Urk H., Bouwstra J., A.P., 2012. RGD containing recombinant gelatin. Available at: <https://www.google.com/patents/US20100062531>.
- Bos, P.K. et al., 2001. Growth factor expression in cartilage wound healing: Temporal and spatial immunolocalization in a rabbit auricular cartilage wound model. *Osteoarthritis and Cartilage*, 9(4), pp.382–389. Available at: <https://www.ncbi.nlm.nih.gov/pubmed/11399103>.
- Bose, S. & Tarafder, S., 2012. Calcium phosphate ceramic systems in growth factor and drug delivery for bone tissue engineering: A review. *Acta Biomaterialia*, 8(4), pp.1401–1421. Available at: <http://dx.doi.org/10.1016/j.actbio.2011.11.017>.
- Boskey, A.L., 2007. Mineralization of bones and teeth. *Elements*, 3(6), pp.385–391.
- Bouwstra J., Sutter M., Kluijtmans S., Hennink W., W.J., 2010. Controlled release composition comprising a recombinant gelatin. , p.11. Available at: <https://www.google.com/patents/US8357397>.
- Van Boxtel, H., 2013. Porous tissue scaffolds.
- Brum, A.M. et al., 2015. Connectivity Map-based discovery of parbendazole reveals targetable human osteogenic pathway. *Proceedings of the National Academy of Sciences of the United States of America*, 112(41), pp.12711–6. Available at: <http://www.pnas.org/content/112/41/12711.full.pdf%5Cnhttp://ovidsp.ovid.com/ovidweb.cgi?T=JS&PAGE=reference&D=emed13&NEWS=N&AN=2015443837%5Cnhttp://www.ncbi.nlm.nih.gov/pubmed/26420877%5Cnhttp://www.pubmedcentral.nih.gov/articlerender.fcgi?artid=PMC461161>.
- Bulstra, S.K. et al., 1993. Thionin staining of paraffin and plastic embedded sections of cartilage. *Biotechnic & histochemistry*, 68(1), pp.20–28. Available at: <https://www.ncbi.nlm.nih.gov/pubmed/7680580>.
- Butoescu, N. et al., 2009. Dexamethasone-containing PLGA superparamagnetic microparticles as carriers for the local treatment of arthritis. *Biomaterials*, 30(9), pp.1772–1780. Available at: <http://www.sciencedirect.com/science/article/pii/S0142961208009885>.
- Calabrese, G. et al., 2016. Collagen-Hydroxyapatite scaffolds induce human adipose derived stem cells osteogenic differentiation in Vitro. *PLoS ONE*, 11(3), pp.1–17. Available at: <http://journals.plos.org/plosone/article?id=10.1371/journal.pone.0151181>.
- Campodoni, E. et al., 2016. Development of innovative hybrid and intrinsically magnetic nanobeads as a drug delivery system. *Nanomedicine*, 11(16), pp.2119–2130. Available at: <http://www.futuremedicine.com/doi/abs/10.2217/nnm-2016-0101?journalCode=nnm>.
- Cheraghipour, E., Javadpour, S. & Mehdizadeh, A.R., 2012. Citrate capped superparamagnetic iron oxide nanoparticles used for hyperthermia therapy. *J. Biomedical Science and Engineering*, 5(December), pp.715–719. Available at: <https://www.scirp.org/journal/PaperInformation.aspx?PaperID=25767>.
- Choi, Y.C. et al., 2013. Human gelatin tissue-adhesive hydrogels prepared by enzyme-mediated biosynthesis of DOPA and Fe³⁺ ion crosslinking. *Journal of Materials Chemistry B*, 2(2), pp.201–209. Available at: <http://pubs.rsc.org/en/content/articlelanding/2014/tb/c3tb20696c%5Cnhttp://pubs.rsc.org/en/Content/Ar>

ticleLanding/2014/TB/C3TB20696C#!divAbstract%5Cnhttp://pubs.rsc.org/en/content/articlepdf/2014/tb/c3tb20696c.

- Chomoucka, J. et al., 2010. Magnetic nanoparticles and targeted drug delivering. *Pharmacological Research*, 62(2), pp.144–149. Available at: <http://dx.doi.org/10.1016/j.phrs.2010.01.014>.
- Costa, P.F., 2015. Bone Tissue Engineering Drug Delivery. *Current Molecular Biology Reports*, pp.87–93. Available at: <http://link.springer.com/10.1007/s40610-015-0016-0>.
- Cui, F.-Z., Li, Y. & Ge, J., 2007. Self-assembly of mineralized collagen composites. *Materials Science and Engineering: R: Reports*, 57(1), pp.1–27. Available at: <http://www.sciencedirect.com/science/article/pii/S0927796X07000526>.
- Dang, P.N. et al., 2016. Controlled dual growth factor delivery from microparticles incorporated within human bone marrow-derived mesenchymal stem cell aggregates for enhanced bone tissue engineering via endochondral ossification. *Stem cells translational medicine*, 5(2), pp.206–217. Available at: <https://www.ncbi.nlm.nih.gov/pubmed/26702127>.
- Dang, P.N. et al., 2016. Guiding Chondrogenesis and Osteogenesis with Mineral-Coated Hydroxyapatite and BMP-2 Incorporated within High-Density hMSC Aggregates for Bone Regeneration. *ACS Biomaterials Science and Engineering*, 2(1), pp.30–42.
- Davis, H.E. et al., 2011. Osteogenic response to BMP-2 of hMSCs grown on apatite-coated scaffolds. *Biotechnology and Bioengineering*, 108(11), pp.2727–2735.
- Delgado-López, J.M. et al., 2012. Crystallization of bioinspired citrate-functionalized nanoapatite with tailored carbonate content. *Acta Biomaterialia*, 8(9), pp.3491–3499. Available at: <http://www.sciencedirect.com/science/article/pii/S1742706112002048>.
- Denry, I. & Kuhn, L.T., 2016. Design and characterization of calcium phosphate ceramic scaffolds for bone tissue engineering. *Dental Materials*, 32(1), pp.43–53. Available at: <http://dx.doi.org/10.1016/j.dental.2015.09.008>.
- Dong, X. et al., 2007. Understanding adsorption-desorption dynamics of BMP-2 on hydroxyapatite (001) surface. *Biophysical journal*, 93(3), pp.750–759. Available at: <http://dx.doi.org/10.1529/biophysj.106.103168>.
- Dormer, N.H. et al., 2012. Osteogenic Differentiation of Human Bone Marrow Stromal Cells in Hydroxyapatite-Loaded Microsphere-Based Scaffolds. *Tissue Engineering. Part A*, 18(7–8), pp.757–767. Available at: <http://www.ncbi.nlm.nih.gov/pmc/articles/PMC3313610/>.
- Dorozhkin, S. V., 2011. Calcium orthophosphates. , (December), pp.121–164. Available at: <https://www.ncbi.nlm.nih.gov/pmc/articles/PMC3549886/>.
- Dorozhkin, S. V., 2009. Nanodimensional and nanocrystalline apatites and other calcium orthophosphates in biomedical engineering, biology and medicine. *Materials*, 2(4), pp.1975–2045. Available at: <http://www.mdpi.com/1996-1944/2/4/1975>.
- Drexler, J. & Powell, H., 2011. Dehydrothermal Crosslinking of Electrospun Collagen. *Tissue Engineering Part C: Methods*, 17(1), pp.9–17. Available at: <https://www.ncbi.nlm.nih.gov/pubmed/20594112>.

-
- Engel, E. et al., 2009. Biomaterials for tissue engineering of hard tissues. In M. Santin, ed. *Strategies in Regenerative Medicine*. Springer, pp. 1–42. Available at:
https://link.springer.com/chapter/10.1007%2F978-0-387-74660-9_3.
- Fernandez-Yague, M.A. et al., 2015. Biomimetic approaches in bone tissue engineering: Integrating biological and physicommechanical strategies. *Advanced Drug Delivery Reviews*, 84, pp.1–29. Available at: <http://dx.doi.org/10.1016/j.addr.2014.09.005>.
- Ferreira, A.M. et al., 2012. Collagen for bone tissue regeneration. *Acta Biomaterialia*, 8(9), pp.3191–3200. Available at: <http://dx.doi.org/10.1016/j.actbio.2012.06.014>.
- Florencio-Silva, R. et al., 2015. Biology of Bone Tissue: Structure, Function, and Factors That Influence Bone Cells. *BioMed Research International*, 2015, pp.1–17. Available at: <http://www.hindawi.com/journals/bmri/2015/421746/>.
- Gaihre, B. et al., 2008. Gelatin stabilized iron oxide nanoparticles as a three dimensional template for the hydroxyapatite crystal nucleation and growth. *Materials Science and Engineering C*, 28(8), pp.1297–1303. Available at: <http://dx.doi.org/10.1016/j.msec.2008.01.001>.
- Gan, S.D. & Patel, K.R., 2013. Enzyme Immunoassay and Enzyme-Linked Immunosorbent Assay. *Journal of Investigative Dermatology*, 133(9), pp.1–3. Available at:
<http://www.sciencedirect.com/science/article/pii/S0022202X15363879>.
- Gil, S. & Mano, J.F., 2014. Magnetic composite biomaterials for tissue engineering. *Biomater. Sci.*, 2, pp.812–818. Available at: <http://dx.doi.org/10.1039/C4BM00041B>.
- Gilde, F. et al., 2012. Secondary structure of rhBMP-2 in a protective biopolymeric carrier material. *Biomacromolecules*, 13(11), pp.3620–3626. Available at:
<https://www.ncbi.nlm.nih.gov/pubmed/22967015>.
- Gloria, A. et al., 2013. Magnetic poly(ϵ -caprolactone)/iron-doped hydroxyapatite nanocomposite substrates for advanced bone tissue engineering. *Journal of the Royal Society Interface*, 10(80), p.20120833. Available at: <http://www.ncbi.nlm.nih.gov/pmc/articles/PMC3565733/>.
- Gomes, S.R. et al., 2013. In vitro evaluation of crosslinked electrospun fish gelatin scaffolds. *Materials Science and Engineering C*, 33(3), pp.1219–1227. Available at:
<http://dx.doi.org/10.1016/j.msec.2012.12.014>.
- Gomez-Morales, J. et al., 2013. Progress on the preparation of nanocrystalline apatites and surface characterization: Overview of fundamental and applied aspects. *Progress in Crystal Growth and Characterization of Materials*, 59(1), pp.1–46. Available at:
<http://www.sciencedirect.com/science/article/pii/S0960897412000332>.
- Groeneveldt, L.C. et al., 2014. Enamel Matrix Derivative has No Effect on the Chondrogenic Differentiation of Mesenchymal Stem Cells. *Frontiers in bioengineering and biotechnology*, 2(September), p.29. Available at:
<http://www.pubmedcentral.nih.gov/articlerender.fcgi?artid=4151337&tool=pmcentrez&rendertype=abstract>.

-
- Gu, W. et al., 2013. Nanotechnology in the targeted drug delivery for bone diseases and bone regeneration. *International Journal of Nanomedicine*, 8, pp.2305–2317. Available at: <http://www.ncbi.nlm.nih.gov/pmc/articles/PMC3699134/>.
- Gupta, A.K. & Gupta, M., 2005. Synthesis and surface engineering of iron oxide nanoparticles for biomedical applications. *Biomaterials*, 26(18), pp.3995–4021. Available at: <http://www.sciencedirect.com/science/article/pii/S0142961204009317>.
- Hartgerink, J.D., Beniash, E. & Stupp, S.I., 2001. Self-Assembly and Mineralization of Peptide-Amphiphile Nanofibers. *Science*, 294(5547), p.1684 LP-1688. Available at: <http://science.sciencemag.org/content/294/5547/1684.abstract>.
- Harvey, E.J., Henderson, J.E. & Vengallatore, S.T., 2010. Nanotechnology and bone healing. *Journal of orthopaedic trauma*, 24 Suppl 1(3), pp.S25-30. Available at: <http://www.ncbi.nlm.nih.gov/pubmed/20182231>.
- Haugh, M.G., Jaasma, M.J. & O'Brien, F.J., 2009. The effect of dehydrothermal treatment on the mechanical and structural properties of collagen-GAG scaffolds. *Journal of Biomedical Materials Research - Part A*, 89(2), pp.363–369. Available at: <https://www.ncbi.nlm.nih.gov/pubmed/18431763>.
- Heidari, F. et al., 2015. In situ preparation of iron oxide nanoparticles in natural hydroxyapatite/chitosan matrix for bone tissue engineering application. *Ceramics International*, 41(2, Part B), pp.3094–3100. Available at: <http://www.sciencedirect.com/science/article/pii/S0272884214017052>.
- Hellman, B., 2011. The regulatory path from concept to market. In R. Lanza, R. Langer, & J. P. Vacanti, eds. *Principles of Tissue Engineering (Third Edition)*. Academic press, pp. 20–30.
- Herrera, B. & Inman, G.J., 2009. A rapid and sensitive bioassay for the simultaneous measurement of multiple bone morphogenetic proteins. Identification and quantification of BMP4, BMP6 and BMP9 in bovine and human serum. *BMC cell biology*, 10, p.20. Available at: <http://www.pubmedcentral.nih.gov/articlerender.fcgi?artid=2663541&tool=pmcentrez&rendertype=abstract>.
- Higashi, T. et al., 1993. Orientation of erythrocytes in a strong static magnetic field. *Blood*, 82(4), pp.1328–1334.
- Hing, K.A. et al., 2006. Effect of silicon level on rate, quality and progression of bone healing within silicate-substituted porous hydroxyapatite scaffolds. *Biomaterials*, 27(29), pp.5014–5026. Available at: <http://www.sciencedirect.com/science/article/pii/S0142961206004601>.
- Hoffman-Antenbrink, M., Von Rechenberg, B. & Hofmann, H., 2009. *Superparamagnetic nanoparticles for biomedical applications*,
- Huang, B. et al., 2016. Facilitated receptor-recognition and enhanced bioactivity of bone morphogenetic protein-2 on magnesium-substituted hydroxyapatite surface. *Scientific reports*, 6(October 2015), p.24323. Available at: <http://www.nature.com/srep/2016/160414/srep24323/full/srep24323.html>.
- Iafisco, M. et al., 2014. Biomimetic magnesium-carbonate-apatite nanocrystals endowed with strontium ions as anti-osteoporotic trigger. *Materials Science and Engineering C*, 35(1), pp.212–219.

-
- Ivey, K.N. et al., 2008. MicroRNA Regulation of Cell Lineages in Mouse and Human Embryonic Stem Cells. *Cell Stem Cell*, 2(3), pp.219–229.
- Jeevithan, E. et al., 2014. Type II Collagen and Gelatin from Silvertip Shark (*Carcharhinus albimarginatus*) Cartilage: Isolation, Purification, Physicochemical and Antioxidant Properties. *Marine Drugs*, 12(7), pp.3852–3873. Available at: <http://www.ncbi.nlm.nih.gov/pmc/articles/PMC4113802/>.
- Kaygili, O. et al., 2014. Dielectric properties of Fe doped hydroxyapatite prepared by sol-gel method. *Ceramics International*, 40(7 PART A), pp.9395–9402. Available at: <http://dx.doi.org/10.1016/j.ceramint.2014.02.009>.
- Kim, H.Y. et al., 2016. Development of Porous Beads to Provide Regulated BMP-2 Stimulation for Varying Durations: In Vitro and in Vivo Studies for Bone Regeneration. *Biomacromolecules*, 17(5), pp.1633–1642. Available at: <http://pubs.acs.org/doi/abs/10.1021/acs.biomac.6b00009>.
- King, W.J. & Krebsbach, P.H., 2012. Growth factor delivery: how surface interactions modulate release in vitro and in vivo. *Advanced drug delivery reviews*, 64(12), pp.1239–1256. Available at: <http://www.sciencedirect.com/science/article/pii/S0169409X12001007>.
- Kon, E., Delcogliano, M., et al., 2010. Orderly osteochondral regeneration in a sheep model using a novel nano-composite multilayered biomaterial. *Journal of Orthopaedic Research*, 28(1), pp.116–124. Available at: <https://www.ncbi.nlm.nih.gov/pubmed/19623663>.
- Kon, E., Filardo, G., et al., 2010. Platelet autologous growth factors decrease the osteochondral regeneration capability of a collagen-hydroxyapatite scaffold in a sheep model. *BMC musculoskeletal disorders*, 11, p.220. Available at: <https://www.ncbi.nlm.nih.gov/pubmed/20875101>.
- Koopman, G. et al., 1994. Annexin V for flow cytometric detection of phosphatidylserine expression on B cells undergoing apoptosis. *Blood*, 84(5), pp.1415–1420. Available at: <https://www.ncbi.nlm.nih.gov/pubmed/8068938>.
- Kotani, H. et al., 2002. Strong static magnetic field stimulates bone formation to a definite orientation in vitro and in vivo. *Journal of Bone and Mineral Research*, 17(10), pp.1814–1821.
- Kramer, E., Zilm, M. & Wei, M., 2013. A Comparative Study of the Sintering Behavior of Pure and Iron-Substituted Hydroxyapatite. *Bioceramics Development and Applications*, 3(1), pp.1–9. Available at: <http://www.omicsonline.com/open-access/a-comparative-study-of-the-sintering-behavior-of-pure-and-iron-substituted-hydroxyapatite-2090-5025.1000067.pdf?aid=19909>.
- Kumar, C.S.S.R. & Mohammad, F., 2011. Magnetic Nanomaterials for Hyperthermia-based Therapy and Controlled Drug Delivery. *Advanced drug delivery reviews*, 63(9), pp.789–808. Available at: <http://www.ncbi.nlm.nih.gov/pmc/articles/PMC3138885/>.
- LaConte, L., Nitin, N. & Bao, G., 2005. Magnetic nanoparticle probes. *Materials Today*, 8(5, Supplement 1), pp.32–38. Available at: <http://www.sciencedirect.com/science/article/pii/S136970210500893X>.
- Landi, E. et al., 2006. Biomimetic Mg- and Mg₂CO₃-substituted hydroxyapatites: synthesis characterization and in vitro behaviour. *Journal of the European Ceramic Society*, 26(13), pp.2593–2601. Available at: <http://www.sciencedirect.com/science/article/pii/S0955221905006680>.

-
- Lee, J. & Yun, H.-S., 2014. Effect of hydroxyapatite-containing microspheres embedded into three-dimensional magnesium phosphate scaffolds on the controlled release of lysozyme and in vitro biodegradation. *International journal of nanomedicine*, 9, pp.4177–4189. Available at: <https://www.ncbi.nlm.nih.gov/pubmed/25214782>.
- Leijts, M.J.C. et al., 2012. Effect of Arthritic Synovial Fluids on the Expression of Immunomodulatory Factors by Mesenchymal Stem Cells: An Explorative in vitro Study. *Frontiers in Immunology*, 3, p.231. Available at: <http://www.ncbi.nlm.nih.gov/pmc/articles/PMC3410447/>.
- Lienemann, P.S., Lutolf, M.P. & Ehrbar, M., 2012. Biomimetic hydrogels for controlled biomolecule delivery to augment bone regeneration. *Advanced Drug Delivery Reviews*, 64(12), pp.1078–1089. Available at: <http://dx.doi.org/10.1016/j.addr.2012.03.010>.
- Lin, K.L. et al., 2013. Hollow magnetic hydroxyapatite microspheres with hierarchically mesoporous microstructure for pH-responsive drug delivery. *Crystengcomm*, 15(15), pp.2999–3008. Available at: <http://pubs.rsc.org/en/Content/ArticleLanding/2013/CE/c3ce26683d#!divAbstract>.
- Liu, M. et al., 2013. Tissue engineering stratified scaffolds for articular cartilage and subchondral bone defects repair. *Orthopedics*, 36(11), pp.868–73. Available at: <http://www.ncbi.nlm.nih.gov/pubmed/24200433>.
- Livak, K.J. & Schmittgen, T.D., 2001. Analysis of Relative Gene Expression Data Using Real-Time Quantitative PCR and the $2^{-\Delta\Delta CT}$ Method. *Methods*, 25(4), pp.402–408. Available at: <http://www.sciencedirect.com/science/article/pii/S1046202301912629>.
- Long, F., 2011. Building strong bones: molecular regulation of the osteoblast lineage. *Nature Reviews Molecular Cell Biology*, 13(1), pp.27–38. Available at: <http://dx.doi.org/10.1038/nrm3254>.
- Lopez-Lopez, M.T. et al., 2015. Generation and characterization of novel magnetic field-responsive biomaterials. *PLoS ONE*, 10(7), pp.1–17. Available at: <http://journals.plos.org/plosone/article?id=10.1371/journal.pone.0133878>.
- Ma, P.X., 2008. Biomimetic Materials for Tissue Engineering. *Advanced drug delivery reviews*, 60(2), pp.184–198. Available at: <http://www.ncbi.nlm.nih.gov/pmc/articles/PMC2271038/>.
- Marques, C. et al., 2014. Multifunctional materials for bone cancer treatment. *International Journal of Nanomedicine*, 9, pp.2713–2725.
- Di Mauro, V. et al., 2016. Bioinspired negatively charged calcium phosphate nanocarriers for cardiac delivery of MicroRNAs. *Nanomedicine*, 11(8), pp.891–906. Available at: <https://www.ncbi.nlm.nih.gov/pubmed/26979495>.
- Mehta, S., 2008. *Commercializing Successful Biomedical Technologies*, Available at: <http://commercialbiotechnology.com/article/view/259>.
- Meng, J. et al., 2010. Paramagnetic nanofibrous composite films enhance the osteogenic responses of pre-osteoblast cells. *Nanoscale*, 2(12), pp.2565–2569. Available at: <http://www.ncbi.nlm.nih.gov/pubmed/20949222>.
- Meng, J. et al., 2013. Super-paramagnetic responsive nanofibrous scaffolds under static magnetic field

-
- enhance osteogenesis for bone repair in vivo. *Scientific reports*, 3, p.2655. Available at: <http://www.nature.com/srep/2013/130913/srep02655/full/srep02655.html>.
- Mercado, D.F. et al., 2014. Paramagnetic Iron-Doped Hydroxyapatite Nanoparticles with Improved Metal Sorption Properties. A Bioorganic Substrates Mediated Synthesis. *Applied materials and interfaces*, 6(6), pp.3937–3946. Available at: <http://pubs.acs.org/doi/abs/10.1021/am405217j>.
- Mertens, M.E. et al., 2014. Iron oxide-labeled collagen scaffolds for non-invasive MR imaging in tissue engineering. *Advanced Functional Materials*, 24(6), pp.754–762. Available at: <https://www.ncbi.nlm.nih.gov/pmc/articles/PMC3837415/>.
- Miller, S.C. et al., 1989. Bone lining cells: structure and function. *Scanning microscopy*, 3(3), pp.953–960. Available at: <https://www.ncbi.nlm.nih.gov/pubmed/2694361>.
- Minuth, W.W., Strehl, R. & Schumacher, K., 2006. *Tissue engineering: From cell biology to artificial organs*, John Wiley & Sons.
- Mitsionis, A.I., Vaimakis, T.C. & Trapalis, C.C., 2010. The effect of citric acid on the sintering of calcium phosphate bioceramics. *Ceramics International*, 36(2), pp.623–634. Available at: <http://www.sciencedirect.com/science/article/pii/S0272884209003691>.
- Mumcuoglu, D. et al., 2016. BMP-2 release from synthetic collagen peptide particles. *Frontiers in Bioengineering and Biotechnology*, (1596). Available at: http://www.frontiersin.org/bioengineering_and_biotechnology/10.3389/conf.FBIOE.2016.01.01596/full
- Mura, S., Nicolas, J. & Couvreur, P., 2013. Stimuli-responsive nanocarriers for drug delivery. *Nature Materials*, 12(11), pp.991–1003. Available at: <http://dx.doi.org/10.1038/nmat3776>.
- Murti, G.K., Moharir, A. & Sarma, V., 1970. Spectrophotometric determination of iron with orthophenanthroline. *Microchemical Journal*, 15, pp.585–589. Available at: <http://www.sciencedirect.com/science/article/pii/0026265X70901013>.
- Nakamura, M. et al., 2016. Hydroxyapatite with High Carbonate Substitutions Promotes Osteoclast Resorption through Osteocyte-like Cells. *ACS Biomaterials Science and Engineering*, 2(2), pp.259–267.
- Nandi, S.K. et al., 2015. Converted marine coral hydroxyapatite implants with growth factors: In vivo bone regeneration. *Materials Science and Engineering: C*, 49, pp.816–823. Available at: <http://www.sciencedirect.com/science/article/pii/S0928493115000880>.
- Oliveira, M.B. & Mano, J.F., 2011. Polymer-based microparticles in tissue engineering and regenerative medicine. *Biotechnology Progress*, 27(4), pp.897–912. Available at: <https://www.ncbi.nlm.nih.gov/pubmed/21584949>.
- Oryan, A. et al., 2014. Bone regenerative medicine: classic options, novel strategies, and future directions. *Journal of orthopaedic surgery and research*, 9(1), p.18. Available at: <http://www.biomedcentral.com.ezlibrary.technion.ac.il/content/pdf/1749-799X-9-18.pdf>
<http://www.ncbi.nlm.nih.gov/pubmed/24628910>
<http://www.pubmedcentral.nih.gov/>
-

articlerender.fcgi?artid=PMC3995444.

- Pankhurst, A. et al., 2003. Applications of magnetic nanoparticles in biomedicine. *Journal of Physics D: Applied Physics*, 36(13), p.R167. Available at: <http://stacks.iop.org/0022-3727/36/i=13/a=201>.
- Panseri, S. et al., 2012. Magnetic Hydroxyapatite bone substitutes to enhance tissue regeneration: Evaluation in vitro using osteoblast-like cells and in vivo in a bone defect. *PLoS ONE*, 7(6), pp.4–11. Available at: <https://www.ncbi.nlm.nih.gov/pubmed/22685602>.
- Panseri, S. et al., 2016. Magnetic Labelling of Mesenchymal Stem Cells with Iron-Doped Hydroxyapatite Nanoparticles as Tool for Cell Therapy. *Journal of Biomedical Nanotechnology*, 12(5), pp.909–921. Available at: <http://openurl.ingenta.com/content/xref?genre=article&issn=1550-7033&volume=12&issue=5&spage=909>.
- Panseri, S. et al., 2013. Modifying bone scaffold architecture in vivo with permanent magnets to facilitate fixation of magnetic scaffolds. *Bone*, 56(2), pp.432–439. Available at: <http://dx.doi.org/10.1016/j.bone.2013.07.015>.
- Papadopoulos, N.G. et al., 1994. An improved fluorescence assay for the determination of lymphocyte-mediated cytotoxicity using flow cytometry. *J.Immunol.Methods*, 177, pp.101–111. Available at: <http://www.sciencedirect.com/science/article/pii/0022175994901473>.
- Pareta, R., Taylor, E. & Webster, T., 2008. Increased osteoblast density in the presence of novel calcium phosphate coated magnetic nanoparticles. *Nanotechnology*, 19(26), p.265101. Available at: <http://stacks.iop.org/0957-4484/19/i=26/a=265101>.
- Pashuck, E.T. & Stevens, M.M., 2012. Designing regenerative biomaterial therapies for the clinic. *Science translational medicine*, 4(160), p.160sr4. Available at: <http://www.ncbi.nlm.nih.gov/pubmed/23152328>.
- Patrício, T. et al., 2017. New bioactive bone-like microspheres with intrinsic magnetic properties obtained by bio-inspired mineralisation process. *Materials and Engineering: Part C*, In press,.
- Patrício, T. et al., 2014. Fabrication and characterisation of PCL and PCL/PLA scaffolds for tissue engineering. *Rapid Prototyping Journal*, 20(2), pp.145–156. Available at: <http://dx.doi.org/10.1108/RPJ-04-2012-0037>.
- Perez, R.A. et al., 2014. Therapeutic bioactive microcarriers: Co-delivery of growth factors and stem cells for bone tissue engineering. *Acta Biomaterialia*, 10(1), pp.520–530. Available at: <http://dx.doi.org/10.1016/j.actbio.2013.09.042>.
- Perez, R.A. et al., 2015. Therapeutically relevant aspects in bone repair and regeneration. *Materials Today*, 18(10), pp.573–589. Available at: <http://www.sciencedirect.com/science/article/pii/S1369702115002102>.
- Pérez, R.A. et al., 2013. Naturally and synthetic smart composite biomaterials for tissue regeneration. *Advanced Drug Delivery Reviews*, 65(4), pp.471–496. Available at: <http://dx.doi.org/10.1016/j.addr.2012.03.009>.
- Poinern, G.E.J., Brundavanam, R.K. & Fawcett, D., 2013. Nanometre Scale Hydroxyapatite Ceramics for

-
- Bone Tissue Engineering. *American Journal of Biomedical Engineering*, 3(6), pp.148–168. Available at: <http://article.sapub.org/10.5923.j.ajbe.20130306.04.html>.
- Polo-Corrales, L., Latorre-Esteves, M. & Ramirez-Vick, J.E., 2014. Scaffold Design for Bone Regeneration. *Journal of nanoscience and nanotechnology*, 14(1), pp.15–56. Available at: <http://www.ncbi.nlm.nih.gov/pmc/articles/PMC3997175/>.
- Pon-On, W. et al., 2013. Physicochemical and biochemical properties of iron-loaded silicon substituted hydroxyapatite (FeSiHAp). *Materials Chemistry and Physics*, 141(2–3), pp.850–860. Available at: <http://dx.doi.org/10.1016/j.matchemphys.2013.06.014>.
- Prasertsung I., M.R. & Damrongsakkul S., W.C., 2010. Surface modification of dehydrothermal crosslinked gelatin film using a 50 Hz oxygen glow discharge. *Surface and Coatings Technology*, 205, pp.133–138. Available at: https://www.researchgate.net/publication/240378564_Surface_modification_of_dehydrothermal_crosslinked_gelatin_film_using_a_50_Hz_oxygen_glow_discharge.
- Qiao, C.Y. et al., 2015. Sustained release poly (Lactic-co-glycolic acid) microspheres of bone morphogenetic protein 2 plasmid/calcium phosphate to promote in vitro bone formation and in vivo ectopic osteogenesis. *American Journal of Translational Research*, 7(12), pp.2561–2572. Available at: <https://www.ncbi.nlm.nih.gov/pmc/articles/PMC4731657/>.
- Quinlan, E. et al., 2015. Long-term controlled delivery of rhBMP-2 from collagen-hydroxyapatite scaffolds for superior bone tissue regeneration. *Journal of Controlled Release*, 207, pp.112–119. Available at: <http://dx.doi.org/10.1016/j.jconrel.2015.03.028>.
- Radulovic, M. & Godovac-Zimmermann, J., 2011. Proteomic approaches to understanding the role of the cytoskeleton in host-defense mechanisms. *Expert review of proteomics*, 8(1), pp.117–126. Available at: <http://www.ncbi.nlm.nih.gov/pmc/articles/PMC4261605/>.
- Ramírez-Rodríguez, G.B. et al., 2016. Biomimetic mineralization of recombinant collagen type I derived protein to obtain hybrid matrices for bone regeneration. *Journal of Structural Biology*. Available at: <http://dx.doi.org/10.1016/j.jsb.2016.06.025>.
- Rosset, E.M. & Bradshaw, A.D., 2016. SPARC/osteonectin in mineralized tissue. *Matrix Biology*, 52, pp.78–87. Available at: <https://www.ncbi.nlm.nih.gov/pubmed/26851678>.
- Roveri, N. & Iafisco, M., 2010. Evolving application of biomimetic nanostructured hydroxyapatite. *Nanotechnology, science and applications*, 3(1), pp.107–125. Available at: <https://www.ncbi.nlm.nih.gov/pmc/articles/PMC3781698/>.
- Russell, J. & Bertram, T., 2011. Moving into the Clinic. In R. Lanza, R. Langer, & J. P. Vacanti, eds. *Principles of Tissue Engineering (Third Edition)*. Academic press, pp. 20–30.
- Russo, A. et al., 2012. A new approach to scaffold fixation by magnetic forces: Application to large osteochondral defects. *Medical Engineering and Physics*, 34(9), pp.1287–1293. Available at: <http://dx.doi.org/10.1016/j.medengphy.2011.12.019>.
- Saiz, E. et al., 2013. Perspectives on the role of nanotechnology in bone tissue engineering. *Dental*

-
- Materials*, 29(1), pp.103–115. Available at: <http://dx.doi.org/10.1016/j.dental.2012.08.001>.
- Sandri, M. et al., 2010. Collagen based scaffold for biomedical applications. *Journal of Biotechnology*, 150, pp.29–29. Available at: <http://linkinghub.elsevier.com/retrieve/pii/S016816561000475X>.
- Santos, L.J., Reis, R.L. & Gomes, M.E., 2015. Harnessing magnetic-mechano actuation in regenerative medicine and tissue engineering. *Trends in Biotechnology*, 33(8), pp.471–479. Available at: <http://dx.doi.org/10.1016/j.tibtech.2015.06.006>.
- Schwartz, D., Sofia, S. & Friess, W., 2006. Integrity and stability studies of precipitated rhBMP-2 microparticles with a focus on ATR-FTIR measurements. *European Journal of Pharmaceutics and Biopharmaceutics*, 63(3), pp.241–248. Available at: <http://www.sciencedirect.com/science/article/pii/S0939641106000440>.
- Sensenig, R. et al., 2012. Magnetic nanoparticle-based approaches to locally target therapy and enhance tissue regeneration in vivo. *Nanomedicine (London, England)*, 7(9), pp.1425–42. Available at: <http://www.pubmedcentral.nih.gov/articlerender.fcgi?artid=3543693&tool=pmcentrez&rendertype=abstract>.
- Shibuya, N. & Jupiter, D.C., 2015. Bone Graft Substitute: Allograft and Xenograft. *Clinics in Podiatric Medicine and Surgery*, 32(1), pp.21–34. Available at: <http://www.sciencedirect.com/science/article/pii/S0891842214000846>.
- Shimizu, K. et al., 2007. Bone tissue engineering with human mesenchymal stem cell sheets constructed using magnetite nanoparticles and magnetic force. *Journal of Biomedical Materials Research Part B: Applied Biomaterials*, 82B(2), pp.471–480. Available at: <http://dx.doi.org/10.1002/jbm.b.30752>.
- Silva, a, Silva-Freitas, É. & Carvalho, J., 2012. Magnetic Particles in Biotechnology: From Drug Targeting to Tissue Engineering. *Advances in Applied Biotechnology*, pp.237–256. Available at: <http://www.intechopen.com/books/advances-in-applied-biotechnology/magnetic-particles-in-biotechnology-from-drug-targeting-to-tissue-engineering>.
- Di Silvio, L., 2007. Bone tissue engineering and biomineralization. In *Tissue Engineering Using Ceramics and Polymers*. pp. 319–334. Available at: <https://books.google.com/books?id=dQekAgAAQBAJ&pgis=1>.
- Singh, R.K. et al., 2014. Potential of magnetic nanofiber scaffolds with mechanical and biological properties applicable for bone regeneration. *PLoS ONE*, 9(4). Available at: <http://journals.plos.org/plosone/article?id=10.1371/journal.pone.0091584>.
- Skaat, H. et al., 2012. Magnetic Scaffolds Enriched with Bioactive Nanoparticles for Tissue Engineering. *Advanced Healthcare Materials*, 1(2), pp.168–171. Available at: <http://dx.doi.org/10.1002/adhm.201100056>.
- Skinner, H.C.W. & Ehrlich, H., 2014. *Biomineralization*, Available at: <http://linkinghub.elsevier.com/retrieve/pii/B9780080959757008044>.
- Solorio, L.D. et al., 2013. High-density cell systems incorporating polymer microspheres as microenvironmental regulators in engineered cartilage tissues. *Tissue engineering. Part B, Reviews*,

-
- 19(3), pp.209–20. Available at:
<http://www.pubmedcentral.nih.gov/articlerender.fcgi?artid=3627432&tool=pmcentrez&rendertype=abstract>.
- Sprio, A. et al., 2016. Nature-Inspired Nanotechnology and Smart Magnetic Activation: Two Groundbreaking Approaches Toward a New Generation of Biomaterials for Hard Tissue Regeneration. In *Advanced Techniques in Bone Regeneration*. Available at:
<http://www.intechopen.com/books/advanced-techniques-in-bone-regeneration/nature-inspired-nanotechnology-and-smart-magnetic-activation-two-groundbreaking-approaches-toward-a->.
- Sprio, B. et al., 2016. Bio-inspired assembling/mineralization process as a flexible approach to develop new smart scaffolds for the regeneration of complex anatomical regions. *Journal of the European Ceramic Society*, 36(12), pp.2857–2867. Available at: <http://dx.doi.org/10.1016/j.jeurceramsoc.2016.01.005>.
- Sprio, S. et al., 2010. Biomimesis and biomorphic transformations: New concepts applied to bone regeneration. *Journal of Biotechnology*, 156(4), pp.347–355. Available at:
<http://dx.doi.org/10.1016/j.jbiotec.2011.07.034>.
- Sprio, S. et al., 2012. Hybrid scaffolds for tissue regeneration: Chemotaxis and physical confinement as sources of biomimesis. *Journal of Nanomaterials*, 2012. Available at:
<https://www.hindawi.com/journals/jnm/2012/418281/>.
- Stark, G., 2005. Functional consequences of oxidative membrane damage. *The Journal of membrane biology*, 205(1), pp.1–16. Available at: <https://www.ncbi.nlm.nih.gov/pubmed/16245038>.
- Stevens, M.M., 2008. Biomaterials for bone tissue engineering. *Materials Today*, 11(5), pp.18–25. Available at: [http://dx.doi.org/10.1016/S1369-7021\(08\)70086-5](http://dx.doi.org/10.1016/S1369-7021(08)70086-5).
- Stevens, M.M. & George, J.H., 2005. Exploring and Engineering the Cell Surface Interface. *Science*, 310(5751), p.1135 LP-1138. Available at:
<http://science.sciencemag.org/content/310/5751/1135.abstract>.
- Surovell, T. & Stiner, M., 2001. Standardizing Infra-red Measures of Bone Mineral Crystallinity: an Experimental Approach. *Journal of Archaeological Science*, 28, pp.633–642. Available at: [internal-pdf:/Surovell%7B_%7Dand%7B_%7DStiner-2001-JAS.pdf%5Cnhttp://www.sciencedirect.com/science/article/B6WH8-45RFJ1J-17/1/78f9905876fa4c873d6276ba21fc9fd7%5Cninternal-pdf:/Surovell_and_Stiner-2001-JAS.pdf%5Cnhttp://www.sciencedirect.com/science/article/B6WH8-45RFJ1](http://internal-pdf/Surovell%7B_%7Dand%7B_%7DStiner-2001-JAS.pdf%5Cnhttp://www.sciencedirect.com/science/article/B6WH8-45RFJ1J-17/1/78f9905876fa4c873d6276ba21fc9fd7%5Cninternal-pdf/Surovell_and_Stiner-2001-JAS.pdf%5Cnhttp://www.sciencedirect.com/science/article/B6WH8-45RFJ1).
- Tampieri, A. et al., 2016. Biologically Inspired Nanomaterials and Nanobiomagnetism : A Synergy among New Emerging Concepts in Regenerative Medicine. In *Bio-Inspired Regenerative Medicine: Materials, Processes, and Clinical Applications*. pp. 978–981. Available at:
<https://books.google.pt/books?id=NhjYCwAAQBAJ&pg=PR5&lpg=PR5&dq=Biologically+Inspired+Nanomaterials+and+Nanobiomagnetism+:+A+Synergy+among+New+Emerging+Concepts+in+Regenerative+Medicine+1+.+1+The+New+Concept+of+Bio-Inspiration+toward+Biomimetics&source=bl>.
- Tampieri, A. et al., 2003. Biologically inspired synthesis of bone-like composite: Self-assembled collagen

-
- fibers/hydroxyapatite nanocrystals. *J Biomed Mater Res*, 67, pp.618–625. Available at: <https://www.ncbi.nlm.nih.gov/pubmed/14566805>.
- Tampieri, A. et al., 2008. Design of graded biomimetic osteochondral composite scaffolds. *Biomaterials*, 29(26), pp.3539–3546. Available at: <https://www.ncbi.nlm.nih.gov/pubmed/18538387>.
- Tampieri, A. et al., 2012. Intrinsic magnetism and hyperthermia in bioactive Fe-doped hydroxyapatite. *Acta Biomaterialia*, 8(2), pp.843–851. Available at: <http://dx.doi.org/10.1016/j.actbio.2011.09.032>.
- Tampieri, A. et al., 2014. Magnetic Bioinspired Hybrid Nanostructured Collagen – Hydroxyapatite Scaffolds Supporting Cell Proliferation and Tuning Regenerative Process. *Applied materials and interfaces*, 6, pp.15697–15707. Available at: <http://pubs.acs.org/doi/abs/10.1021/am5050967>.
- Tampieri, A. et al., 2011. Mimicking natural bio-mineralization processes: A new tool for osteochondral scaffold development. *Trends in Biotechnology*, 29(10), pp.526–535. Available at: <http://dx.doi.org/10.1016/j.tibtech.2011.04.011>.
- Tan, H. et al., 2009. RGD modified PLGA/gelatin microspheres as microcarriers for chondrocyte delivery. *Journal of Biomedical Materials Research - Part B Applied Biomaterials*, 91(1), pp.228–238. Available at: <https://www.ncbi.nlm.nih.gov/pubmed/19388090>.
- Tang, D. et al., 2016. Biofabrication of bone tissue: Approaches, challenges and translation for bone regeneration. *Biomaterials*, 83, pp.363–382. Available at: <http://dx.doi.org/10.1016/j.biomaterials.2016.01.024>.
- Tang, Z. et al., 2014. Biodegradable magnetic calcium phosphate nanoformulation for cancer therapy. *European Journal of Pharmaceutics and Biopharmaceutics*, 87(1), pp.90–100. Available at: <http://dx.doi.org/10.1016/j.ejpb.2014.01.003>.
- Toxqui, L. & Vaquero, M.P., 2015. Chronic iron deficiency as an emerging risk factor for osteoporosis: a hypothesis. *Nutrients*, 7(4), pp.2324–2344. Available at: <https://www.ncbi.nlm.nih.gov/pubmed/25849944>.
- Tsang, E.J. et al., 2011. Osteoblast interactions within a biomimetic apatite microenvironment. *Annals of Biomedical Engineering*, 39(4), pp.1186–1200. Available at: <https://www.ncbi.nlm.nih.gov/pmc/articles/PMC3069334/>.
- Vallet-Regi, M. & Gonzalez-Calbet, J.M., 2004. Calcium phosphates as substitution of bone tissues. *Progress in Solid State Chemistry*, 32(1–2), pp.1–31. Available at: <http://www.sciencedirect.com/science/article/pii/S0079678604000111>.
- Vandelli, M.A. et al., 2004. Microwave-treated gelatin microspheres as drug delivery system. *Journal of Controlled Release*, 96, pp.67–84. Available at: <https://www.ncbi.nlm.nih.gov/pubmed/15063030>.
- Verseijden, F. et al., 2009. Angiogenic capacity of human adipose-derived stromal cells during adipogenic differentiation: an in vitro study. *Tissue engineering. Part A*, 15(2), pp.445–452. Available at: <http://eutils.ncbi.nlm.nih.gov/entrez/eutils/elink.fcgi?dbfrom=pubmed&id=18652540&retmode=ref&cmd=prlinks%5Cnpapers2://publication/doi/10.1089/ten.tea.2007.0429>.
- Viti, F. et al., 2016. Osteogenic differentiation of MSC through calcium signaling activation:

-
- Transcriptomics and functional analysis. *PLoS ONE*, 11(2), pp.1–21. Available at:
<http://journals.plos.org/plosone/article?id=10.1371/journal.pone.0148173>.
- Walmsley, G.G. et al., 2015. Nanotechnology in bone tissue engineering. *Nanomedicine: Nanotechnology, Biology, and Medicine*, 11(5), pp.1253–1263. Available at:
<http://dx.doi.org/10.1016/j.nano.2015.02.013>.
- Wang, D. et al., 2013. One-pot synthesis of magnetic, macro/mesoporous bioactive glasses for bone tissue engineering. *Science and Technology of Advanced Materials*, 14(2), p.25004. Available at:
<http://stacks.iop.org/1468-6996/14/i=2/a=025004?key=crossref.4e7f704d967d41c8f50154e18f82ca6c>.
- Wang, G., Babada, M.E. & Uluda, H., 2011. Bisphosphonate-Derivatized Liposomes to Control Drug Release from Collagen / Hydroxyapatite Scaffolds. *Molecular Pharmaceutics*, 8, pp.1025–1034. Available at: <https://www.ncbi.nlm.nih.gov/pubmed/21557579>.
- Wang, L. & Nancollas, G.H., 2009. Calcium Orthophosphates: Crystallization and Dissolution. , 108(11), pp.4628–4669. Available at: <https://www.ncbi.nlm.nih.gov/pmc/articles/PMC2743557/>.
- Wang, P. et al., 2014. Bone tissue engineering via nanostructured calcium phosphate biomaterials and stem cells. *Bone Research*, 2(July), p.14017. Available at: <http://www.nature.com/articles/boneres201417>.
- Wang, Q. et al., 2017. Magnetic iron oxide nanoparticles accelerate osteogenic differentiation of mesenchymal stem cells via modulation of long noncoding RNA INZEB2. *Nano Research*, 10(2), pp.626–642. Available at: <http://link.springer.com/10.1007/s12274-016-1322-4>.
- Wang, Q. et al., 2016. Nanomaterials promise better bone repair. *Materials Today*, 19(8), pp.451–463. Available at: <http://dx.doi.org/10.1016/j.mattod.2015.12.003>.
- Wang, Z.-L. et al., 2015. Gelatin-derived sustainable carbon-based functional materials for energy conversion and storage with controllability of structure and component. *Science Advances*, 1(1), pp.1–9. Available at: <http://advances.sciencemag.org/content/1/1/e1400035.abstract>.
- Wegst, U.G.K. et al., 2014. Bioinspired structural materials. *Nature materials*, 14(1), pp.23–36. Available at: <http://www.sciencemag.org/content/319/5866/1053.short%5Cnhttp://www.nature.com/doifinder/10.1038/nmat4089%5Cnhttp://www.ncbi.nlm.nih.gov/pubmed/25344782>.
- Weiner, S. & Bar-Yosef, O., 1990. States of preservation of bones from prehistoric sites in the Near East: A survey. *Journal of Archaeological Science*, 17(2), pp.187–196. Available at:
<http://www.sciencedirect.com/science/article/pii/030544039090058D>.
- Westrin, M. et al., 2015. Osteogenic differentiation of human mesenchymal stem cells in mineralized alginate matrices. *PLoS ONE*, 10(3), pp.1–16. Available at:
<https://www.ncbi.nlm.nih.gov/pubmed/25769043>.
- Wimpenny, I., Markides, H. & El Haj, A.J., 2012. Orthopaedic applications of nanoparticle-based stem cell therapies. *Stem Cell Research & Therapy*, 3(2), p.13. Available at:
<https://www.ncbi.nlm.nih.gov/pmc/articles/PMC3392773/>.
- Woodruff, M.A. et al., 2012. Bone tissue engineering: From bench to bedside. *Materials Today*, 15(10), pp.430–435. Available at: [http://dx.doi.org/10.1016/S1369-7021\(12\)70194-3](http://dx.doi.org/10.1016/S1369-7021(12)70194-3).

-
- Wu, C. et al., 2011. Multifunctional magnetic mesoporous bioactive glass scaffolds with a hierarchical pore structure. *Acta Biomaterialia*, 7(10), pp.3563–3572. Available at: <http://dx.doi.org/10.1016/j.actbio.2011.06.028>.
- Wu, S. et al., 2014. Biomimetic porous scaffolds for bone tissue engineering. *Materials Science and Engineering R: Reports*, 80(1), pp.1–36. Available at: <http://dx.doi.org/10.1016/j.mser.2014.04.001>.
- Xu, H.-Y. & Gu, N., 2014. Magnetic responsive scaffolds and magnetic fields in bone repair and regeneration. *Frontiers of Materials Science*, 8(1), pp.20–31.
- Xu, J. et al., 2014. Application of iron magnetic nanoparticles in protein immobilization. *Molecules*, 19(8), pp.11465–11486. Available at: <https://www.ncbi.nlm.nih.gov/pubmed/25093986>.
- Yang, Z. et al., 2005. Preparation and characterization of magnesium doped hydroxyapatite–gelatin nanocomposite. *Journal of Materials Chemistry*, 15(18), p.1807. Available at: <http://pubs.rsc.org/en/Content/ArticleLanding/2005/JM/b418015c#!divAbstract>.
- Yang, Z. et al., 2008. Substitution of manganese and iron into hydroxyapatite: Core/shell nanoparticles. *Materials Science and Engineering C*, 14(2), pp.1774–1780. Available at: <http://dx.doi.org/10.1016/j.tibtech.2013.06.005>.
- Yonezawa, T. et al., 2008. Easy preparation of stable iron oxide nanoparticles using gelatin as stabilizing molecules. *Japanese Journal of Applied Physics*, 47(2), pp.1389–1392. Available at: <http://iopscience.iop.org/article/10.1143/JJAP.47.1389/pdf>.
- Zeng, X.B. et al., 2012. Magnetic responsive hydroxyapatite composite scaffolds construction for bone defect reparation. *International Journal of Nanomedicine*, 7, pp.3365–3378. Available at: <https://www.ncbi.nlm.nih.gov/pmc/articles/PMC3405892/>.
- Zhang, J. et al., 2014. The size of surface microstructures as an osteogenic factor in calcium phosphate ceramics. *Acta Biomaterialia*, 10(7), pp.3254–3263. Available at: <http://dx.doi.org/10.1016/j.actbio.2014.03.021>.
- Zhang, W. et al., 2003. Nucleation sites of calcium phosphate crystals during collagen mineralization. *Journal of the American ...*, 54(186871), pp.2002–2004. Available at: <http://onlinelibrary.wiley.com/doi/10.1111/j.1151-2916.2003.tb03422.x/abstract>.
- Zhou, H. et al., 2007. Adsorption mechanism of BMP-7 on hydroxyapatite (001) surfaces. *Biochemical and biophysical research communications*, 361(1), pp.91–96.
- Zhu, X. et al., 2015. Functionalized graphene oxide-based thermosensitive hydrogel for magnetic hyperthermia therapy on tumors. *Nanotechnology*, 26(36), p.365103. Available at: <https://www.ncbi.nlm.nih.gov/pubmed/26291977>.

Annex I

Preliminary investigations on microspheres production with low amount of mineral phase

Brief introduction

Preliminary investigations on microspheres production were performed during the secondment in Fujifilm Manufacturing Europe B.V. (The Netherlands). RCP was mineralised with iron doped hydroxyapatite at 25 °C and 40 °C with mineral extend of 10 wt% and final biomineralised slurry contained 5 wt% of RCP. Chemical, physical, morphological, degradation and preliminary tests on magnetisation were presented. Those results were fundamental to define the appropriate characterisation techniques as well as the feasibility of DHT crosslinking method.

Materials and Methods

Chemical, physical and morphological characterisation were followed the information presented in the chapter 2.

Results

Phase composition was presented in the section 3.1.2. SEM results showed that the emulsification process allowed to produce microspheres with different materials and properties (Figure 1). RCP microspheres presented a smooth surface and well defined geometry. Biomineralised microspheres exhibited a roughness surface and heterogeneous size and shape. On the other hand, biomineralised magnetic microspheres at 25°C showed higher roughness compared to the samples biomineralised at 40°C.

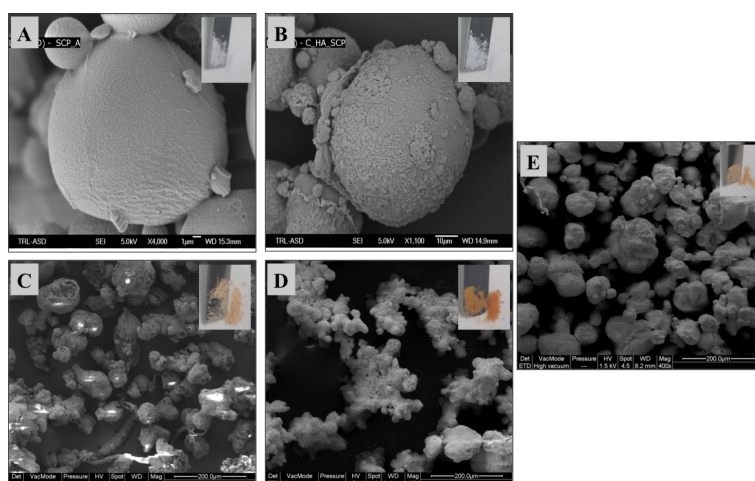


Figure 1. SEM micrographs of the as-produced microspheres A) RCP; B) RCP/HA (90:10, 40 °C); C) RCP/FeHA (90:10; 3:2; 25 °C); D) RCP/FeHA (90:10; 3:2; 40 °C); E) RCP/FeHA (90:10; 5:4; 40 °C).

The amount of different elements (Ca, P and Fe) in the microspheres was determined by ICP-OES (Table 1). RCP and RCP/HA microspheres were used as control materials. In RCP microspheres Ca, P and Fe were detected. The presence of these elements is likely related to the used method in the development of RCP. For example, gelatin obtained by denaturation of collagen contains divalent metal ions, such as calcium, copper, iron and zinc that can form ionic bonds with the carboxylic acid groups on the gelatin polypeptides (Xing et al. 2014).

By comparing RCP/FeHA 25°C (3:2) and RCP/FeHA 40°C (3:2), the real amount of Fe in the samples was higher at 40 °C, indicating that the temperature favoured the entrance of iron into the crystal lattice (Tampieri et al. 2014). Decrease in Ca/P ratio was showed and is close to the theoretical one Ca/P ratio (1.67). Probably, this behaviour was related to the nucleation of Fe and partial replacement of Ca with Fe ions, which was also confirmed by XRD analysis. TGA analyses were performed to evaluate the mineral amount inside of the biomineralized samples. The theoretical ratio composition of the hybrid microspheres (RCP/HA and RCP/FeHA) was 90:10wt%. Mineral amount in the mineralised materials range between 20-30 wt%, as reported in table 1.

Table 1. Chemical amount evaluation and mineral composition of the microspheres, obtained by ^a ICP-OES and ^b TGA/DSC analysis.

	RCP	RCP/HA	RCP/FeHA (90:10, 3:2, 25°C)	RCP/FeHA (90:10, 3:2, 40°C)	RCP/FeHA (90:10, 5:4, 40°C)
Ca (wt%)^a	0.046±0.01	0.563±0.03	0.321±0.01	0.379±0.01	0.409±0.02
P (wt%)^a	0.172±0.02	0.272±0.02	0.120±0.05	0.118±0.04	0.184±0.03
Fe (wt%)^a	0.005±0.01	---	0.071±0.01	0.073±0.01	0.082±0.01
Ca/P (mol)^a	0.210±0.11	1.597±0.34	2.067±2.05	2.488±1.87	1.716±0.69
(Fe+Ca)/P (mol)^a	0.226±0.11	---	2.397±2.37	2.832±2.13	1.965±0.79
Fe/Ca (mol %)^a	7.376±6.29	---	15.945±2.73	13.797±2.03	14.541±2.19
Fe/(Ca+Fe) (mol %)^a	0.069±0.06	---	0.137±0.02	0.121±0.02	0.127±0.02
% of organic phase in the samples (≈)^b	90	78:22	78:22	82:18	70:30

Hybrid microspheres with Fe were preliminary tested to assess magnetization by using a neodymium magnet (Figure 2) and all biomineralised microspheres presented magnetic behaviour. According to the ICP results the sample produced at 25°C probably have less magnetization compared to the samples produced at 40°C. Analysing the samples produced at 40°C, the sample with 3:2 (Fe²⁺/Fe³⁺) ratio present better magnetic properties. These preliminary tests allow to concluded that the temperature and the (Fe²⁺/Fe³⁺) ratio are important parameters to produce magnetic microspheres for further tissue engineering applications.

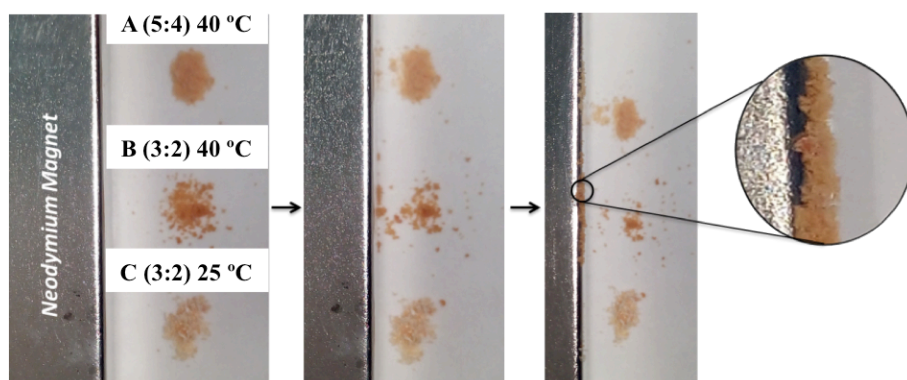


Figure 2. Preliminary evaluation of magnetic properties of the microspheres, by neodymium magnet.

DHT treatment was carried out by placing the dried magnetic microspheres in separately aluminium foil packet inside an oven at 160°C, during 24h and 48h.

Figure 3 shows the morphological properties of microspheres obtained by SEM after 24h and 48h of DHT treatment. The results showed that the geometry, morphology and microspheres size were not affected by the treatment. The roughness morphology was due to the presence of the mineral phase on the surface of the microspheres.

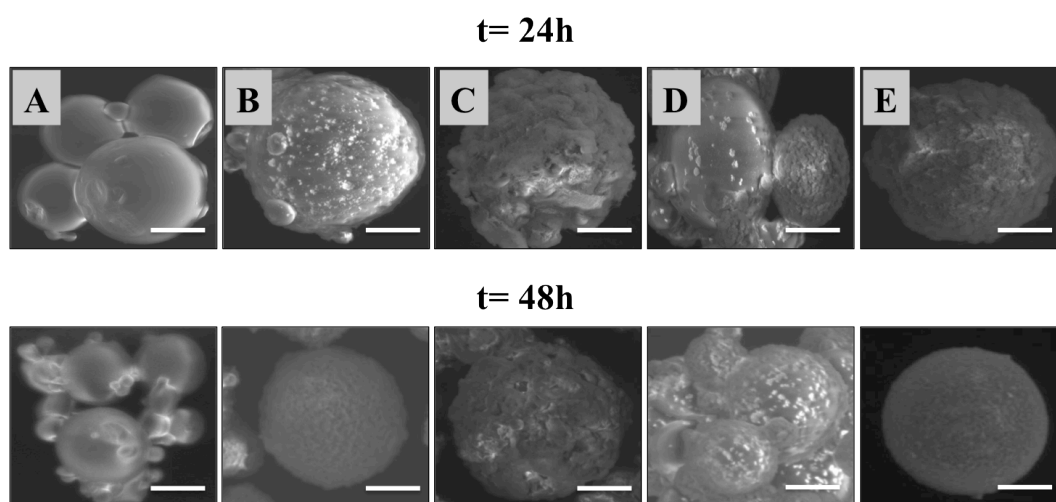


Figure 3. Crosslinked microspheres, A) RCP; B) RCP/HA (90:10, 40 °C); C) RCP/FeHA (90:10; 3:2; 25 °C); D) RCP/FeHA (90:10; 3:2; 40°C); E) RCP/FeHA (90:10; 5:4; 40°C), (Scale bar: 20 µm).

The following results were referred to RCP/FeHA (90:10; 3:2; 40°C) microspheres. As showed in the previous results, apparently the DHT method did not influence the microspheres properties. According to this, the thermal, chemical and magnetic properties of the magnetic microspheres were also evaluated. In the DSC graph (Figure 4, left), three relevant peaks were showed: water loss of RCP (≈ 80 °C), DHT crosslinking temperature (≈ 160 °C) and the starting point of polymer degradation (at ≈ 260 °C). All samples present similar thermal behaviour, in terms of denaturation and degradation starting point. The results indicated that the temperature and the exposition time of the material to DHT treatment do not influence the thermal properties and no evident material degradation was occurred. Figure 4 (right), shows the real amount

of organic phase present in the microspheres before and after treatment, that also does not reveal significant changes on the as-produced materials, after DHT crosslinking.

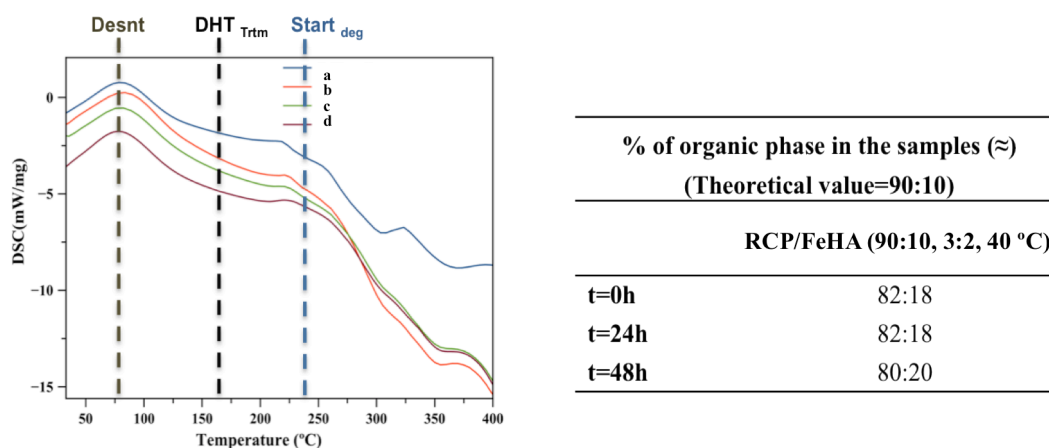


Figure 4. Thermal properties of the materials before and after DHT crosslinking, a) RCP; b) RCP/FeHA (40 °C, 3:2), t = 0; c) RCP/FeHA (40 °C, 3:2), t = 24h; d) RCP/FeHA (40 °C, 3:2), t = 48h, (Desnt) RCP desnaturation; DHT_{Trtm}) temperature used in the DHT treatment; Start_{deg}) starting the degradation of RCP).

The effect of crosslinking processes on organic-inorganic interactions and on the phase composition of the samples was evaluated by FTIR (Figure 5A) and XRD (Figure 5B), respectively.

The FTIR spectra of RCP before crosslinking treatment showed three main peaks of amide groups ($\approx 1240\text{cm}^{-1}$ (Amide I), 1550cm^{-1} (Amide II), 1650cm^{-1} (Amide III)). The biomineralized samples also presented the main peaks of RCP and endorse the presence of calcium phosphate (CaP) nucleated into RCP structure, indicated by $\approx 1026\text{cm}^{-1}$ asymmetrical stretching (ν_3) of PO_4^{3-} from apatite (Wei et al. 2014; Cai et al. 2011), $\approx 960\text{cm}^{-1}$ very weak peak that correspond to $\nu_1\text{PO}_4^{3-}$, presence of CaP in RCP material, $\approx 870\text{cm}^{-1}$ $\nu_2\text{CO}_3$ vibrational mode that can substitute for PO_4^{3-} in the HAp lattice (Chang et al. 2006; Wei et al. 2014). Regarding to the spectrums after DHT treatment, main groups of RCP and CaP were presented. The decrease of intensity of Amide II peak, $\approx 1553\text{cm}^{-1}$, indicated the conversion of RCP free amide groups to amine groups (Haugh et al. 2009).

The effect of temperature and exposition time of DHT crosslinking on the phase composition of hybrid magnetic was analysed by XRD. XRD pattern (Figure 5B) before and after DHT presents a broad peak at $\approx 20^\circ 2\theta$ (*), due to the higher amount of RCP into bio-hybrid materials and also were presented the characteristic peaks of hydroxyapatite (** in Figure 5) (Koutsopoulos, 2002). This result indicates that the temperature and the exposition time do not influence the phase composition of the materials and also do not induce formation of any secondary phase, such as magnetite. It is also evident the maintenance of the magnetic properties after 24h and 48h of treatment (Figure 5C).

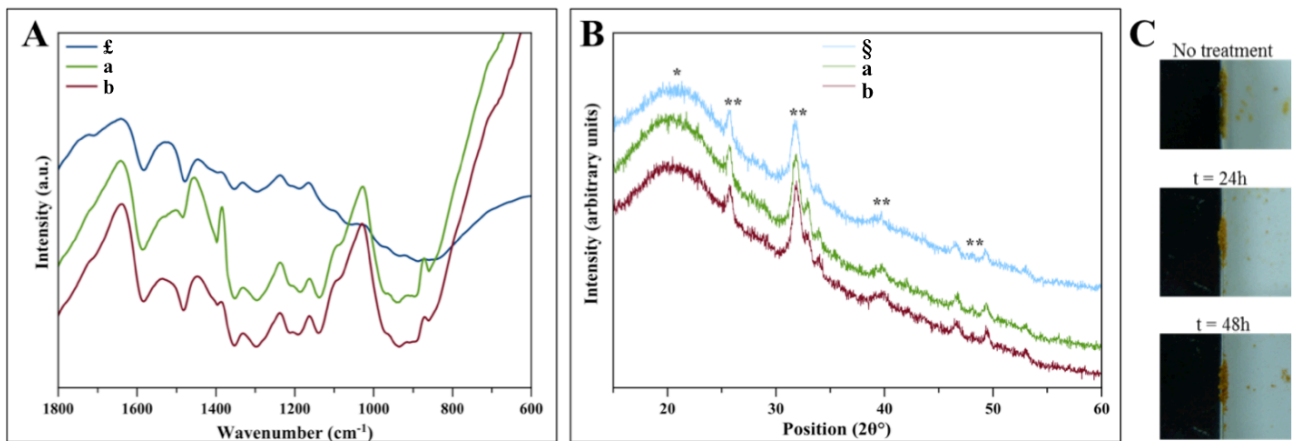


Figure 5. Chemical and magnetic characterisation of the magnetic microspheres analysed by FTIR (A), XRD (B) and neodymium magnet (C), (£) RCP; a) RCP/FeHA (90:10; 3:2; 20 mol %), $t = 24\text{h}$; b) RCP/FeHA (90:10; 3:2; 20 mol %), $t = 48\text{h}$; §) RCP/FeHA (90:10; 3:2; 20 mol %), $t = 0$).

Investigations on the swelling ratios were carried out by immersing the samples in PBS solution (pH 7.4), during 24h. The sample used in this study was RCP/FeHA (90:10; 3:2; 40°C), after 24h of DHT crosslinking. Optical microscope was used to evaluate the microspheres size at different times. Optical micrographs (Figure 6) show an increase of the particle size and a well-defined geometry, due to the medium absorption. According to the results of the optical micrographs and the graph (Figure 6 A, 6 B) it is possible to observe a higher absorption of medium, during the first hours. After that, magnetic microspheres reach the equilibrium state, which is due to the osmotic phenomena that promote a relaxation of the hybrid material matrix (Valente et al. 2013). Microspheres composed by iron doped hydroxyapatite presented less water content due to the interaction of FeHA with RCP matrix, that reduce the hydrophilicity of RCP by the electrostatic binding of carboxyl or amine groups with calcium and phosphate (Figure 6B) (Lee et al. 2014).

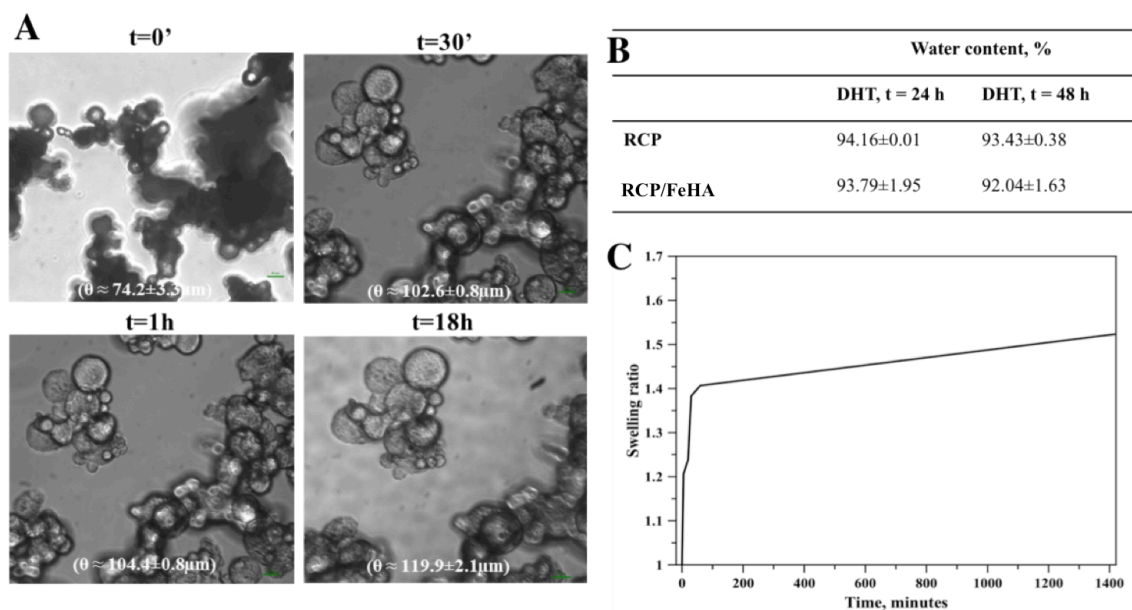


Figure 6. Swelling ratio and water content of RCP/FeHA (90:10; 3:2; 40°C), after 24h DHT crosslinking.

Magnetic microspheres (i.e. RCP/FeHA (90:10; 3:2; 40°C)) were immersed in PBS solution (pH 7.4) and placed on orbital incubator at ≈ 100 rpm, at 37°C, during 30 days and the medium was replaced 3 times. Morphological, chemical, thermal and magnetic preliminary characterisation was performed in order to evaluate the stability/degradation of the magnetic particles after 30 days immersed in PBS.

Figure 7 presents the surface morphology of the microspheres before and after 30 days immersed in PBS. SEM micrographs show that after 30 days in PBS the surface morphology became rougher and also a decrease of particles size was evident, probably due to the degradation of RCP in the microspheres. This result was also confirmed by FTIR (Figure 8A) and TGA (Figure 8B) analysis. Looking to the crosslinked hybrid magnetic materials after 30 days of immersion in PBS, peaks at $\approx 601\text{ cm}^{-1}$ and $\approx 566\text{ cm}^{-1}$ appeared. These two peaks are related to the triply degenerated bending mode of $\nu_4\text{PO}_4$ of calcium phosphate (Delgado-López et al. 2012); probably this can indicate some degradation of RCP on magnetic microspheres. Regarding to the thermogravimetric graph (Figure 8B), the samples without and with treatment present a similar weight loss. After 30 days of immersion in PBS in both situations the degradation of the organic material occurred. Comparing to the organic material percentage on the microspheres after 30 days in PBS, the weight loss was approximately of 20% and 8.75%, respectively to $t=24\text{h}$ and $t=48\text{h}$ of DHT treatment. After 30 days immersed in PBS the magnetic properties were still evident in the samples (Figure 8C).

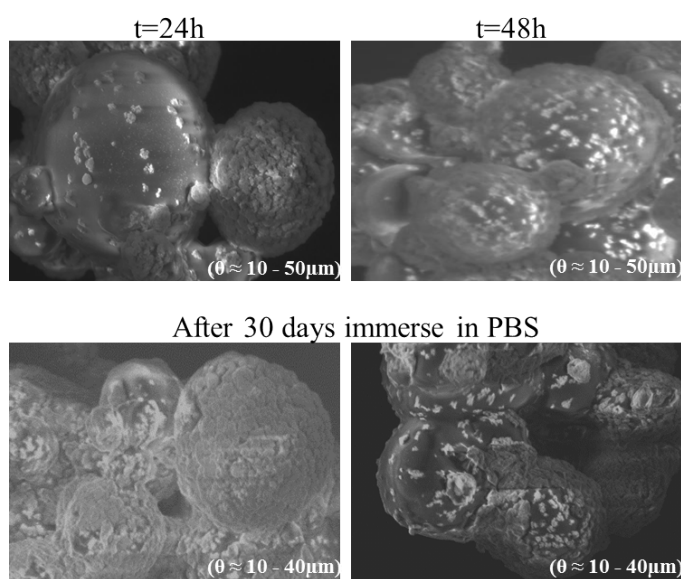


Figure 7. Morphological characterisation after immersed during 30 days in PBS.

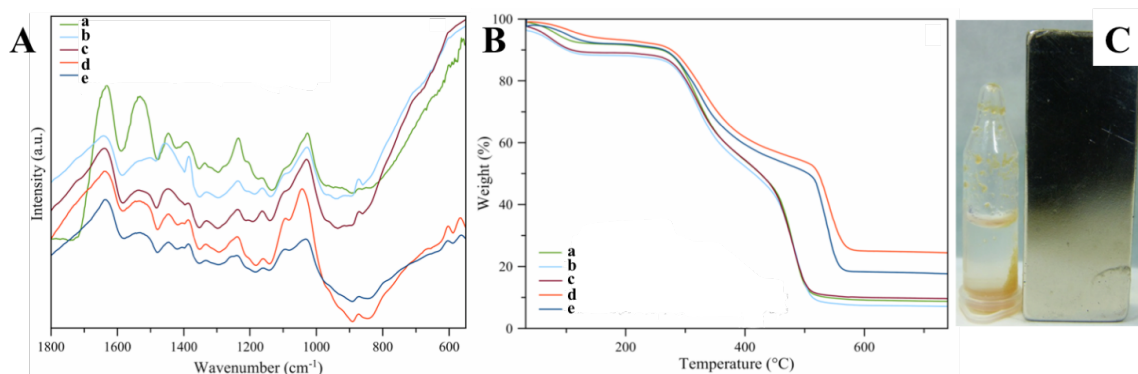


Figure 8. Magnetic microspheres (RCP/FeHA (90:10, 40 °C)) evaluation after 30 days immersed in PBS. A) Chemical characterisation; B) Thermal characterisation; C) Preliminary magnetic properties, (a) no crosslinked; b) crosslinked at $t = 24\text{h}$; c) crosslinked at $t = 48\text{h}$; d) crosslinked at $t = 24\text{h}$ and after 30 days; e) crosslinked at $t = 48\text{h}$ and after 30 days).

Final remarks

- Microspheres were produced by emulsification process;
- Dehydrothermal crosslinking enable suitable crosslinking of the microspheres, after 24h and 48h;
- DHT process does not influence the morphological, chemical, thermal and magnetic properties of the samples;
- No evident presence of secondary phases after DHT crosslinking;
- Magnetic microspheres presented higher swelling ratio and water content after 24h immersed in PBS;
- After 30 days immersed in PBS the degradation of the microspheres was observed by morphological, chemical and thermal characterisation, while magnetic properties were not influenced.

References

- Cai Q., Xu Q., Feng Q., Cao X., Yang X., Deng X. (2011), Biomineralization of electrospun poly(l-lactic acid)/gelatin composite fibrous scaffold by using a supersaturated simulated body fluid with continuous CO_2 bubbling, *Applied Surface Science*, 257 (2011) 10109– 10118.
- Chang M. C., Douglas W. H., Tanaka J. (2006), Organic-inorganic interaction and the growth mechanism of hydroxyapatite crystals in gelatin matrices between 37 and 80°C, *J Mater Sci: Mater Med*, 17: 387–396, DOI 10.1007/s10856-006-8243-9.
- Delgado-López, J. M., Iafisco, M., Rodríguez, I., Tampieri, A., Prat, M., & Gómez-Morales, J. (2012). Crystallization of bioinspired citrate-functionalized nanoapatite with tailored carbonate content. *Acta biomaterialia*, 8(9), 3491-3499.
- Koutsopoulos, S. (2002). Synthesis and characterization of hydroxyapatite crystals: a review study on the analytical methods. *Journal of biomedical materials research*, 62(4), 600-612.
- Lee, J., & Yun, H. S. (2014). Hydroxyapatite-containing gelatin/chitosan microspheres for controlled release of lysozyme and enhanced cytocompatibility. *Journal of Materials Chemistry B*, 2(9), 1255-1263.

Haugh, M. G., Jaasma, M. J., & O'Brien, F. J. (2009). The effect of dehydrothermal treatment on the mechanical and structural properties of collagen-GAG scaffolds. *Journal of Biomedical Materials Research Part A*, 89(2), 363-369.

Tampieri A., Iafisco M., Sandri M., Panseri S., Cunha C., Sprio S., Savini E., Uhlarz M., Herrmannsdörfer T. (2014), Magnetic bio-inspired hybrid nanostructured collagen-hydroxyapatite scaffolds supporting cell proliferation and tuning regenerative process. *ACS applied materials & interfaces*.

Wei W., Sun R., Jin Z., Cui J., Wei Z., Hydroxyapatite-gelatin nanocomposite as a novel adsorbent for nitrobenzene removal from aqueous solution, *Applied Surface Science* 292 (2014) 1020– 1029.

Xing Q., Yates K., Vogt C., Qian Z., Frost M. C., Zhao F. (2014), Increasing mechanical strength of gelatin hydrogels by divalent metal ion removal, *Scientific reports*, 4.

Annex II

List of Publications

Tatiana F. Patrício, Monica Montesi, Silvia Panseri, Michele Iafisco, Monica Sandri, Anna Tampieri, Simone Sprio Effect of superparamagnetic microspheres on osteogenic differentiation of MC3T3-E1 (*in preparation*);

Tatiana F. Patrício, Silvia Panseri, Monica Sandri, Anna Tampieri, Simone Sprio. New bioactive bone-like microspheres with intrinsic magnetic properties obtained by bio-inspired mineralisation process. *Materials and Engineering: Part C (in press - accepted manuscript)*;

Michele Miragoli, Paola Ceriotti, Michele Iafisco, Marco Vacchiano, Nicolò Salvarani, Alessio Alogna, Pierluigi Carullo, Gloria Belén Ramírez-Rodríguez, Tatiana Patrício, Silvana Pinelli, Rossella Alinovi, Marco Erreni, Stefano Rossi, Gianluigi Condorelli, Heiner Post, Anna Tampieri, & Catalucci Daniele. Inhalation Therapy Delivers Nanoparticle-Based Therapeutic Biomolecules To The Diseased Heart (*Under submission*)

Di Mauro, V., Iafisco, M., Salvarani, N., Vacchiano, M., Carullo, P., Ramírez-Rodríguez, G. B., Patrício T., ... & Catalucci, D. (2016). Bioinspired negatively charged calcium phosphate nanocarriers for cardiac delivery of MicroRNAs. *Nanomedicine*, 11(8), 891-906;

Sandhöfer, B., Meckel, M., Delgado-López, J. M., Patrício, T., Tampieri, A., Rösch, F., & Iafisco, M. (2015). Synthesis and preliminary in vivo evaluation of well-dispersed biomimetic nanocrystalline apatites labeled with positron emission tomographic imaging agents. *ACS applied materials & interfaces*, 7(19), 10623-10633;

Conferences:

T. M. Fernandes Patrício, D. Mumcuoglu, J. Nickel, M. Montesi, S. Panseri, M. Sandri, S. Kluijtmans, A. Tampieri and S. Sprio. New magnetic microspheres obtained by bio-inspired synthesis, for controlled release of BMP-2 in bone tissue engineering. (<http://eventi.cnism.it/materials2016/submission/view/1307>)

Iafisco, M., Di Mauro, V., Salvarani, N., Ramírez-Rodríguez, G. B., Patrício, T., Miragoli, M., ... & Tampieri, A. Bio-inspired negatively-charged calcium phosphate nanocarriers for cardiac delivery of therapeutic molecules.

Fernandes Patrício, T., Sprio, S., Sandri, M., Gostynska, N., Montesi, M., Panseri, S., ... Tampieri, A. (2016). Bio-inspired superparamagnetic microspheres for bone tissue engineering applications. *Frontiers in Bioengineering and Biotechnology*, (2734). article. <http://doi.org/10.3389/conf.FBIOE.2016.01.02734>

T. M. Fernandes Patrício, S. Sprio, M. Sandri, M. Montesi, S. Panseri, A. Tampieri (2015), "Hybrid Superparamagnetic Collagen-like Peptide - Microparticles applied on Bone Tissue Regeneration", *Tissue engineering: Part A*, V. 21, Supplement 1-152 (4th TERMIS World Congress).